Online Monitoring and Analysis of Water Quality in Offshore Oil & Gas Production

Hansen, Dennis Severin

DOI (link to publication from Publisher):
https://doi.org/10.5278/vbn.phd.eng.00080

Publication date:
2020

Document Version
Publisher's PDF, also known as Version of record

ONLINE MONITORING AND ANALYSIS OF WATER QUALITY IN OFFSHORE OIL & GAS PRODUCTION

BY
DENNIS SEVERIN HANSEN

DISSERTATION SUBMITTED 2020

AALBORG UNIVERSITY
DENMARK

Online Monitoring and Analysis of Water Quality in Offshore Oil & Gas Production

Ph.D. Dissertation

Dennis Severin Hansen

Dissertation submitted December 19, 2020

Dissertation submitted: December 19, 2020

PhD supervisor: Associate Prof. Zhenyu Yang
Aalborg University

PhD committee: Associate Professor Matthias Mandø (chairman)
Aalborg University

Principal Consultant Ming Yang
TÜV SÜD National Engineering Laboratory

Professor Simon Ivar Andersen
Technical University of Denmark

PhD Series: Faculty of Engineering and Science, Aalborg University

Department: Department of Energy Technology

ISSN (online): 2446-1636
ISBN (online): 978-87-7210-866-7

Published by:
Aalborg University Press
Kroghstræde 3
DK – 9220 Aalborg Ø
Phone: +45 99407140
aauf@forlag.aau.dk
forlag.aau.dk

Printed in Denmark by Rosendahls, 2021

"Wonder is the beginning of wisdom."

– SOCRATES

Abstract

70% of the world's oil production derives from matured hydrocarbon fields. Water is together with oil trapped in the reservoirs and becomes a byproduct of the oil production, which steadily increases over time. In the Danish sector alone, the oil to water ratio (water cut) reached 80% in 2015, and the required amount of energy to treat the volumes of produced water before ocean discharge to comply with legislation increases. Another solution is to reinject the produced water into the reservoir to gain more sustainable production and comply with discharge legislation. Produced water reinjection has gained increasing attention in the last decades as it can increase yield and reduce oil discharge. However, the presence of solid particles, crude oil, and chemicals in the produced water, when reinjecting into the reservoir, introduces other complications in the injection water treatment process and the reservoir. Ideally, injection water should be sterile, non-scaling, free of suspended solids and oil to prevent plugging the reservoir rock's pores and reduce permeability. Furthermore, corrosion due to the presence of dissolved gases and microbially influenced corrosion bacteria should be prevented. A treatment process for achieving these ideal conditions is challenged to yield economic payoffs. The current solutions for measuring water quality are based on manual sampling, which suffers from being time-consuming and may not suffice to retain a high and consistent injection water quality. Despite the long history of implementing online quality monitors for measuring particle and oil droplet concentrations and sizes, there is no consensus regarding which method provides the most reliable estimate leaving petroleum engineers with an array of choices.

An extensive review study has been carried out of how different water quality issues can add to the suspended solids concentration that can potentially cause injectivity decline in the injection water treatment facility or, even worse, cause formation damage. Furthermore, the complexity of selecting quality monitors that reliably measure the concentration and sizes of suspended solids in the process has been heavily reviewed. Through the review process, online microscopy analyzers were deemed the best candidates for measuring single-particle properties within an injection water treatment process. Two different microscopy analyzers for measuring suspended particles have been validated,

including four identical fluorescence-based monitors for measuring oil-in-water concentrations. For each monitor type, a thorough calibration validation has been proposed to investigate their accuracy and reliability. The four identical fluorescence-based monitors for measuring oil-in-water concentrations revealed that the calibration procedure using a weighted least square yields higher reproducibility compared to ordinary least square due to the heteroskedastic behavior. The experimental validation results of the four fluorescence-based monitors showed a high precision between each other. However, due to its high sensitivity to fluorescent substances (fluorophores), they will be challenged in a dynamic separation facility with continuous changes of the fluorophores. The two different types of microscopy analyzers showed promising results in estimating known particle sizes and were able to measure oil-in-water concentrations with high precision in steady-state. A trailing moving average window of 1min was proposed resulting as a feasible solution for continuous measurements. It is acknowledged that an issue will arrive at shallow concentrations as the required number of oil droplets will not be captured within the expected relative error to represent the size distribution. Additionally, the classification procedure for both microscopy analyzers needs further validation.

Lastly, a connection between an industrial human-machine interface software and an academic used software were established to reduce the gap between academic research and industrial implementation. The connection was successfully established, and a case study of a model-predictive control method in the industrial used software was presented. The industrial human-machine interface software connection is a beneficial tool when, i.e., the presentation of water quality should be furtherly investigated.

Resumé

70% af verdens olieproduktion stammer fra aldrende oliefelter. Vand er sammen med olie fanget i reservoirerne og er derfor et biprodukt af olieproduktionen. Grundet udtømningen af oliefelterne stiger biproduktet af produceret vand støt hvert år. Alene i den danske sektor nåede olie/vand-forholdet 1/5 i 2015. Den nødvendige mængde energi til at behandle det producerede vand før udledning til havet stiger løbende, for at overholde udledningslovgivningen. En anden løsning er at geninjicere det producerede vand ned i reservoiret for at opretholde en mere bæredygtig produktion og overholde udledningslovgivningen. Injektion af produceret vand har fået øget opmærksomhed i de sidste årtier, da det kan øge det totale udbytte og reducere olieudledningen. Dog bliver behandlingsprocessen mere kompliceret når det producerede vand introduceres til injektionsprocessen, hvor tilstedeværelsen af faste partikler, råolie og kemikalier skal filtreres og behandles før det injiceres ned i reservoiret. Ideelt set skal injektionsvandet være sterilt, fri for krystallisering, faste partikler og olie for at forhindre tilstopning af den interne porestruktur i reservoiret, og derved reducere permeabiliteten. Derudover bør gaskorrosion og mikrobiel korrosion forhindres. Men økonomisk set vil det være svært at opnå profit af olieproduktionen, hvis der tilstræbes en ideel behandlingsproces.

De nuværende målemetoder af vandkvalitet er baseret på manuelle prøvetagninger, som kan være tidskrævende, og vil derfor ikke være tilstrækkelig til at opretholde en høj og ensartet kvalitet af injektionsvandet. På trods af mange års implementering af forskellige typer af online enheder til måling af partikelstørrelser og koncentrationer er der ingen enighed om hvilken metode der giver den mest pålidelige måling, hvilket resulterer i at olieingeniører står tilbage med et svært valg når der skal investeres i nye måleenheder.

En gennemgribende undersøgelse er blevet udført omkring hvilke forskellige partikulære stoffer der kan være til stede i injektionsvandet, og dermed øge den samlede koncentration af suspenderede stoffer. De suspenderede stoffer kan potentielt forårsage reduktion af den injicerede vandmængde i injektionsprocessen, eller forårsage formationsskader i reservoiret. Derudover er kompleksiteten ved at vælge den rette type af måleenhed til at måle koncentrationer og partikelstørrelser af suspenderede stoffer i injektionsprocessen blevet undersøgt. Ud

fra analysen blev online mikroskopienheder konkluderet til at være de bedste kandidater til måling af forskellig partiklers fysiske egenskaber i en injektionsproces.

To forskellige online mikroskopienheder til måling af suspenderede partikler er blevet testet. Herudover er fire identiske fluorescensbaserede enheder til måling af olie-i-vand koncentrationer også blevet testet. For hver af de to enhedstyper er der givet en grundig kalibreringsvalidering for at undersøge deres nøjagtighed og pålidelighed. De fire identiske fluorescensbaserede enheder til måling af olie-i-vand koncentrationer efterviste at kalibreringsproceduren med anvendelse af en vægtet mindste kvadraters metode, giver øget reproducerbarhed sammenlignet med almindelig mindste kvadraters metode på grund af den heteroskedastiske opførsel af prøvetagningen under kalibreringen. De eksperimentelle valideringsresultater for de fire fluorescensbaserede enheder viste høj præcision mellem hinanden. Men på baggrund af deres høje følsomhed over for fluorescerende stoffer (fluoroforer) vil de blive udfordret i et dynamisk separationsanlæg med kontinuerlige ændringer af fluoroforer.

De to forskellige typer mikroskopienheder viste lovende resultater ved estimering af kendte partikelstørrelser, og var i stand til at måle olie-i-vand koncentrationer med høj præcision i stationær tilstand. Et glidende gennemsnitsvindue på 1min blev påvist som en mulig løsning til at måle koncentrationen kontinuerligt. Det erkendes dog at et af problemerne ved målinger af partikler og koncentrationer med online mikroskopienheder kan opstå, hvis et given antallet af partikler ikke opfanges inden for en acceptabel usikkerhed af størrelsesfordelingen. Klassificeringsproceduren for begge mikroskopienheder kræver yderligere validering.

Til sidst blev der etableret en forbindelse mellem en industriel brugerflade (HMI) og et akademisk software for at reducere afstanden mellem akademisk forskning og industriel implementering. Forbindelsen blev succesfuldt oprettet, hvilket er præsenteret i et casestudie med en demonstration af en model forudsigelig kontrol (MPC) metode på i industrielle brugerflade. Den industrielle brugerflade er et nyttigt værktøj når præsentationen af vandkvaliteten bør undersøges yderligere.

Contents

Thesis Details

Thesis Title:	Online Monitoring and Analysis of Water Quality in Offshore Oil & Gas Productions
Ph.D. Student:	Dennis Severin Hansen
Supervisor:	Associate Prof. Zhenyu Yang, Aalborg University, DK

The body of the thesis consists of the following papers:

[A] D. S. Hansen, M. V. Bram, S. M. Ø. Lauridsen, and Z. Yang, "Online Quality Measurements of Total Suspended Solids for Offshore Reinjection: A Review Study" *Energies*, MDPI, p. 53, 2020. [submitted for publication]

[B] D. S. Hansen, M. V. Bram, and Z. Yang, "Efficiency investigation of an offshore deoiling hydrocyclone using real-time fluorescence- and microscopy-based monitors," in *2017 IEEE Conference on Control Technology and Applications (CCTA)*. Mauna Lani, HI: IEEE, 27-30 Aug. 2017, pp. 1104–1109. Doi: 10.1109/CCTA.2017.8062606

[C] D. S. Hansen, S. Jespersen, M. V. Bram, and Z. Yang, "Uncertainty Analysis of Fluorescence-Based Oil-In-Water Monitors for Oil and Gas Produced Water," *Sensors*, vol. 20, no. 16, p. 36, 2020. Doi: 10.3390/s20164435

[D] D. S. Hansen, S. Jespersen, M. V. Bram, and Z. Yang, "Offshore Online Measurements of Total Suspended Solids using Microscopy Analyzers" *IEEE Sensors Journal*, IEEE, p. 10, 2020. [submitted for publication]

[E] D. S. Hansen, S. Jespersen, M. V. Bram, and Z. Yang, "Human Machine Interface Prototyping and Application for Advanced Control of Offshore Topside Separation Processes," in *IECON 2018 - 44th Annual Conference of the IEEE Industrial Electronics Society*. Washington, DC: IEEE, 21-23 Oct. 2018, pp. 2341–2347. Doi: 10.1109/IECON.2018.8591309

In addition the following publications have also been made:

[**1**] P. Durdevic, S. Pedersen, M. Bram, D. Hansen, A. Hassan, and Z. Yang, "Control Oriented Modeling of a De-oiling Hydrocyclone," *IFAC-PapersOnLine*, vol. 48, no. 28, pp. 291–296, 2015. Doi: 10.1016/j.ifacol.2015.12.141

[**2**] M. V. Bram, A. A. Hassan, D. S. Hansen, P. Durdevic, S. Pedersen, and Z. Yang, "Experimental modeling of a deoiling hydrocyclone system," in *2015 20th International Conference on Methods and Models in Automation and Robotics (MMAR)*. Miedzyzdroje: IEEE, 24-27 Aug. 2015, pp. 1080-1085, Doi: 10.1109/MMAR.2015.7284029

[**3**] D. Hansen, M. Bram, P. Durdevic, S. Jespersen, and Z. Yang, "Efficiency evaluation of offshore deoiling applications utilizing real-time oil-in-water monitors," in *Oceans 2017 - Anchorage*. Anchorage, AK: IEEE, 18-21 Sep. 2017, p. 6. Available: https://ieeexplore.ieee.org/document/8232154

[**4**] P. Durdevic, C. Raju, M. Bram, D. Hansen, and Z. Yang, "Dynamic Oil-in-Water Concentration Acquisition on a Pilot-Scaled Offshore Water-Oil Separation Facility," *Sensors*, vol. 17, no. 124, p. 11, 2017. Doi: 10.3390/s17010124

[**5**] M. V. Bram, L. Hansen, D. S. Hansen, and Z. Yang, "Grey-Box Modeling of an Offshore Deoiling Hydrocyclone System," in *2017 IEEE Conference on Control Technology and Applications (CCTA)*. Mauna Lani, HI: IEEE, 27-30 Aug. 2017, pp. 94–98. Doi: 10.1109/CCTA.2017.8062446

[**6**] P. Andreussi, M. Bonizzi, P. Ciandri, S. Pedersen, and D. S. Hansen, "The use of a low-cost gas-liquid flow meter to monitor severe slugging," in *18th International Conference on Multiphase Production Technology*, Cannes: BHR Group, 7-9 Jun. 2017, pp. 413–424.

[**7**] M. V. Bram, L. Hansen, D. S. Hansen, and Z. Yang, "Hydrocyclone Separation Efficiency Modeled by Flow Resistances and Droplet Trajectories," *IFAC-PapersOnLine*, vol. 51, no. 8, pp. 132–137, 2018. Doi: 10.1016/j.ifacol.2018.06.367

[**8**] M. V. Bram, L. Hansen, D. S. Hansen, and Z. Yang, "Extended Grey-Box Modeling of Real-Time Hydrocyclone Separation Efficiency," in *2019 18th European Control Conference (ECC)*. Naples: IEEE, 25-28 Jun. 2019. pp. 3625–3631. Doi: 10.23919/ECC.2019.8796175

[**9**] M. V. Bram, S. Jespersen, D. S. Hansen, and Z. Yang, "Control-Oriented Modeling and Experimental Validation of a Deoiling Hydrocyclone System," *Processes*, vol. 8, no. 9, p. 33, 2020. Doi: 10.3390/pr8091010

[**10**] M. V. Bram, J. Calliess, S. Roberts, D. S. Hansen, Z. Yang, "Analysis and Modeling of State-Dependent Delay in Control Valves," In *IFAC World Congress 2020* (IFAC-PapersOnLine). Berlin: Elsevier, 11-17 Jul. 2020. [Accepted/In press]

[**11**] Z. Yang, P. Durdevic, S. Jespersen, and D. S. Hansen, "Potential of using Real-time OIW Monitoring for Control of Produced Water Treatment in Offshore Oil & Gas Production," *Advances in Science, Technology & Innovation*, Springer, 2020, p. 2. [Accepted/In press]

This thesis has been submitted for assessment in partial fulfillment of the Ph.D. degree. The thesis is based on the submitted or published scientific papers that are listed above. The thesis's body consists directly of the Papers A−E, where Papers 1−11 are additional papers related to offshore oil and gas. As part of the assessment, co-author statements have been made available to the assessment committee and available at the faculty.

Preface

This thesis is submitted as a collection of papers to fulfill the requirements for the degree of Doctor of Philosophy at the Department of Energy Technology, Aalborg University, Denmark. The entire work has been conducted at the Department of Energy Technology, Aalborg University, Denmark. The work was done in close collaboration with Total Denmark in the period September 2017 to December 2020 under the supervision of Associate Professor Zhenyu Yang. The project was supported by the Danish Hydrocarbon Research and Technology Centre and Aalborg University joint project: "Injection Water Quality and Control, Aalborg University, Pr-no: 878040". A direct thanks to the contact person at Total, Steven M. Ø. Lauridsen, for his support and collaboration during the project.

I gratefully thank all the colleagues from the Department of Energy Technology, Aalborg University, for providing a friendly research environment. I want to thank my supervisor Zhenyu Yang for his professional opinion on navigating in the academic research society and always finding time for discussions. Thanks to my project colleagues: Stefan Jespersen, Leif Hansen, Kasper Jepsen, Simon Pedersen, and Petar Durdevic, for providing great feedback, collaboration, and valuable discussions. Special thanks to my colleague, former fellow student, and friend, Mads V. Bram, for more than nine years of professional teamwork; it has been an honor. Lastly, I would like to express my gratitude to my girlfriend and my two kids, which has been part of my journey to hand in my Ph.D. thesis. They have been the foundation outside the research environment where I could relax.

Dennis Severin Hansen
Aalborg University

Abbreviations

ASM	Abnormal Situation Management
CCD	Charge-coupled device
CMOS	Complementary metal–oxide–semiconductor
DS	Danish Standard
EIA	Energy Information Administration
ESV	Edge strength value
FRV	Focus rejection value
GC-FID	Gas chromatography-flame ionization detector
GHG	Greenhouse gases
HMI	Human machine interface
IEA	International Energy Agency
ISO	International Organization for Standardization
IW	Injection water
IWT	Injection water treatment
MIC	Microbially influenced corrosion
MPC	Model predictive control
OCED	Organisation for Economic Co-operation and Development
OiW	Oil-in-water
OLS	Ordinary least square
OPC	Open platform communications
OPEX	Operational expenditure
OSPAR	Oslo and Paris convention

P&ID	Piping and instrumentation diagram
PDR	Pressure different ratios
PID	Proportional, integral, and derivative
PLC	Programmable logic controller
PMT	Photomultiplier tube
ppm	Parts per million
PSD	Particle size distribution
PW	Produced water
PWRI	Produced water reinjection
RET	Resonance energy transfer
RFU	Relative fluorescence unit
SAE	Society of Automotive Engineers
SCADA	Supervisory control and data acquisition
TDS	Total dissolved solids
THV	Threshold value
TPES	Total primary energy supply
TSS	Total suspended solids
UV	Ultraviolet
WLS	Weighted least square

Nomenclature

$[c_0, c_1]$	Slope and the intercept on the ordinate axis for the predicted variance function
$[x, y]$	Cartesian coordinates
α	non-zero exponential constant, for log-normal distribution $\alpha = 2$
$\bar{}$	Arithmetic mean
β	Basis number, for the count basis $\beta = 0$
δ	Relative error
$\hat{}$	Prediction
μ	Mean
μ_0	Mean of the log-normal distribution
ω	Intermediate parameter
ω_i	Weighting factor
σ	Population Standard deviation
σ_0	Standard deviation of the log-normal distribution
$_0$	Set of observations
$_i$	Index observation from 1 to n
a	Slope
b	The intercept on the ordinate axis
c	constant dependent on α and β
CI	Confidence interval of linear regression curve
DOF	Degree of freedom
e	Error between predicted and observed data
k	Coverage factor
n	Number of observations
n^*	Minimum number of required counted particles
$OiW_{repeat.}$	OiW concentration results with repeatability uncertainties from the reference method

$OiW_{reprod.}$	OiW concentration results with reproducibility uncertainties from the reference method
PI	Prediction interval of linear regression curve
s	Sample standard deviation
SS_{xx}	Weighted sum of square
SSE	Sum of square errors
$t_{0.025}$	t-score with two-tailed 95% confidence interval
u	Defined confidence level with its represented z-score value, for 95% confidence interval $u = 1.96$
X_N	Number of counted particles

Part I

Extended Summary

Chapter 1

Introduction and Motivation

1.1 Introduction

While the fossil fuel-based energy consumption in developed countries approaches a plateau and we are entering a new era of climate change, striving to reduce the carbon dioxide (CO_2) emission during the coming decades, production of oil is still expected to increase by 0.6% globally to meet the increasing demands the next 30 years [1, 2]. With an increasing population in developing countries and increasing energy demands, the Energy Information Administration (EIA) predicts that by 2050, natural gas, crude oil, and other liquids will still account for 48.4% of all combined energy sources, unless radical changes occur, as shown in Fig. 1.1 [2]. The total primary energy supply (TPES) in Fig. 1.1, refers to the amount of energy aggregate from production and imports without including exported energy.

If the estimations that are shown in Fig. 1.1 are correct, oil will account for $\sim$27% of the total energy consumption, hence the oil and gas industry will be a significant part of the worlds energy consumption during the next 30 years [4, 5]. Therefore, there is a strong incentive and a responsibility for the oil and gas industry to minimize greenhouse gases (GHG) emissions by investing in innovative solutions and exploring new technologies [6]. However, it must be taken into account that countries like Denmark, and many other developed European countries, have a goal of being CO_2 neutral within the next few decades. This is also shown in Fig. 1.1, as Organisation for Economic Co-operation and Development (OCED) countries are estimated to reduce the energy consumption from oil by 5.5*p.p.*, though OCED members represent a wide range of different countries around the world. Even if Denmark achieves to become CO_2 neutral in 2050, Denmark only accounts for 1‰ of the total

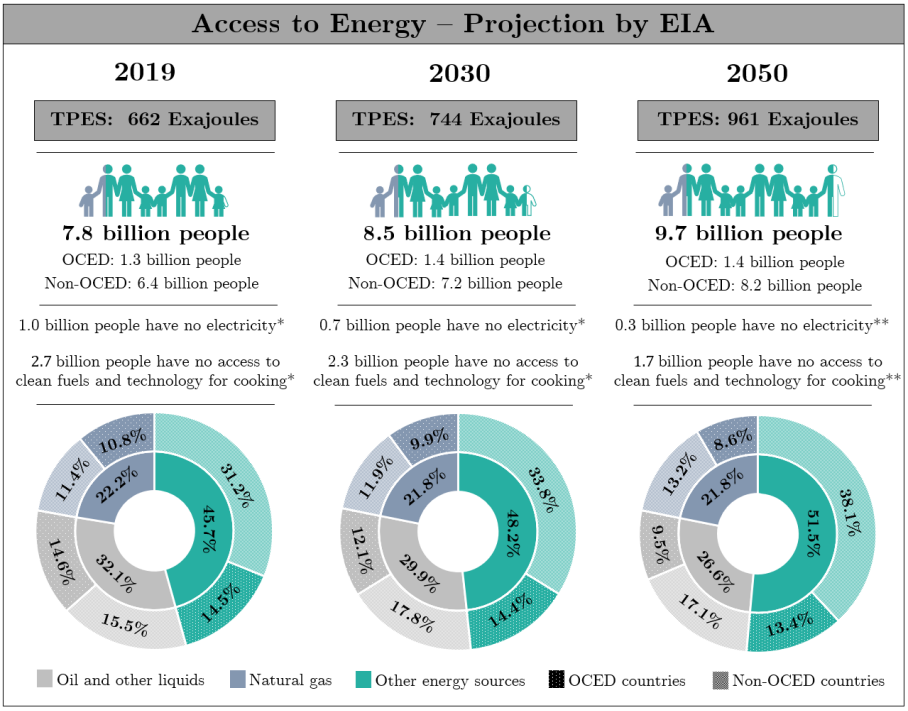

*Based on estimated data from the International Energy Agency (IEA) [3].
**Assuming a continuing gain of 3.34% and 1.40% annually for access to electricity and clean-cooking, respectively, based on the projected data from 2016 to 2030 by IEA [3].

Fig. 1.1: The presented data show the projection by EIA over a 31-years period [4]. Oil and other liquids include all types of crude oil, natural gas plant liquids, and biofuels. the other energy sources include coal, nuclear, and renewables, with renewables estimated to increase by an annually average of 3.1% worldwide. Thus, it is estimated to surpass energy consumption from oil and other liquids in 2047. Figure is from Paper A.

CO_2 emissions globally. Denmark's achievement of having a net-zero emission in 2050 must therefore be found in the positive return of being an inspiration for other countries to increase their ambition to reduce their CO_2 emissions. If this is not the case, pioneering countries such as Denmark should consider whether there is a risk of introducing "carbon leakage" instead, which will have a negative effect on the global CO_2 reduction [7]. Carbon leakage refers to the phenomenon of stricter GHG emissions regulations only causes production to increase in other countries with more lenient legislation [7]. That could be the case with the Danish oil and gas sector as they have the lowest carbon intensity from the upstream processes in the world [8]. The low carbon intensity is a positive outcome of a long history of stricter legislation and documentation regarding offshore production in the North Sea, governed by Oslo and Paris

convention (OSPAR) regulations and national legislation. One can, therefore, raise the question: "Can Denmark support disadvantageous actions to the environment by stopping the offshore oil production too soon through carbon leakage?"

In the transition to more sustainable production, and as the underground hydrocarbon reservoirs mature, offshore oil and gas production faces another difficult challenge; the increasing amount of produced water (PW). PW is the byproduct during the extraction of oil or gas. Producers in the Danish part of the North Sea have since 1986 injected water back into the underground reservoir to such an extent that the extracted mixture consists of more than 90% PW, as shown in Fig. 1.2 [9, 10]. In addition, the amount of oil produced from the reservoirs decreases over time, which has caused Denmark to no longer be a net exporter of oil as the Danish oil consumption exceeded the oil production in 2018 [11]. Therefore, it raises the second question: "How long can the operation remain financially feasible?" [12].

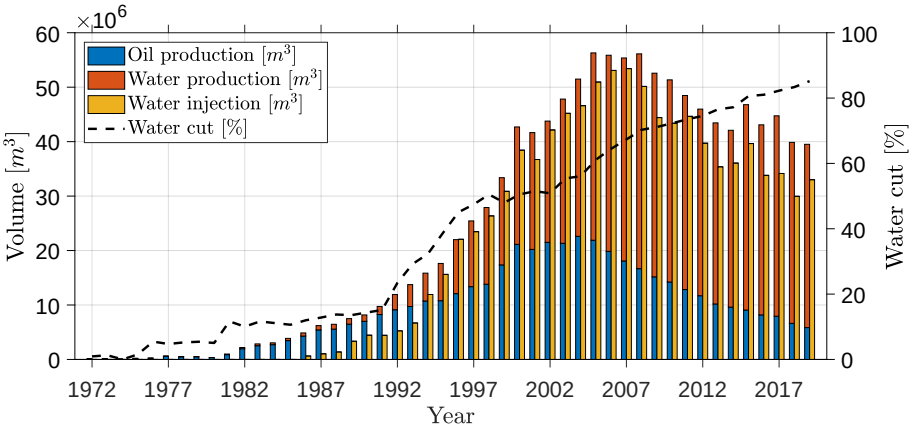

Fig. 1.2: The bar chart shows the annual production of oil and water, and amount of water that is injected in the Danish sector of the North Sea. The data are annually published by Danish Energy Agency [9]. Figure is from Paper A.

A general trend towards more sustainable production, guided by discharge legislation that introduces stricter legislation and strives to achieve zero discharge, improved enhanced recovery techniques, such as produced water reinjection (PWRI) have received increasing attention. The Danish part of the North Sea's current regulation states that oil-in-water (OiW) concentration must be less than 30ppm before discharging into the ocean. The Danish Environmental Protection Agency furthermore states that the total annual quantity of oil discharged into the North Sea must be less than 222t/yr based on an agreement from 2017/2018 [13–16]. As an increasing amount of water is pro-

duced, the limit of the total discharged oil becomes more significant, especially as the former Mærsk Oil in 2015 reached 96% of the allowed total amount of oil discharge [14, 15].

In 2014 the OSPAR commission reported that 16 installations failed to meet the 30ppm discharge legislation, where each of the installations exceeded an annual average concentration of dispersed oil discharge [17]. Several of the platforms reported that the reason for not achieving the standard was due to PWRI failure, which questions whether the OiW concentration in the PW is even considered when reinjecting. Increasing the PWRI ratio has the potential to increase yields and reduce oil emissions while complying with national and local regulations and minimizing negative environmental impacts [18–20]. The injection water (IW) is mainly injected to maintain reservoir pressure, which drives reservoir production. The secondary purpose is to sweep the reservoir, by displacing the oil to flow towards the production wells and thereby increase the oil production [21, 22].

In Denmark, $33.7 \cdot 10^6 \mathrm{m}^3$ of water was produced, and $33.0 \cdot 10^6 \mathrm{m}^3$ of water was injected during 2019, of which ∼14% of the IW consists of PW according to the Danish Environmental Protection Agency [23], while the remaining IW consists of treated seawater. To further increase the PWRI ratio, it must be economically feasible for acquiring sufficient quality to avoid accidental formation damage. Current offshore platforms rely on offline measurements of both OiW and total suspended solids (TSS) concentration, where OiW concentrations of PW must be measured manually at least twice daily. In comparison, reports of TSS concentrations from injection water treatment (IWT) facilities are not governed by legislation but governed by the producer's own choice. How often the TSS concentrations are measured can vary widely. Both manual reporting methods for OiW and TSS suffer from being time-consuming and may not suffice to increase the PWRI ratio. To increase the PWRI ratio, the IW quality must be high and consistent. Effective control of PW and IW involves appropriate treatment, discharge, and monitoring. Monitoring PW discharge can also help protect the receiving environment. Accurate water analysis is essential to gain an understanding of the dispersed conditions in PW and IW to identify changes in the process. Therefore, the operator must have confidence in the data that are obtained from the monitor. Accurate information on the amount of oil and particles, sizes, and classification of particles in IW can be used for decision support, reporting, or even advanced control to achieve better operation in the treatment process, all of which benefits water-intensive operation [20]. Therefore, the importance and awareness of accurate online water quality measurements have received more attention the last decades within the oil and gas industry. Based on a preliminary feasibility study, this thesis investigated two promising online monitor types: a fluorescence-based monitor for measuring the OiW concentration and two different microscopy analyzers for measuring particles. All three types of monitors are shown in Fig. 1.3.

Fig. 1.3: The three types of online monitors used in the experiments described in this thesis: (**a**) Jorin ViPA; (**b**) Canty InFlow; (**c**) Turner TD-4100XDC.

1.1.1 Fluorescence-Based Monitor

The types of monitors described in this thesis, both microscopy and fluorescence spectroscopy, uses light in their measurement principles. Light is the smallest quantity of energy that can be transported. Light can be described in terms of a stream of photons traveling as a wave-particle duality at the speed of light [24]. A photon is an elementary particle that only can be created or destroyed. Looking at light in the electromagnetic spectrum, the visible light that the human eye is sensitive to only covers a very narrow range of the entire spectrum, as shown in Fig. 1.4 [25], from near-ultraviolet (UV) at a wavelength of 380nm to deep red at 710nm [25].

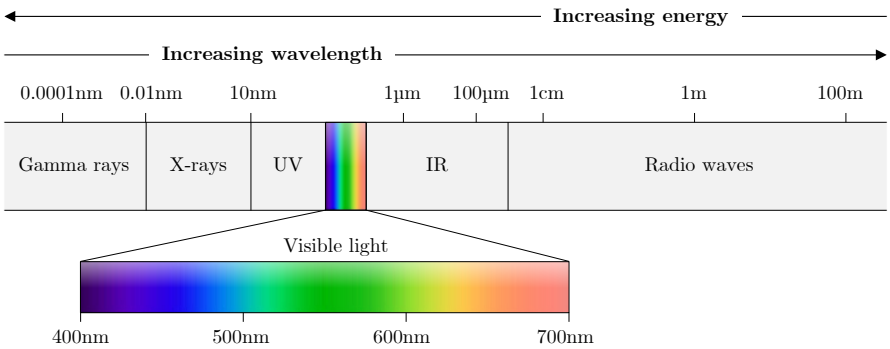

Fig. 1.4: The electromagnetic spectrum, with a zoom-in on the visible spectrum from roughly $(400 - 700)$nm.

The intensity of light is defined by the number of photons passing through a unit area in a unit of time. That will be the case when using optical microscopes to analyze samples manually by using the eyesight.

Fluorescence occurs as the incoming photons raise the electrons' energy in a fluorophore molecule to an excited state, for instance, in aromatic hydrocarbons. The electron then loses some energy as heat due to the molecule's vibrations, and lastly, the electron returns to the ground state by releasing a new photon with a longer wavelength [26]. This fluorescence process is often illustrated by the Jablonski diagram as shown in Fig. 1.5.

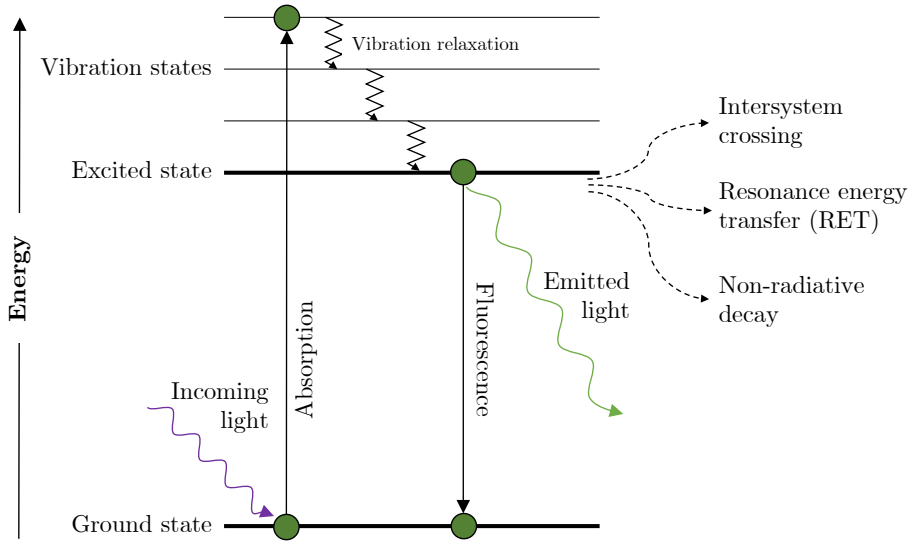

Fig. 1.5: An illustration of a Jablonski diagram, showing the interaction of a fluorophore molecule with a photon with the outcome of an emitted florescent photon.

Since energy has been lost during the process due to vibrational relaxations, the emitted fluorescent photon has lower energy, hence longer wavelength than the excitation photon. Outcomes other than the emission of light can occur, such as non-radiative decay, where energy is released by heat through vibrations, and no photon is emitted. Other less common events are intersystem crossing from the excited state to the triple-state where relaxation from the triplet state to the ground state can occur, also known as phosphorescence [26]. Additionally, resonance energy transfer (RET) is when energy transfers from a fluorescent donor to a fluorescent acceptor when the emission spectrum of the fluorescent donor overlaps with the excitation spectrum of the fluorescent acceptor [27]. Furthermore, the intensity of fluorescence can be decreased by a wide range of molecular interactions, collectively known as quenching. According to Lakowicz [26], quenching can occur by different mechanisms, such as

collisional, excited state reactions, molecular rearrangements, energy transfer, and ground-state complex formation.

The presented fluorescence-based monitor in this thesis detects the content of fluorescent aromatic hydrocarbons in the oil-water-mixture. The fluorescence compound unit is measured as relative fluorescence unit (RFU), which is then transformed to parts per million (ppm) through a calibration curve.

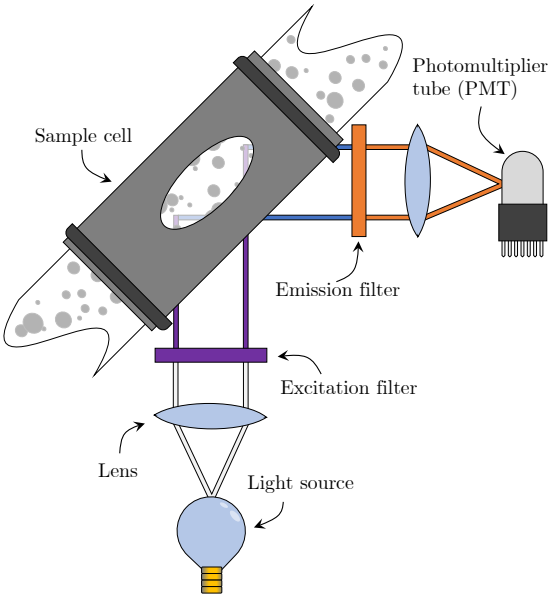

Fig. 1.6: The fluorescence detection structure of the monitor.

Fig. 1.6 illustrates five main components of the fluorescence-based monitor [28]:

- Light source
- Excitation filter
- Sample cell
- Emission filter
- Light detector

Fig. 1.6 shows the working principle of the fluorescence-based monitor for illustration purposes and exact structure and composition of lenses is possibly different [25, 26]. Each component is briefly described in the following paragraphs. Selecting each component depends on the composition of the fluorophore molecule and its fluorescent excitation region; therefore, the components are selected by the manufacturer to detect the type of oil injected into

the experiments.

Light source: The installed near-UV light source emits photons in a wide range of wavelengths. The emitted wavelengths of the light source, published by the Turner Designs [29], is in a range of $\sim(300-400)$nm.

Excitation filter: The excitation filter narrows the range of wavelengths emitted by the light source. Although the specific region of the excitation filter is confidential, it is likely in the range of $(300-400)$nm according to the document published by Turner Designs [30] and the product numbers of instruments used in this work.

Sample cell: Within the sample cell, the water sample is exposed to the transmitted light after the excitation filter, and the sample ideally emits fluorescence light.

Emission filter: The emitted light passes through the emission filter that narrows the range of wavelengths to ensure only the desired wavelengths are transmitted to the light detector. Again, the emission filter's specific region is confidential, but it is likely in the range of $(410-600)$nm.

Light detector: The light detector is a photomultiplier tube (PMT) in the fluorescence-based monitor. The PMT changes the incoming photon into electrons and amplifies the number of electrons. The output signal from the PMT is current pulses. Based on the current pulses, a relation with the concentration of OiW flowing through the sample cell can be established through calibration.

1.1.2 Online Microscopy Analyzers

Continuous online microscopy measurements is a dynamic image analysis method according to International Organization for Standardization (ISO) [31]. This is contrary to the static image analysis method that mostly relates to manual sampling by an optical microscope. Online microscopy utilizes a high-resolution video camera to capture images of the sample stream [2, 16]. These digital images are recorded by a charge-coupled device (CCD) or complementary metal–oxide–semiconductor (CMOS) in the camera converting the readings to a two-dimensional grid of pixels. A photon of light falling on the photodiode of the electronic sensor releases a photoelectron from the silicon photodiode. Pixel-by-pixel, the readout amplifier, converts the photoelectrons into a voltage signal, which is then converted to a digital value. The digital value can then be displayed as a greyscale image on a computer for further analysis [25]. Both online microscopy analyzers used in this work for measuring TSS are similar in their design. An illustration of an online microscopy analyzer is shown in

Fig. 1.7, consisting of a camera, lens, light source, view cell, and a dedicated computer. The computer is installed with a software program that analyzes the images captured by the camera.

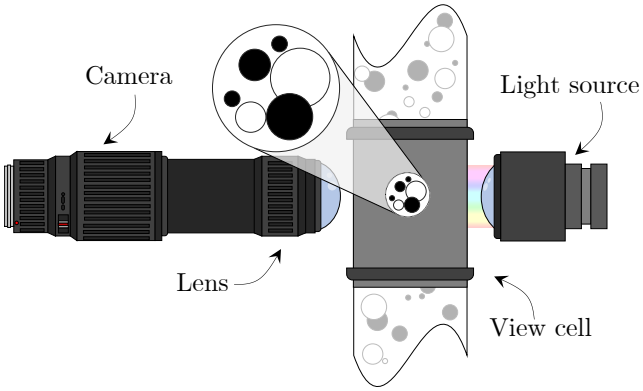

Fig. 1.7: Illustration of a microscopy analyzer's physical parts, consisting of a camera, lens, light source, and a view cell. Figure is the graphical abstract from Paper D.

Both monitors are based on bright field illumination technique, forming a dark image of particles in focus with a bright background. Bacteria can be difficult to capture with a bright field due to being opaque. The specifications of both microscopes are shown in Table 1.1.

Table 1.1: Specifications of the Canty InFlow and Jorin ViPA. Table is from Paper D.

	Jorin ViPA	Canty InFlow
Pixel length	0.375µm/pixel	0.513µm/pixel
Resolution	1292×964 pixels	1920×1200 pixels
Frame rate	∼30fps	∼30fps

In order to measure the different properties of the IW, the IW flows through a view cell where images are captured with ∼30fps for both online microscopy analyzers. The properties of the TSS can then be measured, such as the particle size, projected area, sphericity, aspect ratio, and equivalent volume. Thus, it is even possible to distinguish between particles and classify them, based on their properties. Table 1.2 shows three different images of captured particles in a process.

Table 1.2: Data information obtained from three different images captured in an experiment.

	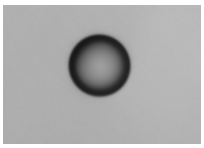	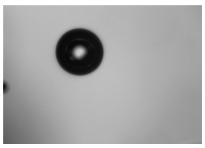	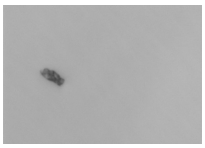
	Oil droplet	**Air bubble**	**Solid particle**
Avg. Feret diameter	72.1616	38.6725	22.9672
Area	4038.1875	1153.9688	291.9375
Perimeter	227.9835	121.8554	75.3347
Aspect ratio	0.9927	0.9975	0.5046
Shape factor	0.9763	0.9766	0.6464
Convexity	1.0102	1.0002	0.9253
Optical density	0.5290	0.7057	0.3195

*Data obtained with Jorin ViPA, based on calibration described in Chapter 4. More property parameters do exist in both microscopy analyzers; this is only a sample of some parameters.

A significant disadvantage of online microscopy analysis is related to the narrow depth of field within the view cell that is captured by the microscopes; thus the measured flow must be a representative homogeneous mixture of the process. An illustration of the narrow depth of field is shown in Fig 1.8.

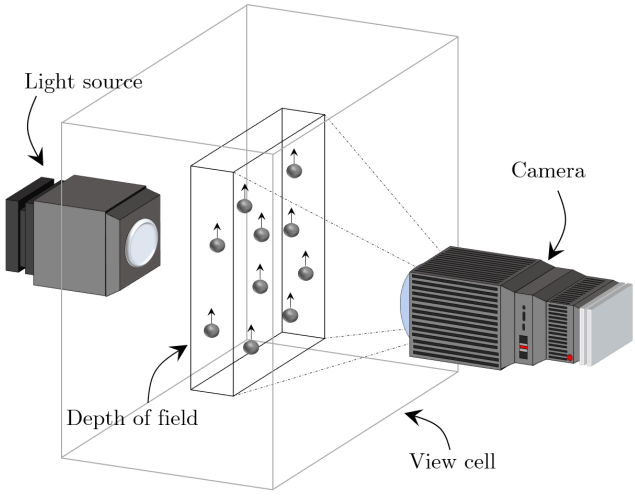

Fig. 1.8: The narrow depth of field within the view cell. Figure is from Paper D.

1.2 Motivation for Online Monitoring

In general, all online quality monitors can presumably be assumed to work well when they are exposed to a known non-hazard environment, and they are properly calibrated (especially by manufacturing personnel) [32–34]. Despite most methods of measuring particles and oil droplets' sizes and concentrations are well-established methods, none has become a standard operation in the oil and gas industry. Although, the Danish Environmental Agency grants every second-year permission of use, discharge, and other disposals of substances and materials, including oil and chemicals in the North Sea, to different ownerships. In the permission, oil and gas companies are obligated to continue logging the OiW concentration by installed online OiW monitors for process optimization [23]. There exist several commercially available monitors for detecting concentrations and sizes of particles and oil droplets, based on different measurement techniques. Some have a broad application focus, where other monitors are designed specifically for the oil and gas industry. Most of the technologies existing today for measuring particle sizes have been developed several decades ago and are commercially distributed by several manufacturers. Therefore, the development of new technologies seems to be scarce, yet the improvement of well-established technologies is still possible. It is also important to realize that the measurement technique is often not the main reason for the error source in the observed results [35]. Merkus [35], Allen [36], and Leschonski [37] all emphasize that the main source of errors are related to sampling and poorly instrument preparation, e.g., improper installment and calibration. The following list highlights multiple issues incountered during the experimental work of this thesis, including calibration and sampling, as mentioned by Merkus, Allen, and Leschonski.

Calibration The procedure of how the instrument must be calibrated should be thoroughly described. Furthermore, some instruments include too much freedom in the calibration procedure, leading to subjective justification in the calibration procedure. Thus, the instrument's measurement is a direct function of the operator's calibration procedure and will change according to operators.

Sampling To minimize the uncertainty related to sampling, the procedure must follow the ISO 3171. The sampling procedure is already integrated at most offshore platforms. Nevertheless, the comparison of samples between online monitors and manual reference samples are not documented.

Cleaning and maintenance An automated cleaning procedure is necessary to reduce inconvenient fouling that can reduce the accuracy of the measurement. It is recommended that the cleaning procedure is fully controllable and have the opportunity to sequential execute the cleaning procedure. The maintenance should comply with the manufacturer's request to limit the non-operational period of the instrument. Even worse, if some parts degrade over time, they must frequently be replaced according to the manufacturer's recommendation; consequently, the accuracy of measurement decreases if calibration is not often executed to compensate for the degradation, e.g., the lumen of lamps.

Measurement and reporting errors Measurement errors can occur due to several reasons: particles differentiate from the measurement range, inadequate selection of size distribution model to represent the true distribution, and human error of reporting incorrectly. The latter case's consequence can occur from manual mistakes of labeling correctly or inadequate presentation of the data to an operator. Other measurement errors can also occur due to the instrument's poor electrical installment, vibration, and electrical created noise from other devices or materials.

Instrument's limitations Operators must have sufficient knowledge of the instrument's limitations. This is especially important at the instrument's installment, when calibrating the instrument, and if abrupt changes occur in measurement data.

Performance specifications Knowing the instrument's performance capability concerning the standard operating procedure will strengthen the instrument's reliability.

Reference method To minimize the uncertainty between the reference method and the instrument, it is recommended that they share the same target and even calls for manufacturers to incorporate a manual sampling procedure in relation to the instrument. The performance specification of the reference method (repeatability and reproducibility) in the entire measurement range should be executed for a fair evaluation of the results measured by the instrument and the reference method. Note, the oil and gas industry in

the North Sea follows the OSPAR reference method using a gas chromatography-flame ionization detector (GC-FID) for measuring OiW concentration. There does not exist any regulation for measuring particle sizes in the oil and gas industry, but it is recommended to follow the related ISO standards.

Documentation The user manual and guidance of the instrument, both hardware and software, should be well documented to help the user obtain knowledge about the instrument most sufficiently.

The dominance of the main source of errors listed above is strongly dependent on the type of particles, material properties, concentrations, particle shapes, size variance, and manufacturer. The sum of all errors may often result in doubtful and misleading measurements at field-installations [33, 38, 39]. Measuring the quality of the PW or IW is not only limited to environmental concerns. Seen from an economic perspective, accurate measurements can also benefit from treatment processes, localization of possible contaminates, decision support (i.e., should the PW be discharged or reinjected?), and process optimization, all of which can extend the reservoirs' economic life.

1.3 Paper Motivation

The thesis is divided into two parts: an extended summary and a part containing the papers. The extended summary covers the background and motivation for the project and ties each paper's contributions together. The second part consists of the contributing Papers A−E. An overview of the contributions in terms of papers and how they relate is shown in Fig. 1.9. The remaining of this section describes the motivation for each of the contributing papers.

1.3.1 Motivation for Paper A [2]

The importance of controlling the water quality of the IW is well known in the oil and gas society to be a direct function of injectivity decline and has since the 1940s been known to affect the injection rate [40, 41]. Depending on whether fracturing is undesirable or not, a relatively low concentration of particles can result in rapid reductions in well injectivity. Numerous studies have referenced different plugging tendencies that can affect the injection rate [42–45]. Few of them described that monitoring the process is extremely important to keep a sufficient water quality, e.g., Patton [46], Bennion et al. [47], and Ogden [34], but none of them addresses the complexity of selecting quality monitors that reliably measure the concentration and/or sizes of suspended solids in the

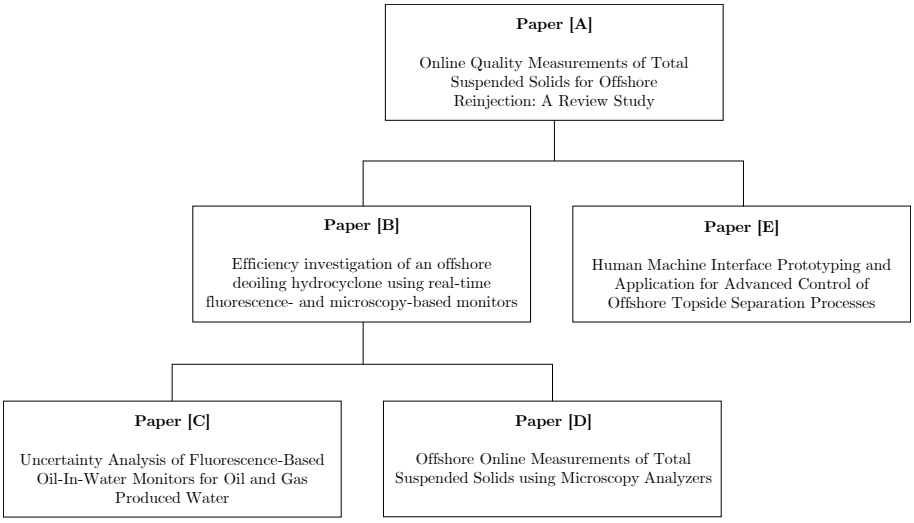

Fig. 1.9: Overview of the enclosed papers.

process. To the author's knowledge, Paper A is the first to extensively address how different water quality issues can add to the suspended solid concentration and which types of monitors are good candidates.

1.3.2 Motivation for Paper B [48] and C [32]

As the general trend towards more sustainable production by reducing oil discharge to the ocean, PWRI has gained increasing attention in the last decade. PWRI has the potential to extend the reservoirs' economic life by minimizing water discharge to comply with national regulations. To increase the PWRI ratio, the injected water quality, including both seawater and PW, must be high and consistent. Effective management of retaining a high and consistent quality involves appropriate treatment and monitoring. Monitoring the OiW concentration of PW can also help protect the receiving environment when PW is discharged. To the author's knowledge, no online monitors have been accepted as a reference method for measuring OiW concentration. For the acceptance of online monitors for measuring OiW concentration, accuracy, and robustness must be high. As UV fluorescence monitors are the most widespread application used for online measurement of OiW concentrations in PW offshore, a well-known fluorescence-based monitor in the oil and gas industry was investigated. Paper B focused on the application for continuously calculating the hydrocyclone's efficiency by measuring the OiW concentration. By maintaining a high separation efficiency before discharge or reinjection, two option occurs: increasing the production or maintaining a lower OiW concentration for ac-

commodating PWRI. In joined cooperation, Bram et al. have reinvestigated the hydrocyclone's performance even further in several papers [49–52]. Paper C aimed to evaluate the reliability of measuring OiW concentrations using an online fluorescence-based OiW monitor. Paper C questions if the calibration method was adequate, the uncertainty related to the sampling procedure, as well as a hypothetical question of how reliable the reference method (OSPAR GC-FID) is. Paper C thoroughly evaluates the calibration method on four identical fluorescence-based OiW monitors by statistical analysis of their uncertainties. This heavily contributes to the extent to which the data from the specific monitor can be trusted and which assumptions must be considered if implementing a fluorescence-based OiW monitor.

1.3.3 Motivation for Paper D [53]

Based on the extensive review study in Paper A, online microscopy analyzers were deemed to be the best candidate to measure sizes and concentrations of suspended solids. Two online microscopes familiar in the oil and gas industry were investigated. As the two online microscopes' calibration procedure is highly based on the perception of what image objects are in focus, the procedure for calibrating the three main parameters must be consistent for reducing the calibration uncertainties. The three main calibration parameters that have been evaluated in Paper D are threshold value (THV), edge strength value (ESV)/focus rejection value (FRV), and depth of field. To evaluate both microscopes' performance to measure concentrations in steady-state and real-time, oil was selected as a verification object as the fluorescence-based monitor investigated in Paper C can benchmark both microscopes' ability to measure concentrations. Paper D thoroughly evaluates both microscopes' ability to measure OiW concentrations both in steady-state and real-time. Paper D concluded to what extent online microscopy analyzers can be used for measuring TSS sizes and concentrations accurately, and which reservation must be taken if implementing an online microscopy analyzer for measuring TSS. Furthermore, the estimated particle size distribution (PSD) that is presented to the operator must be a sufficient statistically representation of the true PSD and the uncertainty of the estimated PSD must be kept within a predefined bound. Paper D investigated the minimum number of counted particles to present an adequate PSD within a defined confidence interval and the amount of relative error that is allowed.

1.3.4 Motivation for Paper E [54]

Based on the number of output properties withdrawn from the different online quality monitors, the complexity of displaying the data for an operator comprehensively increases. This will especially be the case for microscopy analyzers as

several properties can be displayed, and each type of particle can be classified. Even if online quality monitors only outputs one value, other additional information could be valuable to be displayed, such as an uncertainty interval from the monitor, if that will help the acceptance of OiW monitors as mentioned in Paper C. Paper E presents a solution to incorporate the graphical design of measured properties most conveniently to an operator, seen from a developer point of view. A connection between Simulink Real-Time and ABB human machine interface (HMI) software via an open platform communications (OPC) server has been established, sending and receiving information. By doing so, new solutions from, e.g., the academic society, can be presented in a familiar environment to industrial partners. That is particularly useful, as it will reduce the concerns related to the solution development in an academic used software, which may not be applicable in a programmable logic controller (PLC) system nor be representable in an HMI software. To demonstrate the established connection's usefulness, a case study was carried out to visualize a developed model predictive control (MPC) solution's behavior. The MPC solution used as a case study is thoroughly described by Hansen et al. [55]; thus, at no given time was the underlying control theory discussed in Paper E.

Chapter 2

State of the Art of Online TSS Monitoring

In this section, the review article (Paper A) is summarized, covering the main challenges associated with measuring the water quality related to TSS. This section is divided into two parts: Sec. 2.1; injection water characteristics and formation damage mechanisms, and Sec. 2.2; selection of online monitoring for measuring TSS.

2.1 Injection Water Characteristics and Formation Damage Mechanisms

IW has been known for several decades to be a solution to increase the cost recovery ratio [40, 41, 56–60]. The main reason for injecting water into the reservoir is to maintain the reservoir pressure, which naturally drives the production. The second reason is to sweep the reservoir. A common well pattern consists of four injection wells surrounding a production well, forming a five-spot pattern to displace the oil occupied in the pores of the underground porous media toward the production well. If necessary, other patterns can be selected to increase the injection rate, such as a seven-point or nine-point pattern. The IW quality was already observed in the early 1940s to affect the recovery process significantly [2, 40, 41]. Water quality of IW is typically referred to in terms of suspended solids as these directly affects the production of oil from the reservoir [42, 46]. This renders the IW quality problem to be a weighting of net present value, where low operational expenditure (OPEX) must be weighted against longer and more sustainable production. Ideally, the IW should be non-scaling and free of suspended solids and organic matter; thus, the injectivity rate is maintained without any degradation in the reservoirs'

operational lifetime. The IWT process should be protected against corrosion, erosion, and microbiological growth [61]. The pursuit of achieving perfectly clean IW is expensive, to such a degree that operation will seize to be profitable. The geological formation and geographical location of the reservoir are the two factors that determine the physical, chemical, and biological properties of the oilfield [62]. Balancing between the IW quality and the economically profitable estimation of the reservoir lifetime is highly dependent on location and formation. For operators to maintain an adequate IW quality for the specific formation, they must have confidence in the measured data [34, 54, 63]. Even though off-line sampling is often necessary to apply with the reference method, the response time of off-line sampling is long and it can be challenging to maintain a consistent quality during operation. Online installations of proper and reliable monitors will increase the awareness in cases were the process deviates from normal operation behavior within a short period of time compared to off-line samplings [42]. In Paper A, the concerns of measuring the water quality related to TSS were investigated on an IWT facility illustrated in Fig. 2.1.

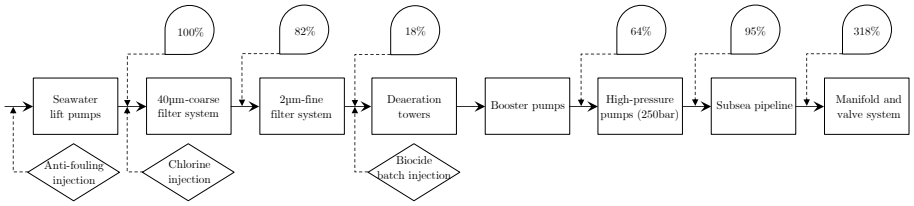

Fig. 2.1: The block diagram illustrating a IWT facility located in the Danish sector of the North Sea. Each percentage represents the TSS concentration measured manually at different locations on the IWT facility. The exact concentrations are confidential. Figure is from Paper A.

As a benchmark, the results that were manually measured from an IWT facility located in the Danish sector of the North Sea raised the importance of investigating IW's characteristics and what type of online monitoring will be most helpful to improve the IW quality. Photos from the manual experiment following Danish Standard (DS) 207 and the results are shown in Fig. 2.2.

With nearly a seventeenfold increment of the TSS concentration mean after the fine filter system to after the subsea transportation pipeline, indicating the addition of TSS such as scales, corrosion deposits, and microbial grows; assuming the filtration systems works as intended. This also concludes that the instrument that measure the particle size distribution should be able to measure within an overall TSS concentration from >30.5mg/L ($\mu + 2\sigma$) to ∼0mg/L. As TSS are added within the process, it is difficult to conclude the particles' actual sizes based on the TSS concentration results.

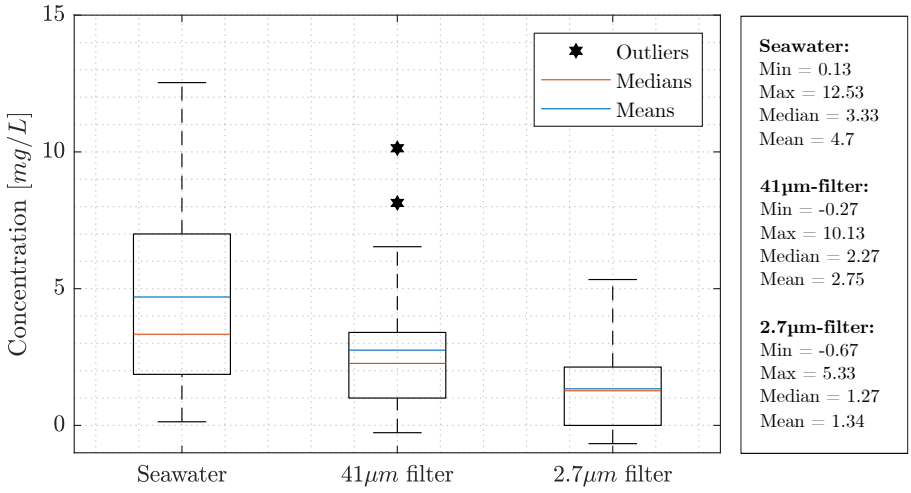

(a)

(b)

Fig. 2.2: Results and photos of the manual experiment of measuring TSS concentration: (**a**) box plot representation of between each filtration: unfiltered seawater, 41µm-filter, and 2.7µm-filter. Figure is from Paper A; (**b**) photos of the DS 207 experimental execution of the IW from the benchmarked IWT facility.

For determining the different influences of the IW quality, a block diagram is illustrated in Fig. 2.3, followed by a description for each of the IW's characteristics and their formation damage mechanisms.

Other important properties of water are the effects of temperature, acidity, and salinity. The main IW quality characteristics, listed in Fig. 2.3, are summarized in the following list in relation to suspended solids:

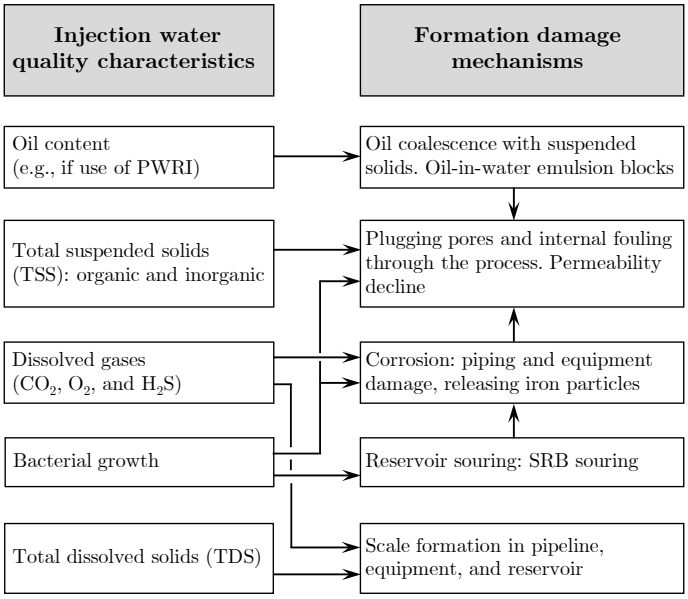

Fig. 2.3: The block diagram illustrates how main IW quality characteristics can negatively effect the injection rate, IWT process, and formation. Figure is from Paper A.

Total suspended solids: The definition of TSS and total dissolved solids (TDS) must be established. There is a general confusion of the definition, as TSS and TDS's definitions are by Baird et al. [64] discriminated by a 2µm filter. The confusion is easily observed in Table 2.1. In the thesis, TSS is defined as anything in the water that can be trapped by a filter, making the definition filter size-dependent [65]. TDS then becomes anything, other than the carrying phase fluid, that passes the selected filter.

Table 2.1: Different definitions of TSS and TDS. Table is from Paper A.

Definitions of TSS and TDS used in different studies	**Source**
TDS defined as materials that are soluble in water	[16, 34, 66]
TDS defined as materials that passes through a 2µm-filter	[67, 68]
TDS is indirectly defined as materials that are soluble in water	[69–71]
TDS is indirectly defined as materials that passes through a 2µm-filter	[42, 59, 72, 73]
Undefined or too uncertain to tell	[45, 47, 62, 74]

Oil content: Historically, mostly seawater has been used as IW, but due to the increasing environmental awareness, the discharge policies may require PWRI to reduce the discharge of crude oil even further. Especially, as described in Sec. 1.1, the former Mærsk Oil discharged 96% of allowable oil to the ocean in 2017/2018. The increasing attention to PWRI and the presence of oil must be considered when evaluating the IW quality. The presence of crude oil can affect the IWT process and the reservoir in direct and indirect ways such as agglomeration-effect of oil with other matters, asphaltenes deposits, and emulsion blocks [46].

Total dissolved solids: IW with high concentrations of dissolved solids is the foundation of scales in pipelines and instruments. If scales deposit in the process, several issues can occur; it can decrease the injectivity, and more severely completely plug parts of the process. The scales can also deposit into the treatment train, thus, increasing the TSS concentration after the filtration system. Scales often occur when PW and seawater mixes, as seawater can contain significant concentration of sulfate (SO_4^{2-}) and carbonate (CO_3^{2-}), while PW or formation water contains calcium (Ca^{2+}), barium (Ba^{2+}), and strontium (Sr^{2+}) [75].

Dissolved gases: The presence of dissolved gases do not add to the TSS concentration. Similar to TDS, dissolved gases affect the TSS concentration indirectly by promoting an electrochemical reaction between steel and the contacting aqueous phase, creating a corrosive environment that eventually facilitates corrosion deposits that adds to the TSS [34, 76]. The high concentrations of dissolved gases are the main source of corrosion together with growth aerobic organisms that play a role in microbially influenced corrosion (MIC) [77, 78]. The most common dissolved gases that causes corrosion are O_2, CO_2 (sweet), and H_2S (sour) [77, 79, 80]. The presence of O_2 is the most corrosive gas of these three, that is capable of causing serious damage well below concentrations of 1ppm [77, 81–83].

Bacterial growth: When discussing negative influence of microorganisms in IWT processes it is often referred to as MIC, that accelerate the corrosion inside the process, which indirectly adds to the TSS concentration through corrosion deposits. The presence of biofilm and microorganisms above a certain size can also contribute to the TSS concentration directly by physically plugging pores or by bridging. The development of biofilm is shown in Fig. 2.4. Another side-effect of microorganisms in the process is biofouling, which can physically block parts of the process, especially in the filtration system. How much of the corrosion in a process is related to MIC can be challenging to measure, but studies predict that MIC accounts for (20−30)% in the oil and gas industry, and some studies even predict around 50% [78, 84–86].

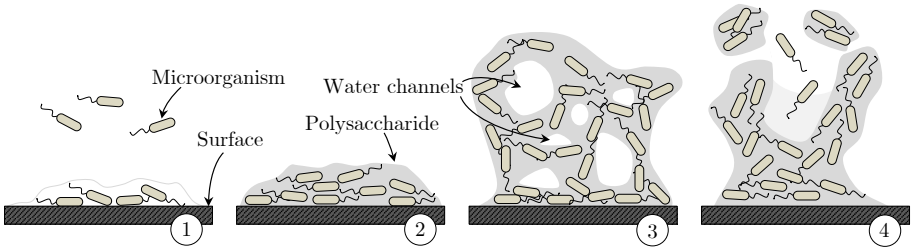

Fig. 2.4: The illustration shows four development stages of biofilm: ① adhering of free floating biofilm producing bacteria to surfaces in the process. ② colonization inside EPS. ③ biofilm is produced and the *in-situ* ecosystem is nourished by water channels to grow [87]. ④ The biofilm reaches critical environmental factors and which the biofilm detaches from the colony. Figure is from Paper A.

2.2 Online Monitoring of Total Suspended Solids

There exist several methods to estimate the concentration and size distribution of both OiW and TSS related to the oil and gas industry. Different measurement techniques have been developed to fulfill the task: ultrasonic spectroscopy, electrical sensing zone, light scattering, light obscuration, and microscopy analysis. Despite the long history of implementing quality monitors for measuring particle sizes, there is no consensus as to which method provides the most reliable estimate, leaving petroleum engineers with a bewildering array of choices [74]. Through a the discrimination process, Paper A concluded that microscopy has the highest potential for measuring particle sizes. The selection was based on two parts:

1. A rough selection based on different measurement techniques, defined by ISO standards, related to measuring particle sizes suspended in a liquid. Table 2.2 highlights if the different measurement techniques apply to on-/in-line installment and their overall size ranges.

2. The second selection was based on the measurement techniques in general pros and cons, without drawing any conclusion on specific manufacturers' equipment.

Two decisive factors favorise microscopy analyzers compared to other online monitors for measuring TSS. As the sample of particles in an IWT process can consist of a wide variety of different matters and diverse sizes, most other methods are challenged by the assumption that even though a size distribution can be obtained fast, the highly sophisticated methods for measuring particles presume perfectly spherical, and the influence of particles' shapes are not taken into account [37]. Many of the other methods are still suitable for measuring particle sizes when the particles of interest are dominant in the process,

Table 2.2: Particle size analysis methods presented in ISO standards. Table is from Paper A.

Particle size analysis' methods	ISO standard(s)	Overall size range [µm]	On-/in-line capable
Sieving	2591-1 3310-1 to -3 20977	$5 - 125$*	✗
Gravitational sedimentation	13317-1 to -4	$0.5 - 100$	✗
Centrifugal sedimentation	13318-1 to -3	$0.1 - 5$	✗
Electrical sensing zone	13319	$0.4 - 1,200$	✓
Laser diffraction	13320	$0.1 - 3,000$	✓
Image analysis methods	13322-1 to -2	$(0.25)1 - 500$*	✓
Small-angle X-ray scattering	17867	$0.001 - 0.14$	✗(✓)
Scanning electron microscopy	19749**	$40.01 - 500$*	✗
Ultrasonic attenuation spectroscopy	20998	$0.01 - 3,000$	✓
Transmission electron microscopy	21363**	$0.001 - 5$*	✗
Light obscuration	21501-3	$1 - 100$	✓
Dynamic light scattering	22412	$0.02 - 3$* $(\ll 10)$	✓

* No typical size range was given within the ISO standards, found according to Merkus [35].

** ISO standard under development.

such as crude oil after the treatment process at the topside production process offshore. Even though microscopy can provide more single-particle properties than most of other methods, microscopy is only more valuable if additional information such as shapes and classification is applied. I.e., an equivalent diameter obtained from microscopy is particularly not more informative than other methods. The second noteworthy advantage of microscopy analysis over other methods is the ability to discriminate captured suspended solids manually. The manual justification is useful for improving the classification procedure and for evaluating the captured images.

Table 2.3 presents a non-exhaustive list of five different microscopy analyzers published in Paper A. Table 2.3 provides a comparative overview of the different microscopy analyzers based on their design and options available. The assortment of microscopy analyzers is based on their diversity in:

- View
- Classification options
- Connection
- Detection range
- Familiarity

The software process performance and ability to acquire samples by each manufacturer cannot be evaluated without any hands-on experience with each equipment, which has not been covered in Paper A. Alternatively, a brief description

Table 2.3: Comparison of five different microscopy analyzers. Table is from Paper A.

Manufacturer Instrument name	**Jorin** ViPA	**J.M. Canty** InFlow	**Grundfos** Bacmon	**ParticleTech** oCelloScope	**SOPAT** MM2, Ma
Familiar with the oil and gas industry	✓	✓	✗	✗	(✓)*
Distinguish between solids, droplets, and bubbles	✓	✓	(✓)	(✓)	✓
Categorize different solid types	✓	✓	✓	✓	✓
Distinguish bacteria and abiotic particles	✗	✗	✓	✓	✗
Training classification (neural network, machine learning)	✗	✓	✓	✗	✗
View	2D	2D	3D	3D	2D
Connection	At-line/on-line	At-line/on-line/(in-line)	At-line/on-line	At-line	In-line
Measurement range [µm]	<150**	$0.7 - 480$	0.6<**	$0.5 - 2000$	$0.5 - 90$, $1.5 - 280$
Pressure range [bar]	<120	<689	$2 - 10$	–	$0.01 - 3$, $0.01 - 320$
Temperature range [°C]	<120	–	$5 - 40$	$20 - 40$ (operation temp.)	$0 - 50$
Flow velocity [m/s]	$0.03 - 2.1$ $(0.05 - 4)$L/min	$0.25 - 2.74$	Batch operation, 10min cycle	Batch operation, 10min cycle	–
Frame rate [Hz]	30	30	–	–	15
Cleaning procedure	Manually with flexible stick	Automatically vapor removal system	Flushed between each batch cycle for 1min	Flushed between each batch	Automatically liquid cleaner (Ceramat Sensor Lock-Gate)
ATEX approved	✓	✓	✗	✗	✗, ✓

*Applied at a testing facility related to upstream oil-water separation process. However, to the authors knowledge it has not been installed at a fully integrated upstream separation process.
**Minimum or maximum measurement range is not explicitly defined.

of each microscope's limitations and advantages based on the manufacturer's specifications has been evaluated. By incorporating the advantages from each of the five different microscopy analyzers, such as automatic cleaning procedures, machine learning classification procedures, 3D image analysis, and manually defined particle classes by colors after the analysis, microscopy analyzers can further be improved. Furthermore, a microscopy analyzer system can always benefit from higher resolution, better software design, and more detailed user manuals [2].

Similar to TSS monitors, there are many different techniques and manufacturers for measuring OiW concentrations and droplet sizes; however, a review of those has not been published in Paper A. Several other studies have focused on OiW monitors, with UV fluorescence being the most widespread technique for online measurement of oil in PW [16, 33, 88, 89].

2.3 Conclusion

Water analysis in the oil and gas industry can yield highly informative analytical information to an operator. The analysis can assist in identifying the

quality of production, when contamination appears in parts of the production zone when there is an increasing tendency for corrosion and scale deposition, and for evaluating process design changes. However, for water analysis to be useful, the water analysis must be representatively sampled, and the sample must be withdrawn, analyzed, and interpreted correctly.

This chapter investigated different water quality problems related to TSS that can affect the injectivity rate and the system. As manual water analysis is a time-consuming process, which translates to a slow reaction time, where critical process deviations are observed too late, resulting in process failures. To investigate this, several techniques were evaluated for measuring TSS. Where through a discrimination process based on results in several studies, the author strongly believes measuring different TSS properties with microscopy will bring the most promising results compared to other techniques. Even as several online microscopy analyzers exist on the market, the instrumental design and software design must still further be improved. However, microscopy analyzers' ability to perform shape analysis is the prerequisite for closing the link between the assumption of particles being spherical and the practical results obtained.

Chapter 3

Online Monitoring of Oil-in-Water Concentration

With UV fluorescence as the most widespread application used for measuring the OiW concentration in PW offshore, an investigation of the instrument's reliability was investigated in Paper C. The uncertainty related to the reference method was questioned to have a negative impact on the acceptance of online monitors, moreover the sampling procedure. Four fluorescence-based monitors (Turner TD4100-XDC) was statistically investigated by examining their calibration method, their robustness to different interferences, and their reproducibility between each other. However, the OiW concentrations were not validated according to the reference method (OSPAR GC-FID) in Paper C. Unlike Paper C, Paper B is a typical example of using quality monitors prior to evaluating their performance. Paper B investigates the efficiency of offshore deoiling hydrocyclone in the pilot-plant facility.

The pilot-plant used in both papers is shown in Fig. 3.1, however smaller standalone systems have also been constructed to execute the experiments in Paper C. The pilot-plant has, in the past, been used for other studies to test and develop new control algorithms, validating the separation efficiency of different treatment methods, fault detection and diagnosis, and evaluating the performance of various instruments [52, 55, 90–93].

A piping and instrumentation diagram (P&ID) of the pilot-plant facility is shown in Fig. 3.2, where only the support and hydrocyclone subsystems were used in the experiment executed in Paper B and C.

Fig. 3.1: Photos of the pilot-plant. Left: the pilot-plant; top middle: two of the three online monitor types on a movable skid; bottom middle: the Matlab Simulink Real-Time interface of the pilot-plant; top right: example of the OiW mixture in the buffer tank; bottom right: barrel of the Midland non-detergent Society of Automotive Engineers (SAE) 30 oil used.

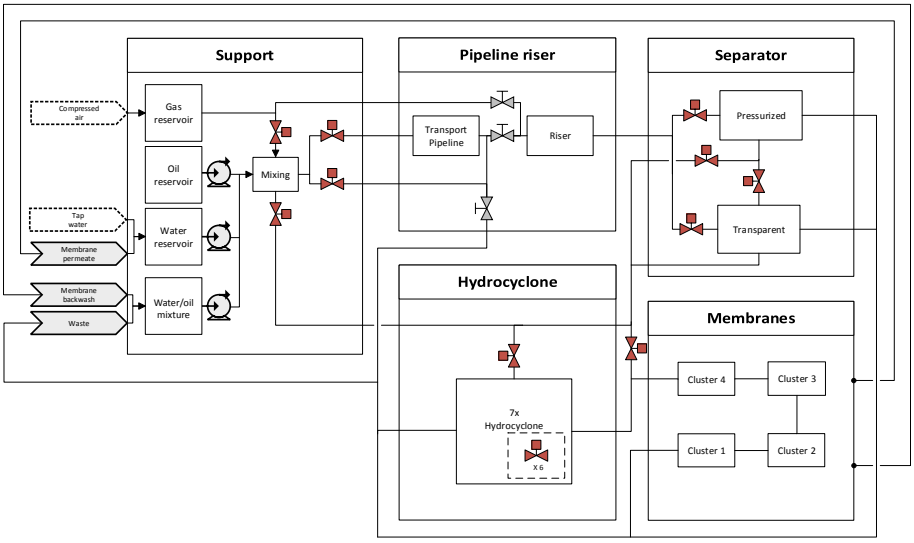

Fig. 3.2: A complete overview of pilot-plant bypass structure at Aalborg University located on Esbjerg campus. Figure is from Paper C.

3.1 Applying Online Oil-in-Water Monitors

With the increasing attention to reducing ocean discharge of oil, obtaining an accurate OiW concentration online is valuable in the pursuit to continuously measure discharged PW. The main priority of online OiW monitors' installment is to fulfill the governmental requirement of oil discharge. Secondly, reliable OiW monitors can be installed at unmanned installations, where currently only one sample set is collected during each planned visit [94]. Another advantage of proper installed OiW monitors is the requirement for new state-of-the-art control solutions and integrated models, published in several studies, that could economically increase the production [52, 92, 95]. However, as discharge regulations are clearly defined, the operation is up to the producers' economic strategy.

On the basis of Paper B, including OiW monitors, it will be beneficial for innovative solutions for increasing the separation process with the use of measured OiW concentration as a feedback signal for control. As hydrocyclones are commonly used as the last separation stage before discharging, it is a natural area to strive for the highest separation efficiency without sacrificing the production rate. Hydrocyclones utilize rotating flow to expose the fluid to large centripetal forces in order to enhance the separation process by forcing the water to the cyclone wall, and the lighter oil will migrate towards the center [49, 96, 97]. The hydrocyclone's separation principle is illustrated in Fig. 3.3.

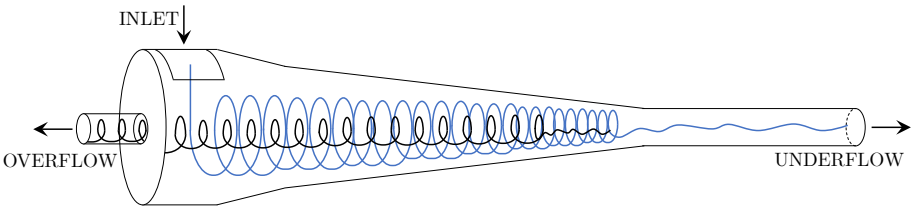

Fig. 3.3: Illustration of an offshore deoiling hydrocyclone consisting of a single liner. Figure is modified from Paper B.

The performance of current offshore hydrocyclones is indirectly controlled by maintaining a pressure different ratios (PDR) [97, 98]. Thus, direct efficiency control for deoiling hydrocyclones will be achievable with OiW monitors' installment before and after the hydrocyclone. Bram et al. [52] have published an extensive joined work on control-oriented modeling for the deoiling hydrocyclone system using OiW monitors for model validation.

3.2 Calibration of Multiple Identical Fluorescence-Based Monitors

Calibration is the process of comparing the measured value from an instrument with a known value. It is highly essential to calibrate the instrument to ensure the measurements have good accuracy. The installation's environment will affect the measuring device; it may be necessary to take precautions if the instrument is highly sensitive to changes, such as harsh environments, vibration, temperature, pressure, and flow. The calibration published in Paper B follows the guideline documented by the manufacturer, as shown in Fig. 3.4, where at least two samples must be taken [28].

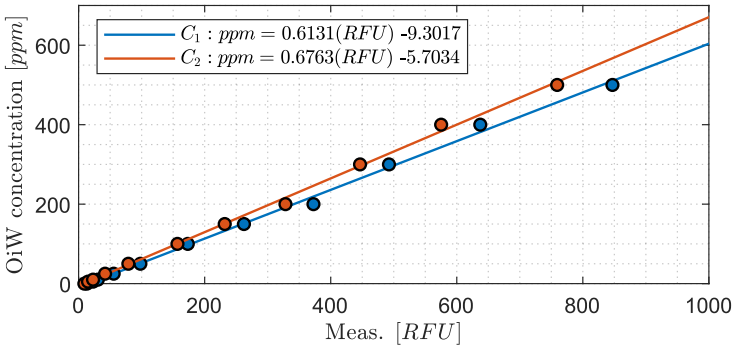

Fig. 3.4: Ordinary least square calibration regression based on eleven measured RFU values for both fluorescence-based monitors. Figure is modified from Paper B.

Multiple points are necessary to verify whether the relation follows a linear or nonlinear trend. For both calibration in Paper B and C, the relationship between measured RFU and injected OiW concentration follows a linear trend. The calibration procedure in Paper B was executed on two identical fluorescence-based monitors within a calibration range of $(0-500)$ppm, and in Paper C the calibration range is $(0-300)$ppm, as shown in Fig. 3.5. However, below 10% of the entire RFU range was only covered, which may have challenged the instrument's sensitivity in Paper B. For Paper C, 400ppm was chosen as the highest value of interest by adjusting the instrument's sensitivity. 400ppm were selected as the OiW concentration before entering the deoiling hydrocylone based on different studies [99, 100].

In Paper B, the default calibration procedure documented by the manufacturer uses ordinary least square (OLS) regression to fit the measured RFU value with the injected OiW concentration; thus, a homoscedastic random error must be assumed. Paper C investigated whether OLS regression is the most optimal calibration procedure. The results using OLS and weighted least

square (WLS) was compared in Fig. 3.5, based on the same 70 sample points for each of the four identical monitors at the following OiW concentrations: $(0, 10, 20, 50, 100, 150, 300)$ppm, ten samples for each concentration.

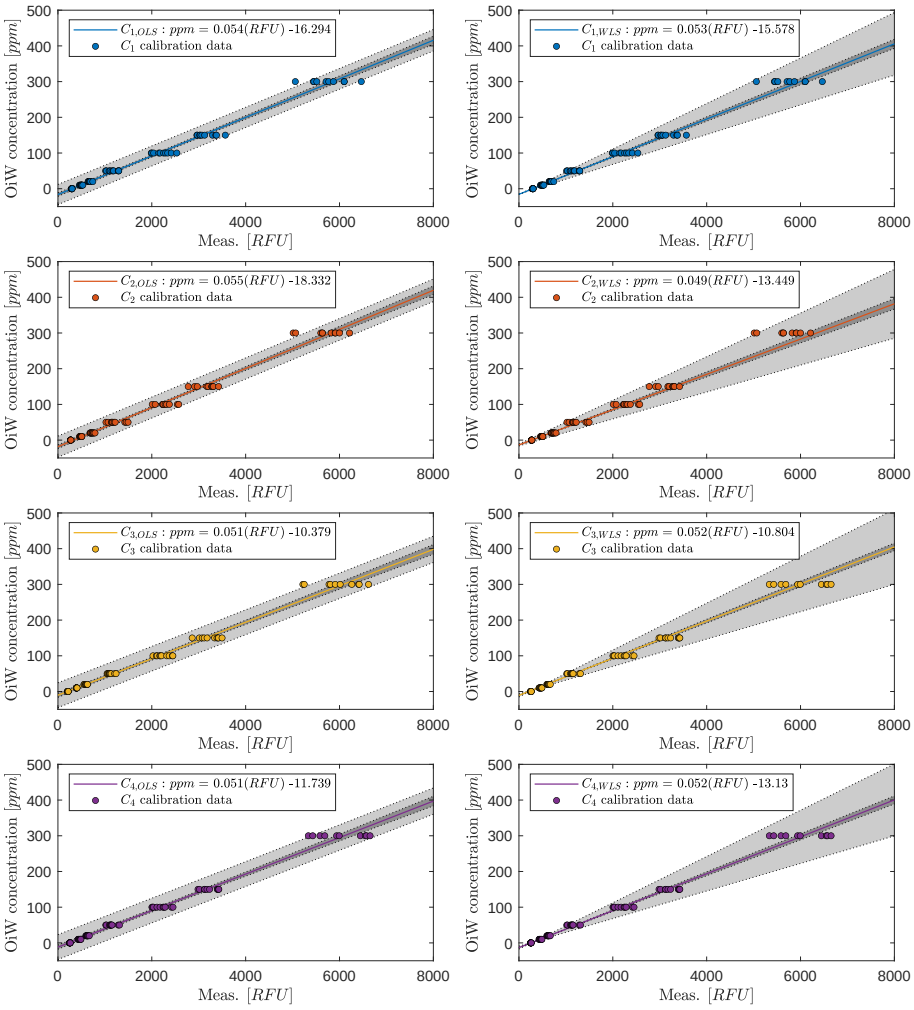

Fig. 3.5: Two different least square regression procedures for each of the four OiW monitors. Left column: linear regressions using OLS; right column: linear regressions using WLS. Figure is from Paper B.

Due to fairness, the procedure presented by the manufacturer and shown in Fig. 3.4 was not executed for OLS. Even though the weighting factor (w_i) for $i = 0, 1, 2..., n$ does not affect the regression result using OLS, including the number of samples (n) will still positively affect the calibration procedure. The

most significant disadvantage of WLS is determining the w_i, as w_i is unknown. Using the reciprocal of the variance (σ^{-2}) for each calibration concentration is a reasonable candidate of w_i.

Fig. 3.5 is mathematically presented in equations: (3.1)−(3.13). A more detailed description of the equations can be found in Paper C, where

$$y = ax + b, \tag{3.1}$$

$$b = \frac{SS_{xy}}{SS_{xx}}, \tag{3.2}$$

and

$$a = \overline{y} - b\overline{x}. \tag{3.3}$$

a and b are the slope and the intercept on the ordinate axis, respectively. SS_{xx} and SS_{xy} are the weighted sum of squares and the weighted sum of cross-products, respectively, and $\overline{x}$ and $\overline{y}$ are the arithmetic weighted means. To calculate the prediction interval (PI) and confidence interval (CI), the following equations are used:

$$\overline{x} = \frac{\sum_{i=1}^{n} w_i x_i}{\sum_{i=1}^{n} w_i}, \tag{3.4}$$

$$\overline{y} = \frac{\sum_{i=1}^{n} w_i y_i}{\sum_{i=1}^{n} w_i}, \tag{3.5}$$

$$SS_{xx} = \sum_{i=1}^{n} w_i (x_i - \overline{x})^2, \tag{3.6}$$

$$SS_{xy} = \sum_{i=1}^{n} w_i (x_i - \overline{x})(y_i - \overline{y}), \tag{3.7}$$

$$SSE = \sum_{i=1}^{n} w_i (y_i - \hat{y})^2, \tag{3.8}$$

$$\hat{s} = \sqrt{\frac{SSE}{DOF}}, \tag{3.9}$$

$$CI = ax_0 + b \pm t_{0.025}\hat{s}\sqrt{\frac{1}{n} + \frac{(x_0 - \overline{x})^2}{SS_{xx}}}, \tag{3.10}$$

and

$$PI = ax_0 + b \pm t_{0.025}\hat{s}\sqrt{\frac{1}{w_0} + \frac{1}{n} + \frac{(x_0 - \overline{x})^2}{SS_{xx}}}. \tag{3.11}$$

SSE is the sum of squared errors, $\hat{s}$ is the predicted sample standard deviation, DOF is the degrees of freedom, and $t_{0.025}$ is the t-score with two-tailed 95%

confidence. The only difference between OLS and WLS is w_i. For OLS and WLS, $w_i = 1$ and $w_i = s_i^{-2}$, respectively. The notation "$\hat{}$" denotes predicted value and the subscript "$_0$" denotes the set of observations. As the true variance of the calibration region is unknown, w_0 is estimated based on the predicted variance function:

$$s(\hat{y}) = c_1\hat{y} + c_0 \tag{3.12}$$

and

$$w_0 = s^{-2}(\hat{y}), \tag{3.13}$$

where c_0 and c_1 are obtained from least square method on known sample standard deviation (s_i) in $y_i = (0, 10, 20, 50, 100, 150, 300)$ppm. Eq. (3.12) may only be a suboptimal representation of the variance function for the OiW monitor, alternative candidates to represent the variance function are published by Noblitt et al. [101]. Whether WLS is a better calibration procedure than OLS is evaluated based on the experimental results in Fig. 3.6. The evaluation is executed on the same 100min experiment with addition of oil in steps starting at 0ppm: (5, 10, 20, 40, 80, 160, 320, 400)ppm.

The deviation between the OiW monitors calibrated using WLS was in every OiW concentration smaller compared to calibration with OLS, as shown in Table 3.1 and observed in Fig. 3.6. This is especially evident at low OiW concentrations where the deviation of WLS is two to three times smaller than with OLS. Whereas, at higher OiW concentrations, the deviation between both methods is low. This tendency agrees with the theory that a linear unweighted regression tends to fit points at the upper calibration levels compared to lower calibration levels due to the square errors measured in absolute values.

Table 3.1: Data results from the experiment shown in Fig. 3.6. Table is from Paper C.

X_{pred} [ppm]	Biggest div. between $\overline{C}_1$, $\overline{C}_2$, $\overline{C}_3$, $\overline{C}_4$ with OLS [ppm]	Biggest div. between $\overline{C}_1$, $\overline{C}_2$, $\overline{C}_3$, $\overline{C}_4$ with WLS [ppm]	Biggest div. from $\overline{C}_{OLS}$ [ppm]	Biggest div. from $\overline{C}_{OLS}$ [%]	Biggest div. from $\overline{C}_{WLS}$ [ppm]	Biggest div. from $\overline{C}_{WLS}$ [%]
0	4.34	1.56	2.30	–	0.86	–
5	3.43	1.54	1.95	35.1	0.82	13.8
10	2.55	1.70	1.64	15.8	1.00	9.4
20	2.26	1.54	1.50	8.0	0.82	4.4
40	3.31	2.10	1.86	5.0	1.08	3.0
80	7.55	5.33	4.76	6.5	2.85	4.0
160	17.42	13.46	11.21	7.5	7.64	5.3
320	36.41	33.88	24.75	7.8	21.42	6.9
400	55.14	52.91	34.46	8.3	33.83	8.4

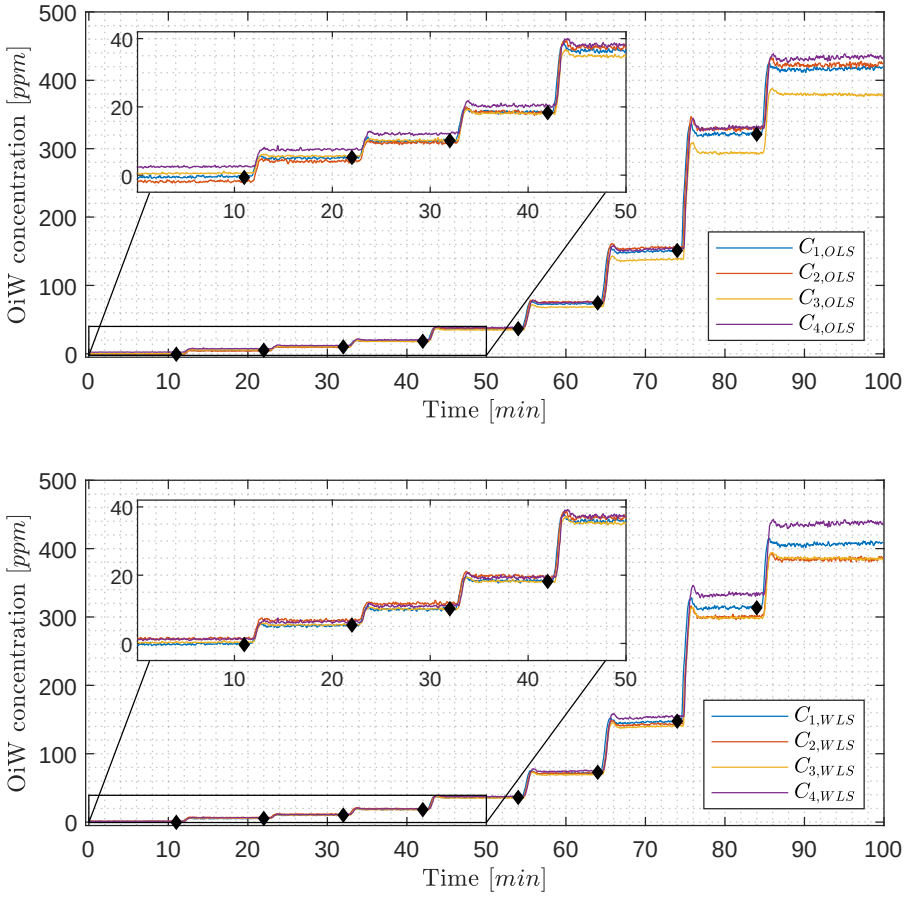

Fig. 3.6: Eight times oil was added with the intention to achieve the OiW concentrations: $(5, 10, 20, 40, 80, 160, 320, 400)$ppm starting at 0ppm, during the 100min experiment. The black diamonds mark when each different OiW concentrations were added. The top located plot shows the results using OLS as calibration procedure, and the bottom located plot shows the results using WLS as calibration procedure. Figure is modified from Paper C.

3.3 Uncertainties

Uncertainties will always be present in measurement results; however, the uncertainty sources' influences vary greatly depending on the procedure, instrument, and environment. The magnitudes of the deviations caused by uncertainty sources are usually unknown and can thus only be estimated. In this section, different uncertainties related to measuring OiW concentration with fluorescence-based monitors are addressed. The combined uncertainty using

the GC-FID reference method, with a 95% confidence interval, can be calculated based on data presented in ISO 9377-2 [102], without introducing the uncertainty related to sampling from the production target. Based on the data, between $127 - 156$ number of results were obtained in $35 - 41$ laboratories on four different OiW concentrations ranging between $(0.57 - 3.61)$mg/L. If assuming the oil producers use the same laboratory and personal, and the uncertainties of the reference method are scalable in the entire range of interest, then the uncertainty by the reference method lies within:

$$OiW_{repeat.} = x \pm (5.9 - 27.6)\%, k = 1.96, norm, \tag{3.14}$$

where k is the coverage factor assuming the uncertainty is normally distributed. The uncertainty increase if different laboratories and personal are used to measure the OiW concentration obtained:

$$OiW_{reprod.} = x \pm (18.8 - 79.4)\%, k = 1.96, norm \tag{3.15}$$

The data from ISO 9377-2 and the calculation of the uncertainties are described in Paper C. Even though the reproducibility value may not be constant in the entire range of interest, the reproducibility value certainly includes noteworthy uncertainties that should be addressed to promote the industrial use of online OiW monitors by quantifying the trustworthiness of the measurements.

3.3.1 Sampling

By recapitulating the reference method's previous conditions, the uncertainties related to extracting a representative sample, transportation, and storage of heterogeneous oily PW were not addressed. Uncertainties related to sampling are often dominant and occasionally may exceed 90% of the total measurement uncertainty [103]. Another study by Lava et al. [104] states that the sampling uncertainty may influence 75% of the total variance of measurement uncertainty [104]. However, estimating the uncertainty related to sampling can be challenging, but the uncertainty associated with the sampling process must inevitably contribute to the total uncertainty of the measured OiW concentration [103]. A great deal of minimizing of sampling uncertainty has been done by standardizing the sampling procedure in ISO 3171 [105], whereas storage and transportation of the sampling should follow the ISO 9377-2 [102] and ISO 5667-3 [106]. To give a certain understanding of where different uncertainty sources can occur from in the standards for PW, a list of different procedures that must be fulfilled before an analysis can can be executed onshore:

- The sample should be taken from rising flow in a vertical pipe section, with an isokinetic center lined pitot, in a fully developed turbulent region.

- The distance between the intake opening of the sampling pitot tube and the sampling end-point to where the sample is bottled should be as short as possible to avoid dead volume in the sampling system.
- PW must be flushed through the sampling end-point at least three times to ensure potential residing residue replacement from prior measurements.
- The sample should be preserved by acidifying it to a low pH (pH<2) to kill bacteria that can degrade the oil if the sample cannot be analyzed immediately.
- The sample must be bottled and stored in the absence of light and cooled to $(4-8)$°C, to avoid the growth of bacteria, but also to directly avoid the possibility of degradation of petroleum components by photochemical reaction [106, 107].

If the last two bullet points about storage and transportation are disregarded, the uncertainty related to sampling between the manual GC-FID reference method and an online OiW monitor can be reduced greatly if the same sample is measured by sharing target at the exact same time.

3.3.2 Influencing Properties Related to the Fluorescence-Based Monitors

Two different influencing properties were investigated in Paper C: the presence of gas bubbles and flow rate changes. Other known influencing properties from the literature that can affect fluorescence-based monitors are:

- The ratio between aromatic and aliphatic hydrocarbons.
- Inner filter effects.
- Chemical quenchers.
- Degradation of physical parts over time.

Some of the influences have been discussed in Paper C.

Gas bubbles' influence on an OiW monitor: The presence of air bubbles is known from several studies to influence the measurement results of many quality monitors [33, 108–112]. The same was suspected of the fluorescence-based monitors in Paper C, as a false high measurement was observed when visible air bubbles were apparent in the buffer tank in the start-up of each experiment and slowly converged as air bubbles slowly dissipated to the surrounding environment. According to literature, the change in fluorescence intensity with respect to the presence of air bubbles occurs as the fluorescence spectrum is distorted by the scattered light caused by gas bubbles [112].

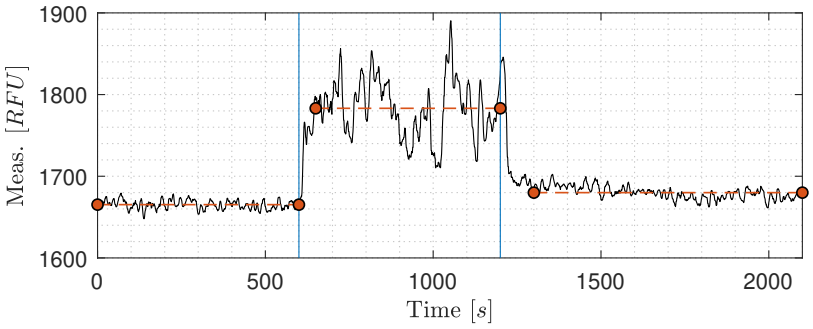

Fig. 3.7: The results measured by the OiW monitor. Gas bubbles are injected in the time period $(10-20)$min of the 35min experiment. Figure is from Paper C.

Fig. 3.7 shows the results of introducing air bubbles into the process. The experiment's execution consisted only of tap water to minimize the number of unknown influences, such as a shift in the volume of oil droplets entering the OiW monitor. Air was consistently added into the process from 600s to 1200s as shown in Fig. 3.7. In the period of injecting air into the system, the RFU measurement increased by 118RFU equivalent to 6.2ppm if using the WLS calibration procedure presented in Fig. 3.5. It is noteworthy to highlight that when only air was present in the view cell (with some uncertainty to small micro/macro water droplets), the measurement was $(80-90)$RFU. This insinuates a sweet spot when the presence of air bubbles by volume overtakes its effect of distorting the fluorescence spectrum. As only tap-water was used in the experiment, further investigation should examine different OiW concentrations with the presence of gas bubbles and how the volume and sizes of gas bubbles influence the results.

Repeatability investigation of flow-dependency on an OiW monitor: As previous joined studies by Bram et al. [52] suspected the OiW monitors to be flow-dependent, an investigation was carried out in Paper C. One OiW monitor was gravity fed with both tap water and demineralized water at two different flow rates: 1.1L/min and 1.7L/min, as shown in Fig. 3.8. Both flow rates were selected as they lie within the recommended range of $(1-2)$L/min by the manufacturer. Each box in Fig. 3.8 shows the median, 25^{th} and 75^{th} percentiles. The whiskers at each box represent the most extreme data points that are not considered as outliers.

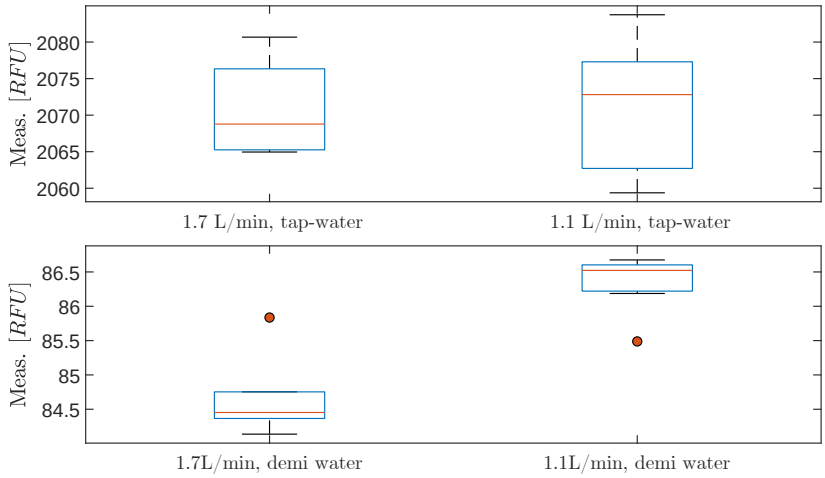

Fig. 3.8: The results of gravity feeding an OiW monitor with both demineralized water and tap water at two different flow rates: 1.1L/min and 1.7L/min. Figure is from Paper C.

The results showed insignificant flow-dependency at both types of water, with a difference in grand median of 4.0RFU for demineralized water and of 2.1RFU for tap water. Equivalently, if WLS calibration is considered, the difference in grand medians in ppm values for both types of water will be 0.2ppm and 0.1ppm, respectively. Although the influence of the RFU readings is insignificant compared to, e.g., air bubbles, the experiment interestingly showed the opposite, as was documented by Bram et al. [52], that the measurement of RFU is lower with a high flow rate. As concluded in Paper C, the suspected flow-dependency discussed by Bram et al. [52] must occur due to insufficient representation of the process flow rather than a change in flow rate.

3.4 Conclusion

An evaluation of four identical fluorescence-based monitors (Turner TD4100-XDC) was executed to determine the precision and sensitivity to measure aromatic oil content in water. The calibration method of the OiW monitor revealed that WLS yields a higher reproducibility between the four monitors, compared to the OLS method. Additionally, uncertainties related to sampling, calibration, and some variation in the process parameters were investigated. The latter uncertainties concerns: flow-dependency and the presence of gas bubbles in the flow stream. The results showed that the fluorescence-based monitors are not or at least insignificantly flow-dependent within its recommended flow rate range by the manufacturer. The results of gas bubbles showed a notably increase of the OiW concentration by 6.2ppm. However, further investigation

must be examined to prove the relation between gas bubbles and OiW concentrations. Whether the OiW monitor is feasible to measure OiW concentrations accurately in highly dynamic separation facilities with continuous fluid composition changes is questionable. Nevertheless, they are still of interest for measuring the separation efficiency of the hydrocyclones to enhance their deoiling performance, assuming the parameter effects on the OiW monitors are scalable.

Chapter 4

Online Monitoring of Total Suspended Solids

Based on the conclusion in Chapter 2, microscopy is believed to be the best candidate for measuring TSS in an IWT facility due to their direct observation that can measure single-particle properties and thereby able to classify particles [37]. The specifications of the two online microscopy analyzers: Jorin ViPA and Canty InFlow, are shown in Table 1.1. The calibration method of both microscopy analyzers was examined in Paper D to highlight the subjective assumptions related to calibrating the equipment. Paper D proposed one solution of how the calibration procedure could be performed to increase reproducibility related to the calibration uncertainties. The fluorescence-based monitor, described in Chapter 3, was used as a benchmark to evaluate both online microscopes' performance to measure different OiW concentrations accurately and in real-time.

The test setup used for evaluating both microscopes is shown in Fig. 4.1. The setup is equipped with a centrifugal pump, flowmeters, pressure transmitters, and control valves. The setup is designed for the purpose of testing quality monitors that is installed on-line (sidestream). One significant advantage of online sampling is the applicability regardless of process dimensions in size and flow rate, however, a large number of images is required to yield representative sample of the mainstream [2]. In Paper D, all three quality monitors (Jorin ViPA, Canty Inflow, and Turner TD-4100XDC) were equipped in series on a sidestream. By manipulating the control valves, the setup is configurable to direct the liquid through the sidestream with a constant flow rate within the recommended flow velocity of each quality monitor.

Fig. 4.1: Photos of the skid-mounted test setup. Left: the test setup for testing different online quality monitors; top middle: electrical control panel; bottom middle: the supply tank with a mounted mixer; right: calibration particles manufactured by BS-Partikel.

4.1 Calibrating Online Microscopy Analyzers

For calibrating and validating both online microscopes, known polystyrene particle sizes produced by BS-Partikel were used. A known particle size with a μ and σ of 20.1(0.4)µm was selected for calibrating both microscopes. Two other known particle sizes were used for validating the calibration: 9.8(0.3)µm and 40.3(0.9)µm.

To calibrate both microscopes, three calibration parameters must be tuned: THV, ESV/FRV, and depth of field. Although, tuning the virtual depth of field is only necessary when concentration measurements are needed. The THV consists of values in the range of $0-255$, from black to white. The ESV/FRV are edge detection methods to determine the particles' edge. Jorin ViPA's ESV is in a range of $0-10$, where Canty InFlow's FRV ranges from $0-1000$. The virtual depth of field determines the volume of captured images to match the known concentration.

Selecting THV and ESV/FRV is based on the petroleum engineers' perception of which objects are considered adequately in focus when calibrating the microscope. Fig. 4.2, presents eleven different particles with the same nominal size captured by Jorin ViPA. The numbers in Fig. 4.2 represent the range of ESV. Fig. 4.2 shows particles in different degrees of focus, from where the subjective assumption must be made; which particles are considered sufficiently sharp and at which greyscale value of the particles' periphery should be included to represent its area.

One solution for calibrating the microscopy analyzers was suggested in Paper D, to keep a temporary high ESV followed by adjusting the THV until

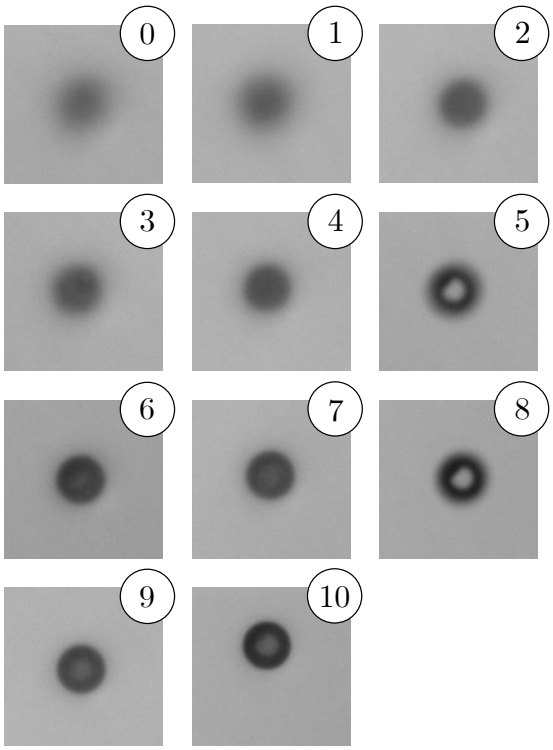

Fig. 4.2: Eleven different particles captured by Jorin ViPA each with the corresponding ESV ranging from $0-10$. Figure is from Paper D.

the PSD matches the distribution of the known particle size. When increasing ESV/FRV less particles will be captured, and when decreasing ESV/FRV more particles that are less in focus can be underestimated. This complicates the selection of ESV/FRV as these tradeoffs are chosen by the petroleum engineer. However, as the measurement of particle sizes is dependent on the THV and ESV/FRV, other values may yield a better representation of the PSD. The calibration results of the known particle size: 20.1(0.4)µm, from each microscope is shown in Fig. 4.3 and 4.4.

The calibration method was validated by recirculating two other known particle sizes together with the known calibration particle size: 9.8(0.3)µm, 20.1(0.4)µm, and 40.3(0.9)µm. The μ and s for each known particle size, measured by Jorin ViPA and Canty InFlow are shown in Table 4.1. The data were obtained by truncating the entire experiment results at each known particle size with a duration of $\pm$4µm from the known μ by the manufacturer.

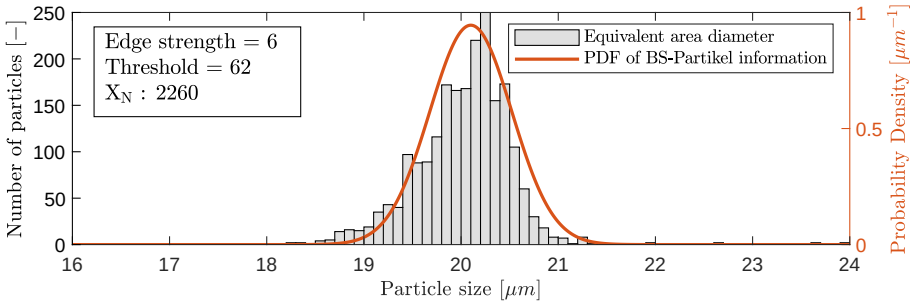

Fig. 4.3: The results of the selected calibration parameters: THV = 62 and ESV = 6 for Jorin ViPA. Figure is from Paper D.

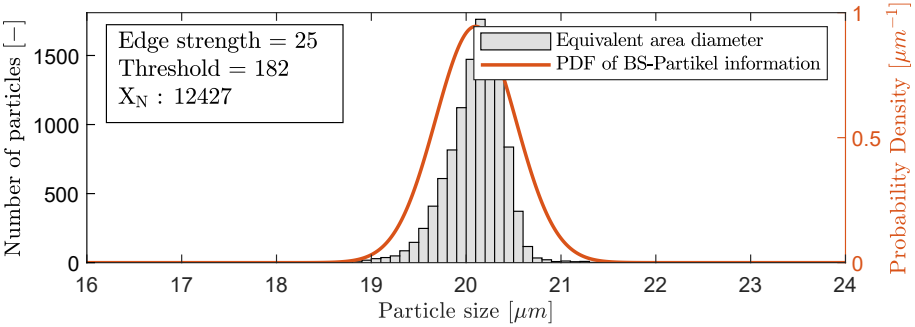

Fig. 4.4: The results of the selected calibration parameters: THV = 182 and ESV = 25 for Canty InFlow. Figure is from Paper D.

Table 4.1: The μ and σ results of recirculating three known particle sizes for 2h. Table is modified from Paper D.

	Known $\mu(\sigma)$ [µm]	$\mu_{estimat.}$ [µm]	$\sigma_{estimat.}$ [µm]
Canty InFLow	9.8(0.3)	9.5	0.6
	20.1(0.4)	20.0	0.6
	40.3(0.9)	40.9	0.5
Jorin ViPA	9.8(0.3)	9.6	0.6
	20.1(0.4)	20.3	1.0
	40.3(0.9)	41.4	0.6

4.2 Performance Validation

Both microscopes' ability to measure concentrations based on classified particles was evaluated. Oil droplets were selected as verification object as the

fluorescence-based monitor was available to benchmark their ability to measure the OiW concentration. A 6h experiment was executed on the test setup as shown in Fig. 4.1. To ensure consistency in the PSD throughout the experiment, the pump speed was fixed to maximum speed, and the flow rate was maintained constant through the sidestream by manipulating the control valve after the quality monitors. Six nominal OiW concentrations were analyzed $(55, 100, 150, 200, 250, 400)$ppm, by injecting oil between each concentration. Fig. 4.5 shows the results of measuring the OiW concentration in steady-state, by outputting the mean concentration every minute. The results in Fig. 4.5 are shown in Table 4.2.

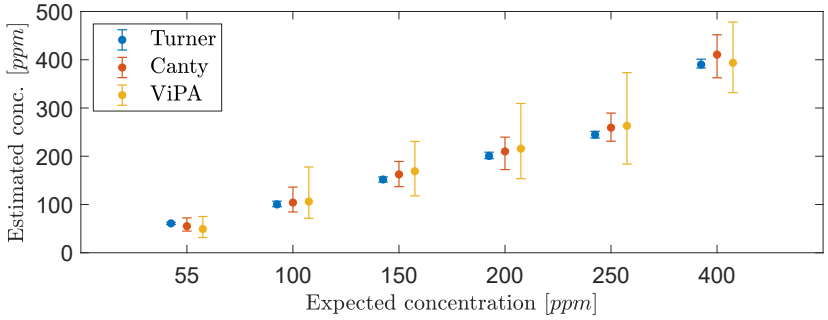

Fig. 4.5: Each error bar represents the steady-state measurement obtained with both microscopes each minute. The error bars shows the μ, minimum, and maximum OiW concentration of a 30min duration for each OiW concentration. The error bars of the fluorescence-based monitor are based on measurements every 10s. Figure is from Paper D.

Table 4.2: Associated results to Fig. 4.5. Table is modified from Paper D.

Expected conc.		55ppm	100ppm	150ppm	200ppm	250ppm	400ppm
Turner TD-4100XDC	min:	56.2	94.7	146.1	193.9	237.6	379.0
	μ:	60.9	100.1	151.8	200.7	244.6	390.0
	max:	67.7	105.4	159.5	207.7	255.8	398.4
Jorin ViPA	min:	31.6	71.4	118.0	153.5	183.7	331.9
	μ:	49.2	106.1	168.9	215.7	263.1	393.6
	max:	75.1	177.8	230.7	309.3	373.4	478.0
Canty InFlow	min:	44.9	84.6	136.9	172.4	231.2	362.6
	μ:	55.1	104.0	162.4	210.0	259.3	410.6
	max:	72.3	136.1	189.2	239.6	289.4	451.7

Both microscopes showed promising results in measuring OiW concentrations in real-time. Fig. 4.6 and 4.7 show the real-time measurement at the expected 55ppm OiW concentration. A trailing moving average window of 1min

was used, although extending the averaging window will naturally smooth the measurements. However, depending on the plant's dynamics, important information might be lost by selecting a too large window.

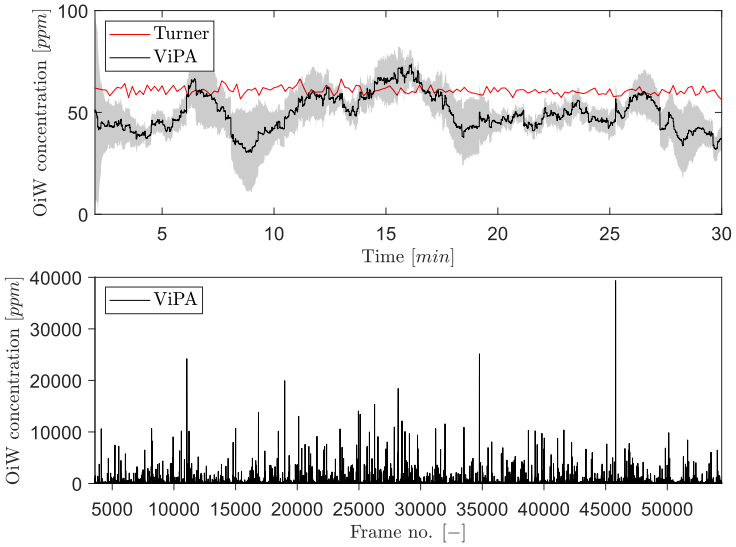

Fig. 4.6: Real-time OiW concentration measurement estimated by Jorin ViPA at the expected OiW concentration of 55ppm. A 95% confidence interval of the averaging window is shadowed behind the signal. The bottom graph shows the volume based OiW concentration in each image captured. Figure is from Paper D.

As the number of captured particles affects the accuracy of the PSD it is necessary to sample a sufficient amount of particles. The estimation of the number of particles that must be counted to achieve a given statistically accuracy was investigated in Paper D. As an example Fig. 4.8 and 4.9 represent the PSD measured by the two microscopes at an expected OiW concentration of 55ppm. Furthermore, the mean and standard deviation of the log-normal distributions, μ_0 and σ_0, is presented in Fig. 4.8 and 4.9, together with the number of counted particles, X_N.

Masuda and Iinoya [113] proposed a mathematical procedure to determine the minimum number of particles that must be counted, n^*, within a defined confidence interval, u, and the amount of error, δ, allowed. Thus, the relative error to a certain time can be estimated based on number of particles observed. n^* is determined by:

$$\log(n_*) = -2\log(\delta) + \log(\omega), \tag{4.1}$$

where

$$\omega = u^2\alpha^2 s^2(2c^2s^2 + 1). \tag{4.2}$$

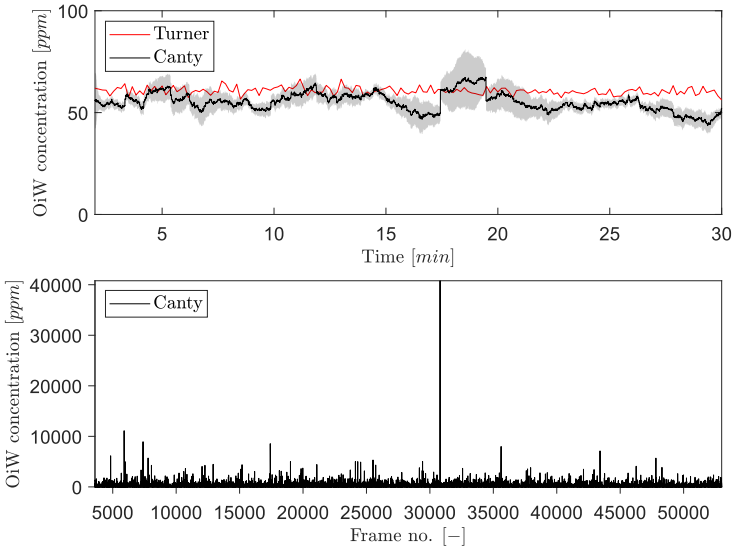

Fig. 4.7: Real-time OiW concentration measurement estimated by Canty Inflow at the expected OiW concentration of 55ppm. A 95% confidence interval of the averaging window is shadowed behind the signal. The bottom graph shows the volume based OiW concentration in each image captured. Figure is from Paper D.

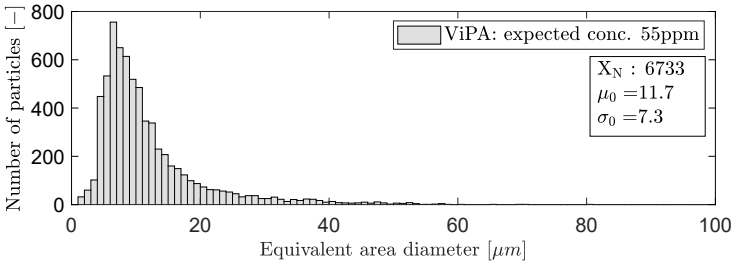

Fig. 4.8: The PSD obtained by Jorin ViPA based on the expected concentration of 55ppm. Figure is from Paper D.

α is a non-zero exponential constant (for log-normal distribution $\alpha = 2$) [114]. Lastly, the constant, c, is:

$$c = \beta + \frac{\alpha}{2} \tag{4.3}$$

where β is a basis number, for the count basis $\beta = 0$ [53]. Table 4.3 shows the relative error within 95% confidence interval of the PSDs for each measured OiW concentration, based on different obtained time intervals.

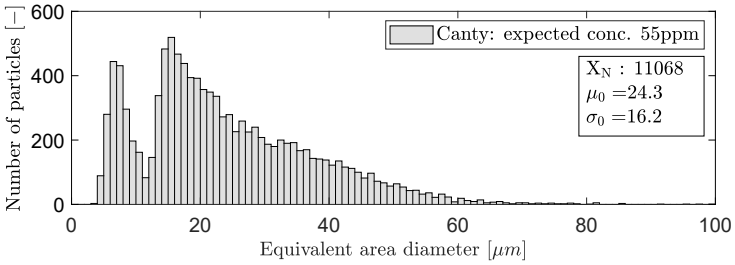

Fig. 4.9: The PSD obtained by Canty InFlow based on the expected concentration of 55ppm. Figure is from Paper D.

Table 4.3: Measured δ within 95% confidence interval based on different durations for each OiW concentration measurement of both microscopes.

Expected conc.		55ppm	100ppm	150ppm	200ppm	250ppm	400ppm
Jorin ViPA	1min:	19.8%	16.9%	13.7%	13.2%	12.2%	10.5%
	5min:	8.6%	7.7%	6.3%	5.7%	5.2%	4.5%
	10min:	6.1%	5.3%	4.5%	4.0%	3.7%	3.3%
	30min:	3.5%	3.0%	2.6%	2.3%	2.2%	1.9%
Canty InFlow	1min:	15.4%	13.6%	11.0%	9.2%	1.7%	1.5%
	5min:	7.5%	6.4%	5.5%	4.8%	4.5%	4.1%
	10min:	5.3%	4.5%	3.8%	3.3%	3.1%	2.9%
	30min:	2.98%	2.6%	2.2%	1.9%	1.8%	1.6%

The results in Table 4.3 shows the potential δ of presenting the PSD within a 95% confidence interval, based on the number of particles captured by both microscopes. If $\delta < 5\%$ is sufficient, the time interval of presenting the data must be at least 5min, although at lower concentrations the duration must be further increased. For obtaining a PSD with $\delta = 1\%$, approximately $100,000 - 130,000$ particles for Canty InFlow and $90,000 - 100,000$ particles for Jorin ViPA must be counted based on the measured OiW concentrations.

4.3 Conclusion

Both microscopes' calibration procedure relies on the petroleum engineers' ability to determine what is acceptably sharp. The calibration procedure of both microscopes consists of three main parameters: THV, ESV/FRV, and depth of field, all of which must be manually tuned in order to measure the single-particle properties accurately. A calibration procedure was determined as a solution to keep a consistent procedure for calibrating the microscope. The

calibration procedure results showed high accuracy in measuring three different known particle sizes in a validation experiment, indicating a useful calibration procedure.

To evaluate both microscopes' performance to measure OiW concentrations in steady-state and real-time, oil was selected as a verification object as the fluorescence-based monitor can benchmark the microscopes ability to measure concentrations. Both measurements showed reasonable results in relation to the fluorescence-based monitor and the expected OiW concentration. A trailing moving average window of 1min was applied to evaluate both microscopes ability to measure the OiW concentration in real-time. Although depending on the plant's dynamics, it can be discussed whether the moving average window should be extended to smooth the continuous measurement even further. The errors related to the statistical representation of a particle size distribution were presented. A mathematical procedure proposed by Masuda and Iinoya [113] was used to determine the minimum number of particles that must be counted within a defined confidence interval and the amount of error allowed. An example was given of how long time it will take to obtain a satisfying particle size distribution by preferring a 95% of the data to be included within different relative errors.

Chapter 5

Graphical Interface on Industrial Software

Having a good understanding of the uncertainties associated with the online monitors would improve their industrial acceptance. Even though proper calibration is vitally important to ensure reliable measurement, presenting the data to an operator in an appropriate manner is at least as important. The traditional visualization approach is usually based on the assumption that calibration data are exact and, thus, the visual representation of uncertainty is ignored [115]. It is essential to convey the uncertainty in the right format in order for an operator to swiftly comprehend the process's current state, which can range from simple text to dynamic graphical representations, as discussed in Paper E. It is necessary to determine how best to present the data to an operator when there are uncertainties related to the data and how different representations can affect users' understanding of the uncertainty, all of which can affect the operator's decisions and actions. Inaccurate interpretation of the data can potentially lead to costly failures. According to Abnormal Situation Management (ASM) consortium, abnormal events cause $(3-8)\%$ production loss of the plant's capacity, where 42% of those are due to human incidents (operators), 36% are due to degradation and failures of equipment, and 22% are due to process operation [116]. $(3-8)\%$ production is equivalent to $\$(45-120)$ million lost annually in oil production in the Danish sector alone, with the assumption of a crude oil price at \$41 per barrel of oil, and the annual production of oil in 2019 of $5.851 \cdot 10^6 \mathrm{m}^3$ [9, 116]. Based on these aspects, it is essential to consider what should be displayed to the operator and how it should be displayed in order to strengthen the operator's comprehension of the system state. Operators can miss out on important information due to the large number of data streams flooding the operator's screens [117]. Therefore, suggestions are given to emphasize the "human factors" when designing HMI software for the

operators [117]. The HMI software is the graphical interface of the supervisory control and data acquisition (SCADA) system used offshore, on which the operator controls the process. For a simple system with a well-defined operating point, the task of identifying abnormal situations might be easy. However, for a complex interdependent system, where the optimal operating point varies due to uncontrollable inputs, the situation could be much harder to interpret [52]. In addition to incorporating water quality monitors into the decision support solution, either manually or through control feedback information, the data's presentation and interpretation must be evaluated. The water quality monitors should output accurately information and easy to interpret for an operator before having the potential to improve product quality, increase production, or lower OPEX, as mentioned in Sec. 1.1.

5.1 Human Machine Interface: a Case Study

Paper E presents a case study to compare MPC to conventional proportional, integral, and derivative (PID) control on the pilot-plant facility, as shown in Fig. 3.1. The case study of the control solution comparison uses the four configuration sections, as shown in Fig. 3.2: support, pipeline riser, separator, and hydrocyclone to execute the experiment. A design approach is given for displaying and explaining the control for the operators. This is based on uniting the fast prototyping capability of Simulink Real-Time with an industrial graphical interface HMI software with OPC as the central node in the communication system. The selection of establishing a connection between Simulink Real-Time and HMI is the basis of experimental execution that is particularly useful when developers aim to increase the readiness level of new solutions.

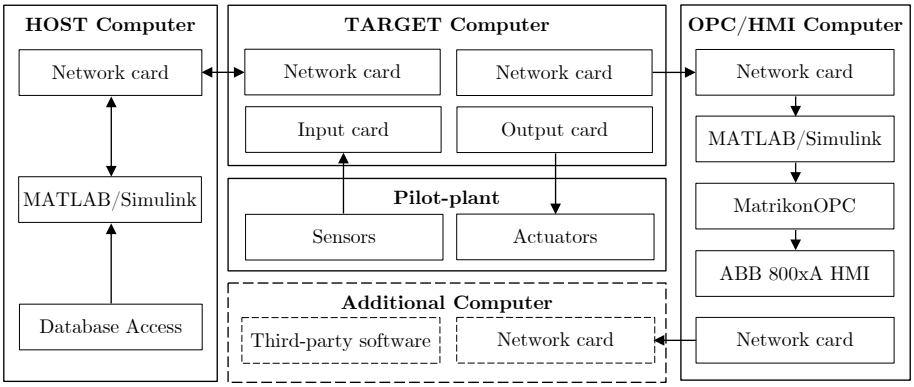

Fig. 5.1: The established connection between different computing systems of the pilot-plant. Each block represents a physical computer dedicated to the pilot-plant with its respective software and hardware. Figure is modified from Paper E.

Fig. 5.1 shows the connection of three dedicated computers and an optional connection to an additional computer if a third-party software should be evaluated.

Although this thesis does not cover the design of new offshore control solutions in the oil and gas sector, the case study was particularly useful at the time to investigate the potential of the communication establishment between Simulink Real-Time and the HMI software. The design solution of the MPC algorithm used for this case study has been published by Hansen et al. [55]. The graphical interface presentation of MPC algorithm is presented in Fig. 5.2. The PID control operation was ghosted on the MPC operation's presentation to evaluate their different performance under the exact same operating conditions of the pilot-plant facility. By comparing the visual design of the data presented in the HMI software shown in Fig. 5.2, and the image in Fig. 3.1 showing the Simulink Real-Time interface, it is much more challenging to comprehend the Simulink Real-Time interface, especially if larger quantities of data must be evaluated at the same time.

Based on the MPC case study, it will be beneficial to evaluate how to present the data from the quality monitors presented in this thesis. Especially if a third-party software connection through, e.g., OPC is not an option at a platform offshore, information must be delivered as signals to the PLC as part of the SCADA system. Although OiW concentration is not troublesome to deliver as a signal, delivering representative particle sizes within each class in continuous statistical batches can be more problematic.

5.2 Conclusion

The scaled pilot-plant provides a suitable testing environment for developing new features to the upstream offshore oil and gas industry, as it is capable of running different sections of the plant in series or bypass sections. To further mimic industrial practice, the plant's data were expanded by establishing a connection between Simulink Real-Time (academic used software) and ABB 800xA HMI software (industrial used software). The proposed connection can increase the adoption speed of new technological approaches by lowering the gap between academic research and industrial implementation when creating new solutions with a high innovation rate.

To demonstrate the connection functionality, a case study was carried out by investigating how to improve the operators' comprehension of the MPC procedure and how different controllers' performance can be presented in real-time by ghosting previous experiments. Although this work does not directly concern online quality monitoring, the data's presentation and interpretation can be investigated in an industrial used software in a safe testing facility.

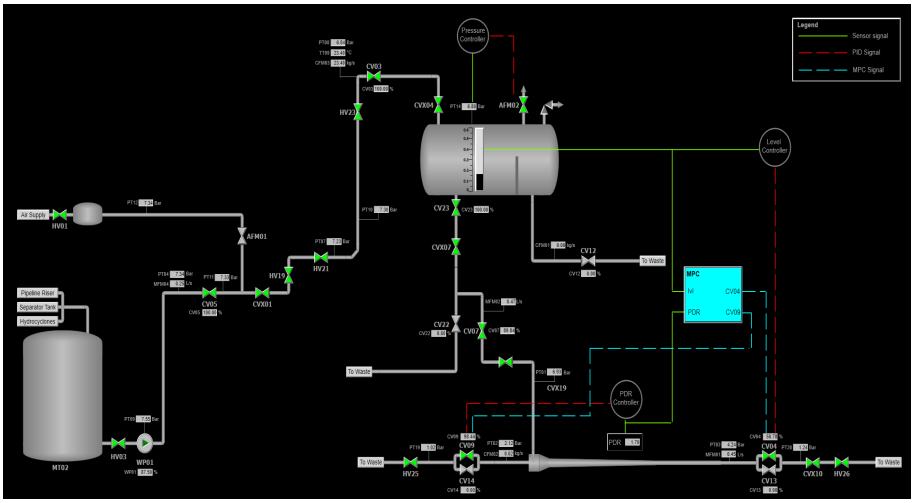

(a)

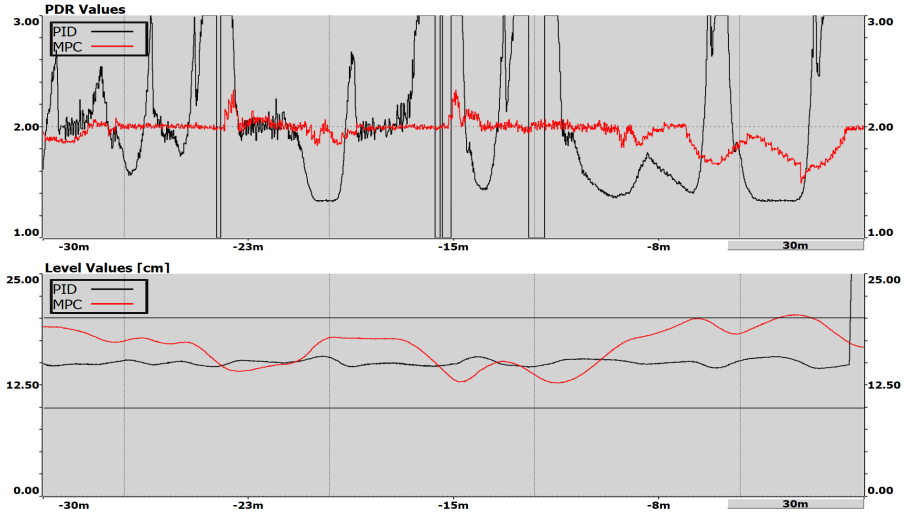

(b)

Fig. 5.2: The industrial used HMI interface: (**a**) shows the graphical design of the pilot-plant. (**b**) shows an example of a trend curve that can be visualized in the HMI software. In this particular example, the trend curve shows the level within the separator tank and the PDR of the hydrocylone with two different control algorithms: MPC and PID. Figures are from Paper E

Chapter 6

Closing Remarks

With growing requirements for increasing operational efficiency and environmental sustainability, the application use of online water quality monitors will increase in the years to come, whether it is in the water industry to enhance the drinking water quality or wastewater disposal or in the oil and gas industry to enhance the produced water discharge or to reinject the produced water into the reservoir. In this thesis, the challenges associated with online water quality measurements in the IWT process are addressed, emphasizing OiW concentration and TSS measurements. The thesis aims to increase the awareness of online monitors for the offshore oil and gas industry and highlights the challenges within online quality monitors. The main contributions of this work can be summarized to:

- An extensive literature review on what IW quality characteristics can be considered as TSS, which affects the reservoir's economic lifetime. Furthermore, no similar review study has discussed the complexity of selecting quality monitors that can reliably measure suspended solids' sizes and concentrations in an IWT process. Online Microscopy analyzers were deemed the best candidates to measure suspended solids based on the review study.

- Uncertainty analysis and calibration evaluations of online fluorescence-based monitors. The evaluated online fluorescence-based monitors showed a high reproducibility between each other using a weighted least square method to execute the calibration procedure. The performance of measuring OiW concentration with the fluorescence-based monitor showed promising results. However, the fluorescence-based monitor is highly sensitive to changes in the oil's aromatic content, which is a considerable limitation that will affect the fluorescence-based monitor's performance when oil is produced from different production wells.

- Calibration and performance evaluations of online microscopy analyzers. The evaluated online microscopy analyzers showed promising results in measuring particle sizes and concentrations. Furthermore, they were reasonable to measure OiW concentrations in both steady-state and real-time by using a trailing moving average window.
- Defined methodology to integrate and test novel process solutions with industrial used software. An industrial used software program was established to expand the in-house pilot-plant's data information to mimic the industrial practice of newly developed features, which includes presentation of water quality data.

Based on the literature review proposed in Paper A, the type of IW characteristics that can affect the increment of TSS concentration was comprehensively investigated, and the formation damage mechanism it can advance. While controlling water quality in the IWT process has been highlighted as the main key to increase the useful lifetime of the reservoir in several studies, most of these studies state that formation damage can be prevented or reduced, but they rely on the hypothesis that online accurate measurements are available.

In the second part of the review proposed in Paper A, a discrimination process was executed for petroleum engineers to reduce the number of choices when selecting instruments to measure TSS' quantity and size distribution in their IWT process. Measuring the single-particle properties with an online microscopy analyzer was concluded to be the best candidate to achieve TSS measurements in an offshore IWT process. To measure both OiW concentrations and single-particle properties online, each measurement type's advantages and limitations were divided into three papers, where Paper B and C cover evaluation of a fluorescence-based monitor to measure OiW concentration, and Paper D investigated two types of microscopy analyzers for measuring TSS. Four identical fluorescence-based monitors were examined in Paper C to estimate the OiW concentration. The calibration method of the OiW monitor revealed that WLS yields a higher reproducibility between the four monitors than the OLS method. Furthermore, an uncertainty analysis of sampling, calibration of the instrument, OiW concentration measurements with the reference method, and different variations in the process parameters were explored. Paper B proposed the application use of quality monitors on an offshore production treatment process for measuring the separation efficiency of a hydrocyclone. The use of fluorescence-based monitors to measure the separation efficiency of a deoiling hydrocyclone showed promising results capable of accurately measuring OiW concentrations under certain conditions. Paper D revealed that two types of online microscopy analyzers were able to measure known particle sizes and concentrations with high accuracy. Further examination of their ability to classify several different particles is necessary. Lastly, an expansion of the pilot-plant's interface was established in Paper E by integrating an industrial

used software program to be able to improve the presentation of the data from new features such as online water quality monitors. In conclusion, as there is no consensus on which method provides the most reliable estimate of TSS in an IWT process, the author has put a considerable effort into investigating what measurement type will be most promising for measuring TSS.
By acknowledging the uncertainty related to measuring the different kinds of water qualities in an IWT facility, future work may take into account these uncertainties when new water quality monitors need to be investigated or developed monitors need improvements. Accurate water analysis is essential to identify process changes and promotes sophisticated process optimization and control to be implemented into any water system.

References

[1] EIA, "International Energy Outlook 2019," U.S. Energy Information Administration, Washington, DC, USA, Tech. Rep., p. 169, 2019.

[2] D. S. Hansen, M. V. Bram, and Z. Yang, "Online Quality Measurements of Total Suspended Solids for Offshore Reinjection: A Review Study," *Energies*. MDPI, 2020, p. 53, 2020, [Submitted].

[3] IEA, "Energy Access Outlook 2017," ser. World Energy Outlook, International Energy Agency, Paris, France, Tech. Rep., p. 11, 2017.

[4] EIA, "International Energy Outlook 2019: World Energy Projection System Plus," Washington, DC, USA, 2019. [Online]. Available: www.eia.gov/aeo (Accessed 2020-05-19).

[5] SEI, IISD, ODI, Analytics Climate, CICERO, and UNEP, "The Production Gap: The discrepancy between countries' planned fossil fuel production and global production levels consistent with limiting warming to 1.5°C or 2°C," The Production Gap, Tech. Rep., p. 70, 2019.

[6] IPIECA, "Meeting energy needs: The unique role of oil and gas," ser. The Paris Puzzle, The global oil and gas industry association for environmental and social issues, London, UK, Tech. Rep., p. 2, 2014.

[7] Klimarådet, "Kendte Veje og Nye Spor til 70 Procents Reduktion: Retning og iltag for de næste ti års klimaindsats i Danmark," Klimarådet, Copenhagen, Denmark, Tech. Rep., p. 154, 2020.

[8] M. S. Masnadi, H. M. El-Houjeiri, D. Schunack, Y. Li, J. G. Englander, A. Badahdah, J.-C. Monfort, J. E. Anderson, T. J. Wallington, J. A. Bergerson, D. Gordon, J. Koomey, S. Przesmitzki, I. L. Azevedo, X. T. Bi, J. E. Duffy, G. A. Heath, G. A. Keoleian, C. McGlade, D. N. Meehan, S. Yeh, F. You, M. Wang, and A. R. Brandt, "Global carbon intensity of crude oil production," *Science*. Washington, DC, USA: AAAS, 2018, vol. 361, no. 6405, pp. 851–853, 2018. doi: 10.1126/science.aar6859

[9] Danish Energy Agency, "Yearly production, injection, flare, fuel and export in SI units 1972-2019," Danish Energy Agency, Esbjerg, Denmark, Tech. Rep., 2020.

[10] I. Larsen, "Denmark's Oil and Gas Production – and Subsoil Use 09," Energistyrelsen, Copenhagen, Denmark, Tech. Rep., p. 156, 2010.

[11] Danish Energy Agency, "Ressourceropgørelse og prognoser," Danish Energy Agency, Esbjerg, Denmark, Tech. Rep., p. 9, 2018.

[12] U. Ahmed, "Making the Most of Maturing Fields," *Oilfield Review*, D. Williamson and R. Gir, Eds. Houston, TX, USA: Schlumberger, 2004, vol. 16, no. 2, pp. 1–1, 2004.

[13] OSPAR Commission, "Produced Water Discharges from Offshore Oil and Gas Installations 2007-2012," London, UK, Tech. Rep., p. 2, 2014.

[14] Miløstyrelsen, "Generel tilladelse for Mærsk Olie og Gas A/S (Mærsk Olie) til anvendelse, udledning og anden bortskaffelse af stoffer og materialer, herunder olie og kemikalier i produktions- og injektionsvand fra produktionsenhederne Halfdan, Dan, Tyra og Gorm for perioden 1. januar 2017 - 31. december 2018." Mærsk Olie og Gas A/S, Copenhagen, Denmark, Tech. Rep., p. 11, 2016.

[15] D. S. Hansen, M. V. Bram, and Z. Yang, "Efficiency investigation of an offshore deoiling hydrocyclone using real-time fluorescence- and microscopy-based monitors," in *2017 IEEE Conference on Control Technology and Applications (CCTA)*. Mauna Lani, HI, USA: IEEE, 2017, pp. 1104–1109. doi: 10.1109/CCTA.2017.8062606

[16] M. Yang, "Measurement of Oil in Produced Water," in *Produced Water*, 1st ed., K. Lee and J. Neff, Eds. New York, NY, USA: Springer, 2011, ch. 2, pp. 57–88. ISBN 978-1-4614-0045-5. doi: 10.1007/978-1-4614-0046-2

[17] OSPAR Commission, "OSPAR report on discharges, spills and emissions from offshore oil and gas installations in 2014," OSPAR, London, UK, Tech. Rep., p. 54, 2016.

[18] S. Maxwell, "Implications of Re-Injection of Produced Water on Microbially Influenced Corrosion (MIC) in Offshore Water Injection Systems," in *CORROSION 2005*. Houston, TX, USA: NACE International, 2005, p. 9.

[19] OSPAR Commission, "List of Decisions, Recommendations and Other Agreements Applicable within the Framework of the OSPAR Convention - Update 2018," OSPAR, London, UK, Tech. Rep., p. 22, 2018.

[20] E. Blanchard, "Oil in Water Monitoring is a Key to Production Separation," *Offshore*. Nashville, TN, USA: Endeavor Business Media, 2013, vol. 73, no. 11, pp. 104–105, 2013.

[21] D. J. Hartmann and E. A. Beaumont, "Predicting Reservoir System Quality and Performance," in *Handbook of Petroleum Geology: Exploring for Oil and Gas Traps*, 1st ed., ser. Handbook of petroleum geology, E. A. Beaumont and N. H. Foster, Eds. Tulsa, OK, USA: The American Association of Petroleum Geologists, 1999, vol. 3, ch. 9, p. 154. ISBN 9780891816027. doi: 10.1306/TrHbk624C9

[22] C. M. Marle, "Oil entrapment and mobilization," in *Basic Concepts in Enhanced Oil Recovery Processes*, 1st ed., ser. Critical Reports on Applied Chemistry Volume 33, M. Bavière, Ed. Paris, France: Elsevier, 1991, vol. 33, ch. 1, pp. 3–39. ISBN 1-85166-617-6

[23] Miløstyrelsen, "Generel tilladelse for Total E&P Danmark A/S (TOTAL) til anvendelse, udledning og anden bortskaffelse af stoffer og materialer, herunder olie og kemikalier i produktions- og injektionsvand fra produktionsenhederne Halfdan, Dan, Tyra og Gorm for perioden 1. januar 2019 - 31. december 2020." Total E&P Danmark A/S, Copenhagen, Denmark, Tech. Rep., p. 12, 2018.

[24] Andor, "What is Light? - An overview of the properties of light," Oxford Intruments, Bognor Regis, UK, Tech. Rep., p. 3, 2019.

[25] J. Sanderson, *Understanding Light Microscopy*, 1st ed., ser. Royal Microscopical Society. Chichester, UK: Wiley, 2019. ISBN 9780470973752. doi: 10.1002/9781118696736

[26] J. R. Lakowicz, *Principles of Fluorescence Spectroscopy*, 3rd ed., J. R. Lakowicz, Ed. Boston, MA, USA: Springer, 2006. ISBN 0387312781. doi: 10.1007/978-0-387-46312-4

[27] X. Zhu and T. Gao, "Spectrometry," in *Nano-Inspired Biosensors for Protein Assay with Clinical Applications*, 1st ed., G. Li, Ed. Amsterdam, Netherlands: Elsevier, 2019, ch. 10, pp. 237–264. ISBN 9780128150535. doi: 10.1016/B978-0-12-815053-5.00010-6

[28] Turner Designs Hydrocarbon Instruments, "E09 TD-4100XDC Oil in Water Monitor User Manual," Turner Designs, Fresno, CA, USA, Tech. Rep., p. 272, 2014.

[29] Turner Designs, "Lamp, Near U.V. SKU: 10-049," San Jose, CA, USA. [Online]. Available: https://www.turnerdesigns.com/product-page/lamp-near-u-v (Accessed 2020-10-28).

[30] Turner Designs, "10-AU Field Fluorometer," San Jose, CA, USA, pp. 1–2. [Online]. Available: https://www.turnerdesigns.com/10au-field-laboratory-fluorometer (Accessed 2020-10-28).

[31] ISO, "Particle Size Analysis – Image Analysis Methods – Part 2: Dynamic Image Analysis Methods," ser. ISO 13322-2, Geneva, Switzerland, Tech. Rep., p. 24, 2006.

[32] D. Severin Hansen, S. Jespersen, M. V. Bram, and Z. Yang, "Uncertainty Analysis of Fluorescence-Based Oil-In-Water Monitors for Oil and Gas Produced Water," *Sensors*. Basel, Switzerland: MDPI, 2020, vol. 20, no. 16, p. 36, 2020. doi: 10.3390/s20164435

[33] J. Zhang, "RPSEA Subsea Produced Water Discharge Sensor Lab Test Results and Recommendations Final Report," Clearlew Subsea LLC, Houston, TX, USA, Tech. Rep. 3, p. 351, 2016.

[34] B. L. Ogden, "Water Technology: Understanding, Interpreting and Utilizing Water Analysis Data," in *Southwestern Petroleum Short Course Conference 2008*. Lubbock, TX, USA: Southwestern Petroleum Short Course, 2008, p. 12.

[35] H. G. Merkus, *Particle Size Measurements - Fundamentals, Practice, Quality*, 1st ed., ser. Particle Technology Series, Vol. 17. Houten, Netherlands: Springer, 2009. ISBN 978-1-4020-9015-8. doi: 10.1007/978-1-4020-9016-5

[36] T. Allen, *Powder Sampling and Particle Size Determination*, 1st ed. Amsterdam, Netherlands: Elsevier, 2003. ISBN 9780080539324. doi: 10.1016/B978-0-444-51564-3.X5000-1

[37] K. Leschonski, "Particle Characterization, Present State and possible Future Trends," *Particle & Particle Systems Characterization*, K. Leschonski, B. Scarlett, G. Jimbo, and B. H. Kaye, Eds. Weinheim, Germany: Wiley, 1986, vol. 3, no. 3, pp. 99–103, 1986. doi: 10.1002/ppsc.19860030302

[38] P. Durdevic, C. Raju, M. Bram, D. Hansen, and Z. Yang, "Dynamic Oil-in-Water Concentration Acquisition on a Pilot-Scaled Offshore Water-Oil Separation Facility," *Sensors*. Basel, Switzerland: MDPI, 2017, vol. 17, no. 1, p. 11, 2017. doi: 10.3390/s17010124

[39] A. Henriksen, "Online Oil-in-Water Monitoring Experience," Carrickfergus, UK, p. 30, 2008. [Online]. Available: http://www.advancedsensors.co.uk/wp-content/uploads/statoil-hydro-technical-presentation--qpc.pdf (Accessed 2020-11-07).

[40] W. F. Cerini, W. R. Battles, and P. H. Jones, "Some Factors Influencing the Plugging Characteristics of an Oil-well Injection Water," *Transactions of the AIME*. Los Angeles, CA, USA: Society of Petroleum Engineers, 1946, vol. 165, no. 1, pp. 52–63, 1946. doi: 10.2118/946052-G

[41] E. C. Babson, J. E. Sherborne, and P. H. Jones, "An Experimental Water-flood in a California Oil Field," *Transactions of the AIME*. Richardson, TX, USA: Society of Petroleum Engineers, 1944, vol. 160, no. 1, pp. 25–33, 1944. doi: 10.2118/945025-G

[42] K. M. Bansal and D. D. Caudle, "A New Approach for Injection Water Quality," in *SPE Annual Technical Conference and Exhibition*. Washington, DC, USA: Society of Petroleum Engineers, 1992, pp. 383 – 396. doi: 10.2118/24803-MS

[43] J. H. Barkman and D. H. Davidson, "Measuring Water Quality and Predicting Well Impairment," *Journal of Petroleum Technology*. Richardson, TX, USA: Society of Petroleum Engineers, 1972, vol. 24, no. 7, pp. 865–873, 1972. doi: 10.2118/3543-PA

[44] J. F. Pautz, M. E. Crocker, and C. G. Walton, "Relating Water Quality and Formation Permeability to Loss of Injectivity," in *SPE Production Operations Symposium*. Oklahoma City, OK, USA: Society of Petroleum Engineers, 1989, pp. 565–576. doi: 10.2118/18888-MS

[45] D. B. Bennion, D. W. Bennion, F. B. Thomas, and R. F. Bietz, "Injection Water Quality - A Key Factor to Successful Waterflooding," in *Annual Technical Meeting*, vol. 37, no. 6. Calgary, Canada: Petroleum Society of Canada, 1994, pp. 53–62. doi: 10.2118/94-60

[46] C. C. Patton, "Water Quality Control and Its Importance in Waterflooding Operations," *Journal of Petroleum Technology*. Richardson, TX, USA: Society of Petroleum Engineers, 1988, vol. 40, no. 9, pp. 1123–1126, 1988. doi: 10.2118/18459-PA

[47] D. B. Bennion, F. B. Thomas, D. Imer, T. Ma, and B. Schulmeister, "Water Quality Considerations Resulting in the Impaired Injectivity of Water Injection and Disposal Wells," *Journal of Canadian Petroleum Technology*. Calgary, Canada: Petroleum Society of Canada, 2001, vol. 40, no. 06, pp. 54 – 61, 2001. doi: 10.2118/01-06-05

[48] D. S. Hansen, M. V. Bram, P. Durdevic, S. Jespersen, and Z. Yang, "Efficiency evaluation of offshore deoiling applications utilizing real-time oil-in-water

monitors," in *Oceans 2017 - Anchorage*. Anchorage, AK, USA: IEEE, 2017, p. 6.

[49] M. V. Bram, L. Hansen, D. S. Hansen, and Z. Yang, "Grey-Box Modeling of an Offshore Deoiling Hydrocyclone System," in *2017 IEEE Conference on Control Technology and Applications (CCTA)*. Mauna Lani, HI, USA: IEEE, 2017, pp. 94–98. doi: 10.1109/CCTA.2017.8062446

[50] M. V. Bram, L. Hansen, D. S. Hansen, and Z. Yang, "Hydrocyclone Separation Efficiency Modeled by Flow Resistances and Droplet Trajectories," *IFAC-PapersOnLine*, S. Skogestad, Ed. Esbjerg, Denmark: Elsevier, 2018, vol. 51, no. 8, pp. 132–137, 2018. doi: 10.1016/j.ifacol.2018.06.367

[51] M. V. Bram, L. Hansen, D. S. Hansen, and Z. Yang, "Extended Grey-Box Modeling of Real-Time Hydrocyclone Separation Efficiency," in *2019 18th European Control Conference (ECC)*. Naples, Italy: IEEE, 2019, pp. 3625–3631. doi: 10.23919/ECC.2019.8796175

[52] M. V. Bram, S. Jespersen, D. S. Hansen, and Z. Yang, "Control-Oriented Modeling and Experimental Validation of a Deoiling Hydrocyclone System," *Processes*. Basel, Switzerland: MDPI, 2020, vol. 8, no. 9, p. 33, 2020. doi: 10.3390/pr8091010

[53] D. S. Hansen, S. Jespersen, M. V. Bram, and Z. Yang, "Offshore Online Measurements of Total Suspended Solids using Microscopy Analysis," *IEEE Sensors Journal*. IEEE, 2020, p. 10, 2020, [Submitted].

[54] D. S. Hansen, S. Jespersen, M. V. Bram, and Z. Yang, "Human Machine Interface Prototyping and Application for Advanced Control of Offshore Topside Separation Processes," in *IECON 2018 - 44th Annual Conference of the IEEE Industrial Electronics Society*. Washington, DC, USA: IEEE, 2018, pp. 2341–2347. doi: 10.1109/IECON.2018.8591309

[55] L. Hansen, P. Durdevic, K. L. Jepsen, and Z. Yang, "Plant-wide Optimal Control of an Offshore De-oiling Process Using MPC Technique," *IFAC-PapersOnLine*, S. Skogestad, Ed. Esbjerg, Denmark: Elsevier, 2018, vol. 51, no. 8, pp. 144–150, 2018. doi: 10.1016/j.ifacol.2018.06.369

[56] A. G. Ostroff, "Injection Water Problems Identified By Laboratory Analysis," in *Middle East Technical Conference and Exhibition*. Manama, Bahrain: Society of Petroleum Engineers, 1981, pp. 523 – 526. doi: 10.2118/9632-MS

[57] J. F. Carll, *The geology of the oil regions of Warren, Venango, Clarion, and Butler Counties; including surveys of the Garland and Panama conglomerates in Warren and Crawford, and in Chautauqua Co., N. Y., descriptions of oil well rig and tools, and a discussion of the preglacial and postglacial drainage of the Lake Erie country.*, 1st ed., ser. Report of progress. Washington, DC, USA: Harrisburg: Board of Commissioners for the Second geological survey, 1880. ISBN 978-1-362-59079-8

[58] A. C. Simmons, "Recent Developments in Water Flooding in the Bradford District," in *Drilling and Production Practice*. Amarillo, TX, USA: American Petroleum Institute, 1938, pp. 260–266.

[59] A. R. Ellenberger and J. H. Holben, "Flood Water Analyses and Interpretation," *Journal of Petroleum Technology*. Richardson, TX, USA: Society of Petroleum Engineers, 1959, vol. 11, no. 6, pp. 22–25, 1959. doi: 10.2118/1199-G

[60] J. W. Watkins, F. R. Willett Jr, and C. E. Arthur, "Conditioning Water for Secondary-Recovery in Midcontinent Oil Fields," Bureau of Mines, Bartlesville, OK, Washington, DC, USA, Tech. Rep., p. 164, 1952.

[61] M. Yari, H. Mansouri, H. Esmaili, and S. A. Alavi, "A Study of Microbial Influenced Corrosion in Oil and Gas Industry," in *International Conference of Oil, Gas, Petrochemical and Power Plant*, vol. 1. Tehran, Iran: Civilica, 2012, p. 11. doi: 10.13140/RG.2.1.3117.8089

[62] M. S. H. Bader, "Seawater versus produced water in oil-fields water injection operations," *Desalination*. Amsterdam, Netherlands: Elsevier, 2007, vol. 208, no. 1-3, pp. 159–168, 2007. doi: 10.1016/j.desal.2006.05.024

[63] J. Rochon, M. R. Creusot, P. Rivet, C. Roque, and M. Renard, "Water Quality for Water Injection Wells," in *SPE Formation Damage Control Symposium*, Society of Petroleum Engineers. Lafayette, LA, USA: Society of Petroleum Engineers, 1996, pp. 489–503. doi: 10.2118/31122-MS

[64] R. B. Baird, A. D. Eaton, and E. W. Rice, *Standard methods for the examination of water and wastewater*, 23rd ed., L. L. Bridgewater, Ed. Washington, DC, USA: American Public Health Association, American Water Works Association, and Water Environment Federation, 2017. ISBN 978-087553-287-5

[65] A. F. Ismail, K. C. Khulbe, and T. Matsuura, "RO Membrane Fouling," in *Reverse Osmosis*, 1st ed. Amsterdam, Netherlands: Elsevier, 2019, ch. 8, pp. 189–220. ISBN 978-0-12-811468-1. doi: 10.1016/B978-0-12-811468-1.00008-6

[66] M. N. Allhands, "The Efficient Removal of Organic and Inorganic Suspended Solids – Old Problem, New Technology," *Water Online Newsletter*. Horsham, PA, USA: VertMarkets, 2003, p. 11, 2003.

[67] M. C. Kennicutt, "Water Quality of the Gulf of Mexico," in *Habitats and Biota of the Gulf of Mexico: Before the Deepwater Horizon Oil Spill*, 1st ed., C. H. Ward, Ed. New York, NY, USA: Springer, 2017, vol. 1, ch. 2, pp. 55–164. ISBN 978-1-4939-3445-8. doi: 10.1007/978-1-4939-3447-8

[68] C. E. Boyd, "Dissolved Solids," in *Water Quality*, 2nd ed., C. E. Boyd, Ed. Cham, Switzerland: Springer, 2015, ch. 4, pp. 71–100. ISBN 978-3-319-17445-7. doi: 10.1007/978-3-319-17446-4

[69] C. Gao, "Factors affecting particle retention in porous media," *Emirates Journal for Engineering Research*. Al Ain, United Arab Emirates: United Arab Emirates University, 2007, vol. 12, no. 3, p. 7, 2007.

[70] H. A. Nasr-El-Din and A. A. Al-Taq, "Water Quality Requirements and Restoring the Injectivity of Waste Water Disposal Wells," in *SPE Formation Damage Control Conference*. Lafayette, LA, USA: Society of Petroleum Engineers, 1998, pp. 565–573. doi: 10.2118/39487-MS

[71] J. Zheng, B. Chen, W. Thanyamanta, K. Hawboldt, B. Zhang, and B. Liu, "Offshore produced water management: A review of current practice and challenges in harsh/Arctic environments," *Marine Pollution Bulletin*. Elsevier, 2016, vol. 104, no. 1-2, pp. 7–19, 2016. doi: 10.1016/j.marpolbul.2016.01.004

[72] J. R. Coleman and W. G. McLelland, "Produced Water Re-Injection; How Clean is Clean?" in *SPE Formation Damage Control Symposium*. Lafayette, LA, USA: Society of Petroleum Engineers, 1994, p. 5. doi: 10.2118/27394-MS

[73] J. E. Donham, "Offshore Water Injection System: Problems and Solutions," in *Offshore Technology Conference*. Houston, TX, USA: Offshore Technology Conference, 1991, pp. 53–57. doi: 10.4043/6782-MS

[74] C. C. Patton, "Injection-Water Quality," *Journal of Petroleum Technology*. Richardson, TX, USA: Society of Petroleum Engineers, 1990, vol. 42, no. 10, pp. 1238–1240, 1990. doi: 10.2118/21300-PA

[75] A. B. B. Merdhah and A. A. M. Yassin, "Calcium and Strontium Sulfate Scale Formation Due to Incompatible Water," in *International Graduate Conference on Engineering and Science 2008*. Skudai, Malaysia: Universiti Teknologi Malaysia, 2008, p. 9.

[76] M. Koteeswaran, "CO_2 and H_2S corrosion in oil pipelines," Master's thesis, University of Stavanger, Faculty of Mathematics and Natural Science, Stavanger, Norway, 2010.

[77] D. Brondel, F. Montrouge, R. Edwards, A. Hayman, D. Hill, S. Mehta, and T. Semerad, "Corrosion in the Oil Industry," *Oilfield Review*. Houston, TX, USA: Schlumberger, 1994, vol. 6, no. 2, pp. 4–18, 1994.

[78] T. L. Skovhus, D. Enning, and J. S. Lee, *Microbiologically Influenced Corrosion in the Upstream Oil and Gas Industry*, 1st ed., T. Skovhus, D. Enning, and J. Lee, Eds. Boca Raton, FL, USA: CRC Press, 2017. ISBN 978-1-4987-2656-6. doi: 10.1201/9781315157818

[79] G. R. Ruschau and M. Al-Anezi A, "Appendix S - Oil and Gas Exploration and Production," in *Corrosion Cost and Preventive Strategies in the United States*. McLean, VA, USA: Federal Highway Administration, 2001, ch. Appendix S, p. 14.

[80] L. Popoola, A. Grema, G. Latinwo, B. Gutti, and A. Balogun, "Corrosion problems during oil and gas production and its mitigation," *International Journal of Industrial Chemistry*. Berlin, Germany: Springer, 2013, vol. 4, no. 35, p. 15, 2013. doi: 10.1186/2228-5547-4-35

[81] P. Durdevic, C. S. Raju, and Z. Yang, "Potential for Real-Time Monitoring and Control of Dissolved Oxygen in the Injection Water Treatment Process," *IFAC-PapersOnLine*, S. Skogestad, Ed. Esbjerg, Denmark: Elsevier, 2018, vol. 51, no. 8, pp. 170–177, 2018. doi: 10.1016/j.ifacol.2018.06.373

[82] R. Heidersbach, "Corrosion in Oil and Gas Production," in *Microbiologically Influenced Corrosion in the Upstream Oil and Gas Industry*, 1st ed., T. L. Skovhus, D. Enning, and J. S. Lee, Eds. Boca Raton, FL, USA: CRC Press, 2017, ch. 1, pp. 3–34. ISBN 9781498726566. doi: 10.1201/9781315157818

[83] E. F. Diaz, J. G. Gonzalez-Rodriguez, A. Martinez-Villafañe, and C. Gaona-Tiburcio, "H_2S corrosion inhibition of an ultra high strength pipeline by carboxyethyl-imidazoline," *Journal of Applied Electrochemistry*. Dordrecht, Netherlands: Springer, 2010, vol. 40, no. 9, pp. 1633–1640, 2010. doi: 10.1007/s10800-010-0149-z

[84] V. S. Sastri, "Corrosion Causes," in *Challenges in Corrosion: Costs, Causes, Consequences, and Control*, 1st ed., ser. Wiley Series in Corrosion, R. W. Revie, Ed. Hoboken, NJ, USA: Wiley, 2015, ch. 3, pp. 127–204. ISBN 9781119069614. doi: 10.1002/9781119069638.ch5

[85] B. J. Little and J. S. Lee, *Microbiologically Influenced Corrosion*, 1st ed. Hoboken, NJ, USA: Wiley, 2006. ISBN 9780470112458. doi: 10.1002/047011245X

[86] E. Heitz, H.-C. Flemming, and W. Sand, *Microbially influenced corrosion of materials: scientific and engineering aspects*, 1st ed. Berlin, Germany: Springer, 1996. ISBN 978-3-642-80019-1

[87] R. Vasudevan, "Biofilms: Microbial Cities of Scientific Significance," *Journal of Microbiology & Experimentation*, S. Wood, Ed. Edmond, OK, USA: MedCrave Group, 2014, vol. 1, no. 3, pp. 1–16, 2014. doi: 10.15406/jmen.2014.01.00014

[88] Z. Latif, "Towards Continuous Online Oil-in-Water Measurement for Regulatory Purposes," Ph.D. dissertation, Coventry University, Coventry, UK, 2020.

[89] D. L. Gallup, "Advances in Oil-in-Water Monitoring Technology," in *Analytical Methods in Petroleum Upstream Applications*, 1st ed., C. Ovalles and C. E. Rechsteiner Jr., Eds. Boca Raton, FL, USA: CRC Press, 2015, ch. 3, pp. 51–58. ISBN 9780429170058. doi: 10.1201/b18109

[90] K. L. Jepsen, S. Pedersen, and Z. Yang, "Control pairings of a deoiling membrane crossflow filtration process based on theoretical and experimental results," *Journal of Process Control*. Elsevier, 2019, vol. 81, pp. 98–111, 2019. doi: 10.1016/j.jprocont.2019.05.009

[91] S. Pedersen, P. D. Løhndorf, and Z. Yang, "Influence of riser-induced slugs on the downstream separation processes," *Journal of Petroleum Science and Engineering*. Amsterdam, Netherlands: Elsevier, 2017, vol. 154, pp. 337–343, 2017. doi: 10.1016/j.petrol.2017.04.042

[92] P. Durdevic and Z. Yang, "Application of H_∞ Robust Control on a Scaled Offshore Oil and Gas De-Oiling Facility," *Energies*. Basel, Switzerland: MDPI, 2018, vol. 11, no. 2, p. 18, 2018. doi: 10.3390/en11020287

[93] E. K. Nielsen, M. V. Bram, J. Frutiger, G. Sin, and M. Lind, "A water treatment case study for quantifying model performance with multilevel flow modeling," *Nuclear Engineering and Technology*, H. G. Kang, Ed. Elsevier, 2018, vol. 50, no. 4, pp. 532–541, 2018. doi: 10.1016/j.net.2018.02.006

[94] Department for Business Energy & Industrial Strategy, "Methodology for the Sampling and Analysis of Produced Water and Other Hydrocarbon Discharges," United Kingdom Government Digital Service, London, UK, Tech. Rep., p. 84, 2018.

[95] M. Vallabhan and C. Holden, "Non-linear control algorithms for de-oiling hydrocyclones," in *2020 28th Mediterranean Conference on Control and Automation (MED)*, no. 978. Saint-Raphaël, France: IEEE, 2020, pp. 85–90. doi: 10.1109/MED48518.2020.9183115

[96] A. B. Sinker, M. Humphris, and N. Wayth, "Enhanced Deoiling Hydrocyclone Performance without Resorting to Chemicals," in *SPE Offshore Europe Oil and Gas Conference and Exhibition*. Aberdeen, UK: Society of Petroleum Engineers, 1999, pp. 405–413. doi: 10.2118/56969-MS

[97] T. Husveg, O. Rambeau, T. Drengstig, and T. Bilstad, "Performance of a deoiling hydrocyclone during variable flow rates," *Minerals Engineering*. Elsevier, 2007, vol. 20, no. 4, pp. 368–379, 2007. doi: 10.1016/j.mineng.2006.12.002

[98] M. V. Bram, A. A. Hassan, D. S. Hansen, P. Durdevic, S. Pedersen, and Z. Yang, "Experimental modeling of a deoiling hydrocyclone system," in *2015 20th International Conference on Methods and Models in Automation and Robotics (MMAR)*. Miedzyzdroje, Poland: IEEE, 2015, pp. 1080–1085. doi: 10.1109/MMAR.2015.7284029

[99] J. Coca-Prados, G. Gutiérrez-Cervelló, and J. M. Benito, "Treatment of Oily Wastewater," in *Water Purification and Management*, 1st ed., ser. NATO Science for Peace and Security Series C: Environmental Security, J. Coca-Prados and G. Gutiérrez-Cervelló, Eds. Dordrecht, Netherlands: Springer, 2011, ch. 1, pp. 1–55. ISBN 978-90-481-9775-0. doi: 10.1007/978-90-481-9775-0_1

[100] M. F. Schubert, F. Skilbeck, and H. J. Walker, "Liquid Hydrocyclone Separation Systems," in *Hydrocyclones*, 1st ed., ser. Fluid Mechanics and its Applications, Vol.12, L. Svarovsky and M. T. Thew, Eds. Dordrecht, Netherlands: Springer, 1992, pp. 275–293. ISBN 978-90-481-4180-7. doi: 10.1007/978-94-015-7981-0_18

[101] S. D. Noblitt, K. E. Berg, D. M. Cate, and C. S. Henry, "Characterizing nonconstant instrumental variance in emerging miniaturized analytical techniques," *Analytica Chimica Acta*. Elsevier, 2016, vol. 915, pp. 64–73, 2016. doi: 10.1016/j.aca.2016.02.023

[102] Dansk Standard, "Water Quality - Determination of Hydrocarbon Oil Index - Part 2: Method using Solvent Extraction and Gas Chromatography," ser. DS/EN ISO 9377-2, DS/ISO, Copenhagen, Denmark, Tech. Rep., p. 19, 2001.

[103] Eurachem/EUROLAB/ CITAC/Nordtest/AMC Guide, "Measurement uncertainty arising from sampling: a guide to methods and approaches," Eurachem, Torino, Italy, Tech. Rep., p. 102, 2019.

[104] R. Lava, F. Zanon, and L. Menegus, "Issues with monitoring and analysis of hydrocarbons in Italy," in *NEL Produced Water Workshop*. Aberdeen, UK: Nel, 2017, p. 41.

[105] Dansk Standard, "Olieproducter. Automatisk prøveudtagning fra rørledninger," ser. ISO 3171, DS/ISO, Charlottenlund, Denmark, Tech. Rep., p. 54, 1999.

[106] Dansk Standard, "Water quality – Sampling – Part 3: Preservation and handling of water samples," ser. DS/EN ISO 5667-3, DS/ISO, Copenhagen, Denmark, Tech. Rep., p. 52, 2018.

[107] R. M. Van der Heul, "Environmental Degradation of petroleum hydrocarbons," Master's thesis, Utrecht University, Faculty of Medicine, Utrecht, Netherlands, 2009.

[108] M. Broadwell, *A Practical Guide to Particle Counting for Drinking Water Treatment*, 1st ed. Boca Raton, FL, USA: CRC Press, 2001. ISBN 9781566703062. doi: 10.1201/9781420033038

[109] A. Sabin, "Problems in Particle Size: Laser Diffraction Observations," *Journal of GXP Compliance*. Burlington, MA, USA: IVT Network, 2011, vol. 15, no. 4, pp. 35–43, 2011.

[110] D. J. McClements, "Ultrasonic Measurements in Particle Size Analysis," in *Encyclopedia of Analytical Chemistry*, R. A. Meyer, Ed. Chichester, UK: Wiley, 2006, ch. 6, pp. 5581–5587. ISBN 978-3-527-31991-6. doi: 10.1002/9780470027318.a1518

[111] P. Scardina, R. D. Letterman, and M. Edwards, "Particle count and on-line turbidity interference from bubble formation," *Journal / American Water Works Association*. New York, NY, USA: Wiley, 2006, vol. 98, no. 7, pp. 97–109, 2006.

[112] Edinburgh Instruments, "Scattering," Livingston, UK, p. 1, 2018. [Online]. Available: https://www.edinst.com/blog/raman-scattering-blog/ (Accessed 2020-07-27).

[113] H. Masuda and K. Iinoya, "Theoretical Study on the Scatter of Experimental Data due to the Particle-Size-Distribution," *Journal of Chemical Engineering of Japan*. J-STAGE, 1971, vol. 4, no. 1, pp. 60–66, 1971. doi: 10.1252/jcej.4.60

[114] A. Jillavenkatesa, S. J. Dapkunas, and L.-S. H. Lum, *Particle Size Characterization: Recommended Practice Guide*, 1st ed., ser. NIST Recommended Practice Guide. Gaithersburg, MD, USA: National Institute of Standards and Technology, 2001. ISBN 9780756718503

[115] J. Chung and S. Wark, "Visualising Uncertainty for Decision Support," Joint and Operations Analysis Division Defence Science and Technology Group, Melbourne, Australia, Tech. Rep., p. 49, 2016.

[116] W. Foslien, "Abnormal Situation Management – Effective Automation to Improve Operator Performance," in *10th Annual Symposium, Mary Kay O'Connor Process Safety Center*, vol. 11, no. 3, College station, TX, USA, 2007, pp. 1–1.

[117] S. Guerlain, G. A. Jamieson, P. Bullemer, and R. Blair, "The MPC elucidator: a case study in the design for human-automation interaction," *IEEE Transactions on Systems, Man, and Cybernetics - Part A: Systems and Humans*. IEEE, 2002, vol. 32, no. 1, pp. 25–40, 2002. doi: 10.1109/3468.995527

Part II

Papers

Paper A

Online Quality Measurements of Total Suspended Solids for Offshore Reinjection: A Review Study

Dennis S. Hansen, Mads V. Bram, Steven M. Ø. Lauridsen, and Zhenyu Yang.

The paper has been submitted to,
Energies, MDPI, 2020.

MDPI

Review

Online Quality Measurements of Total Suspended Solids for Offshore Reinjection: A Review Study

Dennis Severin Hansen [1], Mads Valentin Bram [1], Steven Munk Østergaard Lauridsen[2], and Zhenyu Yang [1,*]

[1] Department of Energy Technology, Aalborg University, Niels Bohrs Vej 8, 6700 Esbjerg, Denmark; dsh@et.aau.dk (D.S.H.); sje@et.aau.dk (S.J.); mvb@et.aau.dk (M.V.B.)
[2] Total, Britanniavej 10, Esbjerg, Denmark; steven.lauridsen@total.com
* Correspondence: yang@et.aau.dk (Z.Y.); Tel.: +45-4128-7438

Version December 19, 2020 submitted to Energies

Abstract: The importance and awareness of accurate online water quality measurements increase every year in the oil and gas sector, whether it is for reducing oil discharge, preparing produced water for reinjection, or improving operational performance. For online measurement techniques to yield valuable analytical information, an understanding of their outputs must be established. Produced water reinjection has gained increasing attention in the last decade, as it can minimize negative environmental impacts by reducing oil discharge and has the potential to extend the reservoirs' economic life. To increase the amount of produced water that is able to be reinjected, the water must be maintained at a sufficient quality to prevent unintended formation damage. Although, the cost of treating the injection water should be justified against periodic well-stimulation. The review paper has thoroughly described different water quality issues related to suspended solids that can occur in an injection water treatment system and how the issues and challenges are often interlinked instead of being independent. A case study of measuring the total suspended solids concentration of seawater sampled from the Danish sector of the North Sea has been carried out to effectively quantify water quality through the process of an injection water treatment facility. Furthermore, numerous on- and in-line techniques have been evaluated as candidates for measuring suspended solids. The last part of the paper discusses future microscopy analyzers' considerations based on five promising online microscopy technologies.

Keywords: offshore oil and gas industry; water quality; total suspended solids; online monitoring; injection water treatment; environment

1. Introduction

Although energy consumption in developed countries is approaching a plateau and we are entering a new era of climate changes that must be reduced over the next several years, oil production is still expected to increase the next 30 years globally [1]. Several countries in Europe, such as Denmark, have the goal of being independent of fossil fuels before 2050 [2]. Even if Denmark achieves net-zero emission by 2050, Denmark's carbon dioxide (CO_2) emissions contribute only 1‰ (based on data from 2017) of the total global emissions, though the emission per capita in Denmark is still ∼26% higher than the average capita in the world [3]. Regardless, Denmark should strive to achieve the goal of becoming CO_2-neutral. Pioneering countries in climate actions can inspire other countries to increase their ambitions by international climate negotiations. Pioneering countries show the pathway by developing and maturing technologies that lower the transition cost outside the country. But if pioneering countries, such as Denmark, must contribute to the global climate action in the most effective way, "carbon leakage" is a crucial element; either way,

the risk of carbon leakage can undermine the effectiveness of the EU's emission mitigation policies [2,4]:

"... need to ensure that the Danish climate actions do not simply move the entire GHG emissions beyond the Danish borders [2]."

The climate consultant company, Klimaråd, highlights the importance of avoiding that the national climate actions lead to significantly increased emissions outside Denmark. Carbon leakage denotes the phenomenon that a stricter regulation of greenhouse gas (GHG)-emission in countries only causes the production to increase in other countries with more lenient legislation [2]. That can occur in three different ways, either by companies moving their production facilities abroad, Danish companies closing down due to the stricter regulations, or the companies reduces the production significantly [2]. In the latter cases, the carbon leakage occurs because foreign companies increase production inversely proportional to the Danish production decline. Thus, an incline in emissions can happen globally if the production by others has a higher carbon intensity rate. This would especially be the case of the oil and gas industry in the Danish sector, which has the lowest carbon intensity from the upstream processes in the world [5]. One can question whether Denmark can afford to prematurely stop oil production if it has a negative effect on GHG-emissions globally? According to the reflection from the European Commission:

"...to preserve the environmental benefit of emission reductions in the Union while measures by third countries do not provide the industry with comparable incentives to reduce emissions, transitional free allocation should continue to installations in sectors and subsectors at risk of carbon leakage [4]."

The European Commission has deemed the oil and gas industry to be at risk of carbon leakage and is allowed free allocation to at least 2030 [4]. Therefore, there is still a strong incentive to keep oil and gas production running in European countries and keep investing in reducing their GHG-emissions. Thus, the oil and gas industry can play a part in the transition to renewable energy globally. According to several studies, the rising demand for oil and gas is mainly due to future growth in energy demand from developing countries [1,6,7]. In the next coming years, millions of people in developing countries are estimated to buy their first refrigerator, air conditioner, and vehicle [6]. Regardless of the energy source selected, it requires developments of new factories, power plants, and grid infrastructure. This entails energy for construction of new buildings, an increased number of transportation and heavy goods vehicles, and demands of both new and existing products [6]. Despite a clear and increasing part of the energy comes from renewable sources, the energy demanded in developing countries is still expected to come from fossil fuels [1,6]. According to the "production gap"-report form 2019: by 2040, the production of oil would be 43% higher compared to the recommended low carbon pathways of 2°C proposed by the UN's Intergovernmental Panel on Climate Change (IPCC) [7]. With an increased population in developing countries and higher energy demand, the Energy Information Administration (EIA) predicts that by 2050, natural gas, crude oil, and other liquids would still account for 48.4% of all combined energy sources, unless radical actions occur, as shown in Fig. 1. Other liquids include all types of natural gas plant liquids, biofuels, etc. [1]. The total primary energy supply (TPES) in Fig. 1, refers to the total amount of primary energy from production and imports subtracting exported energy.

Countries, and especially developing countries, face a difficult trade-off between financial costs, availability, time horizon, environmental foot-print, social acceptance, and policy, all of which influence the decision to pursue one energy source over another [8,9]. Expanding energy services in developing countries while striving to significantly reducing global GHG-emissions is a challenging task that requires sensible decisions to balance between goals. On the one hand, there is a global goal of reducing climate change, and on the other hand, the expansion of energy services in the poorest countries is crucial to pursue the sustainable development goal number seven (SDG7): affordable and clean energy.

SDG7 has a significant impact on many of the other SDGs and are challenging to achieve without [8,9]. Without access to affordable and reliable energy, the productivity of modern agriculture and enabling the distribution of food becomes difficult [8]. It is also essential for the provision of public services, such as education and health care. Lack of access to modern energy services is one of the most significant contributors to poor health and continuing to increase the gap between the rich and poor. The lack of accessible modern energy has a particular effect on human health due to exposure from household air pollution and the use of inefficient stoves paired with wood, coal, and kerosene for cooking [10]. The UN estimates that lack of clean cooking is responsible for nearly four million premature deaths each year, with women and children at the highest risk [9,11]. Fig. 1 shows the EIA's projection if there is no radical change in energy extraction from 2019 to 2050, and the world population is rising as expected. The Data follows a reference case of economic growth of 3.0% per year and an average barrel price of 100$. Furthermore, the reference case includes anticipated changes over time, such as expected regional economic and demographic trends based on forecasters, planned retirements of constructions, changed infrastructures, and assumed incremental of cost-performance trends of known technologies based on historical trends [1]. Crude oil production is projected to be reduced by 5.5% in 2050 compared to the total energy production in 2019. However, the production of crude oil is still estimated to have an average annual increase by 0.6% from 2019 to 2050, even though membered European countries of Organisation for Economic Co-operation and Development (OCED) are estimated to have an average reduction of 4.0% annually from 2019 to 2050.

The presented results in Fig. 1 may be pessimistic, but if the trend just follows a fraction of the projection by EIA, then the oil and gas industry will have a significant impact on the world's energy consumption the years to come [7,13]. Therefore, oil and gas recovery strongly incentifies to continually invest in the most innovative solutions by improving energy efficiency and researching new technologies to minimize GHG-emissions [6]. The rapid growth of the world's population also poses a significant challenge to the world's freshwater supply. The water industry, energy production industry, and agriculture sector are drawing more freshwater from the already scarce freshwater resource in some areas and even contaminates in the process [14]. Wastewater that was once treated as "waste" is now considered a valuable "resource" [15]. An increase of reusing the produced water (PW) to replace freshwater for onshore reinjection processes can be economically and environmentally beneficial. The water-energy nexus is essential to achieve sustainable resource management and is increasingly becoming necessary for the successful realization of development and climate goals [8,14]. The energy sector is a large water user responsible for 10% of global water withdrawals and around 3% of total water consumption, with power plants as the far biggest consumer of 88% of the energy sector's withdrawals [16]. The last 12% of the total energy-water withdrawals come from primary energy production, such as coal, oil, natural gas, and biofuels, with biofuels as the most significant water user. At the same time, 4% of global electricity consumption is used to extract, transfer, and treat water and wastewater, along with 581.5MWh of energy sources, mostly gasoline, for running off-the-grid systems [16]. The energy demand for extracting, transferring, and treating water and wastewater is expected to double by 2040 [8]. Therefore, the importance and awareness of accurate online measurements of water quality increase annually, whether it is the water industry to enhance the drinking water quality and the wastewater disposal, or in the oil and gas industry to enhance the PW discharge or reinjecting it into the reservoir. The importance of offshore fields enlarges as the by-product of water production increases as they are maturing. According to literature, 70% of the world's oil production derives from mature fields [17,18]. As the general trend towards more sustainable production governed by discharge legislation imposing stricter policies, produced water reinjection (PWRI) has gained increasing attention to increase yield and reduce the discharge of oil [18–21]. PWRI has the potential to extend the reservoirs' economic life, decrease water discharge, comply with national and local regulations, and minimize negative environmental impacts. To increase the amount of PWRI, the quality of the injected water (both seawater and PW) must be high and consistent. Effective management of PW and injection water (IW) involves appropriate treatment,

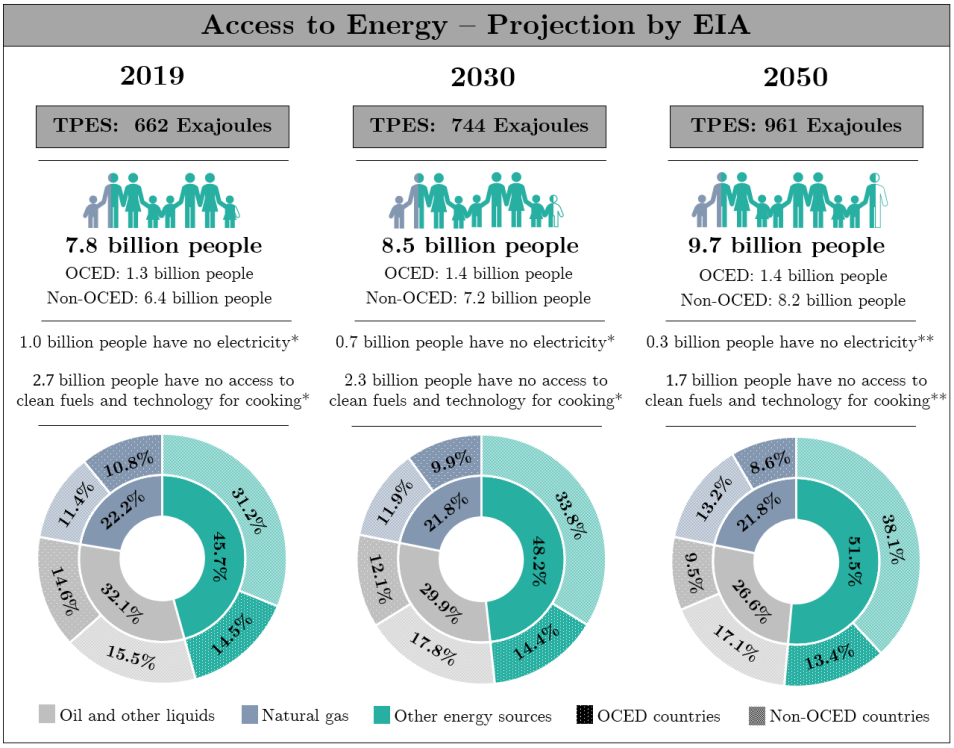

*Based on estimated data from International Energy Agency (IEA) [12].
**Assuming a continuing gain of 3.34% and 1.40% annually for access to electricity and clean-cooking, respectively, based on the projected data from 2016 to 2030 by IEA [12].

Figure 1. Presented data show the 2050 projection by EIA [13]. Totals may not equal the sum of components as a result of independent rounding. Oil and other liquids include all types of crude oil, natural gas plant liquids, biofuels, etc. [1]. With crude oil as the far biggest source predicted to account for ∼82% of the production annually from 2019 to 2050, where biofuels are predicted to account for ∼2%. Other energy sources cover coal, nuclear, and renewables, where renewables have the far biggest increase with an average gain of 3.1% in the world and are estimated to surpass energy consumption by oil and other liquids in 2047. Renewables accounted for ∼16% in 2019 and is estimated to accounts for ∼28% in 2050 of the energy consumed in the world.

discharge, and monitoring. Monitoring the PW discharge can also help to protect the receiving environment. Accurate water analysis is vital to gain an understanding of the dispersed matters of the PW and IW to identify changes in the process. Therefore, the operator must have confidence in the data measured by the monitors. Seen from an economic perspective, accurate information of the amount of oil and particles, their sizes, and classification of particles in the IW can be used for: decision support, reporting, or even advanced control to achieve better operation in the treatment process, all which benefits water-intensive operation [18]. Also, other water quality measurements could be beneficial to measure, such as oxygen concentration and different acid concentrations, although that will not be part of this review study.

This paper aims to examine the challenges associated with inadequate IW quality and what effect different water characteristics can have on a chalk reservoir in the Danish sector of the North Sea. Furthermore, the importance of accurate measurement of total suspended solids (TSS) will be discussed and based on what type of TSS monitor should be selected to provide useful information that

can increase the efficiency of the treatment process. Even though the different methods and designs of TSS monitors reviewed in this paper are related to offshore IW facilities, monitors for measuring particles can very likely be transferred to other domains, such as waterworks and biofuel facilities.

2. Waterflooding

An oil field is a natural hydrocarbon accumulation in pores of a underground porous media [22]. An oil field may contain several separated reservoirs linked together covering a large area. The phenomenon, which leads to the creation of an oil field, is roughly created by layers of sedimentary materials that are trapped under the weight of overlying layers, resulting in increased temperature and pressure, which induces various chemical reactions, transforming the organic materials into oil over millions of years [22]. Water and gas are together with oil trapped in the reservoir when the reservoir is connected to the surface by pipes, it will naturally transport oil due to the pressure in the reservoir is often higher than the hydrostatic pressure. The recovery factor (the recoverable amount of hydrocarbon initially in place) mainly depends on the viscosity of the oil, the permeability of the reservoir, the porosity of the reservoir rocks, and the reservoir drive [23]. The amount of oil produced by the reservoir drive is known as primary oil recovery. For increasing the oil recovery, an injection fluid can be injected to maintain the pressure and to sweep the reservoir. Waterflooding is defined as secondary oil recovery. However, this still leaves about $^2/_3$ of oil in place (OIP) [22]. In 1976 the tertiary recovery process was deployed called enhanced oil recovery (EOR):

"The additional recovery of oil from a petroleum reservoir over that which can be economically recovered by conventional primary and secondary methods" [24].

The main oil recovery stages are:

- Primary oil recovery: ∼(10-15)% of OIP
- Secondary oil recovery: ∼(15-33)% of OIP
- Tertiary oil recovery (EOR): ∼ 45% of OIP [22,25]

The optimization involved is not just increasing the oil recovery percentage, but rather increasing the recovery to cost ratio, as when the recovered oil has less value than operational cost, the operation is no longer profitable [24]. This should not be confused with enhanced recovery, which is considered to be a broader definition [22,25]. In fact, any method used to recover more oil from the reservoir than obtained by primary recovery is considered as enhanced recovery [24]. However, EOR methods are often referred to as tertiary oil recovery as it is the practical best way to evaluate the incremental amount of oil.

Today, 1% of the total oil discovered is roughly equal $^1/_2$ year of the world's energy consumption based on BP's statistical review from 2017 [26]. The 1% of total oil discovered is based on proved reserves. Thus, there is likely more oil left in the reservoirs, which could be economically profitable to extract in the future if: new reservoirs are found, industry practices are improved, new technologies are developed, or the oil price increases. The trend of increasing proved reserves is also supported in BP's statistical review from 2017, as the proven reserves have increased by 48.6% since 1996 [26].

One way of increasing the recovery cost ratio is by focusing on the IW, which has been known for several decades to play a massive role in improving the recovery process [27–33]. Back in 1880, the first waterflooding was executed at Oil Creek, PA (USA), but faced a lot of new and unforeseen issues at that time [28]. Some of the findings Carll [28], back in 1880, obtained from the first waterflooding trails was critical evidence that still today is considered for the modern design of water injection process:

"...oil and gas in their normal conditions, appear to lie in the sand-rock, not as distinct bodies occupying separate portions of the rock."

"...the flooding of an oil district is generally viewed as a great calamity, yet it may be questioned whether a larger amount of oil can not be drawn from the rocks in that way than by any other, for it is certain that all the oil cannot be drawn from the reservoir without the admission of something to take its place"

"...it must naturally travel the fastest towards the point of least resistance."

Due to the amount of new and unforeseen issues, the expended amount of capital usually ended in unproductive efforts to profitable extract enough oil, and the waterflooding method was postponed. First, in the late 1930s, the oil and gas industry rediscovered waterflooding as a potential method in the profitable restoration of old abandoned areas in Bradford and Allegany fields in the northern part of Pennsylvania and the southern part of New York state [29]. The interests in IW projects steadily increased until the late 1940s − early 1950s, where the progress was immensely accelerated, leading to the expertise of the injection water treatment (IWT) processes that exist today [27,30–33]. Already in the early years of waterflooding installations in the 1940s, they observed that the quality of the IW profoundly affects the recovery process [30,31].

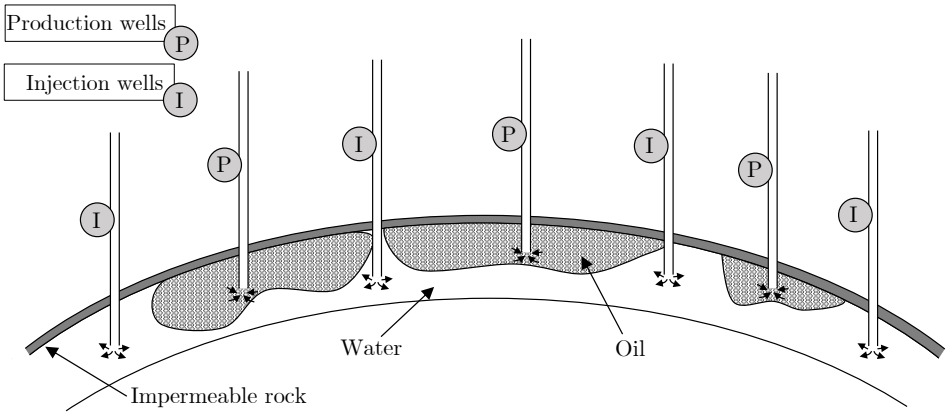

Figure 2. Cross-section of a typical large oil field with distribution of water injection.

The objective of any IW process is to maintain the pressure in the reservoir and to sweep the entire reservoir by injecting water into it without plugging the pores that would hinder the oil production process. Doubtlessly, it would not be useful to maintain the pressure in the reservoir if the production from the field is only the IW, which was one of the main issues Carll observed back in the 1880s. Therefore, the injection and production wells are carefully placed according to local conditions to prevent well short-circuits. Fig. 2 shows a cross-section of distributed water injection in a large field. As injection rates are proportional to oil production, the oil production rate can be affected if the water injection rate is too low to provide enough water volume for maintaining reservoir pressure [34,35]. Contrary, if applying pressures higher than the breakdown pressure of the reservoir, reservoir rocks will deform, and the fractures penetrate further down into the porous media [35]. It is, therefore, a challenge to secure the desired pressure is below the breakdown pressure.

Water quality is usually discussed in terms of plugging tendency, which further complicates the process [36,37]. Furthermore, it should be economically profitable to inject the water into the reservoir. The quality of the water should be completely free of reservoir plugging matters, and not lose the injectivity rate during the lifetime of the waterflooding. Besides, the IWT process must be protected against corrosion, erosion, and microbiological growth, which may lead to high maintenance costs for IWT equipment and extensive use of harmful chemicals [38]. Harmful chemicals are mostly defined in terms of toxic to the marine environment and the health of workers. However, chemicals can also be

harmful to the process, e.g., high concentrations of chlorine increase corrosion, and chemical reactions between mixed IW from different trains are likely to generate scales [39,40]. Ideally, IW should be non-scaling sterile fluids free of suspended solids and organic matter. However, fulfilling these water quality criteria will not be economically profitable, and the question is, therefore: What are the best economical strategies when balancing water quality and formation damage?

IWT most often involves several processes, as described in Sec. 4, such as filtering, additions of chemicals, and deoxygenation to achieve sufficient water quality, all of which affect the expenses of both CAPEX as well as OPEX. The sufficient water quality provokes economic incentives to reduce water quality to a required minimum. Conversely, inadequate water quality can result in dramatic formation damage [36,41]. OPEX is necessary to be addressed to establish an economic basis of the IW quality. OPEX includes chemicals, maintenance, human resources, and energy costs. Any changes in the desired water quality will consequently affect the cost. Reduced water quality requirements may reduce the OPEX, but will generally increase the CAPEX, as, e.g., replacement of instruments may happen earlier than intended. Therefore, the expense of obtaining and preserving good water quality must be balanced against the loss of accumulated production income as a result of decreased oil recovery rate [36,41].

According to different literature around 1980, seawater in the North Sea is generally has a high quality, with a concentration of $(0.2-0.8)$mg/L suspended solids, retained by a 0.8µm-filter [42,43]. However, without disparaging the work done back then, the knowledge and technology must be assumed to have advanced since then, and newer results indicate that the mean concentration in the North Sea is $2.6(3.5)$mg/L [44], where the parentheses indicate the standard deviation throughout 15-month periods covering the seasonal cycle [44]. The results are based on an area that spans from the northern part of Dogger Bank down to the Dover Strait to the eastern coasts of the North Sea to the coast of the UK ($51-56$°N and -2°W-9°E) [44]. Other literature indicate the concentration in the North Sea more loosely as offshore $<$2mg/L, inshore ($>$10mg/L), in shallow intertidal areas ($(50-100)$mg/L and up to 2000mg/L) and 20km offshore $\sim$4mg/L [45,46]. However, they all agree on using the suspended sediment concentration (SSC) analytical method for quantifying the concentrations of suspended-solids in 'natural' water (untreated water) instead of the TSS analytical method [44–47]. The difference is that the SSC analysis uses the whole volume collected, and the volume used is determined by weighing the sample container before and after filtration, where TSS uses subsamples often for making duplicates. The offset from the true value can be high, according to results from Gray et al. [47], The SSC median offset, from the known sediment mass, was $(2-4)$% negatively, where the TSS median had a negative offset of $(6-23)$%. The reason for the relative high deviation from the known sediment mass using TSS is the difficulty of collecting a representative subsample of the original sample when a substantial amount of sand-size particles is present compared to silt- and clay-sized particles. Even though a great amount of effort is put into stirring and shaking a subsample, the settling rate of sand-size particles is relatively fast, following Stokes' law, compared to smaller ones, especially particles finer than 11ϕ where Brownian motion interferes the settling [48]. Another issue of using the TSS method could be the agglomeration-effect of particles, which tends to stick to the sample container. Therefore, a common rule suggests that if the sand-size particles in samples exceed about a quarter of the dry sediment weight, SSC analytical method must be used instead of TSS [47]. Thus, the TSS method is still a valid method to use, especially for wastewater samples. Following the sand-sizing range terms defined by different literature, they all agree on sand-sizes ranges from $({}^{1}/_{16}-2)$mm [49–51]. The different terms of particle scale sizes and their corresponding classification from the cited literature is shown in Table 1. The percentiles in mm-transformation is given by the relation

$$\phi = Log_2 D, \tag{1}$$

were d is the diameter in mm of the measured sediment unit [52].

As previously described, water quality is usually discussed in terms of TSS and their plugging tendency. Other water quality characteristics can directly or indirectly affect the plugging increment and be part of the TSS concentration [37]. Thus, TSS concentration can consist of several water quality characteristics and mechanisms of formation damage. The various water quality characteristics, in terms of TSS, are described in Sec. 3.

Table 1. Particle size scales and terminology by different litterateurs [49–51].

mm	ϕ	Udden (1898) [49]	Wentworth (1922) [50]	Blott and Pye (2012) [51]
2048	-11		Bowlder gravel	Megaclasts
1024	-10			Very large boulder
512	-9			Large boulder
256	-8			Medium boulder
128	-7		Cobble gravel	Small boulder
64	-6			Very small boulder
32	-5		Pebble gravel	Very coarse gravel
16	-4			Coarse gravel
8	-3			Medium gravel
4	-2	Coarse gravel		Fine gravel
2	-1	Gravel	Granule gravel	Very fine gravel
1	0	Fine gravel	Very coarse sand	Very coarse sand
1/2	1	Coarse sand	Coarse sand	Coarse sand
1/4	2	Medium sand	Medium sand	Medium sand
1/8	3	Fine sand	Fine sand	Fine sand
1/16	4	Very fine sand	Very fine sand	Very fine sand
1/32	5	Coarse dust	Silt	Very coarse silt
1/64	6	Medium dust		Coarse silt
1/128	7	Fine dust		Medium silt
1/256	8	Very fine dust		Fine silt
1/512	9	(Clay)	Clay	Very fine silt
1/1024	10			Very coarse clay
1/2048	11			Coarse clay
1/4096	12			Medium clay
1/8192	13			Fine clay
				Very fine clay

3. Injection Water Characteristics and Formation Damage Mechanisms

Two factors determine the sufficient quantities and acceptable quality of the IW: the geological formation and geographical location of the reservoir [53]. A reservoir with high porosity and high permeability tends to sustain its injection rate longer [54].

Porosity is a measure of the pore volume between sediment grains in the reservoir that can contain fluid or gases, and the permeability is a measure of the flowability through the reservoir rocks. The volume of oil, gas, and water in a given reservoir depends directly on porosity. The porosity value is higher when the sediment is well sorted and has a well-packed structure. Porosity is the ratio of the pore volume, V_p, and the total volume, V_T, of the reservoir sediment/rock.

$$\Phi = \frac{V_p}{V_T} \cdot 100 \tag{2}$$

The permeability is also higher in well-sorted sediment, but depends highly on the grain size, due to the fluid flows easier in large pores than in small ones. Permeability, therefore, indicates how easy it is to produce oil or gas. It is mathematically expressed with Darcy's law:

$$k = -\frac{q\mu\Delta L}{A\Delta p}, \tag{3}$$

where k is the permeability, q is the flow rate, μ is the fluid viscosity, A is the cross-sectional area measured volume, Δp is the pressure drop, and ΔL is the length of the measured volume. Permeability is often measured in millidarcy (mD), and the permeability of oil and gas reservoirs are in a range of $(0.1-3000)$mD [55]. The Danish sector of the North Sea is estimated to have a relatively high porosity of $(34-40)$%, but a low permeability $(0.1-10)$mD [56,57]. The low permeability is due to formation of Danish reservoirs often consist of chalk. Chalk reservoirs are mainly composted of single-crystal lathes of calcite produced by the disaggregation of coccoliths [58]. These pore throat sizes range from $(0.1-1)$µm [58,59]. The presence of TSS in the IW can result in rapid injectivity reduction of the injection well, especially due to pore throat sizes in chalk reservoirs. Predicting the well impairment from TSS has been investigated in several studies [60–62]. A common method to estimate the injection time before stimulation of the well is often defined as the injection well half-life. The cost of IWT should, although, be justified against periodic well-stimulation.

For determining the different influences of the IW quality, a block diagram is illustrated in Fig. 3, followed by a description for each of the IW's characteristics and their formation damage mechanisms. Fig. 3 only describes the main root cause's mechanisms of formation damage by the different water quality characteristics, and different mechanisms may interact.

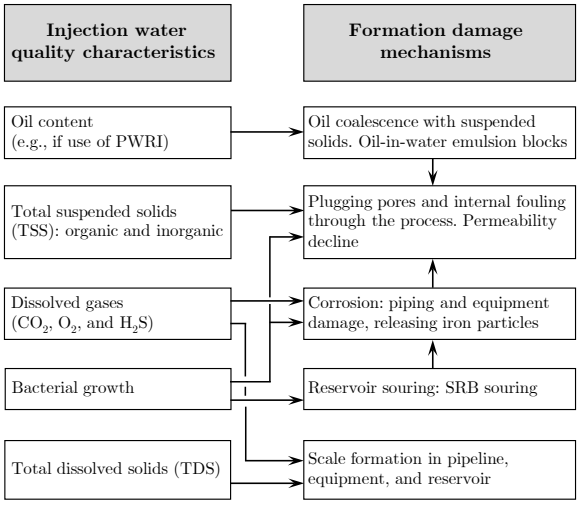

Figure 3. Main potential water quality characteristics and mechanisms of formation damage.

The quality of the IW utilized from different geographical locations varies based on the tolerances of the formation. To secure the quality of the IW fulfills certain criteria for the specific formation, operators must have confidence in the data generated from the measurement equipment, and false data can, therefore, be more harmful than no data [41,63,64]. Injecting water into the reservoir can result in various critical challenges, such as emulsion block, fouling, corrosion, souring, and scale formation. These challenges can be managed and accounted for if proper and reliable monitors are installed to indicate the arising tendency for these challenges occurs [36]. Other important properties

of water is the effect of temperature, acidity, and salinity. The main IW quality characteristics are described in the following subsections: Oil Content 3.1 , Total Suspended Solids 3.2, Total Dissolved Solids 3.3, Dissolved Gases 3.4, and Bacterial Growth 3.5.

3.1. Oil Content

Historically, mostly seawater has been used as IW, but due to the increasing environmental awareness, the discharge policy may require PWRI by means of further reducing the discharge of crude oil. According to the literature, zero discharge policy has become the norm in the industry [19,20,65]. However, in far most cases, there is not enough PW to satisfy injection demands. Therefore, the solution is often a mixture of PW and seawater [66]. In Denmark, 37.5 million m^3 of water was produced, and 44.4 million m^3 of water was injected during 2009, of which $\sim 1/3$ of the IW was reinjected PW [67,68]. Currently, in 2019, Gorm-field is the only field from which PW is expected to be reinjected the next five years, as there are technical reservoir challenges in PWRI at other fields in the Danish sector of the North Sea [69]. According to the Danish Environmental Agency [69] 4.8 million m^3 was projected to be reinjected; thus, only 14.5% of the total 33.0 million m^3 IW was expected to consist of PW in 2019.

As the water cut in the Danish part of the North Sea steadily increases annually and has reached 80% in 2015, as shown in Fig. 4, a high amount of energy is required to handle these large volumes of PW. For some of the matured fields, the water cut even exceeds 90% [54,70,71].

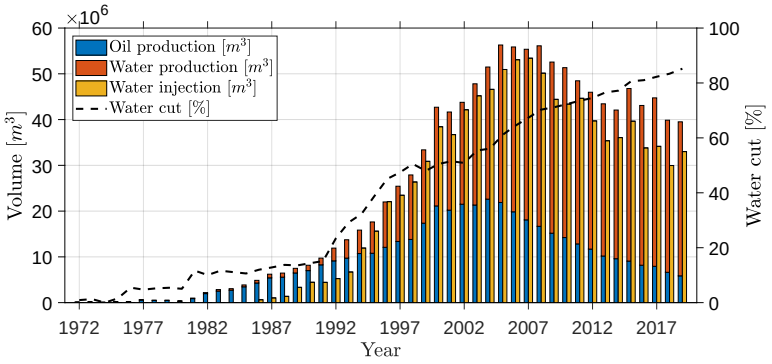

Figure 4. The bar chart shows the yearly oil and water production, water injection, and the water cut. The production data are based on annual reports from the Danish part of the North Sea, published by Danish Energy Agency 1972-2019 [72].

Another issue is the increasing water-cut in the North Sea discharge. The current North Sea discharge legislation states that the dispersed oil concentration in water must be less than 30 parts per million (ppm) and the Danish Environmental Protection Agency furthermore states that the total amount of discharged oil in the Danish sector of the North Sea must be less than 222 tonnes per year in 2017/2018 [65–67,73]. As an increasing amount of water is produced, the limit of the total discharged oil becomes more significant, especially as some oil producers in the Danish sector of the North Sea in 2015 reached 96% of the total amount of discharged oil [65,73]. In 2014 the Oslo and Paris convention (OSPAR) commission reported that 16 installations failed to meet the 30ppm discharged legislation, where each of the installations exceeded an annual average concentration of dispersed oil discharge [74]. Several of them reported that the reason for not achieving the standard was due to PWRI failure. Based on this, it seems that they do not consider the concentration of oil when reinjecting, even though different studies states a common guideline for injection PW containing oil should be below 5ppm

[36,40].

Unfortunately, mixing seawater and PW can result in several other complications than just the presence of crude oil. PW contains crude oil, other organic nutrients, and purification chemicals from the upstream production process, which may result in ideal conditions for bacterial growth, an increment of scales, and corrosion in the IWT process [19]. Another considerable issue of crude oil content is the deposition of suspended organic solids, such as asphaltenes, which have been shown in the literature to decrease the oil production to such a degree that few have prematurely stopped producing in Saudi Arabia [75]. Bacterial growth, scales, corrosion, and asphaltenes will be described in the subsections: 3.2, 3.3, 3.4, and 3.5.

As there is an increasing focus on PWRI, it is relevant to consider the influence of the water quality when oil is present in the IW. The crude oil can reduce the injectivity in several ways, e.g., emulsion blocks and flocculation, where the oil droplets work as an agglomeration whereby particles form larger-sized clusters that can block pores in the porous media. Emulsions are formed when a mixture of oil and water are exposed to intense mixing [75]. This intense mixing creates high shear forces and leads to stable OiW emulsions.

3.2. Total Suspended Solids

To determine whether or not a particle is defined as part of TSS or total dissolved solids (TDS), it is essential to address the standard definition for the examination of water and wastewater determined by the American Public Health Association, American Water Works Association, and Water Environment Federation [76]. The overall definition of TSS and TDS is called total solids, which is defined as:

Total solids – The material left in a sample vessel after evaporation and subsequent oven drying at a defined temperature. Total solids include both total suspended and total dissolved solids, which are physically separated via filtration whether a solids particle is filtered into the "suspended" or "dissolved" portion principally depends on a filter's thickness, area, pore size, porosity, and type of holder, as well as the physical nature, particle size, and amount of solids being filtered [76].

Thus, TSS and TDS are defined as:

TSS – the portion of total solids in an aqueous sample retained on the filter. Note: Some clays and colloids will pass through a 2µm filter [76].

TDS – the portion of total solids in a water sample that passes through a filter with a nominal pore size of 2.0µm under specified condition [76].

If only considering the *"Total solids"*-phrase, particles retained by the selected filter are considered as TSS. Thus, TSS can consist of any substances that are present in seawater and PW: inorganic materials, microorganisms, shells, scales, asphaltenes, clays, etc. Contradictory, TDS (TSS that passes the filter) can also represent a wide range of substances and thereby cause different complications further in the treatment process or formation damages.
However, the *"TSS"*- and *"TDS"*-phrases include extra information that the nominal pore size of the filter must be 2µm, this conclude that portion of total solids retained by a 2µm-filter is considered as TSS and matters that passes through the filter is considered as TDS. This definition might be confusing and problematic when other papers address TDS as "dissolved", which usually refers to a solvent that is soluble in a solution, like salt in water or at least TSS above the molecular range [77]. Table 2 provides an overview of different literature's definition of TDS and TSS. The rest of this work only defines TDS as materials that are soluble in water and TSS as any suspended solids that can be

captured by a filter.

Table 2. Different definitions of TSS and TDS.

Definitions of TSS and TDS used in different studies	Source
TDS defined as materials that are soluble in water	[63,66,77]
TDS defined as materials that passes through a 2µm-filter	[78,79]
TDS is indirectly defined as materials that are soluble in water	[54,80,81]
TDS is indirectly defined as materials that passes through a 2µm-filter	[32,36,82,83]
Too uncertain to tell	[40,53,84,85]

TSS is considered a significant issue that reduces water quality and injectivity [85]. TSS' progression through the porous media is a complicated process, which is determined by several factors such as shapes, sizes, the concentration of TSS, the chemistry of the carrying fluid, the mobilization in the reservoir, the porosity, and pore space in the reservoir. A combination of all influences acting upon the TSS affects the outcome of the TSS' progression through the porous media, whether they pass through the porous media or becomes a part of the plugging mechanisms [54]. The flow rate of the carrying fluid also affects the travel distance of particles inside the porous media. Larger TSS tends to settle faster than smaller ones, and TSS with higher density difference between particles and carrying phase tends to settle faster than lighter ones [54]. Plugging mechanisms distinguish between internal or external cake formation. External cake formation potentially consists of larger particles sealing the pore throat either by itself or by bridging, and internal cake formation happens when small particles invade the pore throats and settle within the pore bodies, either by bridging or decreasing the pore volume due to adsorption or sedimentation [85,86]. Deposited particles reduce the flowing path inside the porous media, thus increasing the possibility of bridging [54]. The four main different plugging mechanisms are illustrated in Fig. 5.

Ideally, a filter system that can persistently clean water from TSS will massively reduce the possibility of cake formation in the reservoir and bacterial growth, which will further reduce corrosion in the system. However, this will likely not be economically feasible. Therefore, some significant factors influencing the overall cost of selecting the right cost-effective filtration system must be treated: reservoir medium size distribution, filter pore size distribution, critical flux of the filters, filtration cost, filtration replacement frequency, maintenance, chemicals, and energy use [87]. The most crucial factor the filter has to fulfill is to secure no or minimum clogging of the porous media in the reservoir. Therefore, filters are selected based on the reservoir porosity/size distribution and a desired bridging factor, like Abrams rule [88]. From literature, filters operating below the critical flux is more economical because of lower energy requirements [86,89]. Filtration below the critical flux is also desirable, as fouling remains irreversible, and the filtration system can be operated in a clean regime. Reducing the pore size of the filters reduces critical flux, and the filtration system is forced to perform a cleaning procedure more frequently. Operation above the critical flux causes fouling, which reduces the critical flux over time.

Bridging of particles is a commonly known phenomenon [43,54,90]. Abram proposed as a rule-of-thumb that particle larger than $^1/_3$ of the pore diameter can bridge at pore throats and form an external filter cake, and particles smaller than $^1/_7$ of the pore diameter are carried through and cause no damage [54,91]. This has, for several years, been generally acceptable guidance for selecting the right filter for the treatment process. However, several experimental studies have proved that due to the complex nature of porous media, a simple norm is inadequate for describing filtration limit [40,85,88,90]. Van Oort et al. [88] suggested to adjust the $^1/_3 - ^1/_7$ rule-of-thumb, based on

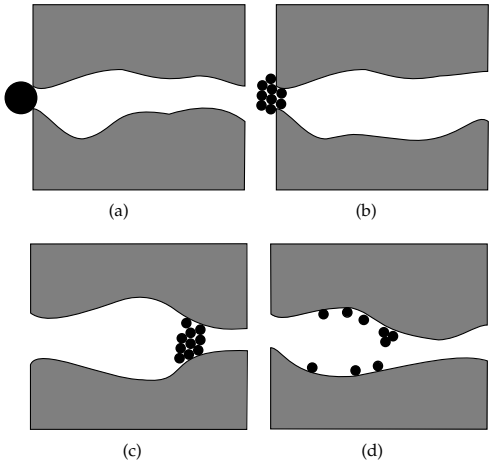

Figure 5. A set of the four main different plugging mechanisms that can occur in the porous media: (a) illustrates complete external cake formation by single suspended solid; (b) illustrates internal cake formation due to small suspended solids bridging; (c) illustrates external cake formation due to larger suspended solids bridging; and, (d) illustrates internal cake formation, either due to adsorption or sedimentation.

new investigations, to $^1/_3 - ^1/_{14}$, which may be more applicable especially at low injection velocities. Newer investigations of TSS have observed, in laminar flow, stable bridging of particles with sizes below $^1/_{14}$ of the pore size in porous media [85]. A fundamental issue of using the $^1/_3$ rule-of-thumb for IWT processes arises as Abram rule only defines that particles should be at least $^1/_3$ of the pore's size to effectively form bridging and not the opposite [91]. This does not conclude that particle below $^1/_3$ of the pore size cannot form a stable bridge and creating cake formation, which some newer studies also indicate by concluding that internal cake formation happened for particles blow $^1/_{14}$ of the porous media pore size distribution [40].

The selection of optimum filtration criteria would suggest a filtration pore size distribution of $^1/_{14}$ of the porous media pore size distribution. Though, this is likely impractical and not economically feasible, especially not in chalk reservoirs due to its small pore sizes. A conservative filtration criterion is suggested by Pautz et al. [90] on $^1/_5$ of the media pore size that usually provides acceptable long-term injectivity.

As TSS represents a wide range of substances, some types of TSS may not be readily removed by the filtration, like asphaltenes. Asphaltene is the heaviest component in crude oil [92]. Under the initial condition of the reservoir, asphaltene is dissolved in crude oil, but as the reservoir is exposed to changes in temperature and pressure, it may affect the asphaltene to precipitate from the crude oil [85]. Asphaltene has the ability to form a viscous coating layer on filter elements in the transportation pipelines and the reservoir. Asphaltenes are also known to stabilize emulsions [75]. As mentioned in subsection 3.1, several wells in some fields in the northwestern part of Saudi Arabia have shown an atypical productivity decline. Production was halted even at water cuts as low as 25%. The results of that study describe the primary cause of the atypical productivity decline is due to the asphaltene present in the reservoir that plugs the porous media [75].

Asphaltenes are highly polar and tend to have an attraction property, as individual micelles attract one another, forming large particle sizes of asphaltenes [85]. Consequently, usual filtration media are often ineffective in removing asphaltene, as the individual asphaltene particles break up in order to pass and coalesce on the other side. The coalescence is very time-dependent, making long

transportation pipelines a good condition for coalescence to occur after the filtration process. Some systems have recorded particles up to 100 times the sizes of particles expected after the filtration system further down the treatment process [85].

Another suspended particle that has a unique behavior as asphaltene is clay. Clay swelling has, for a long time, been recognized as causes of formation damage in the reservoirs [40,92–95]. Clay minerals are extremely small platy-shaped particles smaller than 8ϕ as shown in Table 1 [92]. Even though clay-related problems are often mentioned in relation to well-operation, such as drilling processes, they also occur in the injection processes of waterflooding [93,94]. Reduction in permeability due to clay swelling occurs as a result of decreases in pore body or pore throat size as the volume changes of the clay [94,95]. The phenomenon of clay swelling is a negatively charged imbalance in the clay structure which are stabilized by substitution of a positively charged cation (i.e., Na^+, K^+, Ca^{2+}, Mg^{2+}) into the gap between the individual clay crystals [40]. If an insufficient concentration of these ions is not present around the clay, water can, due to its polar nature, interact with the clay. This causes the clay to physical swell and can cause severe reductions of the permeability in the reservoir as it can expand up to 20 times their original volume [96]. Another phenomenon of clay action is clay deflocculation. Clay deflocculation is caused by the disruption of electrostatic forces, which are causing the clay to be attracted to each other and act as agglomeration for other particles. This phenomenon is described in Fig. 5 as adsorption [40]. Other causes, due to the expansion of the clays, have also been reported to disengage from the pore walls as the clay is swelling and can consequently be transported further down in the pore body until it hits the pore throat area. Thus, they additional acts to bridging or complete pore blocking [40,93].

3.3. Total Dissolved Solids

TDC concentration is a quantification of the cations and anions in the IW. A high concentration of TDS in the IW can cause scales to build up in pipelines and instruments. Scales increase the injection resistance, resulting in a decrease of injectivity over time. In the worst case, it will completely plug the injection trains and equipment. Other consequences could cause equipment failures, emergency shutdowns, increased maintenance costs, and seen from a production point of view; decreased production efficiency [97]. Scale deposition can occur due to supersaturations of the IW. However, supersaturation does not necessarily produce scales; there must be a presence of nucleation. A supersaturated condition is the primary cause of scale formation and occurs when a solution contains dissolved materials that are at higher concentrations than their equilibrium concentration [98]. Supersaturation can be generated in water by changing the pressure and temperature conditions or by mixing two incompatible water types [99]. Changes in pH, CO_2, and hydrogen sulfide (H_2S) could also induce scale formation [99]. Seawater can contain a significant concentration of sulfate (SO_4^{2-}) and carbonate (CO_3^{2-}) ions, while formation water contains cation ions of calcium (Ca^{2+}), barium (Ba^{2+}), and strontium (Sr^{2+}) [100]. When these two water types mixes, supersaturation can occur, which causes calcium carbonate ($CaCO_3$), calcium sulfate ($CaSO_4$), strontium sulfate ($SrSO_4$), and barium sulfate ($BaSO_4$) to deposit within the reservoir rock, as shown in Fig. 6 [100]. Other less common scales have also been reported, such as iron oxide (Fe_2O_3), iron sulfide (FeS), and iron carbonate ($FeCO_3$) [100,101].

3.4. Dissolved Gases

Seawater contains different dissolved gases, were the troposphere is the primary source of gases to seawater. The gases enter or leave the ocean by exchange across the interface between seawater and troposphere [102]. Dissolved gases in the injection process can result in several complications. The two main reasons for removing/reducing dissolved gases are corrosion and the growth of aerobic organisms. There will only be focused on corrosion influenced by dissolved gases in this subsection.

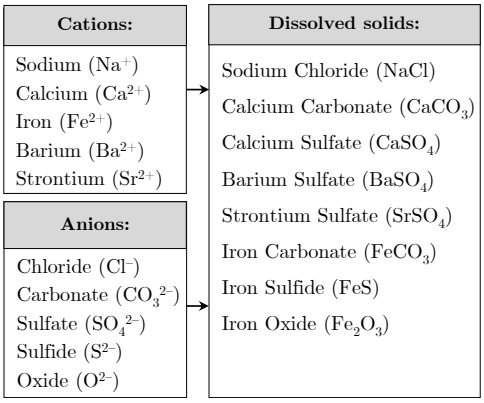

Figure 6. Chemical formula and formation of mineral scales.

The presence of oxygen (O_2) in the IW and its effects on aerobic organisms will be addressed in the subsection 3.5.

The three main dissolved gases that cause corrosion in the oilfield industry are O_2, CO_2, and H_2S [103–105]. When CO_2 and H_2S are dissolved in the water, they form acids. As the concentration of CO_2 and H_2S increases, the pH of the IW will continue to decline, and creating a corrosive environment [63,106]. In the oil and gas industry CO_2-corrosion is often referred to as sweet-corrosion and H_2S-corrosion to as sour-corrosion, where the presence of O_2 can be several times more corrosive than CO_2 and H_2S [107,108]. A comparison between different concentrations of O_2-, CO_2-, and H_2S-gases in water shows that O_2 is 80 times and 400 times more corrosive than CO_2 and H_2S, respectively [103,108]. Corrosion detected in the oil and gas industry involves several mechanisms divided into three different corrosion effects: electrochemical corrosion, chemical corrosion, and physical corrosion, where each corrosion effect covers several types of corrosion [109,110]. Fig. 7 lists some of the corrosion types that can exist. However, this study will not cover each corrosion type, but only draw attention to the existence of different corrosion effects mentioned in different papers [103,106,107,111].

Electrochemical corrosion	Chemical corrosion	Mechanical effects
Galvanic corrosion	Sour corrosion	Cavitation corrosion
Crevice corrosion	Sweet corrosion	Erosion corrosion
Stray current corrosion	Oxygen corrosion	Environmental induced cracking
Pitting corrosion	Concentrated brines	Corrosion fatigue
Intergranular corrosion	Biological effects	Fretting corrosion
Uniform corrosion	Strong acids	

Figure 7. Categorized corrosion effects.

Corrosion has a huge economic impact on the industry; its influences are estimated to cost billion USD annually in the US and explicit 1.3$ billion annually in the oil and gas industry in the US alone [103–105,107]. 43% of the corrosion impact is roughly due to surface pipeline and facility costs, 34% in downhole tubing expenses, and the last 23% in CAPAX related to corrosion [104]. Corrosion is a natural mechanism, as metals tend to return to their natural state by reacting with oxidizing agents present [112]. For corrosion to occur, it requires four elements: anode, cathode, electrolyte, and a metallic/electronic path [110,113]. All metals have a tendency to dissolve or corrode to a greater

or lesser degree; the process is illustrated in Fig. 8 [103]. A typical corrosion process occurs as two dissimilar metals are present in an electrolyte. The anode is the metal that forms the negative pole, and the metal that forms a positive pole is the cathode. The conducting solution (IW) is the electrolyte, and the return path for electronic current flow is through the pipeline-metal between the anode and cathode, as shown in Fig. 8 [113].

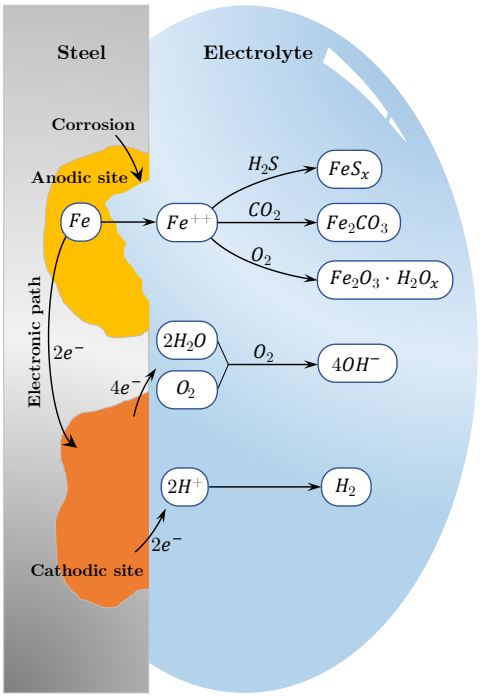

Figure 8. Corrosion on a steel surface due to reaction with the reaction fluid, present of O_2, CO_2, or H_2S. Inspiration from [103].

Anodes and cathodes can form on a single piece of metal that consists of slightly different compositions. The different compositions can be next to each other or very far away (several kilometers) [103]. As the anodic site releases electrons to the cathode site, Fe^{2+} reacts either with O_2, CO_2, or H_2S, which forms the corrosion products: iron sulfide (FeS_x), iron carbonate ($FeCO_3$), or iron oxide ($FeO_3 \cdot H_2O_x$), that often is referred to as rust or corrosion deposits [103,107,108]. However, if no dissolved gases are present to react with Fe^{2+} the tendency to dissolve will heavily be diminished. The O_2 level required to prevent corrosion must be lower than 0.02ppm, as O_2 concentrations above 0.025ppm accelerates corrosion, according to different studies [43,114,115].

Wall thickness reduction is the most considerable risk for pipeline failures [116]. According to data in the period of 1994 – 1999 shows that 25% of all accidents were due to corrosion in transportation pipelines [117]. When corrosion products are not deposited on the surface of the pipelines, very high corrosion rates can reduce the pipeline wall thickness several millimeters per year [106]. Fig. 9 shows three gas concentrations as a function of corrosion rate on carbon steel per year. It clearly shows that over time, with no maintenance, the wall thickness is reduced to such a degree by corrosion that the pipeline will crack in the corroded area causing leaks or damage to the entire pipeline [118,119].

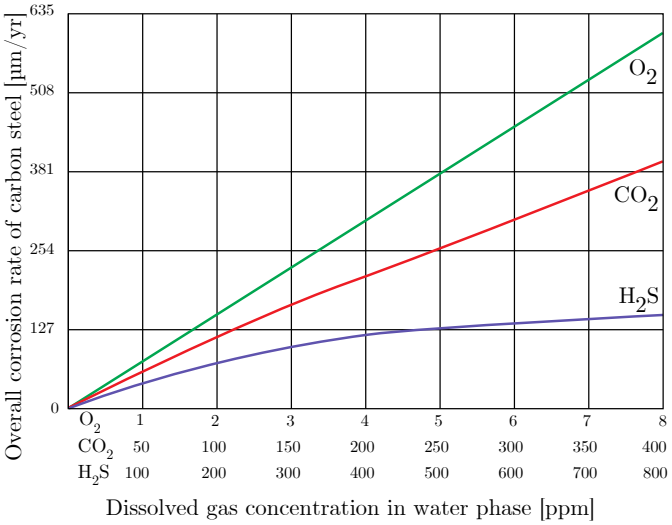

Figure 9. Comparison of corrosion rates exposed to different concentrations of O_2, CO_2, and H_2S disolved in water [103]. Schlumberger. All rights reserved.

The deposit formation of corrosion is another side-effect that acts as TSS; even if the IW is free from TSS after filtration, the TSS concentration can increase through the process [114]. Changes in the internal surface roughness can be another side-effect of corrosion. The pipelines' internal surface roughness is a pipeline system design criteria, and changes of surface roughness can have an economically expenses. Surface roughness influences the flow characteristics in a pipeline by creating unfavorable pressure and energy losses due to friction [120].

3.5. Bacterial Growth

Although the significant effects of microorganism activities in the oil and gas industry were recognized a long time ago, little is known about the effects in the reservoir when continuously introducing microorganisms via waterflooding [121–123]. Microorganisms can cause or contribute to plugging pores and internal fouling throughout the process, and accelerate corrosion of pipelines and equipment. Microorganisms are a highly diverse group of microscopic single-celled organisms and viruses. However, viruses are not considered as an issue in the oil and gas industry as they are extremely small, mostly ranging from $(0.02 - 0.4)$µm, and viruses are not considered as living organisms as, unlike bacteria, viruses cannot reproduce on its own [124,125]. Microorganisms, other than viruses, fall into two classifications: the prokaryotes and eukaryotes. Prokaryotic microorganisms include bacteria and archaea, and eukaryotic microorganisms include algae and fungi [126]. It is estimated that there exist $(4 - 6) \cdot 10^{30}$ prokaryotic microorganism types worldwide and $1.2 \cdot 10^{29}$ occur in the ocean [127,128].

Classification of bacteria are essential for identifying which bacteria are present. Fig. 10 shows how the classification often is carried out [130]. Classifying bacteria is often started on the morphological elements of the organisms, such as shapes, sizes, and colonies, as shown in Fig. 11 [129].

Together with the gram strain method, gram-negative and gram-positive, the microorganisms can be classified into different groups based on the morphological elements. Gram-positive cell walls have a thick murein layer and a cell membrane, whereas gram-negative cell walls have an outer membrane and a thinner murein layer. The gram stain method then stains the gram-positive microorganisms' violet and the gram-negative microorganisms pink, due to their murein layer. Other

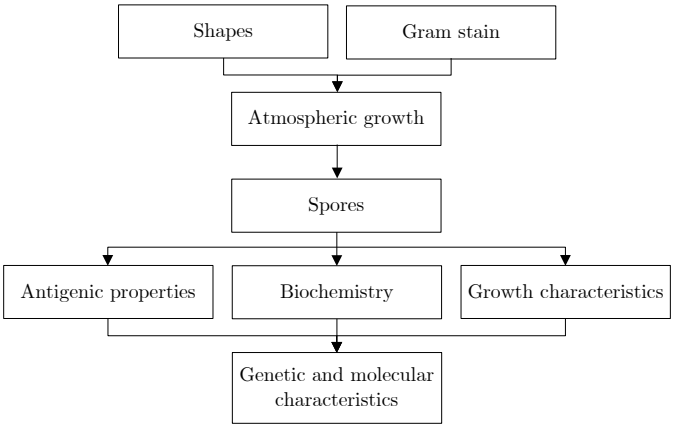

Figure 10. Bacterial taxonomy: classification and identification methods [129].

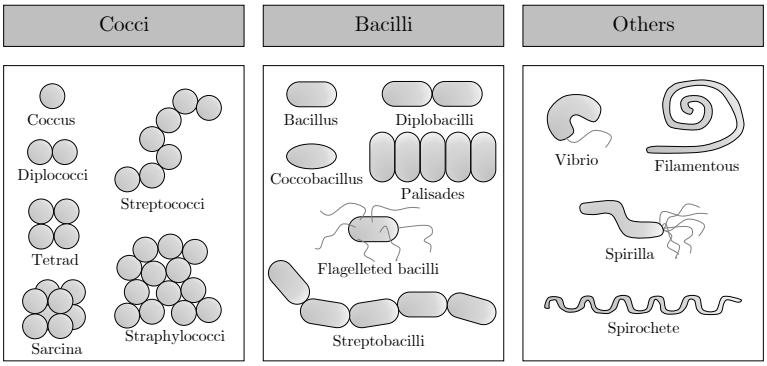

Figure 11. Bacteria come in a variety of shapes, the most common being varieties of cocci and bacilli. Cocci have a spherical, ovoid, or generally round shape and can occur singularly and as groups. They have the ability to stick together and form a pair (diplococci), in long chains (streptococci), and irregularly shaped clusters (staphylococci). Rod-shaped bacteria are called bacilli and occur as single rods or in long chains. Spiral- or helical-shaped bacteria are called spirilla, and vibrio has a curved-rod shape (comma shape) [131].

steps for classifying the microorganisms are based on their atmospheric growth, biochemical properties, antigenic properties, and growth characteristics, such as temperatures and pH. Most recently, next generation sequencing (NGS) is used to understand the evolution of bacteria and their connections to other organisms [129].

Microorganisms require water, nutrients, and electron acceptors for growing, where growth involves both an increase in the size and population [132]. Different bacteria have evolved to grow and survive in widely differing habitats. Whereas nearly all eukaryotic organisms require O_2 to multiply, many species of bacteria can grow under anaerobic conditions [79]. Bacteria are frequently classified in terms of:

- Obligate aerobic bacteria require O_2 to multiply.
- Obligate anaerobic bacteria multiply in the absence of O_2.
- Facultative anaerobic bacteria can multiply in both the present and absent of O_2 due to its metabolism.

- Microaerophilic bacteria need the presence of O_2. Though, at high concentrations of O_2, they are poisoned.
- Aerotolerant microorganisms multiply in the absence of O_2. Though they are not poisoned by O_2 [132].

Even though obligate anaerobic microorganism cannot grow in an O_2 environment, an excellent place to live for an anaerobic organism is below an active colony of aerobic organisms as these consume the O_2 and create anaerobic zones, which serve as habitats for the anaerobic microorganisms [133]. Thus, obligate anaerobe microorganisms, such as sulfate-reducing bacteria (SRB), that are susceptible to O_2 can survive and multiply below aerobic habitats as they are protected by aerobic organisms [133].

Temperature greatly influences the growth and survival of microorganisms. For each specific type of microorganism, there is a minimum temperature below which growth no longer occurs, an optimum temperature range at which the growth is most rapid, and a maximum temperature above which growth is not possible. Other influences on the growth of microorganisms are the pH and salinity concentration.

Most types of marine bacteria can grow in temperature ranging from $(0-40)^{\circ}$C, although some types can survive even above 100°C [40,134]. Even when deep formations surpass temperatures for bacterial growth, in many cases, around the injection wells, a temperated formation can occur due to the long-term water injection. This may result in severe bacterial growth problems down in the reservoir, especially if a biological activity was not considered as an issue [40].

When microorganisms play a role in IWT processes, they are often referred to as microbially influenced corrosion (MIC) and biofouling. MIC has become an acknowledged phenomenon in the oil and gas industry the last decades, starting back in the early 1990s, even though there has been an awareness of maintaining a degree of microbial cleanliness in the IWT processes long before that [121,135,136]. MIC is estimated to account for (20−30)% of all corrosion-related costs in the oil and gas industry, and other studies even report it to account for 50% of the total cost of corrosion [119,121,136,137]. Microorganisms do not produce unique types of corrosion; instead, they accelerate some of the corrosion types mentioned in subsection 3.4, like pitting and stress corrosion [136]. One of the most recognizable presence of MIC is related to reservoir souring, which defines the increasing H_2S level as mentioned in subsection 3.4, especially in a reservoir that initially did not consist of any H_2S [138]. The increasing level of H_2S is often a result of SRB growth in the process.

Biofouling activities in IWT processes can cause materials deterioration and mechanical blockages of fluid transport systems that are consequently increasing energy consumption [139]. Often, biofouling activities in IWT processes are referred to in the filtration system. Biofouling has been known as a contributing factor to more than 45% of all filter fouling and has been reported as a significant problem in membrane filtration by reducing flux rates, increasing the amount of reject water, decreasing permeate quality, and ultimately causing a reduced lifetime of membrane elements [140].

For both biofouling and MIC, biofilm is the root cause. A biofilm is an agglomeration assemblage of microorganisms that are enclosed in an extracellular polymeric substance (EPS) matrix of mainly polysaccharide material [141]. EPS are often referred to as "slime" due to its consistency [133,141].

Fig. 12 indicates four stages of biofilm, where each stage represents different development stages. Biofilm provides a local ecosystem in which the organisms can multiply [133,142]. The biofilm may be comprised of populations of different microorganism types; even microorganisms that are unable to attach to the surface on their own can still attach themselves to the EPS or directly to the earlier development of the colony [143,144]. The multiplication of bacteria inside the biofilm still have their own optimum growth parameters [136]. During the biofilm formation, the outer layers become aerobic, and the inner layers become anaerobic [145].

One of the most important characteristics of biofilm is their increased tolerance to antimicrobial agents,

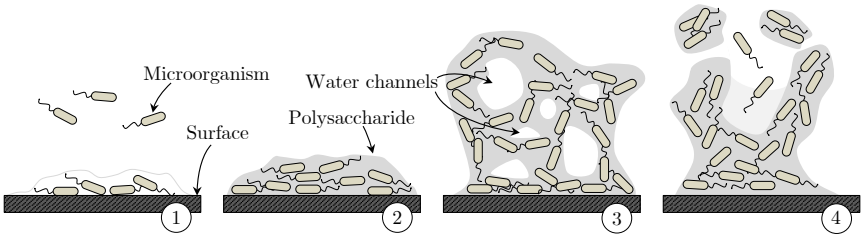

Figure 12. 1.stage indicate free floating biofilm producing bacteria that adheres to the surface of pipelines, filters, equipments, etc. 2.stage form colonization inside EPS, and the attachment becomes irreversible. 3.stage biofilm is formed and the *in-situ* ecosystem is growing by creating water channels allowing the water to keep the biofilm hydrated and nourished [142]. 4.stage reaches critical environmental factors such as the mass or nourishment of the biofilm, that either disperses or colonizes on surfaces further down.

such as biocidal agents (e.g., chlorine). It has been proved that biofilms can tolerate up to 1000 times higher concentrations than planktonic cells [141,145,146]. Biofilms have even been observed in the disinfection pipelines of biocides [133]. Biofilm is resistant to other harsh conditions such as extreme temperatures, pH, high turbulence, and exposure to ultraviolet (UV) light [133]. Another critical characteristic of biofilm is the ability to change the *in-situ* ecosystem from its surrounding; it can change the pH more than three units locally [133,147]. Thus, water samples do not reflect changes of pH value; the pH value can differ significantly in the biofilm from the water phase, where the corrosion process is often taking place.

Biocides are traditionally added to IWT processes to remove biofilm, controlling the MIC, and prevent H_2S production, but the misapplication of biocides can lead to significant issues, including resistance or lack of susceptibility to biocide treatment [148,149]. The primary objective of biocides is to limit the multiplication of numerous microorganisms, which adversely affect the entire process they are in contact with. Although, neither oxidizing (e.g., chlorine) nor non-oxidizing (e.g., glutaraldehyde) biocides penetrate biofilms according to Little et al. [149]. The effectiveness of biocidal agents is highly dependent on the presence of the types of microorganisms [150]. One of the main issues with MIC is the number of different species; there is no single biocide that encounters all conditions. Biocides are therefore chosen based on several factors: economy, environmental toxicity, ease of disposal, effective at targeting the unwanted activities, and effective at low concentrations [150,151]. However, the biggest concerns for operators are related to the effectiveness of long-term chemical treatments, as it is difficult to predict and measure the effectiveness accurately [151].

An alternative to biocide treatment has demonstrated that injection of nitrate can reduce the amount of SRB and their activity, known as bio-competitive exclusion [149,152–154]. The injection of nitrate can induce a shift in the dominant population from SRB to nitrate-reducing bacteria (NRB) [149]. The primary purpose for nitrate addition is to create competition for nutrients, as when NRB and SRB are competing for the same nutrients, NRB outcompetes SRB due to nitrate being a stronger oxidizer than sulfate, and thereby limits the generation of H_2S [149,154]. According to Little et al., the SRB population was decreased, and NRB was increased; after a long-term period, 323 months of nitrate treatment, SRB numbers were reduced 20,000 times, and SRB activity was reduced 50 times [149]. Corrosion measurements decreased from 0.7mm/yr to 0.2mm/yr. Furthermore, another platform that has injected nitrate into its system, to reduce H_2S production, has reported a 1,000 times reduction in SRB numbers, a $10-20$ times reduction in sulfate respiration activity, and a 50% reduction in corrosion [149,152]. However, according to Javaherdashti [152] and Little et al. [149], other researchers have reported failures related to the introduction of bacteria into natural mixed

cultures. E.g., Hubert et al. [155] suggested that bioaugmentation of NRB, which has grown *ex-situ*, was injected along with the nitrate batch if the presents of NRB were missing/low. Though, the considered idea failed regarding the injection of NRB along with nitrate batches. Another study by Xu [156], describes that it is very likely that NRB corrodes the iron if there is a lack of carbon sources under the NRB biofilm [156]. The results by Xu [156] also revealed that pitting corrosion, caused by an NRB-type (*B. licheniformis*), is more aggressive than a typical SRB under strictly anaerobic conditions.

Even though microorganisms are exposed to biocide and are not protected by biofilm, some microorganisms will still survive. Most organisms typically live in unfavorable environments where they experience conditions that are less than ideal for growth and reproduction [148]. A prevalent response to environmental stress for an organism to enter a reversible state of reduced metabolic activity and thereby going into dormancy (non-dividing state) [157]. From that perspective, some studies have even hypothesized that dormancy might be the default form of most microorganisms [158–160]. The dormancy defense mechanism protects the bacteria from exposing itself to unknown environments, where an antimicrobial agent could be present, which they are not resistant to [148,158]. Therefore it can be challenging to analyze different microorganisms' metabolism *ex-situ*. It is therefore notoriously difficult for process engineers and companies to mimic the process in a laboratory, and thereby selecting the most effective biocidal agents to target unwanted activities.

The main types of microorganism associated with corrosion failures are SRB, iron/manganese-oxidizing bacteria (IOB) (also defined as metal-depositing bacteria (MDB) in other studies [133,161]), iron-reducing Bacteria (IRB) (also defined as metal-reducing bacteria (MRB) in other studies [133,161]), as well as slime-forming bacteria (SFB) and acid-producing bacteria (APB). Each type of microbial group that is associated with corrosion failures is described in the following subheadings. Some bacteria cultures can be categorized as different microbial groups, depending on the environment.

Slime-forming bacteria (SFB)

Metabolism: SFB covers a high amount of different bacteria [162]. SFB is a group of bacteria that are capable of producing a EPS, which acts as the foundation for the formation of biofilm. Many of SFB fall within some of the other microbial groups [133,162]. **Formation damage mechanisms:** SFB has a indirectly influence of formation damage by promoting microbial growth inside the biofilm, attachment of other types of MIC, and development of *in-situ* ecosystem underneath a biofilm leads to formation of anodic and cathodic areas, promoting corrosion [163]. **Type ex:** *Vibrio cholerae*, as well as many other *Vibrio* spp., *Clostridium* spp., *Flavobacterium* spp., *Bacillus* spp., *Pseudomonas* spp., *Pseudomonas*, *Aerobacter* [161,164,165]

Sulphate-reducing bacteria/archaea (SRB/SRA)

Metabolism: SRB are stated to be the most troublesome microbial group among MIC in the petroleum industry [166,167]. SRB and SRA, both which primarily perform obligate anaerobic respiration, utilizing sulfate (SO_4^{-2}) as terminal electron acceptor and generate H_2S [135,152]. **Formation damage mechanisms:** Generation of H_2S, which soures the process and their activity, is primarily realized as a pitting attack on the metal surface [133,152]. Some study even observed plugging of the injection well by corrosion deposit flocs due to the increase of H_2S [167]. **Types ex:** *Desulfovibrio*, *Desulfobacter*, *Desulfotomaculum*, [164].

Sulphate-oxidizing bacteria (SOB)

Metabolism: SOB perform aerobic respiration. SOB can convert H_2S, that is produced by SRB, to H_2SO_4 [135]. **Formation damage mechanisms:** The generation of sulfate-producing acids, such as H_2SO_4, are contributors to corrosion. If both SRB and SOB are present these two type of groups almost always accompany each other, when the environmental conditions contains O_2, it is suitable

for the aerobic SOB and vice versa. [152,165,168] **Type ex:** *Thiobacillus* spp., *Paracoccus*, *Xanthobacter*, *Alcaligens*, *Pseudomonas* [164].

Iron-reducing Bacteria (IRB)

Metabolism: Most of the IRB are facultative anaerobes. IRB influences corrosion by reducing insoluble Fe^{+3} oxide layer to soluble Fe^{+3}, or they replace the metal film on the pipeline surface with less stable metal film [152,161,169]. **Formation damage mechanisms:** Exposes the metal beneath corrosion deposits (Fe_2O_3) protective layer to a corrosive environment. IRB also makes the environment more suitable for SRB in a mixed population of microorganisms in the biofilm, as IRB consume the O_2, and the SRB can thereby live under anaerobic conditions [152]. **Type ex:** *Shewanella*, *Pseudomonas* spp [161,168].

Iron/Manganese Oxidizing Bacteria (IOB)

Metabolism: IOB oxidize soluble Fe^{+2} to insoluble Fe^{+3}. IOB form oxides and hydroxides mineral deposits that cover the metal surface and provide O_2-depleted zones where anaerobe microorganisms can propagate [168,169]. **Formation damage mechanisms:** Promote corrosion reactions by the deposition on the metal surface, which decrease or damage the the protective oxide films covered on the surface [133,161]. **Type ex:** *Gallionella*, *Leptothrix*, *Siderocapsa*, *Sphaerotilus*, *Crenothrix*, *Clonothrix* [133,161,164,168].

Acid-producing bacteria (APB)

Metabolism: APB can produce large amounts of organic or inorganic acids as by-products during their metabolism, which can drop the pH in the biofilm into a very acidic environment [133,161]. Production of inorganic acids can be HNO_3, H_2SO_3, H_2SO_4, HNO_2, and H_2CO_3 [133]. E.g. H_2CO_3 can then further disassociate into CO_3^{-2} and CHO_2^{-} which can react with Fe resulting in the corrosion product $FeCO_3$ [168]. **Formation damage mechanisms:** Produce acids that causing metals to dissolve and accelerate corrosion processes [168]. **Type ex:** *Acetobacter*, *Gluconobacter*, *Pseudomonas*, *Thiobacillus*, *Thiothrix*, *Beggiatoa spp.* [133,168].

Nitrate-Reducing Bacteria (NRB)

Metabolism: NRB reduce N_3^{-} to N_2. As previously described, nitrate is often injected into the process to mitigate souring caused by SRB, as NRB can outcompete SRB and thereby reduce H_2S production. Studies proved that NRB efficiently oxidized the cathodic hydrogen from the metal, but unlike SRB cultures, they failed to stimulate the rate of corrosion [170]. **Formation damage mechanisms:** As previous described, corrosion caused by an NRB is more aggressive than SRB under strictly anaerobic conditions **Type ex:** *Arcobacter*, *Bacillus licheniformis*, *Desulfovibrio*.

3.6. Reflection

To summarize Sec. 3, it is essential to understand the different IW characteristics and their formation damage mechanisms on the IWT process if an acceptable online monitor for detecting TSS must be selected. For instance, if only considering TSS as inorganic particles and follow the definition of TSS as particles above 2µm, then an operator could get a hard time to troubleshooting why an increasing TSS concentration further down the treatment process occurs, and determine which type of TSS that increased the overall TSS concentration. The water quality can also be affected by substances like oil, clays, and TDS that have the ability to coalesce, agglomerate, swell, and change states, respectively. All particles that have the ability to pass the filters in the IWT process and changes conditions further downstream that could act to the measurements of TSS, both the size distribution and the concentration. Another example could be troubleshooting why there is an increasing replacement of corroded instruments if only consider dissolved gases as the only

stimulation of corrosion. Furthermore, corrosion and TSS measurements can even affect each other if TSS is considered as any suspended solids, no matter their sizes. Then an increase of MIC types, which are part of the TSS concentration, will likely increase corrosion, which further will increase corrosion deposits that will be included in the TSS concentration further down the IWT process.

Other issues are the performance of measuring OiW. Fjords Processing Ltd executed an extensive investigation of different OiW monitors; many of the OiW monitors that exist can measure solid particles. Though, the results clearly indicated that all the OiW monitors were affected by some, if not all, of the parameter variations, they were exposed to [171]. Most of the parameters must also be taken into account for a TSS monitor, such as particle size variation, the fluid carrier's flow rate, salinity, oil, gas, chemical, temperature variation, and fouling. However, when instruments are installed in a field-environment, a monitor will not be subject to all the different variations listed before, without recalibrations occasionally. Thus, variations such as TSS concentrations and size distribution may change regularly, the flow rate and even chemical concentrations changes daily. How regularly the changes will happen completely dependents on the installation location and the production of a day-to-day basis. In an ideal situation, after the entire IWT process, the water quality, with respect to TSS, should output the same TSS concentration as after the last filtration unit in the IWT facility. Another aspect to consider is the location of measuring TSS in the process, and what type of measurement method can output relevant information to monitor the quality of TSS in the IW.

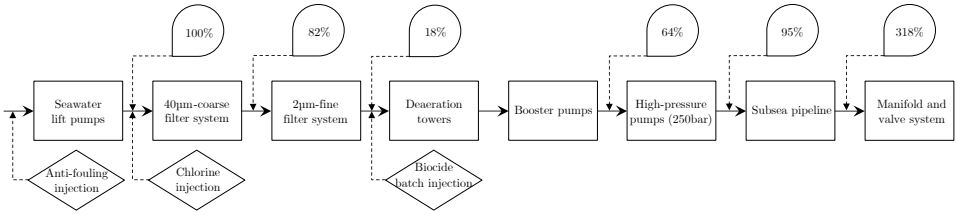

Figure 13. Block diagram of a water injection treatment facility in the Danish sector of the North Sea, with manual TSS concentration ratio at different locations on the IWT facility (exact concentration is confidential).

4. Injection Water Treatment Facility

As IWT consists of various stages, it is important to understand the purpose of each stage and its working principles. Especially with a focus on instrumentation of TSS monitor at different locations on the IWT facility, and which physical process issues could affect the measurements of TSS. A current IWT facility in the Danish sector of the North Sea will be described as a benchmark. The salinity of seawater does not deviate seasonally around the IWT facility, with surface and bottom salinity of $\sim$3.5%, according to former Maersk Oil [172]. The surface temperature is around 7°C during winter and between $(15-19)$°C in summer. The bottom temperature varies from $(6-8)$°C in winter and $(8-18)$°C in summer, where the temperature of the reservoir is typically 80°C [172,173]. As mentioned in Sec. 2, the mean concentration in the North Sea is 2.6(3.5)mg/L around Dogger Bank. The temperature increases through the process, and according to studies, the injection temperature outlet is often around $(18-21)$°C. Although, the temperature can easily increase with 10°C due to a higher injection rate, as the residence time in the subsea pipelines is shortened [173,174].

One of the primary problems in most injection systems, highlighted in several studies, is the entry of dissolved O_2 after the deaeration towers through leaking pumps, seals, hatches, etc. [37,114]. Inadvertently, contaminants may enter the system. The difficulty of preserving water quality is essential and a direct function of the length and complexity of the injection system [37]. The result of water quality in long pipeline systems are often considerably worse than it was after the treatment source [37]. Fig. 13 shows a block diagram of different process stages through an IWT system, where

the process is described in Larsen et al. [173] and Thomsen et al. [174]. The main stages of IWT in Fig. 13 are described in the following subsections.

Seawater Lifting Pumps

A few pumps lift seawater from the ocean to the platform level. These pumps are often controlled by a constant speed, as $3-5$ number of pumps are often required. As the seawater is untreated at this point, the dispersed and dissolved content are highly reactive, thus requiring the pump and piping at these early stages to be highly resilient. Therefore, an anti-fouling agent is added before the lifting pumps to eliminate fouling for this particular benchmarked IWT facility.

Filtering

As solid particles are known to block pores in the reservoir depending on size physically, filters are utilized to remove sufficiently large solid particles. Chlorine is injected before the filter to protect the filters from biological fouling. At this time, there exist multiple solutions, but filtration systems might need improvements as the trend in oil and gas production is getting tighter, which involves injecting PW into the oil reservoir [175]. Some IWT solutions utilize a single-stage filter, where others use two-stage coarse and fine filters. Various types of filters are being used in the solution, such as cartridges, strainers, cyclones, membranes, and granular media types, where granular media types that define sand and nutshell filters are the most common [175]. As multiple of the same filter types are in use simultaneously in each train, it is of interest to divide the filter load equally amongst them as well as having an optimal filter cleaning procedure. The back-flushing cleaning procedure of the filters is commonly triggered by either exhausting a timer or after the delta pressure over the filter exceeds a limit [86]. It is also beneficial to balance the load between the coarse and fine filter states so that one stage is not redundant. As the size distribution of the TSS is unknown, this load balance can be challenging to achieve [176].

Deaeration

As O_2 is unwanted in both the piping and reservoir, the concentration of dissolved O_2 in the water is reduced by deaeration. A common deaeration method is by tray-type vacuum deaeration towers. The operating principle of the trays is to increase the surface area and reduce the travel length of the dissolved O_2. The performance of the deaeration towers is currently measured by analyzing samples of the IW before and after deaeration. However, there are various reliability issues of these measurements as the dissolved O_2 in water should be low after deaeration. According to studies, the acceleration of corrosion occurs when the deaeration O_2 content of the water is above 25ppb [114,115]. The concentration of dissolved O_2 in the samples might change over time, from sample extraction to sample analysis, which cause errors when evaluating the performance [115].

Injection pump, manifold, and valve systems

The booster pumps raise the pressure to $(10-16)$bar before the injection pumps raise the pressure to around $(250-300)$bar [173,174]. The IW is then either directly injection into the nearest wellheads or transported through a $\sim$10km long subsea pipeline, and some of the IW is even further transported $\sim$2km to another wellhead, where it enters the last part before injection into the reservoir [173,174].

5. Total Suspended Solids Dried Weight Measurements

As different IW characteristics and their formation damage mechanisms on an IWT process are well described in Sec. 3, followed by a description how a specific IWT facility is constructed to purify the IW before injection, it is of interest to investigate the location of where online TSS monitors can be beneficial to install, and which type of method, size range, and type of matters the monitor have to measure. Furthermore, it is also necessary to determine how the measurements can be useful to

increase water quality. As the exact TSS concentration are confidential in Fig. 13, a manual experiment of emulating the filtration system was executed. The measurement of TSS followed the Danish standard for "Dry Weight and Loss of Ignition Analysis", which are closely related to the American standard for Total Suspended Solids Dried at $(103 - 105)°C$ [76,177]. The concentration of TSS is calculated as:

$$X = 1000 \cdot \frac{(b - a + c)}{V}, \tag{4}$$

where c is the blank sample's weight loss after drying:

$$c = \frac{a_0 - b_o}{3}. \tag{5}$$

The rest of the variables are: a is the weight of the unused filters [mg], a_0 is the weight of three unused filters for blank sample [mg], b is the weight of the dried blank sample filters with suspended solids [mg], b_0 is the weight of the three washed and dried blank sample filters [mg], and V is the filtered amount of volume [ml]. The three different filters used for determining the concentration of TSS in a specific area and depth in the Danish sector of the North Sea were:

- **41µm-filter:** Nylon filter – Sepctral/Mesh® Woven Filters – follows the U.S.A standard sieves ASTM specification E-11 for a mesh with a permissible variation of ±3µm for a 41µm filter [178].
- **2.7µm-filter:** Glass Microfiber filters – Watman™ 1823-047 Grade GF/D – Particle retention rating at 98% efficiency [179].
- **0.2µm-filter:** Mixed Cellulose ester – Advantec® Membrane filters.

The 41µm- and 2.7µm-filter are used to emulate the two different filtration processes on a specific IWT system. The 41µm-filter emulates the 40µm-coarse filter system, and the 2.7µm-filter emulates the 2µm-fine filter system, that is installed on the IWT system. The 0.2µm-filters are used to retain anything that passes the two emulation filters and is defined as the "TSS sample" in Fig. 14(a).

The 0.2µm-filters are selected as; ideally, no microorganisms nor inorganic particles should pass the filter. The TSS samples are analyzed at four different periods: immediately, after 24 hours, after one week, and after one month, as shown in Fig. 15.

By looking at the future development, this procedure was selected to observe if any evolution of microbial growth has occurred in the seawater after preservation and transportation onshore for analysis. The analysis of variance (ANOVA) test of the samples between each filtration analyzed at different periods does not statistically show any significant evolution, and the null-hypotheses (H_0) fails to be rejected, and the means are likely to be equal for all periods. The ANOVA results are listed in Table 3 for each filtration group.

This likely conclude that preservation of the seawater prevented the growth of microorganisms, and a joined boxplot for each filtration group can represent the TSS concentration, see Fig. 16.

The mean seawater TSS concentration from the experiment reflects the TTS concentration according to the study of 2.6(3.5)mg/L. The mean and standard deviation for each filtration of the measured TSS concentration is estimated to be:

- Unfiltered seawater: 4.7(3.6)mg/L)
- 41µm-filter: 2.8(2.5)mg/L)
- 2.7µm-filter: 1.3(1.5)mg/L)

The executed TSS concentration value can be used to compute a hypothetical value of the TSS concentration evolution throughout the IWT facility, based on the TSS concentration ratios expressed in Fig. 16. Table 4 shows the measured TSS concentration compared with the expected TSS concentration, assuming the mean and standard deviation from the literature of 2.6(3.5)mg/L [44].

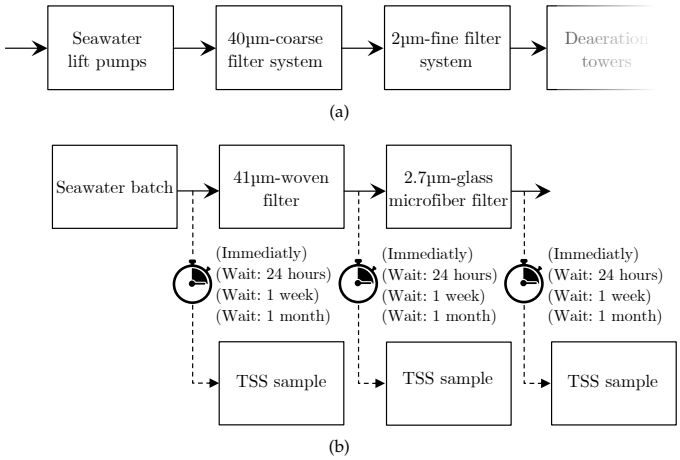

Figure 14. Two flow diagrams of the filtration process offshore and emulation in laboratory: (a) The filtration sections of benchmark IWT process offshore, see Fig. 13 to see the entire flow-diagram of the IWT process; (b) an emulation of the filtration process, where seawater from the intake to the offshore process is collected and tested in laboratory. The seawater is filtered through 41µm-filter and a 2.7µm-filter, to emulate the filtration process offshore, between each filtration a TSS sample is retained by vacuum filtration through a filter with pore sizes of 0.2µm. The TSS samples are analyzed at four different time periods: immediately, after 24 hours, after one week, and after one month.

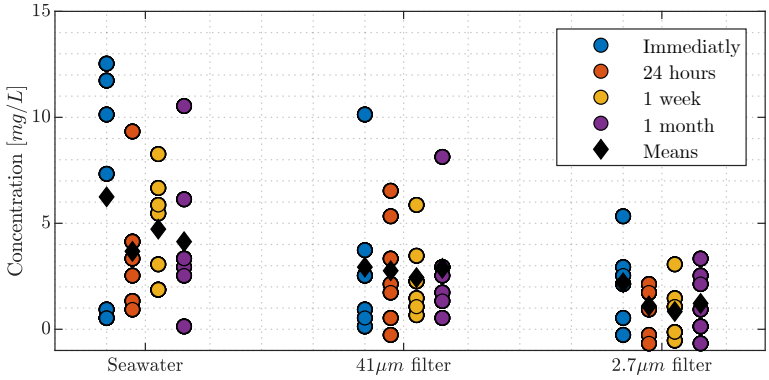

Figure 15. Scatterplot of each sample analyzed at the four different periods.

Though, measurements of TSS concentration are useful to balance the cost of the IWT against the cost of other alternatives, such as periodic well-stimulation, as highlighted in Sec. 3.

The TTS concentrations in Table 4 is in reasonable accordance with the expected TSS concentration in mg/L progress through the system. There could be a substantial uncertainty related to the fact that expected TSS concentration is calculated based on percentage, though, it should be feasible to assume that both TSS concentrations are in the expected range. Thus, the true evolution through the IWT facility may be an addition to the TSS concentration after the fine filter system. With nearly a seventeenfold increment of the mean after the fine filter system to after the subsea transportation pipeline, it clearly indicates the addition of TSS such as scales, corrosion deposits, and microbial grows assuming the filtration systems works as intended. This also concludes that the instrument of monitoring the particle size distribution should be measurable within an overall TSS concentration

Table 3. The ANOVA test results of each sample location at the four different time periods: immediately, after 24 hours, after one week, and after one month.

Unfiltered seawater					
	SS	**df**	**MS**	**F-value**	**P-value**
Between groups	26.35	3	8.78	0.64	0.60
Within groups	329.78	24	13.74		
Total	356.14	27			
41µm-filter					
	SS	**df**	**MS**	**F-value**	**P-value**
Between groups	1.03	3	0.34	0.05	0.98
Within groups	162.93	24	6.79		
Total	163.95	27			
2.7µm-filter					
	SS	**df**	**MS**	**F-value**	**P-value**
Between groups	7.32	3	2.44	1.18	0.34
Within groups	49.55	24	2.06		
Total	56.87	27			

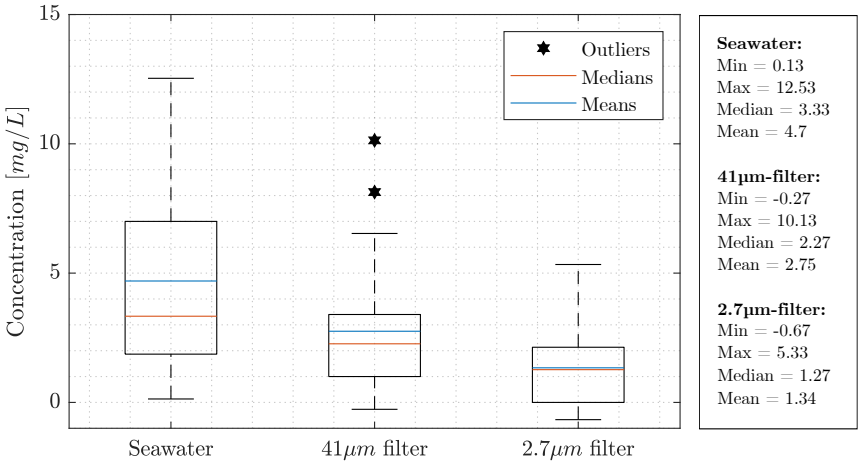

Figure 16. Shared boxplot representation of between each filtration: unfiltered seawater, 41µm-filter, and 2.7µm-filter.

from >30.5mg/L ($\mu + 2\sigma$) to ∼0mg/L. As an increasing amount of TSS is added within the process, though it is difficult to conclude the actual size of particles based on the TSS concentration results.

6. Online Monitoring of Total Suspended Solids

Like many other on-line continuous water quality measurement devices, measurement of TSS requires proper calibration and regular maintenance. Extensive development in the area of implementation of process analytical technology of measuring particle sizes has been investigated for decades. Despite the long history of implementing quality monitors for measuring particle sizes, it has not become a standard operation parameter in the oil and gas industry. However, particle sizes

Table 4. Comparison between the measured TSS concentration and the expected TSS concentration from the literature: 2.6(3.5)mg/L.

	Expected TSS conc. [%]	Expected TSS conc. [mg/L]	Measured TSS conc. [%]	Measured TSS conc. [mg/L]
Seawater lift pumps	100	2.6(3.5)	100	4.7(.6)
Coarse filter system	82	2.1(2.9)	60(69)	2.8(2.5)
Fine filter system	18	0.5(0.6)	28(42)	1.3(1.5)
Booster pumps	64	1.7(2.2)		
High-pressure pumps	95	2.5(3.3)		
Subsea pipeline	318	8.3(11.1)		

are highly essential to increase the performance of IWT processes. It is evident that the particle size distribution significantly affects the quality of the reservoir. Nevertheless, the trustworthy particle size distribution of TSS and their shapes also affect the process control and can be valuable to validate the IWT process design.

In general, TSS monitors work well when they are properly calibrated and well maintained in non-hazard environments. However, in the oil and gas industry, significant variations of mixtures, pressures, chemicals, and temperatures render a harsh environment for the TSS monitors, all of which influence the accurate measurement of the particles in the process. In many cases where the monitors have been installed without proper calibration, maintenance, or actual knowledge of the limitations of the installed monitors, resulted in doubtful and misleading measurements [180]. As described in Sec. 3, the operators must have confidence in the data generated by the monitor, as false data can be more harmful than no data. There exist several commercially available monitors for detecting oil droplets and particle sizes, with different measurement techniques, ranging from technologies based on ultrasonic spectroscopy to electrical sensing zone. However, to the authors' knowledge, no commercialized monitors have been standardized for detecting TSS nor OiW continuously. Another drawback of commercially available monitors is that they are not yet robust and reliable enough to be used as control feedback [171,180].

Currently, different international or industry standard committees, such as International Organization for Standardization (ISO), American Society for Testing and Materials (ASTM), and American Petroleum Institute (API), covers different focus area, ranges, and analysis methods. A new monitor must be compared with the right standard for validating its performance, which on its own, can be difficult. Table 5 and Table 6, contain the main ISO standards related to measuring particle sizes suspended in liquid, that includes definitions, discrimination of different type of TSS, representation, sampling, as well as the technical characteristics and working principles of the most common particle sizing instruments.

As there does not exist one unique reference method for measuring particle sizes, it can be difficult to verify the performance of different measurement techniques. The TSS concentration can be measured and compared according to the ISO 872 by a filter, dry, and weighing the water sample, as executed in Fig. 16. However, it tells nothing about the particle morphologies in the process.

Currently, offshore IWT processes rely on off-line measurements of TSS concentration, but measuring the TSS concentration is highly method-dependent. The measured quantities can, therefore, vary under different operational conditions and between different laboratories. The different reference methods are also limited in detecting all quantities defined within TSS. Thus, different quantities are measured individually, e.g., bacteria and OiW concentration (ISO 8199 and 9377-2). As a result, a very detailed procedure for taking a sample, transportation, storage, and measuring in a laboratory is well described in ISO 5667-3, for manual sampling (ISO 3170), which makes the measurement of TSS not

Table 5. ISO standards for representation of particle size analysis results and related standards

	ISO standard(s)
Representation of particle size analysis results:	
Graphical representation	9276-1
Calculation of particle size distribution	9276-2
Adjustment of an experimental curve to a reference model	9276-3
Characterization of a classification process	9276-4
Size analysis using logarithmic normal probability distribution	9276-5
Representation of particle shape and morphology	9276-6
Repeatability, reproducibility and trueness estimates	21748
Other standards of interest:	
Determination of suspended solids	872
Manual sampling	3170
Automatic pipeline sampling	3171
Preservation and handling of water samples	5667-3
Determination of turbidity	7027
Microbiological examinations by culture	8199
Oil-in-Water concentration	9377-2
Particulate materials — Sampling and sample splitting	14488

Table 6. Relevant ISO standards for Particle size analysis' methods

Particle size analysis' methods	ISO standard(s)	Overall size range [µm]	On-/in-line capable
Sieving	2591-1 3310-1 to -3 20977	$5 - 125$*	✗
Gravitational sedimentation	13317-1 to -4	$0.5 - 100$	✗
Centrifugal sedimentation	13318-1 to -3	$0.1 - 5$	✗
Electrical sensing zone	13319	$0.4 - 1,200$	✓
Laser diffraction	13320	$0.1 - 3,000$	✓
Image analysis methods	13322-1 to -2	$(0.25)1 - 500$*	✓
Small-angle X-ray scattering	17867	$0.001 - 0.14$	✗(✓)
Scanning electron microscopy	19749**	$40.01 - 500$*	✗
Ultrasonic attenuation spectroscopy	20998	$0.01 - 3,000$	✓
Transmission electron microscopy	21363**	$0.001 - 5$*	✗
Light obscuration	21501-3	$1 - 100$	✓
Dynamic light scattering	22412	$0.02 - 3$* ($\ll 10$)	✓

* No typical size range was given within the ISO standards, found according to Merkus [181].
** ISO standard under development.

only method-dependent but also procedure-dependent. Both the method- and procedure-dependency determine the "true" size distribution and TSS concentration introduce a substantial amount of uncertainties, which renders difficulty within validating and compare the performance of the process, but also lose the confidence of new measurement techniques [182,183].

In the ideal world of particle characterization, all particle size analysis' methods within their recommended measurement range, highlighted in Table 6, should yield an unambiguous diameter size of particles under the condition that particles are spherical and homogenous distributed (constant

concentration). Moreover, their chemical composition should be identical, as different properties, such as density, refractive index, and conductivity, would affect the different methods [181]. Even so, the concentration of particles can still affect the output from different measurement techniques. It would be apparent that such ideal conditions of particle sizing would ease the establishment of defining a reference method. It is also clear that in the real world, most particles are not spherical, but have different shapes and chemical composition, and is not homogeneous distributed (deviating concentration) in the sample and some may agglomerate. These differences have all different influences on different measurement techniques. Some are more robust to high sample concentration than others (ultrasonic compared to electrical sensing zone), some have entirely different measurement ranges than others, and some are cable of measuring on-/in-line. Based on measurement ranges and installment capability, it is possible to discriminate which measurement principles are suitable for measuring TSS online. Other influences that can affect the measurement, such as velocity, pressure, temperature, and the presence of gas bubbles, are something that can be accounted for in most processes.

The different automated methods of detecting PSD has the last decades increased considerably, especially due to the increment of computation power and the fact that almost all operating plants in all fields are today entirely controlled automatically. Even with increasing sophistication within each measurement technique, there is still an urge to improve accuracy and increase resolution. There are numerous particle size analysis methods, each with different approaches. Thus, each has its theoretical interpretation and different analyzing procedure of the same particle (spherical or non-spherical shaped). Another drawback, related to the different measurement techniques, suffer from the fact that all particles that are non-spherical are assumed to be spherical [181,182,184]. Consequently, different technologies will yield different PSD, based on the exact same sample, since most methods do not give any information on particle shape, despite being significantly affected by it [181,185].

6.1. Particle Size of Measurements

In this section, the ISO definition of particle size measurement is introduced briefly, as a more in-depth description can be found in the ISO standards; highlighted in Table 5. An understanding of these uncertainties and the sensitivity of these TSS monitors are a prerequisite for successful implementation and comparison of different measurement techniques. Such an understanding could lead to an improved combination of different monitors' technology methods through sensor fusion. More technical descriptions of particle size analysis have been well described, discussed, and compared in different studies [181,185–187]. Some of the most common particle size measurements as highlighted quantify particle sizes differently.

Spherical particles only require to be represented by one parameter; their diameter. For any non-spherical particles, this can only be approximated by an equivalent diameter; either way, more size parameters are needed. Equivalent diameter is defined as the diameter of a spherical particle, which yields the same value of a certain physical property when analyzed under the same conditions as the non-spherical particle [188]. According to ISO standard 9726-2, there are different physical properties that characterize particles:

- Linear dimension
- Projected area
- Surface area
- Volume
- Mass
- Settling rate
- The response of electrical, optical, or acoustical field

Each of these properties can be used to characterize the equivalent diameter of a particle. The isoperimetric quality is only valid if the particles are spherical, as spheres have the largest volume to surface area ratio with a non-empty inner body [189]. The equivalent projected area diameter is

the diameter of a sphere having the same projected area as the particle. That is often the case for particle size analyzers, as the particle has a specific orientation when passing the monitor, such as microscopy and light scattering. The equivalent projected area diameter of a particle, d_A, can be calculated equivalent to circle area:

$$d_A = \left(\frac{4A}{\pi}\right)^{1/2}, \tag{6}$$

where A is the projected area. Depending on the orientation of the particle, d_A can both be smaller or larger compared to the other equivalent diameters in a continuous flow stream. The equivalent projected area diameter in a stable position is mostly larger compared to the other equivalent diameters, d_{As}. Surface diameter, d_S, and volume diameter, d_V, are defined, such that each of them reflects a three-dimensional geometric characteristic of an individual particle. Surface diameter is given as the diameter of a sphere having the same surface area as the particle, which is expressed by

$$d_S = \sqrt{\frac{S}{\pi}}, \tag{7}$$

where S is the particle surface area. A volume equivalent diameter is the diameter of a sphere having the same volume as the particle, which is defined by

$$d_V = \left(\frac{6V}{\pi}\right)^{1/3}, \tag{8}$$

where V is the particle volume. For non-porous particles consisting of one material, the mass equivalent diameter, d_M, is equal to d_V. Stokes equivalent diameter, d_{St}, corresponds to the diameter of a sphere with the same final settling velocity as the particle in stokes regime with the same density, defined by Stokes' law:

$$d_{St} = \sqrt{\frac{18\mu v_t}{g\Delta\rho}}, \tag{9}$$

where v_t is the settling velocity, g is the acceleration due to gravity, μ the dynamic viscosity of the carrier liquid (IW), $\Delta\rho$ are the densities of the carrier liquid and the particle. Lastly, the equivalent sieve diameter, d_{sieve}, corresponds to the diameter of a sphere passing through a defined square sized mesh. These are the most frequently used analyze methods of representing a particle size with only one size parameter. Other methods to quantify the particle size exist, especially for image analysis, e.g., Feret diameter, Martins diameter, and convex perimeter.

The relationship between particle analyzers using equivalent diameter to represent the size of particles are very important to address, as a comparison of different analyzing equipment using a different physical property to characterize particles can give different distributions. Thus, care should be taken if one compares the data from a different type of analyzing equipment and expect related outcomes. Table 7 gives a theoretical analysis of the outcome by obtaining different equivalent diameters on several convex particles having the same volume of $V = 1000\mu m^3$, together with its relative value compared to a sphere.

In summary, the equivalent diameter is still a necessity information to calculate for measuring the PSD in processes. Especially in a process where the particle of interest is the majority, e.g., measuring the oil droplets from PW treatment processes.

6.2. Instrumentation

Each measurement technique can be divided into online methods, that deliver data in a process-relevant time window, and manual methods. A further subdivision of the measurement

Table 7. Theoretical characterization of different convex particles based on different physical properties.

Shape	3D ill.	Orientation O_1	Orientation O_2	Dimensions: d, $d \times h$, $l \times w \times h$ [µm]	d_A* [µm] O_1	d_A* [µm] O_2	d_S [µm]	d_{St}** [µm] O_1	d_{St}** [µm] O_2
Sphere				12.4	12.4	12.4	12.4	12.4	12.4
Disc				25.2 × 2.0	25.2	8.0	19.2	31.8	8.6
Rectangular prism				7.0 × 7.0 × 20.4	7.9	13.5	14.6	10.1	18.1
Cone				19.5 × 10.0	11.1	19.5	15.2	12.7	24.0
Cylinder				8.0 × 20.0	14.3	8.0	13.9	15.8	8.3
Ellipsoid				12.0 × 10.6 × 15.0	11.3	12.6	12.5***	11.2	12.8
Triangular prism				10.0 × 10.0 × 20.0	8.0	16.9	16.4	9.2	21.2

* d_A and d_{St} is obtained at two orientations: O_1 and O_2.

** The drag force of a sphere and non-spherical particles, is calculated according to the drag prediction approach presented by Ganser [190], where the drag coefficient for a sphere is estimated to be $C_d = 26.7$ at $Re = 1$.

*** Knud Thomsen's approximation of an ellipsoid surface area with a worst error of ±1.061%

methods can be made on the sampling point: in-line, on-line, at-line, or off-line, see Fig. 17.

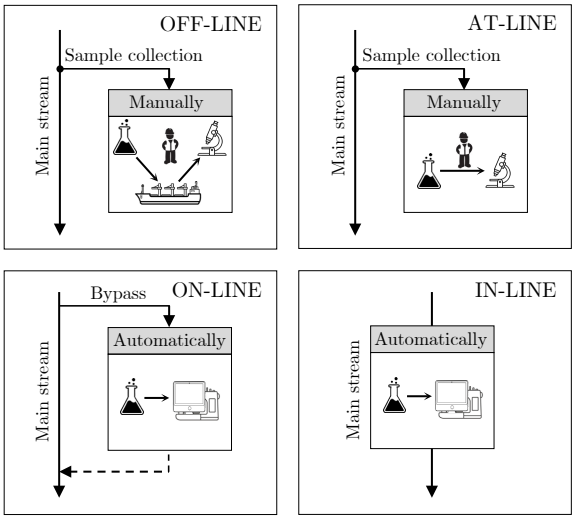

Figure 17. Different sampling methods based on the sampling point: in-line, on-line, at-line, and off-line.

Off-line analysis advantages in the examination of the sample are carried out by experts in laboratories. The sample preparation is adjusted to suit the particular method of analysis and types of quantities being examined. For off-line analysis offshore, the sample needs to be prepared (i.e., diluted, mixed, preservation) to reduce changes under transportation, and a substantial number of samples are needed to verify the trueness of the measurement, which renders it a time-consuming process.

Especially at offshore processes, it can take several days, if not weeks, between sampling collection and the results obtained onshore. For this reason, feedback from the laboratories to the platform has a significantly longer reaction time, which is accentuated when a noteworthy deviation occurs due to faults of the production or even worse process damage.

At-line analysis deviates from off-line analysis by carrying out the sampling analysis closer to the process. Like off-line analysis, at-line analysis is still a manual procedure which demands human resources compared to fully automated analysis procedures as on- and in-line analysis. The at-line location reduces the amount of preparation for transportation. In contrast to off-line analysis, the closer proximity to the process also considerably lower the reaction time, which could have a valuable effect on detecting adverse conditions earlier. The disadvantages compared to off-line analysis is that it may not be an ideal environment due to varying conditions, such as air humidity, temperature, and cleanliness.

On-line analysis differs from the off-line and at-line methods as the sampling is measured automatically, and the reaction time of analyzing the quality of the IW is significantly lowered. The automatic analysis guarantees the possibility of reacting promptly to any deviations from normal operation. TSS measurements have the potential to be used as feedback for improving process control. The disadvantages of on-line analysis, like off-line and at-line, is the risk of a bypassed maldistribution of the heterogeneous mainstream, which may not represent the true process quality. Manual sampling analysis is still necessary to verify the measurement quality of the TSS measurement equipment, which emphasizes the necessity for the equipment to enhance other parts of the process to be worth its investment.

In-line analysis and on-line analysis is closely related and has most of the same advantages and disadvantages. An in-line analysis is done *in-situ* of the process stream directly. Thus, no misrepresentative sampling due to bypassing the flow happens nor disturbances in the process stream. However, the in-line analysis does have some disadvantages; the equipment must be robust within its procedure to prevent shutdowns from carrying out an inspection.

6.3. Particle Size Analysis Methods

Several particle size analysis' methods listed in Table 6, can be discriminated due to the application of measuring on-/in-line with an ideal upper limit of $>$40µm to determine whether the coarse and fine filters are malfunctioning and a lower limit at least $<$2µm to determine the filtration quality. Based on those criteria, the techniques that are applicable for detecting concentration and particle sizes in IW are electrical sensing zone, light scattering, light obscuration, ultrasonic spectroscopy, microscopy, and turbidimetry. Although turbidimetry itself does not have the possibility to measure particle sizes, it is commonly used for measuring water quality. The accuracy of each method, described in different fields of installation, will not be mentioned in this paper as the results may be tendentious. A short description of each method will be given with their advantages and disadvantages, with respect to measuring TSS in IW.

Turbidity method (Turbidimeters):

Turbidity monitors are commonly used in water industries. Turbidity monitors measure the intensity of scattered light due to particles within the water that disrupts the transmitted light path [191]. The detector then measures the scattered light as the light changes direction when it hits the particles. The light energy is then converted to an electric signal which outputs a calibrated nephelometric turbidity units (NTU) value, i.e., if the water is less turbid, less light is scattered, and

thereby low output of NTU. The sensitivity of turbidity monitors may differ between instruments, but ideally, all types of particles, such as silt, clay, algae, organic matter, and microorganisms, scatters the light in the water [192]. One of the most significant advantages of turbidimeters is the ability to detect particles below 1µm in size, all of which can contribute to the overall turbidity value [193]. However, care should be taken if comparing turbidity measurement with TSS concentration, as turbidity is another parameter of measuring water quality. For instance, turbidity also depends on particle sizes, bubbles, color, organic matter ability to absorb light, and microorganism, all of which affect the correlation between turbidity measurements and TSS concentration [192,194,195]. Other conditions can affect the measurement, such as the light scattered by particles at the back of the sample volume, which can be blocked by particles closer to the detector [193]. It is well known in the field of turbidimeters that bubbles affect the turbidity measurement, where particles identical in size, but have different chemical composition, scatter different amounts of light [193]. Even some organic matter such as colored dissolved organic matter (CDOM) can result in an artificially low turbidity measurement as it absorbs light instead of scattering it [194,195]. Nonetheless, it may be unreliable to use turbidimeters for measuring the true TSS concentration, but their strength of measuring the water's turbidity may have the potential in combination with other water quality monitors [193].

Electrical Sensing Zone Method (Coulter Counter):

This instrument was initially developed for sizing blood cells and cell cultures and is widely used for off-line measurements [181,186,187]. The electrical sensing zone (ESZ) method relies on the impedance measurement in a capillary, through which particles within the IW (electrolyte) passes a small orifice. When a particle passes through the measuring gap, they momentarily change the electrical impedance equal to its volume of electrolyte [186]. This change in impedance generates voltage pulses corresponding to the number of particles, whereas the amplitude of the pulse is proportional to the volume of the particles and is used to measure the equivalent volume diameter of the particle. Like the rest of the different particle counters, the operation is continued until a sufficient amount of particles have passed the instrument to achieve a statistically reliable particle size distribution [187]. The ESZ method excels in its high sensitivity and that it is capable of measuring a truly volumetric value of a single particle in contrast to measurement of the oriented cross-section area, relative to the projection direction, in other methods. Nevertheless, its disadvantages for installation in an IWT process surpasses its advantages. The size range of particles is governed by the orifice diameter, where the overall size range is about $(0.4 - 1200)$µm [185].

The lower measurement limit depends on both electric noise and orifice size. Normally, particles with diameters ranging from 2% to a maximum size of $(40 - 60)$% are noted by different studies to be reliably detected [76,181,186,187,196]. The signals of smaller particles are lost due to the signal-to-noise ratio, particles larger than $(40 - 60)$% give an increasingly non-linear response and can block the orifice [181,186,196–199]. The selected orifice diameter can then be estimated based on the particle sizes. As previously concluded in the Sec. 5, for an IWT process, it could be of interest to measure from small micron sizes to very fine sand (4ϕ). The lower limit sets the orifice size, i.e., if 0.4µm should be 2% of the measurement range, the orifice diameter will be 20µm, with a reliable measured size range within $(2 - 60)$%; $(0.4 - 12)$µm or for 40%; $(0.4 - 8)$µm. Although an upper limit of TSS sizes of $(8 - 12)$µm should be enough to detect particles after the fine filter, changes can occur after the filtration unit that may frequently block the ESZ instrument further down the IWT process due to different mechanisms described in Sec. 3. The measurement time is about $(1 - 5)$min and analyzing a small portion at a time, making on-/in-line measurement only applicable for streams with very low flow rates, in a ranges of ml/min, and at low concentrations in a conductive liquid [181,193,200]. Another drawback is that the method cannot distinguish between droplets and different particles [201]. Furthermore, only one particle at a time can be measured accurately within the sensing zone.

Two types of coincidence can be distinguished [186,193,196].

- Primary Coincidence: more than one particle in the sensing zone gives rise to two or more individual pulses which cannot be distinguished and are overestimated as one particle and lower the particle counts.

- Secondary Coincidence: two or more particles below the detectable threshold level, which individually should not be detected, generates a pulse above the threshold level together. Thus, larger numbers of small particles are counted and overestimated [186,196].

Both coincidences increase the higher the concentration is, and the measured concentration should not exceed around 10ppm, according to Merkus [181], although it is highly due to the presence of different types of particles. Lastly, particles with an extreme shape, i.e., thin plates and needles, a large overestimation can appear as the particle may rotate when they are passing the sensing zone, creating an artificial measured volume [186,197].

Static Light Scattering method (Laser Diffraction):

In laser light scattering, the intensity of light scattered by the particles, in an incident beam of light, is determined simultaneously at different scattering angles using an array of photodetectors. Static light scattering, which is sometimes also referred to as laser diffraction, or low-angle laser light scattering, is a well-established technology that has been used for decades for particle size analysis [66]. It is a similar procedure of light scattering used in the turbidimeter design with some significant differences. Both methods measure the intensity of scattered light based on TSS in the IW. The scattered light that interacts with the particles is captured by photodetectors, which converts scattered light to an electric signal.

Laser diffraction counts and analyzes individual particles according to their size, were turbidimeters only measure the amount of scattered light and cannot distinguish the individual particles. Larger particles scatter the light stronger but with low angles than smaller ones, which scatters the light weaker and with a larger angle, assuming identical matter [193,202]. Its advantages from being a well-establish method and its principles and limitation are well described in several textbooks. Light-scattering sensors do also have an advantage in their sensitivity; their total measuring range spans from 0.1µm to 3,000µm depending on the used algorithm, which covers the TSS range of interest in an IWT process [76,181]. However, it can be difficult for light scattering to distinguish between species present in a distribution, such as oil droplets, solid particles, and gas bubbles. Bubble peaks occasionally occur in a process and are therefore essential to identify these peaks as distinct from the particulate to be measured, which can be problematic if the bubble peaks overlap in the PSD with the particles of interest [203]. Like many other particle technologies, it always assumes spherical particles. For non-spherical particles, the diameter of the particle is equivalent to the amount of light scattered, which depends on particle orientation. For platy- and needle-like particles, it often results in an overestimation of their sizes [186]. The pattern of the scattered light resulting from hitting non-spherical particles can be varying as a function of the particle sizes, their shapes, the complex refractive index (the type of material), and the angle of scatter. The refractive index depends on both the light refraction and absorption of particles. The conversion from the angle and intensity of scattering to particle size is determined based either on the principles of Fraunhofer diffraction or Mie scattering theory [76]. Algorithms, based on Mie scattering theory, should ideally be applied for particles below a range of 25µm or 50µm, according to different studies [181,197,204]. The Mie theory requires the knowledge of refractive indices, which are not available for most organic materials and

not directly measurable within the available instruments. Thus, it practically problematic to use in the IWT process if striving for accurate PSD [197]. Alternatively, some laser diffraction instruments extend the lower limit of the Fraunhofer diffraction algorithm, that does not require the refractive index, by collecting the scattered measurements from two or three wavelengths of incident light at a fixed angle [76].

Light Obscuration Method:

Light obscuration is another method using light for measuring particle sizes. Light obscuration, also referred to as light blockage or light extinction measures the diametrically opposite compared to light scattering. Light obscuration measures the light absorbed or reflected away from the photodetector in the sensing zone by the particle. The obscuration of a particle then decreases the intensity on the photodetector generating an electric pulse [196]. Depending on the particle size, larger particles will intuitively block more light [193]. It delivers a measurement of size ranges usually from $(1-2)$µm and above [76,186,193]. Like ESZ, for accurate counting, only one particle must be present in the sensing volume, due to the same reasons described for the ESZ method [196]. Light obscuration particle counters differentiate from the ESZ method for determining particle size, as the method only measures in the two-dimensional plane. Thus, the particle size is determined based on the projected area and not the volume. Light obscuration excels in being less affected by variations in the relative refractive index compared to light scattering [186]. As an example of this, assume two different particles of identical size that passes through the sensing zone of both methods. One particle is crude oil, and the other is stainless steel. Due to their difference in the index of reflection, the particle of stainless steel will reflect considerably more light than the particle of crude oil [186]. Both types have their difficulties when particles refract light as the refracted light passes through the particle, i.e., microorganism, which is almost transparent [193,202]. Its disadvantage, compared to light scattering, is the lower sensitivity.

Ultrasonic Spectroscopy:

Ultrasonic spectroscopy, also referred to as ultrasonic attenuation or acoustic spectroscopy, is a relatively new technique that has emerged in the last couple of years, for online PSD analysis [181,186,202,205,206]. It is considered to have the potential for higher accuracy and feasibility beyond methods using light [186]. Its main advantages are the ability to penetrate opaque systems and still be non-invasive and non-intrusive in its way of measuring [181]. Also, the ultrasonic methods typically make measurements over a range of 1MHz to 200MHz, which enables them to cover a wide range of particle diameter, from 10nm to millimeters [206,207]. The measurement principle is based on ultrasonic waves travel through a sample material at different frequencies. All particles that pass through the measurement volume then transmit, reflect, absorb, or scatter the acoustic energy, equivalent to light methods. Thus, by measuring both the wave velocity and attenuation caused by the particles' morphology, the PSD can be estimated [205,206]. The ultrasonic velocity is the distance the ultrasonic wave moves through the sample per unit time, whereas the attenuation coefficient is a measure of the decrease in the amplitude of the ultrasonic wave per unit distance traveled [207].

The sound attenuation can be deployed in different ways: continuous waves, tone burst, or broadband pulses, all of which have shown their ability to give an estimate of the PSD [205]. The frequency spectrum of the transmitted ultrasonic signal can then be obtained by the application of fast Fourier transform (FFT) [202,208]. There are two approaches to gain the measured signal, through-transmission or pulse-echo. The through-transmission mode receives the ultrasonic signal on the opposite side of the sample volume. In comparison, the pulse-echo mode receives the reflected signal on the same side as the signal excitation [208]. The difficulty of using ultrasonic spectroscopy lies in the need to develop a proper model for determining the complex interactions

between ultrasonic waves and particles' properties, for calculation of the accurate particle size and classification [205,206]. Despite its advantages, it has some technical issues that must be addressed. Mostly, particles are assumed spherical, and the presence of small gas bubbles also obscures the signal in ultrasonic microscopy as they strongly scatter ultrasound [207]. Ultrasonic measurements also require knowledge of different thermophysical properties of the dispersed and continuous phases to interpret ultrasonic spectra, such as density, thermal conductivity, thermal expansion, viscosity, speed of sound in the continuous phase, and heat capacity [206]. Most properties might be known reasonably well for the continuous phase (IW) in the process, though, it is challenging to estimate for the dispersed phase (TSS) [206,207]. McClements [207] concludes that it is necessary to develop a database of the relevant thermophysical properties commonly observed in the dispersed phase of the process [207]. The database is also necessary for further classification of each particle. Even though it is possible to distinguish between oil droplets, solid particles, and gas bubbles, it is not straightforward, according to Zhang [209]. Most of the disadvantages may be solved in the near future as the technology is a less established measurement technique for measuring particle sizes and only a limited number of ultrasonic-based field applications are known in the oil and gas industry (i.e., Mirmorax).

Microscopy and Image Analysis:

For automated digital microscopy analysis of images, there differentiates between static and dynamic analysis. In static image analysis, images of the solution are captured by dispersing it onto a surface for analysis. As the particles are analyzed on a surface, they settle at a stable state and often orientate their largest projection area to the camera. In regard to static image analysis, it is often related to manual sampling or automatic at-line analysis based on integrated algorithms to analyze the solution. Instead, in relation to continuing online measurements in processes, dynamic microscopy analysis of images is used in both on- and in-line installations [185]. Digital microscopy utilizes a high-resolution video camera to capture images of the sample stream [66]. The 2D projection of the particles is then digitalized by conversion into pixels. The most common type of microscope used is called "bright field" as it forms a dark image of particles in focus with a bright background. The resolution of a microscope is a function of the optical magnification, focus quality, numerical aperture, type of immersion media, and also optical characteristics of particles (e.g., bacteria can be difficult to capture with bright field due to being opaque). The fundamental formula expresses the theoretical limit of resolution of a microscope:

$$d_0 = \lambda / 2NA, \tag{10}$$

where d_0 is the shortest distance between to measured points, λ is the wavelength of light used to capture the image, and NA is the numerical aperture. Using visible light closes to near-ultraviolet light (shortest wavelength) gives the highest resolution in the visible light spectrum; green light is often used as the visible light spectrum is centered at about 550nm, and an oil immersion objective lens with an $NA = 1.45$, then the (theoretical) limit of resolution is 190nm [210]. Consequently, particles in closer proximity than 0.2µm appear as a diffuse point, and their size will consequently be overestimated. The exact limitation for measuring the smallest particle size, with a given accuracy, should be specified by each individual manufacture, but usually, the smallest particle that is targeted is around $(1-2)$µm, as smaller particles are limited by the number of pixels that represents the particle. Through image analysis, particles are then identified, counted, and different geometric or physical properties can be calculated, such as the particle size, shape, and volume. For spherically shaped objects, such as droplets or bubbles, the size of the particles can easily be calculated such as Feret diameter or equivalent area diameter. Both oil droplets and gas bubbles are spherical but can be distinguished due to the differences in their optical properties [66]. Non-spherical shapes, microscopy analysis, has its advantage over other methods as being a direct method; it can include shape information. In the case of agglomerated,

spherically shaped particles, the software can classify particles and analyze their individual sizes. Still, for non-spherically shaped particles, it can be challenging to know where the interface is. Even though microscopy image analysis can measure more parameters than indirect methods, it is still facing a challenge to transfer the parameter information from the image into meaningful values. Therefore, often particle sizes are represented as equivalent diameter, though it has the possibility to measure both the width and height of particles. It even can represent other equivalent diameters than based on the projected area, as described in Sec. 6.1, e.g. maximum Feret diameter, equivalent circular perimeter diameter, or least bounding circle. Determination of particle sizes, for microscopy analysis, have, therefore, more freedom in selecting the parameter of interest. One advantage of microscopy over other methods is the fact that the images of the particles being analyzed can be stored and examined manually. By far, the biggest challenge by dynamic microscopy analysis is the limited depth of field. The small field of view should be representative for a given lot and are prone to introduce underrepresented statistics, as only a small fraction of the passing flow is analyzed. According to Shekunov [197], by following ISO 14488, the minimum number of particles should typically be above 1,000,000 particles to achieve a maximum PSD error of $<$1%. Furthermore, the limited depth of field also poses a challenge as particles out of focus is likely to be wrongly perceived.

6.4. Discrimination

From the theoretical background of each technique, as well as from each application described in this section, it is clear that each technique has both advantages and disadvantages. As such, no general advice can be provided about the selection of the most appropriate technique for a given application. Instead, the selection of the TSS monitoring technique depends on the characteristics of the different materials to be analyzed, such as physical form, particle size range, and particle concentration. As a general definition, it can be stated that meaningful particle size results can only be obtained if the provided experiments that are aimed for are well known, as well as the properties of the samples and the characteristics of the techniques used [187]. Most of the described methods in this section suffer from the fact that even though a size distribution may be obtained quickly and the number of particles is counted accurately, the highly sophisticated method for measuring the particle sizes is based on simple mathematical equations of calculation the equivalent diameter of a sphere and the existing shape influence are not taken into the equation [182]. Besides microscopy, which is based on direct observation, all other highlighted techniques in Sec. 6 are indirect methods based on some property of particles, except turbidimetry. For those indirect methods, the particle size is often obtained from characteristics of the sample that are well known and determined based on a calibration curve, assuming the particles to be perfectly spherical. These indirect methods work well in processes where the particles of interest are well known or dominant. However, in processes where the sample is diverse and, to some extend, "unknown", the indirect methods are challenged by their property assumptions. Fig. 18 presents what type of information different types of methods can provide.

As highlighted at the beginning of this section (Sec. 6), turbidity cannot bring any information about the particle size nor particle counts. However, knowing the change in TSS concentration by measuring the turbidity of the IW might be a useful support to the particle analyzer. The data information provided by indirect methods are more sensitive to changes in particulate concentration than turbidimeters, and thus offer additional information about process changes [193]. The challenge should be found in the highly sophisticated indirect methods for measuring the particle sizes are based on the equivalent diameter of a sphere, which bring little or no information about the what type of particles that are present, and can even output particle size measurements incorrectly, when the particles deviate extensively from being spherical. Another significant advantage of microscopy compared to other measurement techniques is the ability to discriminate particles captured by the equipment manually. The manual justification of particle classification is a general disadvantage whenever particle sizes are quantified based on an indirect method. There exist several commercially available image analysis systems. Some are already installed on trial to measure oil droplets and solid

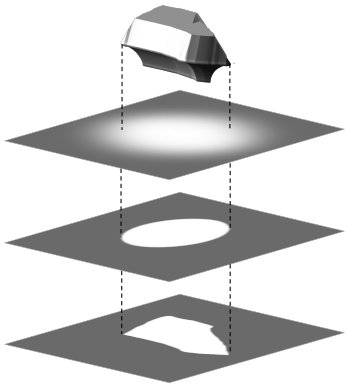

Figure 18. Illustration of data information available based on different type of particle analysis methods.

particles sizes and their concentration in the oil and gas industry. The amount of different applications for each microscopy type of measurement is great. The assortment of microscopy monitors is selected based on diversity in their measurement design, connection, detections, and current presence in the oil and gas industry.

Table 8. A non-exhaustive list with a comparison of five different image analysis monitors' design and options available.

Manufacturer Instrument name	**Jorin** ViPA	**J.M. Canty** InFlow	**Grundfos** Bacmon	**ParticleTech** oCelloScope	**SOPAT** MM2, Ma
Familiar with the oil and gas industry	✓	✓	✗	✗	(✓)*
Distinguish between solids, droplets, and bubbles	✓	✓	(✓)	(✓)	✓
Categorize different solid types	✓	✓	✓	✓	✓
Distinguish bacteria and abiotic particles	✗	✗	✓	✓	✗
Training classification (neural network, machine learning)	✗	✓	✓	✗	✗
View	2D	2D	3D	3D	2D
Connection	At-line/on-line	At-line/on-line/(in-line)	At-line/on-line	At-line	In-line
Measurement range [µm]	<150**	0.7 – 480	0.6<**	0.5< and >2000	0.5 – 90, 1.5 – 280
Pressure range [Bar]	<120	<689	2 – 10	–	0.01 – 3, 0.01 – 320
Temperature range [°C]	<120	–	5 – 40	20 – 40 (operation temp.)	0 – 50
Flow velocity [m/s]	0.03 – 2.1 (0.05 – 4)L/min	0.25 – 2.74	Batch operation, 10min cycle	Batch operation, 10min cycle	–
Frame rate [Hz]	30	30	–	–	15
Cleaning procedure	Manually with flexible stick	Automatically vapor removal system	Flushed between each batch cycle for 1min	Flushed between each batch	Automatically liquid cleaner (Ceramat Sensor Lock-Gate)
ATEX approved	✓	✓	✗	✗	✗,✓

*Applied at a testing facility related to upstream oil-water separation process. However, to the authors knowledge it has not been installed at a fully integrated upstream separation process.
**Minimum or maximum measurement range is not explicitly defined.

It can be challenging to assess each microscopy analyzer's strengths and limitations based on performance in different documentations. Therefore, the list is not based on performance in different publications, but only specifications provided by companies in their manuals, publications, and websites. There is a general tendency for incomplete documentation and guidance of their software's potential. Although the price and complexity of various microscopic monitors vary tremendously, particle examination with microscopy is generally at the high-end of the market, compared to the other methods, i.e., turbidimeters, which only cost a fraction of microscopy analyzers [185]. In addition to being financially expensive to invest in microscopy, the manufacturers offer services, such as courses, installation, and maintenance, which incentivize the manufacturers to retain their documentation as confidential and enhance the demand of their offered services. Although, poorly written or lack of details in user manuals has been well described by Shand [211]. Manufacturers who do not offer a detailed description of the user manual can make the implementation process difficult, particularly if parts of the product is not defined, or of the users find discrepancies between the product and the user manual, and thereby have difficulties determining which one is the true statement [211]. Shand [211] further suggests that the user manual must be written as the same quality that would be expected at the quality of the product. The cost of poorly written user manuals to both the supplier and manufacturer can be high but it is seldom calculated [211]. In Table 8, J.M. Canty InFlow and Jorin ViPA are selected based on the familiarity in the offshore the oil and gas industry [212,213]. That entails that they are ATEX approved, have been in the business for several years, and have the knowledge of the challenges related to offshore installations. Thus, they can handle high pressures, temperatures, and are made of materials that can handle the hazardous environments. Both monitors are similar in their design, where liquid flows through a flow cell while taking pictures from one side of the flow cell window and on the opposite a light source. The monitors then capture the oriented area of the objects perpendicular to the camera with a frame rate of ∼30Hz, respectively. Besides their software-design and selection of different hardware, they basically use the same principles and can output more or less the same parameters of each object. For Jorin ViPA, it is up to the operator to determine the discrimination based on the different parameter ranges selected, which gives freedom and entrust the operators to be specialists in their instrument to use it properly. That may sound positive, but with a lack of detailed description of the instrument software, the freedom to adjust every value can become a challenge to evaluate its influence on the outcome result. The J.M. Canty InFlow uses neural networks/machine learning to classify different objects. That gives the operator the option to train the classifier to become more accurate without tuning every parameter manually to define a class. That increment of the human-computer interaction (HCI) feature should undoubtedly ease the classification process to classify each particle more correctly. Another benefit of the J.M. Canty InFlow compared to Jorin ViPA is the selection of having an automatic cleaning procedure for removing any fouling on the view-cell.

Grundfos Bacmon and ParticleTech oCelloScope are very similar in their design by letting the sample through the flow-cell. The sample is then captured and held still between the inlet and outlet, while the scanning procedure is running. The scanning procedure is executed along the flow-cell with a tilted camera, causing each particle to be recorded several times at different locations. By stacking the sliced image planes of the flow sample, it is possible to create 3D images of the present particles to overcome the limitation of only capturing the oriented area [214,215]. Since the late 1980s, even with the analysis of two-dimensional images, the lack of shape information to predict particle behavior can be woefully inadequate [182]. As stated back then by Leschonski [182]:

"...two-dimensional image cannot yield information on the three-dimensional particle unless the particle is either rotated or cut into slices during analysis."

or

"... three-dimensional shape will at least demand information to be taken from three perpendicular planes."

The Bacmon monitor is specifically developed to distinguish between bacteria and abiotic particles in drinking water. The classification is done by neural networks establishing a boundary between bacteria and abiotic particles in a 59-dimensional parameter space. Theirs developed library includes a prefix of different morphological shapes, such as rods, curved rods, and cocci, as well as various abiotic particle morphologies, e.g., clay [215]. Compared to Grundfos, ParticleTech has a broader application focus, such as crystallization, sand, and fermentation. However, it difficult to distinguish between both units as the available information about the ParticleTech analyzer system is limited. One promising solution presented by ParticleTech is how the manual defined particle classes can be represented by colors after the analysis, which is convenient for operators. Lastly, the two microscopy analyzers: SOPAT MM2 and Ma from Table 8 are similar in their design. The reason for adding both to the list is simply to show that one manufacture can have several products that could be of interest. The same applies to the InFlow by J.M. Canty, which has multiple design selections to customize the unit for each customer need. The SOPAT microscopy analyzers are endoscopic devices that enable in-line installations in the process, assuming that the process has different sensor lock-gates installed. According to Panckow [216], SOPAT microscopy analyzers can automatically output the equivalent diameter and detect irregular shapes by analyzing the edges of expected particles. It should be possible to evaluate each particle manually by means of an integrated interface tool [216]. Their design as an endoscope is what that differentiates them from other microscopy analyzers, like Jorin ViPA and J.M. Canty InFlow. It can be useful in processes where only spot-checks are necessary at different locations, which require only one monitor, or in volumes where accurate on-line sampling are troublesome, like analyzing the homogeneity in a tank at different levels and locations. All five different microscopy analyzers adequately cover the necessary TSS measurement criteria at an offshore IWT process, based on the Sec. 3, to discriminate between different particles, as a minimum between bubbles, droplets, and solids. The authors highly recommend using identical microscopy analyzers in the entire process to reduce the uncertainty between different monitors [66].

The ViPA and the InFlow monitors have the advantage of being familiar with the oil and gas industry. Though, J.M. Canty InFlow may satisfy the application mostly as they have an automatic cleaning procedure and strive to ease the classification process of discriminating different bubbles, droplets, and solids. An automatic cleaning procedure of the view-cell is highly favored, if not a demand. HCI classification process by J.M. Canty InFlow and ParticleTech's colorization of each particle class objects are software features that companies should strive to incorporate in their software design to ease operators' work. However, future microscopy analyzers would draw the benefit of striving for measuring 3D images of particles, e.g., Bacmon and ParticleTech, to remove the limitation of only being the oriented area of particles in a 2D image that is measured. Thus, 3D images enhance the classification of each particle and increase accuracy. However, it should be noted that 3D image analysis introduces more complexity. If a sampling point for on-line monitoring is considered to misrepresent the mainstream, or operators are discerning an undesired maldistribution at specific areas in the process, an alternative could be to design an in-line endoscope analyzer, e.g., SOPAT, to measure the TSS parameters at different levels in the process stream. In-line sensor lock-gates installment also benefits for measure TSS parameters at locations were continuous online monitoring is not a necessity.

7. Conclusion

Although energy consumption in developed countries is approaching a plateau, and we are entering a new era of climate changes that must be reduced over the next several years, global oil production is still expected to increase in the next 30 years, according to EIA. In the world's transition to becoming CO_2-neutral, developed countries have a responsibility not to force the emission of greenhouse gases (GHG) outside their borders, as it can undermine the effectiveness through "carbon

leakage". The oil and gas industry can play a part in the transition by continually investing in the most innovative solutions that improve energy efficiency and researching new technologies that minimize GHG-emissions. The importance and awareness of accurate online water quality measurements increase every year, whether in water industries to enhance the drinking water quality and the wastewater disposal, or in the oil and gas industry to enhance the produce water discharge or reinjecting it into the reservoir. Accurate water analysis can yield valuable analytical information that is necessary to gain an understanding of the dispersed matters of the produced and injected water to identify changes in the process. The water analysis and online measurement of total suspended solids (TSS) can assist in identifying possible contamination in the process and its location, scale deposition corrosion tendencies, support the addition of chemicals in the process, and aid to the design of the injection water treatment (IWT) process if changes are necessary. However, online measurement of TSS must be sampled correctly, analyzed correctly, and interpreted correctly; either way, they can be more harmful than no data. Online measurement of TSS can be used for decision support to indicate whether corrective actions are necessary and assist in confirming the success, or failure, of past actions. Furthermore, online measurement of TSS parameters can even be used for advanced control to achieve better operation in the treatment process, all of which benefit in water-intensive operation. Monitoring the produced water discharge can also help to protect the receiving environment. Even though the methods and designs of different TSS monitors reviewed in this paper are related to offshore IWT facilities, transferring the monitor to other water treatment facilities will be evident, i.e., water treatment and biofuel facilities. The importance of water quality for maintaining long-term water injection of both produced water and seawater has been discussed in detail in this paper. It has been highlighted that the key to maintaining a long-term water injection is usually related directly or indirectly to the water quality. However, the cost of IWT should be justified against periodic well-stimulation.

Reductions in injectivity are mostly a combination of different water quality problems as they are often interlinked, rather than a single problem. Several water quality effects add to the TSS concentration, such as solids, oil content through produced water reinjection, scales, corrosion disposal, and bacterial growth, all of which have been discussed. A case study of measuring the TSS concentration of seawater from the Danish sector of the North Sea has been executed. The results from the case study of the seawater were evaluated in order to effectively quantify water quality through the process of an IWT facility. The results showed that the instrument of monitoring the particle size distribution should be measurable within an overall TSS concentration from $>$30.5mg/L ($\mu + 2\sigma$) to $\sim$0mg/L for this particular IWT facility.

Several on- or in-line techniques have been evaluated as candidates for measuring TSS parameters. Through a discrimination process, based on results in several studies, the author strongly believes measuring different TSS parameters with microscopy will bring the most promising results. Most techniques suffer from the fact that particle sizes are based on the equivalent diameter of a sphere, and the existing shape influence is not taken into the equation. The last part of the paper outlined five different microscopy analyzers for measuring TSS. Each microscopy analyzer has been compared, and an evaluation of future design considerations of microscopy analyzers have been discussed, aiming for more promising results of measuring TSS. Future development of measuring TSS should aim to present shape analysis to increase the accuracy of the TSS parameters and correlate the shape information to other physical particle properties to better classify each particle to its morphology and thereby increase the awareness of the water quality issues for operators.

Author Contributions: Validation, D.S.H and M.V.B; investigation, D.S.H; resources, S.M.Ø.L; data curation, S.M.Ø.L; writing—original draft preparation, D.S.H; writing—review, D.S.H; editing D.S.H, M.V.B, S.M.Ø.L, and Z.Y; supervision, Z.Y.; funding acquisition, Z.Y. All authors have read and agreed to the published version of the manuscript.

Funding: This research was funded by DHRTC projects: "Injection Water Quality and Control" (Proj-no.: 878040).

Acknowledgments: The authors would like to thank the support from the DTU DHRTC and thank the colleagues: L. Hansen, and S. Jespersen from AAU, for many valuable discussions and supports. A special thanks go to colleagues at Total Danmark A/S in Esbjerg for valuable supports.

Conflicts of Interest: The authors declare no conflict of interest.

Abbreviations

The following abbreviations are used in this manuscript:

APB	acid-producing bacteria
API	American Petroleum Institute
ASTM	American Society for Testing and Materials
CDOM	colored dissolved organic matter
EIA	Energy Information Administration
EOR	enhanced oil recovery
EPS	extracellular polymeric substance
ESZ	electrical sensing zone
EU	European Union
FFT	fast Fourier transform
GHG	greenhouse gases
H_0	null-hypotheses
HCI	human-computer interaction
IEA	International Energy Agency
IOB	iron/manganese-oxidizing bacteria
IPCC	Intergovernmental Panel on Climate Change
IRB	iron-reducing Bacteria
ISO	International Organization for Standardization
IW	injection water
IWT	injection water treatment
MIC	microbially influenced corrosion
MDB	metal-depositing bacteria
MRB	metal-reducing bacteria
NGS	next generation sequencing
NRB	nitrate-reducing bacteria
NTU	nephelometric turbidity units
OCED	European countries of Organisation for Economic Co-operation and Development
OIP	oil in place
ppm	parts per million
PW	produced water
PWRI	produced water reinjection
SDG	sustainable development goal
SRB	sulfate-reducing bacteria
SFB	slime-forming bacteria
SSC	suspended sediment concentration
TDS	total dissolved solids
TSS	total suspended solids
UN	United Nation
UV	ultraviolet

References

1. EIA. International Energy Outlook 2019. Technical report, U.S. Energy Information Administration, Washington, DC, 2019.
2. Klimarådet. Kendte Veje og Nye Spor til 70 Procents Reduktion: Retning og iltag for de næste ti års klimaindsats i Danmark. Technical report, Klimarådet, Copenhagen, 2020.
3. Ritchie, H.; Roser, M. CO_2 and Greenhouse Gas Emissions, 2019.

4. European Commission. Supplementing Directive 2003/87/EC of the European Parliament and of the Council concerning the determination of sectors and subsectors deemed at risk of carbon leakage for the period 2021 to 2030. *Official Journal of the European Union, L120* **2019**, *62*, 20–26.
5. Masnadi, M.S.; El-Houjeiri, H.M.; Schunack, D.; Li, Y.; Englander, J.G.; Badahdah, A.; Monfort, J.C.; Anderson, J.E.; Wallington, T.J.; Bergerson, J.A.; Gordon, D.; Koomey, J.; Przesmitzki, S.; Azevedo, I.L.; Bi, X.T.; Duffy, J.E.; Heath, G.A.; Keoleian, G.A.; McGlade, C.; Meehan, D.N.; Yeh, S.; You, F.; Wang, M.; Brandt, A.R. Global carbon intensity of crude oil production. *Science* **2018**, *361*, 851–853. doi:10.1126/science.aar6859.
6. IPIECA. Meeting energy needs: The unique role of oil and gas. Technical report, The global oil and gas industry association for environmental and social issues, London, 2014.
7. SEI.; IISD.; ODI.; Analytics Climate.; CICERO.; UNEP. The Production Gap: The discrepancy between countries' planned fossil fuel production and global production levels consistent with limiting warming to 1.5°C or 2°C. Technical report, The Production Gap, 2019.
8. IPIECA.; UNDP.; IFC. Mapping the Oil and Gas Industry To the Sustainable Development Goals: An Atlas. Technical report, The global oil and gas industry association for environmental and social issues, London, 2017.
9. IEA.; IRENA.; WHO.; WB.; UNSD. Tracking SDG7: The Energy Progress Report. Technical report, The World Bank Group, Washington, DC, 2019.
10. IEA.; IRENA.; WHO.; WB.; UNSD. Tracking SDG7: The Energy Progress Report. Technical report, The World Bank Group, Washington, DC, 2018.
11. United Nations. *The Sustainable Development Goals Report 2019*; The Sustainable Development Goals Report, United Nations Publications: New York, NY, 2019; p. 61. doi:10.18356/55eb9109-en.
12. IEA. Energy Access Outlook 2017. Technical report, International Energy Agency, Paris, 2017.
13. EIA. International Energy Outlook 2019: World Energy Projection System Plus, 2019.
14. Hamiche, A.M.; Stambouli, A.B.; Flazi, S. A review of the water-energy nexus. *Renewable and Sustainable Energy Reviews* **2016**, *65*, 319–331. doi:10.1016/j.rser.2016.07.020.
15. Whalen, T. The Challenges of Reusing Produced Water. *Journal of Petroleum Technology* **2012**, *64*, 18–20. doi:10.2118/1112-0018-JPT.
16. IEA. Water Energy Nexus. Technical report, International Energy Agency, Paris, 2017.
17. Ahmed, U. Making the Most of Maturing Fields. *Oilfield Review* **2004**, *16*, 1–1.
18. Blanchard, E. Oil in Water Monitoring is a Key to Production Separation. *Offshore* **2013**, *73*, 104–105.
19. Maxwell, S. Implications of Re-Injection of Produced Water on Microbially Influenced Corrosion (MIC) in Offshore Water Injection Systems. CORROSION 2005; NACE International: Houston, TX, 2005; p. 9.
20. OSPAR Commission. List of Decisions, Recommendations and Other Agreements Applicable within the Framework of the OSPAR Convention - Update 2018. Technical report, OSPAR, London, 2018.
21. Severin Hansen, D.; Jespersen, S.; Bram, M.V.; Yang, Z. Uncertainty Analysis of Fluorescence-Based Oil-In-Water Monitors for Oil and Gas Produced Water. *Sensors* **2020**, *20*, 36. doi:10.3390/s20164435.
22. Bavière, M. *Basic Concepts in Enhanced Oil Recovery Processes*, 1 ed.; Critical Reports on Applied Chemistry Volume 33, Elsevier: London, 1991; pp. v–viii.
23. Hartmann, D.J.; Beaumont, E.A. Predicting Reservoir System Quality and Performance. In *Handbook of Petroleum Geology: Exploring for Oil and Gas Traps*, 1 ed.; Beaumont, E.A.; Foster, N.H., Eds.; The American Association of Petroleum Geologists: Tulsa, OK, 1999; Vol. 3, *Handbook of petroleum geology*, chapter 9, p. 154. doi:10.1306/TrHbk624C9.
24. Petroleum Council National.; Enhanced Recovery Techniques.; Committee on National Petroleum Council. *Enhanced oil recovery, EOR: an analysis of the potential for enhanced oil recovery from known fields in the United States, 1976 to 2000*, 1 ed.; National Petroleum Council: Washington, DC, 1976; p. 231.
25. Marle, C.M. Oil entrapment and mobilization. In *Basic Concepts in Enhanced Oil Recovery Processes*, 1 ed.; Bavière, M., Ed.; Elsevier: Paris, 1991; Vol. 33, *Critical Reports on Applied Chemistry Volume 33*, chapter 1, pp. 3–39.
26. British Petroleum. BP Statistical Review of World Energy June 2017. Technical report, British Petroleum, London, 2017.
27. Ostroff, A. Injection Water Problems Identified By Laboratory Analysis. Middle East Technical Conference and Exhibition; Society of Petroleum Engineers: Manama, 1981; pp. 523 – 526. doi:10.2118/9632-MS.

28. Carll, J.F. *The geology of the oil regions of Warren, Venango, Clarion, and Butler Counties; including surveys of the Garland and Panama conglomerates in Warren and Crawford, and in Chautauqua Co., N. Y., descriptions of oil well rig and tools, and a discussion of th*, 1 ed.; Report of progress, Harrisburg: Board of Commissioners for the Second geological survey: Washington, DC, 1880; pp. 256–269.
29. Simmons, A.C. Recent Developments in Water Flooding in the Bradford District. Drilling and Production Practice; American Petroleum Institute: Amarillo, TX, 1938; pp. 260–266.
30. Cerini, W.F.; Battles, W.R.; Jones, P. Some Factors Influencing the Plugging Characteristics of an Oil-well Injection Water. *Transactions of the AIME* **1946**, *165*, 52–63. doi:10.2118/946052-G.
31. Babson, E.; Sherborne, J.; Jones, P. An Experimental Water-flood in a California Oil Field. *Transactions of the AIME* **1944**, *160*, 25–33. doi:10.2118/945025-G.
32. Ellenberger, A.R.; Holben, J.H. Flood Water Analyses and Interpretation. *Journal of Petroleum Technology* **1959**, *11*, 22–25. doi:10.2118/1199-G.
33. Watkins, J.W.; Willett Jr, F.R.; Arthur, C.E. Conditioning Water for Secondary-Recovery in Midcontinent Oil Fields. Technical report, Bureau of Mines, Bartlesville, OK, Washington, DC, 1952.
34. Safari, M. Effect of Different Water Injection Rate on Reservoir Performance: A Case Study of Azadegan Fractured Oil Reservoir. International Conference of Oil, Gas, Petrochemical and Power Plant; Scientific Information Database: Tehran, 2012; Vol. 1, p. 8.
35. Yu, K.; Li, K.; Li, Q.; Li, K.; Yang, F. A method to calculate reasonable water injection rate for M oilfield. *Journal of Petroleum Exploration and Production Technology* **2017**, *7*, 1003–1010. doi:10.1007/s13202-017-0356-9.
36. Bansal, K.; Caudle, D. A New Approach for Injection Water Quality. SPE Annual Technical Conference and Exhibition; Society of Petroleum Engineers: Washington, DC, 1992; pp. 383 – 396. doi:10.2118/24803-MS.
37. Patton, C.C. Water Quality Control and Its Importance in Waterflooding Operations. *Journal of Petroleum Technology* **1988**, *40*, 1123–1126. doi:10.2118/18459-PA.
38. Yari, M.; Mansouri, H.; Esmaili, H.; Alavi, S.A. A Study of Microbial Influenced Corrosion in Oil and Gas Industry. International Conference of Oil, Gas, Petrochemical and Power Plant; Civilica: Tehran, 2012; Vol. 1, p. 11. doi:10.13140/RG.2.1.3117.8089.
39. Cantor, A.F.; Park, J.K.; Vaiyavatjamai, P. The Effect of Chlorine on Corrosion in Drinking Water Systems. Technical report, University of Wisconsin-Madison, Madison, WI, 2000. doi:10.1.1.137.1011.
40. Bennion, D.; Bennion, D.; Thomas, F.; Bietz, R. Injection Water Quality - A Key Factor to Successful Waterflooding. Annual Technical Meeting; Petroleum Society of Canada: Calgary, 1994; Vol. 37, pp. 53–62. doi:10.2118/94-60.
41. Rochon, J.; Creusot, M.; Rivet, P.; Roque, C.; Renard, M. Water Quality for Water Injection Wells. SPE Formation Damage Control Symposium; Society of Petroleum Engineers, Society of Petroleum Engineers: Lafayette, LA, 1996; pp. 489–503. doi:10.2118/31122-MS.
42. Mitchell, R.W. The Forties Field Sea Water Injection System. *Journal of Petroleum Technology* **1978**, *30*, 877–884. doi:10.2118/6677-PA.
43. Mitchell, R.W.; Finch, E.M. Water Quality Aspects of North Sea Injection Water. *Journal of Petroleum Technology* **1981**, *33*, 1141–1152. doi:10.2118/8069-PA.
44. Prandle, D.; Hydes, D.J.; Jarvis, J.; McManus, J. The Seasonal Cycles of Temperature, Salinity, Nutrients and Suspended Sediment in the Southern North Sea in 1988 and 1989. *Estuarine, Coastal and Shelf Science* **1997**, *45*, 669–680. doi:10.1006/ecss.1996.0227.
45. Eisma, D.; Cadee, G.C.; Laane, R.W.P.M. Supply of Suspended Matter and Particulate and Dissolved Organic Carbon from the Rhine to the Coastal North Sea. *Transport of Carbon and Minerals in Major World Rivers* **1982**, *52*, 483–506.
46. Aguirre-Gómez, R. Detection of total suspended sediments in the North Sea using AVHRR and ship data. *International Journal of Remote Sensing* **2000**, *21*, 1583–1596. doi:10.1080/014311600209913.
47. Gray, J.R.; Glysson, G.D.; Turcios, L.M.; Schwarz, G.E. Comparability of suspended-sediment concentration and total suspended solids data. Technical Report 00-4191, U.S. Department of the Interior and U.S. Geological Survey, Reston, VA, 2000. doi:10.3133/wri004191.
48. Folk, R.L. *Petrology of Sedimentary Rocks*, 2 ed.; Hemphill Publishing Company: Austin, TX, 1980; p. 184.
49. Udden, J.A. *The Mechanical Composition of Wind Deposits*, 1 ed.; Number 1, Augustana College and Theological Seminary: Rock Island, IL, 1898; p. 69.

50. Wentworth, C.K. A Scale of Grade and Class Terms for Clastic Sediments. *The Journal of Geology* **1922**, *30*, 377–392.
51. Blott, S.J.; Pye, K. Particle Size Scales and Classification of Sediment Types Based on Particle Size Distributions: Review and Recommended Procedures. *Sedimentology* **2012**, *59*, 2071–2096. doi:10.1111/j.1365-3091.2012.01335.x.
52. Krumbein, W.C. Application of Logarithmic Moments to Size Frequency Distributions of Sediments. *Journal of Sedimentary Research* **1936**, *6*, 35–47. doi:10.1306/D4268F59-2B26-11D7-8648000102C1865D.
53. Bader, M. Seawater versus produced water in oil-fields water injection operations. *Desalination* **2007**, *208*, 159–168. doi:10.1016/j.desal.2006.05.024.
54. Gao, C. Factors affecting particle retention in porous media. *Emirates Journal for Engineering Research* **2007**, *12*, 7.
55. Nielsen, B.L.; Nygaard, E.; Reffstrup, J.; Ter-Borch, N. Bjergarters Reservoiregenskaber.
56. Abramovitz, T. Geophysical imaging of porosity variations in the Danish North Sea chalk. *Geological Survey of Denmark and Greenland Bulletin* **2008**, *15*, 17–20.
57. Jørgensen, L.N.; Andersen, P.M. Integrated Study of the Kraka Field. Offshore Europe; Society of Petroleum Engineers: Aberdeen, 1991; pp. 461–474. doi:10.2118/23082-MS.
58. Hardman, R.F.P. Chalk reservoirs of the North Sea. *Bulletin of the Geological Society of Denmark* **1982**, *30*, 119–137.
59. Torsaeter, O. An Experimental Study of Water Imbibition in Chalk From the Ekofisk Field. SPE Enhanced Oil Recovery Symposium; Society of Petroleum Engineers: Tulsa, OK, 1984; Vol. 2, pp. 93–104. doi:10.2118/12688-MS.
60. Barkman, J.; Davidson, D. Measuring Water Quality and Predicting Well Impairment. *Journal of Petroleum Technology* **1972**, *24*, 865–873. doi:10.2118/3543-PA.
61. Shutong, P.; Sharma, M. A Model for Predicting Injectivity Decline in Water-Injection Wells. *SPE Formation Evaluation* **1997**, *12*, 194–201. doi:10.2118/28489-PA.
62. Eylander, J. Suspended Solids Specifications for Water Injection From Coreflood Tests. *SPE Reservoir Engineering* **1988**, *3*, 1287–1294. doi:10.2118/16256-PA.
63. Ogden, B.L. Water Technology: Understanding, Interpreting and Utilizing Water Analysis Data. Southwestern Petroleum Short Course Conference 2008; Southwestern Petroleum Short Course: Lubbock, TX, 2008; p. 12.
64. Hansen, D.S.; Jespersen, S.; Bram, M.V.; Yang, Z. Human Machine Interface Prototyping and Application for Advanced Control of Offshore Topside Separation Processes. IECON 2018 - 44th Annual Conference of the IEEE Industrial Electronics Society; IEEE: Washington, DC, 2018; pp. 2341–2347. doi:10.1109/IECON.2018.8591309.
65. Hansen, D.S.; Bram, M.V.; Yang, Z. Efficiency investigation of an offshore deoiling hydrocyclone using real-time fluorescence- and microscopy-based monitors. 2017 IEEE Conference on Control Technology and Applications (CCTA); IEEE: Mauna Lani, HI, 2017; pp. 1104–1109. doi:10.1109/CCTA.2017.8062606.
66. Yang, M. Measurement of Oil in Produced Water. In *Produced Water*, 1 ed.; Lee, K.; Neff, J., Eds.; Springer-Verlag: New York, NY, 2011; chapter 2, pp. 57–88. doi:10.1007/978-1-4614-0046-2.
67. OSPAR Commission. Produced Water Discharges from Offshore Oil and Gas Installations 2007-2012, 2014.
68. Larsen, I. Denmark's Oil and Gas Production – and Subsoil Use 09. Technical report, Energistyrelsen, Copenhagen, 2010.
69. Miløstyrelsen. Generel tilladelse for Total E&P Danmark A/S (TOTAL) til anvendelse, udledning og anden bortskaffelse af stoffer og materialer, herunder olie og kemikalier i produktions- og injektionsvand fra produktionsenhederne Halfdan, Dan, Tyra og Gorm for perioden 1. Technical report, Total E&P Danmark A/S, Copenhagen, 2018.
70. Danish Energy Agency. Production. Technical report, Danish Energy Agency, Esbjerg, 2016.
71. Hansen, D.; Bram, M.; Durdevic, P.; Jespersen, S.; Yang, Z. Efficiency evaluation of offshore deoiling applications utilizing real-time oil-in-water monitors. Oceans 2017 - Anchorage; IEEE: Anchorage, AK, 2017; p. 6.
72. Danish Energy Agency. Yearly production, injection, flare, fuel and export in SI units 1972-2019, 2020.
73. Miløstyrelsen. Generel tilladelse for Maersk Olie og Gas A/S (Maersk Olie) til anvendelse, udledning og anden bortskaffelse af stoffer og materialer, herunder olie og kemikalier i produktions- og injektionsvand

fra produktionsenhederne Halfdan, Dan, Tyra og Gorm for per. Technical report, Mærsk Olie og Gas A/S, Copenhagen, 2016.
74. OSPAR Commission. OSPAR report on discharges, spills and emissions from offshore oil and gas installations in 2014. Technical report, OSPAR, London, 2016.
75. Kokal, S.; Al-Dawood, N.; Fontanilla, J.; Al-Ghamdi, A.; Nasr-El-Din, H.; Al-Rufaie, Y. Productivity Decline in Oil Wells Related to Asphaltene Precipitation and Emulsion Blocks. *SPE Production & Facilities* **2003**, *18*, 247–256. doi:10.2118/87088-PA.
76. Baird, R.B.; Eaton, A.D.; Rice, E.W. *Standard methods for the examination of water and wastewater*, 23 ed.; American Public Health Association, American Water Works Association, and Water Environment Federation: Washington, DC, 2017; chapter 2, pp. 66 – 82.
77. Allhands, M.N. The Efficient Removal of Organic and Inorganic Suspended Solids – Old Problem, New Technology. *Water Online Newsletter* **2003**, p. 11.
78. Kennicutt, M.C. Water Quality of the Gulf of Mexico. In *Habitats and Biota of the Gulf of Mexico: Before the Deepwater Horizon Oil Spill*, 1 ed.; Ward, C.H., Ed.; Springer New York: New York, NY, 2017; Vol. 1, chapter 2, pp. 55–164. doi:10.1007/978-1-4939-3447-8.
79. Boyd, C.E. Dissolved Solids. In *Water Quality*, 2 ed.; Boyd, C.E., Ed.; Springer International Publishing: Cham, 2015; chapter 4, pp. 71–100. doi:10.1007/978-3-319-17446-4.
80. Nasr-El-Din, H.; Al-Taq, A. Water Quality Requirements and Restoring the Injectivity of Waste Water Disposal Wells. SPE Formation Damage Control Conference; Society of Petroleum Engineers: Lafayette, LA, 1998; pp. 565–573. doi:10.2118/39487-MS.
81. Zheng, J.; Chen, B.; Thanyamanta, W.; Hawboldt, K.; Zhang, B.; Liu, B. Offshore produced water management: A review of current practice and challenges in harsh/Arctic environments. *Marine Pollution Bulletin* **2016**, *104*, 7–19. doi:10.1016/j.marpolbul.2016.01.004.
82. Coleman, J.; McLelland, W. Produced Water Re-Injection; How Clean is Clean? SPE Formation Damage Control Symposium; Society of Petroleum Engineers: Lafayette, LA, 1994; p. 5. doi:10.2118/27394-MS.
83. Donham, J. Offshore Water Injection System: Problems and Solutions. Offshore Technology Conference; Offshore Technology Conference: Houston, TX, 1991; pp. 53–57. doi:10.4043/6782-MS.
84. Patton, C.C. Injection-Water Quality. *Journal of Petroleum Technology* **1990**, *42*, 1238–1240. doi:10.2118/21300-PA.
85. Bennion, D.; Thomas, F.; Imer, D.; Ma, T.; Schulmeister, B. Water Quality Considerations Resulting in the Impaired Injectivity of Water Injection and Disposal Wells. *Journal of Canadian Petroleum Technology* **2001**, *40*, 54 – 61. doi:10.2118/01-06-05.
86. Jepsen, K.; Bram, M.; Pedersen, S.; Yang, Z. Membrane Fouling for Produced Water Treatment: A Review Study From a Process Control Perspective. *Water* **2018**, *10*, 847. doi:10.3390/w10070847.
87. Owen, G.; Bandi, M.; Howell, J.A.; Churchouse, S.J. Economic assessment of membrane processes for water and waste water treatment. *Journal of Membrane Science* **1995**, *102*, 77–91. doi:10.1016/0376-7388(94)00261-V.
88. van Oort, E.; van Velzen, J.; Leerlooijer, K. Impairment by Suspended Solids Invasion: Testing and Prediction. *SPE Production & Facilities* **1993**, *8*, 178–184. doi:10.2118/23822-PA.
89. Kwon, D.Y.; Vigneswaran, S.; Fane, A.G.; Aim, R.B. Experimental determination of critical flux in cross-flow microfiltration. *Separation and Purification Technology* **2000**, *19*, 169–181. doi:10.1016/S1383-5866(99)00088-X.
90. Pautz, J.; Crocker, M.; Walton, C. Relating Water Quality and Formation Permeability to Loss of Injectivity. SPE Production Operations Symposium; Society of Petroleum Engineers: Oklahoma City, OK, 1989; pp. 565–576. doi:10.2118/18888-MS.
91. Abrams, A. Mud Design To Minimize Rock Impairment Due To Particle Invasion. *Journal of Petroleum Technology* **1977**, *29*, 586–592. doi:10.2118/5713-PA.
92. Wang, S.; Civan, F. Preventing Asphaltene Deposition in Oil Reservoirs by Early Water Injection. SPE Production Operations Symposium; Society of Petroleum Engineers: Oklahoma City, OK, 2005; p. 14. doi:10.2118/94268-MS.
93. Permadi, A.K.; Naser, M.A.; Mucharam, L.; Rachmat, S.; Kishita, A. Formation Damage and Permeability Impairment Associated with Chemical and Thermal Treatments: Future Challenges in EOR Applications. In *The Contribution of Geosciences to Human Security*, 1 ed.; Institut Teknologi Bandung.; Kyoto University.; Kyoto University GCOE Program of HSE., Eds.; Logos Verlag: Berlin, 2012; chapter 7, pp. 103–126.

94. Khilar, K.C.; Vaidya, R.; Fogler, H. Colloidally-induced fines release in porous media. *Journal of Petroleum Science and Engineering* **1990**, *4*, 213–221. doi:10.1016/0920-4105(90)90011-Q.
95. Bazin, B.; Esperanza, S.; Le Thiez, P. Control of Formation Damage by Modeling Water/Rock Interaction. SPE Formation Damage Control Symposium; Society of Petroleum Engineers: Lafayette, LA, 1994; pp. 249–258. doi:10.2118/27363-MS.
96. Shrestha, R.A.; Zhang, A.P.; Mateus, E.P.; Ribeiro, A.B.; Pamukcu, S. Electrokinetically Enabled De-swelling of Clay. In *Electrokinetics Across Disciplines and Continents*; Ribeiro, A.B.; Mateus, E.P.; Couto, N., Eds.; Springer International Publishing: Cham, 2016; chapter 3, pp. 43–56. doi:10.1007/978-3-319-20179-5.
97. Merdhah, A.B.B.M. The study of scale formation in oil reservoir during water injection at high-barium and high-salinity formation water. PhD thesis, Universiti Teknologi Malaysia, Skudai, 2008.
98. Amiri, M.; Moghadasi, J. Prediction the Amount of Barium Sulfate Scale Formation in Siri Oilfield using OLI ScaleChem Software. *Asian Journal of Scientific Research* **2010**, *3*, 230–239. doi:10.3923/ajsr.2010.230.239.
99. Amiri, M.; Moghadasi, J.; Jamialahmadi, M. Prediction of Iron Carbonate Scale Formation in Iranian Oilfields at Different Mixing Ratio of Injection Water with Formation Water. *Energy Sources, Part A: Recovery, Utilization, and Environmental Effects* **2013**, *35*, 1256–1265. doi:10.1080/15567036.2010.514596.
100. Merdhah, A.B.B.; Yassin, A.A.M. Calcium and Strontium Sulfate Scale Formation Due to Incompatible Water. International Graduate Conference on Engineering and Science 2008; Universiti Teknologi Malaysia: Skudai, 2008; p. 9.
101. Collins, I.R.; Jordan, M.M. Occurrence, Prediction, and Prevention of Zinc Sulfide Scale Within Gulf Coast and North Sea High-Temperature and High-Salinity Fields. *SPE Production & Facilities* **2003**, *18*, 200–209. doi:10.2118/84963-PA.
102. Chester, R. Dissolved gases in sea water. In *Marine Geochemistry*, 1 ed.; Chester, R., Ed.; Springer: Dordrecht, 1990; chapter 8, pp. 233–271. doi:10.1007/978-94-010-9488-7.
103. Brondel, D.; Montrouge, F.; Edwards, R.; Hayman, A.; Hill, D.; Mehta, S.; Semerad, T. Corrosion in the Oil Industry. *Oilfield Review* **1994**, *6*, 4–18.
104. Ruschau, G.R.; Al-Anezi A, M. Appendix S - Oil and Gas Exploration and Production. In *Corrosion Cost and Preventive Strategies in the United States*; Number FHWA-RD-01-156, Federal Highway Administration: McLean, VA, 2001; chapter Appendix S, p. 14.
105. Popoola, L.; Grema, A.; Latinwo, G.; Gutti, B.; Balogun, A. Corrosion problems during oil and gas production and its mitigation. *International Journal of Industrial Chemistry* **2013**, *4*, 15. doi:10.1186/2228-5547-4-35.
106. Koteeswaran, M. CO_2 and H_2S corrosion in oil pipelines. PhD thesis, University of Stavanger, Stavanger, 2010.
107. Heidersbach, R. Corrosion in Oil and Gas Production. In *Microbiologically Influenced Corrosion in the Upstream Oil and Gas Industry*, 1 ed.; Skovhus, T.L.; Enning, D.; Lee, J.S., Eds.; CRC Press: Boca Raton, FL, 2017; chapter 1, pp. 3–34. doi:10.1201/9781315157818.
108. Diaz, E.F.; Gonzalez-Rodriguez, J.G.; Martinez-Villafañe, A.; Gaona-Tiburcio, C. H_2S corrosion inhibition of an ultra high strength pipeline by carboxyethyl-imidazoline. *Journal of Applied Electrochemistry* **2010**, *40*, 1633–1640. doi:10.1007/s10800-010-0149-z.
109. Stansbury, E.E.; Buchanan, R.A. *Fundamentals of electrochemical corrosion*, 1 ed.; ASM international: Materials Park, OH, 2000; p. 487.
110. Norsworthy, R. Understanding corrosion in underground pipelines: basic principles. In *Underground Pipeline Corrosion*, 1 ed.; Orazem, M.E., Ed.; Woodhead Publishing Series in Metals and Surface Engineering, Woodhead Publishing: Cambridge, 2014; chapter 1, pp. 3–34. doi:10.1533/9780857099266.1.3.
111. Jomdecha, C.; Prateepasen, A.; Kaewtrakulpong, P. Study on source location using an acoustic emission system for various corrosion types. *NDT & E International* **2007**, *40*, 584–593. doi:10.1016/j.ndteint.2007.05.003.
112. Landolt, D. Corrosion and Surface Treatment. In *Electrochemistry*; Feliu-Martinesz, J.M.; Paya, V.C., Eds.; EOLSS Publishers, 2009; chapter 6, pp. 240–271.
113. American Water Works Association. Chemistry of Corrosion. In *M27 - External Corrosion Control for Infrastructure Sustainability*, 3 ed.; De Nileon, G.P.; Gray, M.R.; Armstrong, C.; Beach, M., Eds.; Manual of Water Supply Practices, American Water Works Association: Denver, CO, 2014; chapter 2, pp. 7–24.

114. Byars, H.; Gallop, B. Injection Water + Oxygen = Corrosion and/or Well Plugging Solids. SPE Symposium on Handling of Oilfield Water; Society of Petroleum Engineers: Los Angeles, CA, 1972; pp. 96–102. doi:10.2118/4253-MS.
115. Durdevic, P.; Raju, C.S.; Yang, Z. Potential for Real-Time Monitoring and Control of Dissolved Oxygen in the Injection Water Treatment Process. *IFAC-PapersOnLine* **2018**, *51*, 170–177. doi:10.1016/j.ifacol.2018.06.373.
116. Zardynezhad, S. Consider key factors in pipeline wall thickness calculation and selection. *Gas Processing & LNG* **2015**.
117. Beavers, J.A.; Thompson, N.G. External corrosion of oil and natural gas pipelines. In *ASM handbook Volume 13C: Corrosion: Environments and Industries*, 1 ed.; Cramer, S.D.; Bernard S. Covino, J., Eds.; ASM handbook, ASM International: Materials Park, OH, 2006; chapter 100, pp. 1015–1025. doi:10.31399/asm.hb.v13c.a0004213.
118. Shirazi, S.A.; Mclaury, B.S.; Shadley, J.R.; Roberts, K.P.; Rybicki, E.F.; Rincon, H.E.; Hassani, S.; Al-Mutahar, F.M.; Al-Aithan, G.H. Erosion–Corrosion in Oil and Gas Pipelines. In *Oil and Gas Pipelines: Integrity and Safety Handbook*, 1 ed.; Revie, R.W., Ed.; John Wiley & Sons, Inc.: Hoboken, NJ, 2015; chapter 28, pp. 399–422. doi:10.1002/9781119019213.ch28.
119. Sastri, V.S. Corrosion Causes. In *Challenges in Corrosion: Costs, Causes, Consequences, and Control*, 1 ed.; Revie, R.W., Ed.; Wiley Series in Corrosion, John Wiley & Sons: Hoboken, NJ, 2015; chapter 3, pp. 127–204. doi:10.1002/9781119069638.ch5.
120. Farshad, F.F.; Choate, L.C.; Winters, R.H.; Garber, J.D. Pipeline Optimization - A Surface Roughness Approach. Technical report, University of Louisiana, Lafayette, LA, 2017.
121. Skovhus, T.L.; Enning, D.; Lee, J.S. *Microbiologically Influenced Corrosion in the Upstream Oil and Gas Industry*, 1 ed.; CRC Press: Boca Raton, FL, 2017; pp. v–xxvi. doi:10.1201/9781315157818.
122. Ren, H.; Xiong, S.; Gao, G.; Song, Y.; Cao, G.; Zhao, L.; Zhang, X. Bacteria in the injection water differently impacts the bacterial communities of production wells in high-temperature petroleum reservoirs. *Frontiers in Microbiology* **2015**, *6*, 8. doi:10.3389/fmicb.2015.00505.
123. Ismail, W.A.; Van Hamme, J.D.; Kilbane, J.J.; Gu, J.D. Editorial: Petroleum Microbial Biotechnology: Challenges and Prospects. *Frontiers in Microbiology* **2017**, *8*, 4. doi:10.3389/fmicb.2017.00833.
124. Bouchard, R.P. Is a Virus a Living Creature?, 2017.
125. Wang, I.; Burckhardt, C.J.; Yakimovich, A.; Greber, U.F.; Others. Imaging, Tracking and Computational Analyses of Virus Entry and Egress with the Cytoskeleton. *Viruses* **2018**, *10*, 29. doi:10.3390/v10040166.
126. Cole, L.A. Evolutionary History of Planet Earth. In *Biology of Life: Biochemistry, Physiology and Philosophy*, 1 ed.; Tenney, S., Ed.; Academic Press: Cambridge, MA, 2016; chapter 6, pp. 37–43. doi:10.1016/B978-0-12-809685-7.00006-X.
127. Schloss, P.D.; Handelsman, J. Status of the Microbial Census. *Microbiology and Molecular Biology Reviews* **2004**, *68*, 686–691. doi:10.1128/MMBR.68.4.686-691.2004.
128. Whitman, W.B.; Coleman, D.C.; Wiebe, W.J. Prokaryotes: the unseen majority. *Proceedings of the National Academy of Sciences* **1998**, *95*, 6578–6583. doi:10.1073/pnas.95.12.6578.
129. Gillespie, S.H.; Bamford, K.B. Structure and Classification of Bacteria. In *Medical Microbiology and Infection at a Glance*, 4 ed.; At a Glance, Wiley-Blackwell: Hoboken, NJ, 2012; chapter 1, pp. 8–9.
130. Baron, E.J. Classification. In *Medical Microbiology*, 4 ed.; Baron, S., Ed.; University of Texas Medical Branch: Galveston, TX, 1996; chapter 3.
131. Barnes-Svarney, P.; Svarney, T.E. *The Handy Biology Answer Book*, 2 ed.; The Handy Answer Book, Visible Ink Press: Canton, MI, 2015; pp. 1–496.
132. Barer, M.R. Bacterial growth, physiology and death. In *Medical Microbiology: A Guide to Microbial Infections: Pathogenesis, Immunity, Laboratory Diagnosis and Control*, 18 ed.; Greenwood, D.; Barer, M.R.; Slack, R.C.B.; Irving, W.L., Eds.; Churchill Livingstone: London, 2012; chapter 4, pp. 39–53. doi:10.1016/B978-0-7020-4089-4.00019-6.
133. Beech, I.; Flemming, H.C.; Mollica, A.; Scotto, V. Simple methods for the investigation of of the role of biofilms in corrosion. Technical report, European Commission Federation of Corrosion, 2000.
134. MacLeod, R.A. The Question of the Existence of Specific Marine Bacteria. *Bacteriological reviews* **1965**, *29*, 9–24.
135. Little, B.; Wagner, P.; Mansfeld, F. An Overview of Microbiologically Influenced Corrosion. *Electrochimica Acta* **1992**, *37*, 2185–2194. doi:10.1016/0013-4686(92)85110-7.

136. Little, B.J.; Lee, J.S. *Microbiologically Influenced Corrosion*, 1 ed.; John Wiley & Sons, Inc.: Hoboken, NJ, 2007; p. 280. doi:10.1002/047011245X.
137. Heitz, E.; Flemming, H.C.; Sand, W. *Microbially influenced corrosion of materials: scientific and engineering aspects*, 1 ed.; Springer-Verlag: Berlin, 1996; p. 475.
138. Fischer, D.; Canalizo-Hernandez, M.; Kumar, A. Effects of Reservoir Souring on Materials Performance. In *Microbiologically Influenced Corrosion in the Upstream Oil and Gas Industry*, 1 ed.; Skovhus, T.L.; Enning, D.; Lee, J.S., Eds.; CRC Press: Boca Raton, FL, 2017; chapter 6, pp. 111–137. doi:10.1201/9781315157818.
139. Mittelman, M.W. Bacterial Biofilms and Bifouling: Translational Research in Marine Biotechnology. In *Opportunities for Environmental Applications of Marine Biotechnology*; Vaupel, S., Ed.; National Academies Press: Washington, DC, 2000; chapter 2, pp. 3–7. doi:10.17226/9988.
140. Komlenic, R. Rethinking the causes of membrane biofouling. *Filtration & Separation* **2010**, *47*, 26–28. doi:10.1016/S0015-1882(10)70211-1.
141. Donlan, R.M. Biofilms: Microbial Life on Surfaces. *Emerging infectious diseases* **2002**, *8*, 881–90. doi:10.3201/eid0809.020063.
142. Vasudevan, R. Biofilms: Microbial Cities of Scientific Significance. *Journal of Microbiology & Experimentation* **2014**, *1*, 1–16. doi:10.15406/jmen.2014.01.00014.
143. Nguyen, T.; Roddick, F.; Fan, L. Biofouling of Water Treatment Membranes: A Review of the Underlying Causes, Monitoring Techniques and Control Measures. *Membranes* **2012**, *2*, 804–840. doi:10.3390/membranes2040804.
144. Sauer, K.; Camper, A.K.; Ehrlich, G.D.; Costerton, J.W.; Davies, D.G. Pseudomonas aeruginosa displays multiple phenotypes during development as a biofilm. *Journal of bacteriology* **2002**, *184*, 1140–1154. doi:10.1128/jb.184.4.1140-1154.2002.
145. Macià, M.D.; Rojo-Molinero, E.; Oliver, A. Antimicrobial susceptibility testing in biofilm-growing bacteria. *Clinical microbiology and infection : the official publication of the European Society of Clinical Microbiology and Infectious Diseases* **2014**, *20*, 981–990. doi:10.1111/1469-0691.12651.
146. Mah, T.F.C.; O'Toole, G.A. Mechanisms of biofilm resistance to antimicrobial agents. *Trends in Microbiology* **2001**, *9*, 34–39. doi:10.1016/S0966-842X(00)01913-2.
147. Hall-Stoodley, L.; Costerton, J.W.; Stoodley, P. Bacterial biofilms: from the Natural environment to infectious diseases. *Nature Reviews Microbiology* **2004**, *2*, 95–108. doi:10.1038/nrmicro821.
148. Tidwell, T.J.; Keasler, V.; Paula, R.D. How Production Chemicals Can Influence Microbial Susceptibility to Biocides and Impact Mitigation Strategies. In *Microbiologically Influenced Corrosion in the Upstream Oil and Gas Industry*, 1 ed.; Skovhus, T.L.; Enning, D.; Lee, J.S., Eds.; CRC Press: Boca Raton, FL, 2017; chapter 19, pp. 379–392. doi:10.1201/9781315157818.
149. Little, B.; Lee, J.; Ray, R. New Developments in Mitigation of Microbiologically Influenced Corrosion. Technical report, Naval Research Laboratory Oceanography Division Stennis Space Center, Fort Belvoir, VA, 2007.
150. Turkiewicz, A.; Brzeszcz, J.; Kapusta, P. The application of biocides in the oil and gas industry. *Nafta-Gaz* **2013**, *69*, 103–111.
151. Laura Machuca Suarez. Microbiologically Induced Corrosion Associated with the Wet Storage of Subsea Pipelines (Wet Parking). In *Microbiologically Influenced Corrosion in the Upstream Oil and Gas Industry*, 1 ed.; Skovhus, T.L.; Enning, D.; Lee, J.S., Eds.; CRC Press: Boca Raton, FL, 2017; chapter 18, pp. 361–378. doi:10.1201/9781315157818.
152. Javaherdashti, R. *Microbiologically Influenced Corrosion*, 2 ed.; Engineering Materials and Processes, Springer: London, 2008; p. 216, [arXiv:1011.1669v3]. doi:10.1007/978-1-84800-074-2.
153. Sandbeck, K.; Hitzman, D. Biocompetitive Exclusion Technology: A Field System to Control Reservoir Souring and Increasing Production. The Fifth International Conference on Microbial Enhanced Oil Recovery and Related Biotechnology for Solving Environment Problems; Bryant, R., Ed.; U.S. Department of Energy Office of Scientific and Technical Information: Dallas, TX, 1995; pp. 311–319.
154. Schwermer, C.U.; Lavik, G.; Abed, R.M.M.; Dunsmore, B.; Ferdelman, T.G.; Stoodley, P.; Gieseke, A.; de Beer, D. Impact of Nitrate on the Structure and Function of Bacterial Biofilm Communities in Pipelines Used for Injection of Seawater into Oil Fields. *Applied and Environmental Microbiology* **2008**, *74*, 2841–2851. doi:10.1128/AEM.02027-07.

155. Hubert, C.; Voordouw, G.; Arensdorf, J.; Jenneman, G.E. Control of souring through a novel class of bacteria that oxidize sulfide as well as oil organics with nitrate. *Corrosion 2006* **2006**, p. 10.
156. Xu, D. Microbiologically Influenced Corrosion (MIC) Mechanisms and Mitigation. PhD thesis, Ohio University, Athens, OH, 2013.
157. Jones, S.E.; Lennon, J.T. Dormancy contributes to the maintenance of microbial diversity. *Proceedings of the National Academy of Sciences* **2010**, *107*, 5881–5886. doi:10.1073/pnas.0912765107.
158. Lewis, K. Persister cells, dormancy and infectious disease. *Nature reviews. Microbiology* **2007**, *5*, 48–56. doi:10.1038/nrmicro1557.
159. El-Baky, R. The Future Challenges Facing Antimicrobial Therapy: Resistance and Persistence. *American Journal of Microbiological Research* **2016**, *4*, 15. doi:10.12691/ajmr-4-1-1.
160. Stewart, E.J. Growing Unculturable Bacteria. *Journal of Bacteriology* **2012**, *194*, 4151–4160, [arXiv:1011.1669v3]. doi:10.1128/JB.00345-12.
161. Hu, A. Investigation of sulfate-reducing bacteria growth behavior for the mitigation of microbiologically influenced corrosion (MIC). PhD thesis, Ohio University, Athens, OH, 2004.
162. Klai, N.; Yan, S.; Tyagi, R.D.; Surampalli, R.Y. EPS producing microorganisms from municipal wastewater activated sludge. *Journal of Petroleum & Environmental Biotechnology* **2016**, *7*, 13. doi:10.4172/2157-7463.1000255.
163. Raulio, M. Ultrastructure of biofilms formed by bacteria from industrial processes. PhD thesis, University of Helsinki, Helsinki, 2010.
164. Natarajan, K. Biofouling and Microbially Influenced Corrosion of Stainless Steels. *Advanced Materials Research* **2013**, *794*, 539–551. doi:10.4028/www.scientific.net/AMR.794.539.
165. Borenstein, S.W. Microbiology. In *Microbiologically Influenced Corrosion Handbook*, 1 ed.; Metals and Surface Engineering, Woodhead Publishing: Cambridge, 1994; chapter 2, pp. 8–49. doi:10.1533/9781845698621.8.
166. Coetser, S.E.; Cloete, T.E. Biofouling and Biocorrosion in Industrial Water Systems. *Critical Reviews in Microbiology* **2005**, *31*, 213–232. doi:10.1080/10408410500304074.
167. Okabe, S.; Jones, W.L.; Lee, W.; Characklis, W.G. Anaerobic SRB Biofilms in Industrial Waters Systems: A process Analysis. In *Biofouling and Biocorrosion in Industrial Water Systems*, 1 ed.; Geesey, G.G.; Lewandowski, Z.; Flemming, H.C., Eds.; CRC Press: Boca Raton, FL, 1994; chapter 12, pp. 189–204.
168. Sharma, M.; Voordouw, G. MIC Detection and Assessment A Holistic Approach. In *Microbiologically Influenced Corrosion in the Upstream Oil and Gas Industry*, 1 ed.; Skovhus, T.L.; Enning, D.; Lee, J.S., Eds.; CRC Press: Boca Raton, FL, 2017; chapter 9, pp. 177–212. doi:10.1201/9781315157818.
169. Papavinasam, S. Mechanisms. In *Corrosion Control in the Oil and Gas Industry*, 1 ed.; Gulf Professional Publishing: Houston, TX, 2014; chapter 5, pp. 249–300. doi:10.1016/B978-0-12-397022-0.00005-4.
170. Cord-Ruwisch, R. MIC in Hydrocarbon Transportation Systems. Corrosion Australasia; Australasian Corrosion Association: Perth, WA, 1995; pp. 8–12.
171. Zhang, J. RPSEA Subsea Produced Water Discharge Sensor Lab Test Results and Recommendations Final Report. Technical Report 3, Clearview Subsea LLC, Houston, TX, 2016.
172. Maersk Oil. Maersk Oil ESIA-16 Non-Technical Summary – ESIS Dan. Technical report, Maersk Oil, Esbjerg, 2015.
173. Larsen, J.; Rod, M.H.; Zwolle, S. Prevention of Reservoir Souring in the Halfdan Field by Nitrate Injection. Corrosion 2004; NACE International: New Orleans, LA, 2004; p. 9.
174. Thomsen, U.S.; Markfoged, R.; Meng, R.; Choong, L. Quantification of Microbiologically Influenced Corrosion in Injection Water Pipelines. Corrosion 2017; NACE International: New Orleans, Louisiana, 2017; pp. 3676–3685.
175. Dejak, M. The Next-Generation Water Filter for the Oil and Gas Industry. *Journal of Petroleum Technology* **2013**, *65*, 32–35. doi:10.2118/1013-0032-JPT.
176. Jepsen, K.L.; Bram, M.V.; Hansen, L.; Yang, Z.; Lauridsen, S.M.Ø. Online Backwash Optimization of Membrane Filtration for Produced Water Treatment. *Membranes* **2019**, *9*, 18. doi:10.3390/membranes9060068.
177. Dansk Standard. Vandundersøgelse Suspenderet stof og gløderest: Total non filtrable residue and fixed matter in non filtrable residue. Technical report, Dansk Standard, Copenhagen, 1985.
178. ASTM International. Standard Specification for Woven Wire Test Sieve Cloth and Test Sieves. Technical report, ASTM, West Conshohocken, PA, 2017. doi:10.1520/E0011-17.

179. GE Healthcare. Whatman Grade GF/D Glass Microfiber Filters, Binder Free, 2019.
180. Durdevic, P.; Raju, C.; Bram, M.; Hansen, D.; Yang, Z. Dynamic Oil-in-Water Concentration Acquisition on a Pilot-Scaled Offshore Water-Oil Separation Facility. *Sensors* **2017**, *17*, 11. doi:10.3390/s17010124.
181. Merkus, H.G. *Particle Size Measurements Fundamentals, Practice, Quality*, 1 ed.; Particle Technology Series, Vol. 17, Springer Netherlands: Houten, 2009; p. 534. doi:10.1007/978-1-4020-9016-5.
182. Leschonski, K. Particle Characterization, Present State and possible Future Trends. *Particle & Particle Systems Characterization* **1986**, *3*, 99–103. doi:10.1002/ppsc.19860030302.
183. Severin Hansen, D.; Jespersen, S.; Bram, M.V.; Yang, Z. Uncertainty Analysis of Fluorescence-Based Oil-In-Water Monitors for Oil and Gas Produced Water. *Sensors* **2020**, *20*, 36. doi:10.3390/s20164435.
184. Xu, R.; Andreina Di Guida, O. Comparison of sizing small particles using different technologies. *Powder Technology* **2003**, *132*, 145–153. doi:10.1016/S0032-5910(03)00048-2.
185. Abbireddy, C.O.R.; Clayton, C.R.I. A review of modern particle sizing methods. *Proceedings of the Institution of Civil Engineers - Geotechnical Engineering* **2009**, *162*, 193–201. doi:10.1680/geng.2009.162.4.193.
186. Allen, T. *Powder Sampling and Particle Size Determination*, 1 ed.; Elsevier B.V.: Amsterdam, 2003; p. 682. doi:10.1016/B978-0-444-51564-3.X5000-1.
187. der Meeren, P.V.; Dewettinck, K.; Saveyn, H. Particle Size Analysis. In *Handbook of Food Analysis: Volume 3 Methods, Instruments and Applications*, 2 ed.; Nollet, L.M., Ed.; Taylor & Francis: Boca Raton, FL, 2004; chapter 46, pp. 1805–1824. doi:10.1201/9781482276473-10.
188. Leschonski, K. Representation and Evaluation of Particle Size Analysis Data. *Particle & Particle Systems Characterization* **1984**, *1*, 89–95. doi:10.1002/ppsc.19840010115.
189. Berger, M. *Geometry II*, 1 ed.; Springer: Berlin, Heidelberg, 1987; p. 405. doi:10.1007/978-3-540-93816-3.
190. Ganser, G.H. A rational approach to drag prediction of spherical and nonspherical particles. *Powder Technology* **1993**, *77*, 143–152. doi:10.1016/0032-5910(93)80051-B.
191. Hart, V.S.; Johnson, C.E.; Letterman, R.D. An Analysis of Low-Level Turbidity Measurements. *Journal - American Water Works Association* **1992**, *84*, 40–45. doi:10.1002/j.1551-8833.1992.tb05900.x.
192. Bin Omar, A.; Bin MatJafri, M. Turbidimeter Design and Analysis: A Review on Optical Fiber Sensors for the Measurement of Water Turbidity. *Sensors* **2009**, *9*, 8311–8335. doi:10.3390/s91008311.
193. Broadwell, M. *A Practical Guide to Particle Counting for Drinking Water Treatment*, 1 ed.; CRC Press: Boca Raton, FL, 2001; p. 240. doi:10.1201/9781420033038.
194. Scardina, P.; Letterman, R.D.; Edwards, M. Particle count and on-line turbidity interference from bubble formation. *Journal / American Water Works Association* **2006**, *98*, 97–109.
195. Fondriest Environmental Inc.. Turbidity, Total Suspended Solids and Water Clarity, 2014.
196. Van Gelder, A.M.; Chowdhury, Z.K.; Lawler, D.F. Conscientious particle counting. *Journal / American Water Works Association* **1999**, *91*, 64–76. doi:10.1002/j.1551-8833.1999.tb08751.x8751.x.
197. Shekunov, B.Y.; Chattopadhyay, P.; Tong, H.H.; Chow, A.H. Particle size analysis in pharmaceutics: Principles, methods and applications. *Pharmaceutical Research* **2007**, *24*, 203–227. doi:10.1007/s11095-006-9146-7.
198. Karuhn, R.; Davies, R.; Kaye, B.H.; Clinch, M.J. Studies on the Coulter Counter Part I. Investigation into the Effect of Orifice Geometry and Flow Direction on the Measurement of Particle Volume. *Powder Technology* **1975**, *11*, 157–171. doi:10.1016/0032-5910(75)80040-4.
199. Crowe, C.T.; Schwarzkopf, J.D.; Sommerfeld, M.; Tsuji, Y. *Multiphase Flows with Droplets and Particles*, 2 ed.; CRC Press: Boca Raton, FL, 2011; p. 509. doi:10.1201/b11103.
200. International Standard. Determination of Particle Size Distributions — Electrical Sensing Zone Method. Technical report, ISO, Geneva, 2007.
201. Mikula, R.J. Emulsion Characterization. In *Emulsions: Fundamentals and Applications in the Petroleum Industry*, 1 ed.; Schramm, L.L., Ed.; Advances in Chemistry, Vol. 231, American Chemical Society: Washington, DC, 1992; chapter 3, pp. 79–129. doi:10.1021/ba-1992-0231.ch003.
202. Nabipour, A.; Evans, B.J.; Sarmadivaleh, M.; Kalli, C.J. Methods for Measurement of Solid Particles in Hydrocarbon Flow Streams. SPE - Asia Pacific Oil and Gas Conference and Exhibition; Society of Petroleum Engineers: Perth, WA, 2012; Vol. 1, pp. 702–715. doi:10.2118/158580-MS.
203. Sabin, A. Problems in Particle Size: Laser Diffraction Observations. *Journal of GXP Compliance* **2011**, *15*, 35–43.

204. Dansk Standard. Particle Size Analysis – Laser Diffraction Methods. Technical report, DS/SO, Copenhagen, 2009.
205. Lefebvre, F.; Petit, J.; Nassar, G.; Debreyne, P.; Delaplace, G.; Nongaillard, B. Inline high frequency ultrasonic particle sizer. *Review of Scientific Instruments* **2013**, *84*, 8. doi:10.1063/1.4811847.
206. Adjadj, L.P.; Hipp, A.K.; Storti, G.; Morbidelli, M. Characterization of dispersions by ultrasound spectroscopy. 5th International Symposium on Ultrasonic Doppler Methods for Fluid Mechanics and Fluid Engineering ISUD; Birkhofer, B.H.; Jeelani, S.A.K.; Windhab, E.J., Eds.; Laboratory of Food Process Engineering: Zürich, 2006; Vol. 5, pp. 9–13.
207. McClements, D.J. Ultrasonic Measurements in Particle Size Analysis. In *Encyclopedia of Analytical Chemistry*; Meyer, R.A., Ed.; John Wiley & Sons: Chichester, 2000; chapter 6, pp. 5581–5587. doi:10.1002/9780470027318.a1518.
208. Wrobel, B.M.; Time, R.W. Improved pulsed broadband ultrasonic spectroscopy for analysis of liquid-particle flow. *Applied Acoustics* **2011**, *72*, 324–335. doi:10.1016/j.apacoust.2010.11.013.
209. Zhang, J. RPSEA Technical Gap Analysis Final Report (Phase 1 Final Report). Technical Report 1, Clearview Subsea LLC, Houston, TX, 2015.
210. Sanderson, J. *Understanding Light Microscopy*, 1 ed.; Royal Microscopical Society, Wiley: Chichester, 2019; chapter 30, p. 815. doi:10.1002/9781118696736.
211. Shand, R.M. User manuals as project management tools. II. Practical applications. *IEEE Transactions on Professional Communication* **1994**, *37*, 123–142. doi:10.1109/47.317478.
212. Canty, T.M.; O'Donoghue, A.; Relihan, E. Inline Oil in Water Particle Analysis and Concentration Monitoring for Process Control and Optimisation in Produced Water Plants. TUV NEL's 7th Produced Water Workshop; TUV NEL: Aberdeen, 2009; p. 8.
213. Christensen, K.M. Installation and Testing of a Jorin Visual Process Analyzer Analyzer. Technical report, Idaho National Laboratory, Fuel Cycle Research and Development, Idaho Falls, ID, 2010.
214. Pontius, K. Monitoring of Bioprocesses Opportunities and Challenges. maj, Technical University of Denmark, Kgs. Lyngby, 2019.
215. Højris, B.; Christensen, S.C.B.; Albrechtsen, H.J.; Smith, C.; Dahlqvist, M. A novel, optical, on-line bacteria sensor for monitoring drinking water quality. *Scientific Reports* **2016**, *6*, 1–10. doi:10.1038/srep23935.
216. Panckow, R.P.; Comandè, G.; Maaß, S.; Kraume, M. Determination of Particle Size Distributions in Multiphase Systems Containing Nonspherical Fluid Particles. *Chemical Engineering and Technology* **2015**, *38*, 2011–2016. doi:10.1002/ceat.201500123.

Paper B

Efficiency Investigation of an Offshore Deoiling Hydrocyclone using Real-Time Fluorescence- and Microscopy-Based Monitors

Dennis S. Hansen, Mads V. Bram, Simon Pedersen and Zhenyu Yang.

The paper has been published in the proceeding
2017 IEEE Conference on Control Technology and Applications (CCTA).
Mauna Lani, HI: IEEE, 27-30 Aug. 2017, pp. 1104–1109

2017 IEEE Conference on Control Technology and Applications (CCTA)
August 27-30, 2017. Kohala Coast, Hawai'i, USA

Efficiency Investigation of an Offshore Deoiling Hydrocyclone Using Real-Time Fluorescence- and Microscopy-Based Monitors

Dennis S. Hansen[1,2], Mads V. Bram[1,3] and Zhenyu Yang[1,4]

Abstract— **Offshore oil & gas production is facing an increasing challenge as the water fraction from the production wells rises over time. It is not uncommon that the extracted mixture contains a water-cut of more than 90%. The current North Sea discharge legislation states that the dispersed oil concentration in water must be less than 30 parts per million (ppm). Consequently, the discharge ports are sampled two times per day and analyzed using the OSPAR recommended GC-FID method. However, the variations of Oil-in-Water (OiW) concentration between sampling time points are unknown and could exceed the regulatory limits. This sampling method is commonly used since the current real-time OiW monitoring technology is still quite open and immature. This work focuses on experimental investigation of reliability and accuracy of selected real-time OiW measuring technologies based on two available commercial products. The obtained results indicate that the instrument based on fluorescence technology can provide reasonably fast, reliable, and accurate OiW concentration measurement, while the instrument based on microscopy technology can provide fast and reasonable measurement of the oil droplet's size distribution. This work indicates that it is beneficial to combine both technologies for real-time OiW monitoring before and after the hydrocyclone.**

I. INTRODUCTION

The goal of offshore oil & gas installations is to cost-effectively extract as much oil & gas from the underground hydrocarbon reservoirs as possible, meanwhile complying with the environmental laws and regulations [1]. The produced water is manually sampled two times per day, where the concentration between two sampling time points is unknown and could exceed the regulatory limit [2]. The Danish Environmental Protection Agency furthermore states that the total amount of discharged oil in the North Sea for Mærsk must be less than 202 tonnes per year [3]. As an increasing amount of water is produced, the limit of total discharged oil becomes more significant, especially as the oil discharge in 2015 was 193 tonnes for Mærsk [3]. It is well known in the oil & gas industry that the measurements of OiW concentrations are highly methodology-dependent. Furthermore, the extracted well flows from different fields as well as different time periods can consist of significantly different characteristics and compounds [4]. It is therefore an important task to ensure continuously low OiW concentration in the discharged water, especially as common matured reservoirs contain more than 90% water [5].

[1] Department of Energy Technology, Aalborg University, Esbjerg, Denmark.
[2] dsh@et.aau.dk
[3] mvb@et.aau.dk
[4] yang@et.aau.dk

Hydrocyclones are commonly used in the offshore oil & gas industry as the last stage of the deoiling process before discharging. The hydrocyclones utilize a vortex-based flow to expose the fluid to large centripetal forces, forcing the water to the inner wall of the cyclone and the lighter oil droplets to migrate to the center [6]. This principle is illustrated in Fig. 1.

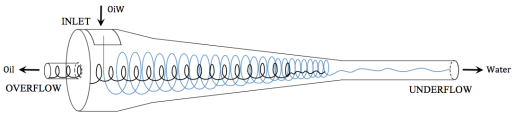

Fig. 1. Operating principle of an offshore deoiling hydrocyclone

Current offshore hydrocyclone control solutions have the objective to achieve a desired separation efficiency (ε) by keeping the Pressure Difference Ratio (PDR) at a desired value [7], [8]. Reports from 1998 suggest that the PDR should be kept at 2-3 [9]. Newer research suggests the PDR to be above 1.8, but the selection of this set-point is highly dependent on the plant and the operating conditions [10]. ε is commonly defined as

$$\varepsilon = 1 - \frac{C_u}{C_i}, \tag{1}$$

where C_u is the volumetric concentration of oil in the water leaving the underflow and C_i is the volumetric concentration of oil in the water entering the cyclone inlet [10], [11]. PDR is defined as

$$PDR = \frac{dP_o}{dP_u} = \frac{P_i - P_o}{P_i - P_u}, \tag{2}$$

where dP_o is the pressure difference between the inlet and overflow and dP_u is the pressure difference between the inlet and underflow [7]. It is clear that whether high efficiency of hydrocyclone performance can be maintained depends on a proper control solution as well as reasonably reliable OiW measurements.

This article investigates two measuring techniques; fluorescence-based and microscopy-based, for real-time measurements of OiW concentration applied to a deoiling hydrocyclone separation setup. The aim of including these measuring techniques to OiW separation systems is to support innovative control solutions based on real-time OiW concentration feedback, or a combined controller using both the well-known PDR solution joined with OiW concentration

feedback. Current control solutions and fault detection and diagnosis will benefit from utilizing these advanced OiW measuring techniques to provide greater understanding of the separation process.

The rest of this paper is organized as: Section II briefs the testing facility and selected OiW monitors; section III illustrates the designed experiments; section IV presents and discusses the experimental results; and lastly the paper is concluded in section V.

II. TESTIING FACILITY AND SELECTED OIW MONITORS

The testing facility used for this study, shown in Fig. 2, consists of an offshore hydrocyclone, flow transmitters (Q), pressure transmitters (P), OiW monitors (C), and control valves (V). To emulate inlet conditions, a water pump and oil injection pump are utilized.

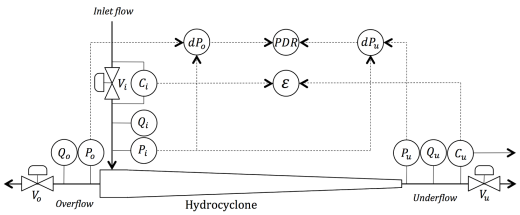

Fig. 2. The deoiling hydrocyclone system used for all experiments

The two different types of OiW monitors selected in this study are microscopy-based Jorin ViPA Model B HF and fluorescence-based Turner TD-4100XDC Online Monitor. These OiW monitors are mounted in series on sidestreams at the inlet and underflow of the hydrocyclone.

Fluorescence-Based Monitoring of OiW Concentration

The Turner TD-4100XDC Online Monitor detects the content of aromatic hydrocarbons in water using fluorometry [12]. The fluorometry principle consists of a light source ① emitting light to the vertical sample cell ③ where the aromatic content of oil absorbs light and fluoresces. The fluorescent light has a lower wavelength and is detected by the light detector ⑤ as shown in Fig. 3. The excitation filter ② and emission filter ④ do not pass light with unwanted wavelengths. The air in the sample cell prevents the liquid mixture from attaching to the walls, which insure that the sample cell is kept clean. The fluorometry is appropriate for measuring OiW concentration as water does not fluoresce, thus only sensitive to aromatic hydrocarbons.

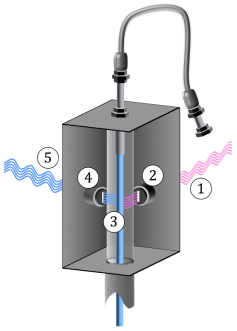

Fig. 3. Illustration of the main components of Turner TD-4100XDC

The Turner TD-4100XDC outputs relative fluorescence units (RFU), that is linear proportional with the OiW concentration, at a sample frequency of 100Hz. The linear function must be calibrated to the specific oil type used in the facility. To measure both inlet and underflow of the hydrocyclone, two Turner TD-4100XDC monitors are calibrated using known solutions of oil in isopropanol as seen in Fig. 4. The dashed lines represent a predicted best fit linear RFU to concentration functions. The slope difference in the two functions indicates that the two fluorescence monitors have slightly different sensitivity to the same solution. However, this difference is accounted for by applying least square calibration functions to their respective measurements. Even though the monitors were calibrated in the range of 0 - 500ppm they had less than $\pm 10\%$ deviations when measuring 1000ppm samples.

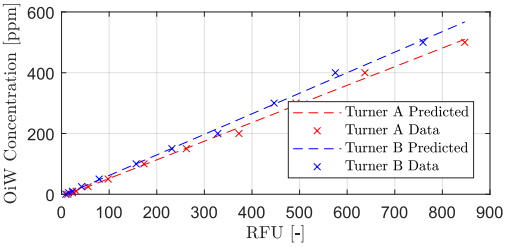

Fig. 4. Least square calibration functions based on eleven measured RFU values

The TD-4100XDC monitors located at the inlet and the underflow of the hydrocyclone enables the possibility to estimate ε at various operating conditions in real-time.

Microscopy-Based Monitoring of OiW Concentration and Droplet Sizes

Analyzing droplet size distribution is important for choosing proper separation equipment that is effective for a specific range of droplet sizes. It is therefore useful to have knowledge of the statistical parameters relating to droplet size

distribution. The produced water entering the hydrocyclone consists of both dispersed and dissolved oil, where only dispersed oil can be separated by the hydrocyclone [13]. The settling time for an oil droplet to migrate to the center of the hydrocyclone is based on Stokes' law

$$v = \frac{D^2 \Delta \rho a}{18\mu}, \tag{3}$$

where v is the settling speed, D is the droplet diameter, $\Delta\rho$ is the density difference between the water and the oil, a is the centripetal acceleration, and μ the dynamic viscosity of the carrying water phase. If the droplet size decreases, ε has the risk to decrease due to the significant reduction of migrating speed.

The Jorin ViPA uses video microscopy to capture images of the particles in the view-cell. This monitor consists mainly of a high-speed camera ① with a narrow focal range ② facing a light source ③ as shown in Fig. 5.

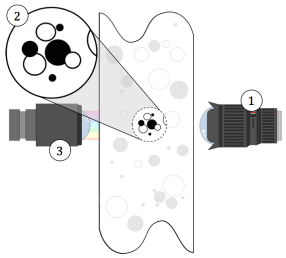

Fig. 5. Illustration of the main components of Jorin ViPA

Image analysis techniques are used to count and distinguish between different particles by analyzing properties of the captured objects such as size, shape factor, and optical density [14]. The shape factor is computed by

$$ShapeFactor = \frac{4\pi Area}{Perimeter^2}, \tag{4}$$

such that perfect circular objects have a shape factor of one. Solid particles often have a larger perimeter and will therefore have a lower shape factor, thus enabling the distinction between solid particles and spherical droplets.

The benefit of using microscopy-based monitors is the ability to count the solid particles and droplets to determine their concentrations. The amount and size of all oil droplets will provide the size distribution that is essential for efficiency analysis.

III. EXPERIMENT DESIGN

The objective of the experiments is to identify the performance of a hydrocyclone at various operating conditions from an OiW perspective. It is therefore essential to obtain measurements from all the pressures, flows, and OiW concentrations in steady state in order to gather the transient data. The steady state OiW concentrations are based on nominal hydrocyclone operating conditions with the aim to use the obtained data for process optimization. For all tests, described in section III, an injection pump was used with a constant speed for oil injection to the inlet. However, changes of Q_i, the mixture's homogeneity, measurement via side streams, and other factors could affect the inlet OiW concentration.

Accuracy of Real-Time OiW Concentrations

To validate the accuracy of the fluorescence-based and microscopy-based monitors, an experiment was executed with an mixture OiW concentration of 100ppm recirculates through both monitors. By analyzing the mean and the fluctuations of the obtained OiW concentration data, the accuracy of the respective OiW monitors can be validated.

Droplets Size Analysis

Two microscopy-based monitors were used to analyze droplet size distributions at the inlet and underflow of the hydrocyclone with the following operating conditions:

- $C_i \approx$ 613ppm by constant oil injection pump speed.
- Constant P_i of 9.5bar by using P_i as feedback for the water pump speed PI-controller.
- Constant PDR of 2 by using PDR as feedback for V_o opening PI-controller.
- Constant Q_i of 0.4L/s by using Q_i as feedback for V_u opening PI-controller.

This test emulates a single steady state operating point with a reasonable PDR reference. This operating condition will provide a nominal representation of the droplet size distribution at the inlet and underflow of the hydrocyclone. It is especially of interest to compare the two oil droplet distributions to statistically identify which ranges of droplet sizes decompose or exit through the overflow. This analysis provides an indication of the droplet size distribution's influence on ε, such as changes of the mean droplet size at the inlet.

Separation Efficiency at Various PDR Values

To identify the behavior of the hydrocyclone's ε when changing the PDR references, an experiment was executed. During this test, the PDR reference was increased in steps, from 1 to 3.5, such that steady state is achieved for each PDR step. Each of the PDR steps was maintained for 4 minutes to generate an average of the measurements. This test uses the following operating conditions:

- $C_i \approx$ 840ppm by constant oil injection pump speed.
- Constant P_i of 9.5bar by using P_i as feedback for the water pump speed PI-controller.
- Specific constant PDR values by using PDR as feedback for V_o opening PI-controller.
- Constant Q_i of 0.4L/s by using Q_i as feedback for V_u opening PI-controller.

The dynamic behavior between each steady state point will give an indication of the dynamic properties of ε and PDR at specific operating conditions.

Separation Efficiency at Various Inlet Flow Rates

To identify the hydrocyclone's ε at various inlet flow rates and PDR references, an experiment is executed with the following operating conditions:

- $C_i \approx$ 400ppm by constant oil injection pump speed.
- Constant P_i of 9bar by using P_i as feedback for the water pump speed PI-controller.
- Specific constant PDR values by using PDR as feedback for V_o opening PI-controller.
- Specific constant Q_i values by using Q_i as feedback for V_u opening PI-controller.

Three tests were executed using PDR references of 1.5, 2.0, and 2.5 by controlling V_o. During each of the three tests, Q_i was increased in steps from 0.23L/s to 0.69L/s. Each steady state flow was maintained for 10 minutes to provide sufficient data for averaging the values of pressures, flows, and OiW measurements, as the system's settling time is approximately 25 seconds. This approach of stepping through a number of specific operating conditions can be utilized to identify other parameters' performance influence on offshore separation systems and applications.

IV. EXPERIMENTAL RESULT AND DISCUSSION

Accuracy of Real-Time OiW Concentrations

A comparison of the real-time OiW concentration measurement of both OiW monitor types is shown in Fig. 6. It is clear that the fluorescence-based measurements (green) fluctuates less than the microscopy-based measurements (red). A low-pass 10^{th}-order butterworth filter with a 4Hz cut-off frequency was applied to the microscopy measurements (blue) to reduce the magnitude of the fluctuations. The fluctuations are most likely due to the random processes involved in the still-image sampling process of flow with low OiW concentration, as multiple images in a row could contain no droplets and single images could contain large amount of droplets, thus complicating the averaging.

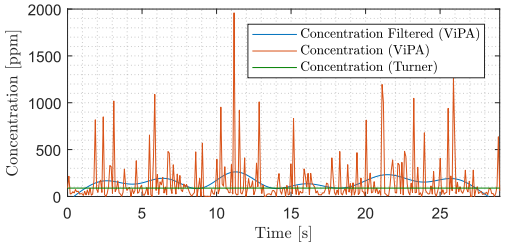

Fig. 6. Real-time OiW concentration measured with fluorescence- and microscopy-based monitors during a period of 30 seconds

Due to the observed stability of the fluorescence-based monitors compared to the microscopy-based monitors, the fluorescence-based monitors were chosen in this study for measuring OiW concentrations. However, the microscopy-based monitors were important for counting and measuring oil droplets to generate size distributions. Fig. 6 is also used as validation experiment, as an oil concentration of 100ppm was injected, where the fluorescence-based monitor mean value was measured at 92ppm and microscopy-based monitor mean value was measured at 147ppm. However, small oil droplets attaching to the pipe wall was observed during the experiments which could cause small offset measurements from the fluorescence-based monitor. Note that composition of oil, such as the amount of aromatic hydrocarbons, changes over time during offshore operation, fluorescence-based monitors must be frequently recalibrated to prevent the measurements from drifting. However, as the composition of oil, such as the amount of aromatic hydrocarbons, changes over time during offshore operation, fluorescence-based monitors must be frequently recalibrated to prevent the measurements from drifting.

Droplet Size Distribution by Microscopy-Based Monitor

The histogram in Fig. 7 is normalized to compare the probability density of the inlet (blue), the underflow (red), and the overlap of the two histograms (purple). The histogram strongly indicates that bigger droplets is either separated or decomposed through the hydrocyclone before leaving the underflow. It should be noted that during this steady state operation, C_i and C_u was measured at 613ppm and 249ppm respectively by the fluorescence-based monitor, resulting in an ε of 59.4%.

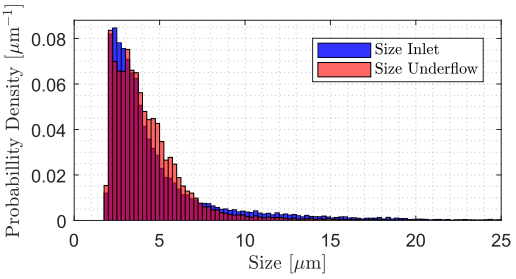

Fig. 7. Normalized histogram of oil droplet size at inlet and underflow

The size distribution in Fig. 7 illustrates that droplets bigger than $7\mu m$ have a tendency to easier be separated. The distribution also indicates that it is difficult for the hydrocyclone to separate small droplets, where the underflow droplet size distribution have a higher percentage than the inlet droplet size distribution, which could be caused by the shearing effect decomposing the droplets.

PDR Dependency of Separation Efficiency

It was observed during the experiments that a PDR of 1 corresponded to V_o being fully closed, a PDR of 3.5 corresponded to V_o being fully open, and a PDR of 1.8 corresponded to the lowest non-zero V_o value of 2.5% open. Note that the V_u was controlled to maintain Q_i during the experiments. The case where V_o was fully closed resulted in

C_i and C_u being equal from a steady state point of view. The general trend in Fig. 8 indicates that PDR has only marginal influence on ε above a specific PDR. However, from an operating point of view, too high PDR values results in undesirable increase of water in Q_o as the opening degree of V_o would be too high.

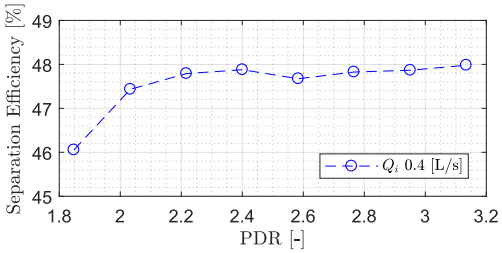

Fig. 8. Separation efficiency at eight different PDR values

The ε and PDR dynamic responses of the experiment are shown in Fig. 9. It is observed that the ε slightly increases as the PDR increases. However, large fluctuations of the estimated ε were observed. The fluctuations of ε could be caused by small variations of Q_i, varying C_i, and/or measurement noise.

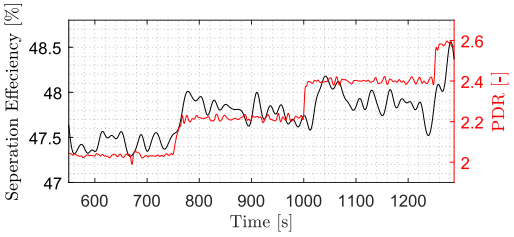

Fig. 9. Dynamic responses of PDR and separation efficiency

Inlet Flow Dependency of Separation Efficiency

The PDR references of 1.5 (blue), 2.0 (red), and 2.5 (black) are shown in Fig. 10, where outlier points (✳) are operation conditions where the PDR-control saturates the overflow valve and can thereby not maintain the PDR reference.

It is clear that the ε is less dependent on the PDR reference compared to Q_i, thus essential to maintain a high Q_i. The similar ε achieved at different PDR references indicates that the PDR should be maintained within a certain range for optimal separation instead of a unique value.

This is mainly due to the fact that the increased flow rate generates a stronger acceleration field resulting in an increased OiW separation [7]. Even though the hydrocyclone requires high flow rates, Q_i is strongly determined by the level-control of the upstream three-phase separator that controls the opening degree of V_u to maintain the interface level.

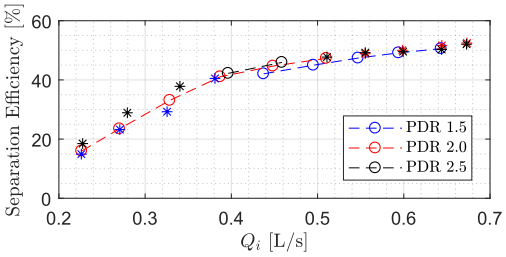

Fig. 10. Separation efficiency at different inlet flow rates

The primary objective is maintaining the water level in the three-phase separator, where PDR is the secondary objective, which directly affects the ε as Q_i fluctuates. If taking both systems into account, further improvements could be made to coordinate both control objectives. E.g. the level-controller could be relaxed to reduce the fluctuations of Q_i.

V. CONCLUSIONS AND FUTURE WORKS

This work indicates that the hydrocyclone performance and concentrations of OiW can be potentially estimated in a real-time manner by utilizing fluorescence- and microscopy-based monitors. Real-time ε of an offshore hydrocyclone was acquired by introducing the OiW monitors at the inlet and the underflow, thus enabling the possibility to identify ε at various operating conditions. The experiments revealed a range of specific operating conditions where a change in PDR has small effect on the ε. This weak dependence between ε and PDR indicates that an optimal PDR range exists rather than a single optimal PDR reference, causing PDR-control solutions to have the opportunity for improvement by exploiting the freedom in this range more effectively. The experiments also revealed that the ε is less dependent on the PDR reference compared to Q_i, thus it is essential to maintain a high Q_i.

The dynamic response measurements in Fig. 9 can be used for system identification to design a model-based control solution utilizing real-time OiW measurements as feedback. This enables the research and development of innovative control solutions utilizing accurate feedback of real-time ε or the combination of ε and PDR as control feedback.

Droplet size distribution in the inlet and underflow can be acquired through microscopy. This enables the design of experiments dedicated to identifying oil droplet size distribution at various system locations. The droplet size analysis can provide solid technical support for choice of proper separation system and thereby achieve an improved separation process. By considering the statistical parameters of droplet size distributions, other operating points should be investigated to indicate what influence the droplet size distribution has on ε and if the inlet mean droplet size of the hydrocyclone is too small to acquire higher ε.

ACKNOWLEDGMENTS

The second author would like to thank support from the DTU DHRTC Sprint Project: Control-oriented modeling of deoiling hydrocyclone system coupled with upstream three-phase separator. The authors would like to thank the colleagues S. Pedersen, K. Jepsen, L. Hansen, and P. Durdevic from AAU, for many valuable discussions and supports.

REFERENCES

[1] Z. Yang, J. P. Stigkæ, and B. Løhndorf, "Plant-wide control for better de-oiling of produced water in offshore oil & gas production," *IFAC Proceedings Volumes*, vol. 46, no. 20, pp. 45–50, 2013.

[2] OSPAR-Commission, *North Sea Manual on Maritime Oil Pollution Offences*. London: OSPAR, 2012.

[3] D. E. P. Agency, "General authorization for maersk oil and gas," Agency, Danish Environmental Protection, Tech. Rep. 1, 2016.

[4] K. Lee and J. Neff, *produced water environmental risks and advances in mitigation technologies*. New York: Springer Link, 2011.

[5] P. Janssen, C. Harris *et al.*, "Emulsion characteristics of high water-cut oil wells," in *SPE Annual Technical Conference and Exhibition*. Society of Petroleum Engineers, 1998.

[6] A. Sinker, M. Humphris, N. Wayth *et al.*, "Enhanced deoiling hydrocyclone performance without resorting to chemicals," in *Offshore Europe Oil and Gas Exhibition and Conference*. Society of Petroleum Engineers, 1999.

[7] T. Husveg, O. Rambeau, T. Drengstig, and T. Bilstad, "Performance of a deoiling hydrocyclone during variable flow rates," *Minerals Engineering*, vol. 20, no. 4, pp. 368–379, apr 2007.

[8] M. V. Bram, A. A. Hassan, D. S. Hansen, P. Durdevic, S. Pedersen, and Z. Yang, "Experimental modeling of a deoiling hydrocyclone system," in *Methods and Models in Automation and Robotics (MMAR), 2015 20th International Conference on*. IEEE, 2015, pp. 1080–1085.

[9] M. Thew and et al., "Cyclones for oil/water separation," *Encyclopedia of Separation Science*, 2000.

[10] G. Young, W. Wakley, D. Taggart, S. Andrews, and J. Worrell, "Oil-water separation using hydrocyclones: An experimental search for optimum dimensions," *Journal of petroleum science and engineering*, vol. 11, no. 1, pp. 37–50, 1994.

[11] L. Svarovsky and M. Thew, *Hydrocyclones: analysis and applications*. Dordrecht: Springer Science & Business Media, 1992, vol. 12.

[12] Turner, "E09 td-4100xdc oil in water monitor," http://www.oilinwatermonitors.com, Turner Designs Hydrocarbon Instruments, 2015, accessed: 15-09-2015.

[13] J. Coca-Prados and G. Gutiérrez-Cervelló, *Water Purification and Management*, ser. NATO Science for Peace and Security Series C: Environmental Security. Springer Netherlands, 2010.

[14] Jorin, "Jorin vipa b hiflo installation, operation and maintenance manual," http://www.jorin.co.uk, Jorin Limited, Leicestershire, 2015, accessed: 23-10-2015.

Paper C

Uncertainty Analysis of Fluorescence-Based Oil-In-Water Monitors for Oil and Gas Produced Water

Dennis S. Hansen, Stefan Jespersen, Mads V. Bram, and Zhenyu Yang.

The paper has been published in
Sensors, vol. 20, no. 16, p. 36, 2020

sensors

MDPI

Article

Uncertainty Analysis of Fluorescence-Based Oil-In-Water Monitors for Oil and Gas Produced Water

Dennis Severin Hansen, Stefan Jespersen, Mads Valentin Bram and Zhenyu Yang *

Department of Energy Technology, Aalborg University, Niels Bohrs Vej 8, 6700 Esbjerg, Denmark; dsh@et.aau.dk (D.S.H.); sje@et.aau.dk (S.J.); mvb@et.aau.dk (M.V.B.)

* Correspondence: yang@et.aau.dk; Tel.: +45-4128-7438

Received: 19 June 2020; Accepted: 6 August 2020; Published: 8 August 2020

Abstract: Offshore oil and gas facilities are currently measuring the oil-in-water (OiW) concentration in the produced water manually before discharging it into the ocean, which in most cases fulfills the government regulations. However, as stricter regulations and environmental concerns are increasing over time, the importance of measuring OiW in real-time intensifies. The significant amount of uncertainties associated with manual samplings, that is currently not taken into consideration, could potentially affect the acceptance of OiW monitors and lower the reputation of all online OiW measurement techniques. This work presents the performance of four fluorescence-based monitors on an in-house testing facility. Previous studies of a fluorescence-based monitor have raised concerns about the measurement of OiW concentration being flow-dependent. The proposed results show that the measurements from the fluorescence-based monitors are not or insignificantly flow-dependent. However, other parameters, such as gas bubbles and droplet sizes, do affect the measurement. Testing the monitors' calibration method revealed that the weighted least square is preferred to achieve high reproducibility. Due to the high sensitivity to different compositions of atomic structures, other than aromatic hydrocarbons, the fluorescence-based monitor might not be feasible for measuring OiW concentrations in dynamic separation facilities with consistent changes. Nevertheless, they are still of interest for measuring the separation efficiency of a deoiling hydrocyclone to enhance its deoiling performance, as the separation efficiency is not dependent on OiW trueness but rather the OiW concentration before and after the hydrocyclone.

Keywords: oil and gas industry; produced water; fluorescence-based monitor; oil-in-water concentration; real-time measurements; interferences; OLS; WLS; reproducibility; uncertainties

1. Introduction

The importance and awareness of accurate real-time measurements of oil-in-water (OiW) are increasing every year, due to the by-product of water production increases as a consequence of maturing offshore fields. According to literature, 70% of the world's oil production is derived from mature fields [1,2]. As the general trend towards more sustainable production governed by discharge legislation imposing stricter policies and striving to achieve zero pollutant discharge, enhanced recovery techniques such as produced water re-injection (PWRI) have gained increasing attention to increase yield and reduce ocean discharge of oil [2–4]. Seen from an economic perspective, accurate information of oil and particle concentration, and the size distribution in the produced water (PW) for either re-injection or discharge, can be used for reporting, decision support, or even advanced control with the aim to achieve better operation in both separation and treatment [2].

PWRI is mainly deployed for reservoir pressure maintenance, which drives the reservoir production and increasing oil production by sweeping the reservoir [5,6]. In the Danish sector of the

North Sea, $^1/_3$ of the PW is re-injected, which is around the average amount of PWRI for offshore processes in Europe (30%) [7–9]. Due to the increased environmental awareness and maturing fields, PWRI is required more often to reduce the emission of crude oil further, thereby oil will be present in the injection water (IW) [7]. This does not simply signify that the quality of the re-injected PW can be lowered. The presence of crude oil and other organic nutrients in PW can result in ideal conditions for bacterial growth, which may further lead to an increase of microbiologically influenced corrosion (MIC) [3]. Other common negative consequences, associated with crude oil in IW, occur due to the agglomeration-effect of oil on solid particles and the formation of asphaltene deposits. The injection of asphaltenes has shown to plug the porous media in the reservoir to such a degree that some fields in Saudi Arabia have prematurely stopped producing [10]. The flocculation of asphaltenes and the agglomeration effect of oil on solid particles have been recorded to increase the size of particles hundredfold, compared to what was expected downstream in the treatment process [11]. Therefore, whether PW is re-injected or discharged, it is essential to maintain a high PW quality for either optimizing the process or controlling the discharge concentration of oil.

Current offshore platforms rely on offline measurements of OiW concentration, but the reference methods vary due to different regulations worldwide, which renders comparison meaningless as measured OiW concentration is highly method-dependent [12–14]. The North Sea legislation (OSPAR) demands at least two manual samples each day using the gas chromatography-flame ionization detector (GC-FID) reference method [15]. OSPAR demands that the dispersed OiW concentration must be less than 30 mg/L, and the Environmental Protection Agency in Denmark further demands that the total amount of discharged oil in the Danish sector of the North Sea must be less than 222 tonnes annually [7,12,14,16]. The environmental risks associated with PW discharges will increase with increasing water production, especially as maturing fields have reached a water cut of 80% in 2015 [17]. For some of the more mature fields, the water cut even exceeds 90% [18,19]. This resulted in the former for Maersk Oil, which in 2015 discharged 193 of the allowed 202 tonnes [16]. Even though the current reference method (OSPAR GC-FID) has its limitations, a reference method is required for meaningful comparisons. Analyzing using the reference method is time-consuming, and the use of manual samplings is not sufficient for increasing production. The discharged OiW concentration between the two manual samples could exceed the regulations [12,14]. Since 2017, the Danish Environmental Protection Agency applied the following in Denmark through Executive Order no. 394 §9 [16].

> *"Online OiW monitors must be in operation and used for process optimization on the treatment plants for PW at all discharge sites ..."*
>
> *"There must be continuous logging of the data, and the data must be stored for at least 5 years ..."*
>
> *"Data collected with the online OiW monitors must be made available to the Danish Environmental Protection Agency if this is desired..."*

Based on the Executive Order no. 394 §9 in Denmark, the oil and gas industry is consistently asked to invest in analytical methods that measure the discharge concentration of oil in PW. This emphasizes the importance of investigating online OiW monitors that could be a good candidate for measuring the same OiW concentration as the OSPAR GC-FID reference method. Continuous OiW measurement can be separated into two primary and two secondary purposes.

Primary purposes:

- Continual compliance with discharge legislation.
- Process optimization.

Secondary purposes:

- Data logging of PW quality for optimizing the re-injection process.
- Data logging for continuous revising of environmental legislation [9].

For measuring OiW concentration, there exist many commercially available online monitors with different measurement techniques designed for the oil and gas industry. However, to the authors' knowledge, none of the non-reference methods have been robust and reliable enough to be accepted as a reference method for measuring OiW concentration. The online OiW monitors often require proper calibration and a non-hazard environment to be reliable. However, at in-field installations, large variations of mixtures, pressures, chemicals, and temperatures render a harsh and non-ideal environment for the monitors. Therefore, many cases where online OiW monitors have been installed without proper calibration and maintenance yielded doubtful and misleading measurements [20–22]. Even though most interferences may be slow and some close to constant, variations such as flow rate, pressure, OiW concentration, droplets/particle sizes, and particle concentration may change frequently. The irregularity of these variations completely depends on the installation, and it is well known that operation can change from one operator shift to another, which will impact the production [22]. Therefore, an online OiW monitor has to be able to maintain performance even when surrounding parameters change from its baseline calibration.

Based on promising results from previous investigations of a fluorescence-based monitor (Turner TD4100-XDC), this paper aims to examine the calibration method, their robustness to different interferences, and their reproducibility between each other. However, the OiW concentrations will not be validated by GC-FID in this paper.

Previous Work Using the OiW Monitor

The Separation research group at Esbjerg campus has previously used the fluorescence-based OiW monitors in different investigations. However, several experiments have raised concern with regards to the monitors' performance when exposed to certain interferences. The OiW monitors have been used to measure the separation efficiency of hydrocyclones and membranes, and different control methods manipulating different parts of the separation process on a pilot-plant at Aalborg University at Esbjerg campus, cf. [12,20,23]. Investigations of the previous papers did not raise any suspicion about the OiW monitors' performance under different flow regimes as the measurements showed the expected outcome. Thus, at no given time was the true accuracy of the OiW concentration expected in the three papers. What especially raised concern was the discussion based on observed flow-dependency in the results by Bram et al. [24].

During the experiments, a significant correlation between the OiW concentration and the flow rate was observed, with OiW concentration measured on the sidestream and flow rate measured on the mainstream of the process. The outcome of the experiments showed that OiW concentration was proportional to the mainstream flow rate, which theoretically should not be true, as the two measurements are independent. Bram et al. [24] discuss whether it is the type and location of sampling point or interference on fluorescence intensity, e.g., gas bubbles, caused by flow-induced turbulence inside the sidestream configuration generated by shear forces.

Whether it is the sidestream sampling point, the separation process, or the instrument itself that causes the difference in OiW measurement will all be evaluated in this paper. The experiments executed on the pilot-plant will be presented in chronological order, too, when the experiments were executed. Experiments on different standalone systems are made independently of the experiments executed on the pilot-plant. The behavior observed by Bram et al. [24] will be recreated and repeated several times to clarify if it is a recurrent phenomenon.

The rest of the paper will discuss the comparison issues between non-reference methods (e.g., Turner 4100XDC) and reference methods (e.g., OSPAR GF-FID) in Section 2, and how that can be a constraint to the slow acceptance of new non-reference methods. Section 3 describes the different method and materials used for executing the experiments. Section 4 describes the experiment designs; Section 5 presents the results of the experiments. Section 6 discusses the outcome of the results, and last a conclusion is drawn in Section 7.

2. Non-Reference Methods Comparison with Reference Methods

For a non-reference method to fully be accepted as an alternative measurement technique in agreement with the OSPAR GC-FID method, it must first have high precision. Besides, it must be calibrated in order to increase trueness to gain high accuracy. The precision of an instrument indicates the uncertainty in the measurement and is referred to as the degree of repeatability and reproducibility in the measurement system [25,26]. Repeatability is the precision under the same conditions of method and equipment, used by the same operator to make measurements on the exact same sample. Reproducibility is the precision determined under the same conditions, but different pieces of equipment are used by different operators to make measurements on the exact same sample [27].

The measurement of OiW concentration is highly method-dependent, e.g., the OSPAR GC-FID method is limited to measuring the total hydrocarbons between C_7 and C_{40} without toluene, ethylbenzene, and xylene (TEX), a modification of the ISO 9377-2 that is limited to measure the total hydrocarbons between C_{10} and C_{40}. While the gravimetric-based method and the USA EPA method measure anything that is extractable by a solvent but not removed during a solvent evaporation process [14]. In addition, the measured quantities can vary under different conditions and even between different laboratories. Therefore, measuring OiW concentration is not only method-dependent but also procedure-dependent. As a result, a very detailed procedure for taking a sample, transportation, storage, and measuring in a laboratory is well described by the International Organization for Standardization (ISO). These detailed standards are necessary for valid comparison and reporting, especially if used to measure PW discharge. However, the method- and procedure-dependency to determine the "true" OiW concentration also introduces a substantial amount of uncertainties.

A cause-and-effect diagram is a common way to present the different contributions to the total measurement uncertainty [28]. The cause-and-effect diagram in Figure 1 shows the uncertainties related to determining the hydrocarbon oil index by following the ISO 9377-2 and the sampling procedure for crude oil in liquid ISO 3171 [29,30]. Thus, not the modified version from OSPAR. The GC-FID method calculates hydrocarbon oil index based on ISO 9377-2 [30]:

$$OiW = CF\frac{Vwf}{m_1 - m_2}, \tag{1}$$

where

$$CF = \frac{A_m - b}{a}. \tag{2}$$

OiW is the hydrocarbon oil index [mg/L]; CF is the linear calibration curve, where a is the slope of the calibration curve; b is the intercept on the y-axis; A_m is the integrated peak area measured of the sample extract; V is the volume of the final extract [mL]; m_1 is the mass of filled sampling bottle [g]; m_2 is the mass of the empty sample bottle [g]; w is the density of the water sample [g/mL]; f is any dilution factor of the sample extracted if necessary.

The measurement uncertainty (u_{meas}) can be divided into sampling (u_{samp}) and analysis (u_{ana}) uncertainties, visualized in Figure 1 with gray and orange, respectively. The parameters in Equation (1) are the representation of the main branches of the uncertainties related to the u_{ana}:

$$u^2_{meas} = u^2_{samp} + u^2_{ana}. \tag{3}$$

For a given OiW concentration of the sample, it is expected that the same analytical uncertainty applies to every measurement result [31]. This is not the case with sample uncertainty, as a greater part is derived from the heterogeneity of the target. The target is defined as the volume of produced water, at a particular time and location, that the sample intends to represent. By following the sampling procedure from ISO 3171, the PW sample should ideally be taken from rising flow in a vertical pipe section, with an isokinetic center lined pitot, in a turbulent region ($RE \gtrsim 10{,}000$) to ensure a representative well-mixed sample of the main flow, and then stored and transported onshore

by following the ISO 9377-2 and ISO 5667-3, respectively. The uncertainties related to sampling are often dominant and occasionally may exceed 90% of the total measurement uncertainty [32]. Another author states that the sampling uncertainty may influence 75% of the total variance of measurement uncertainty [33].

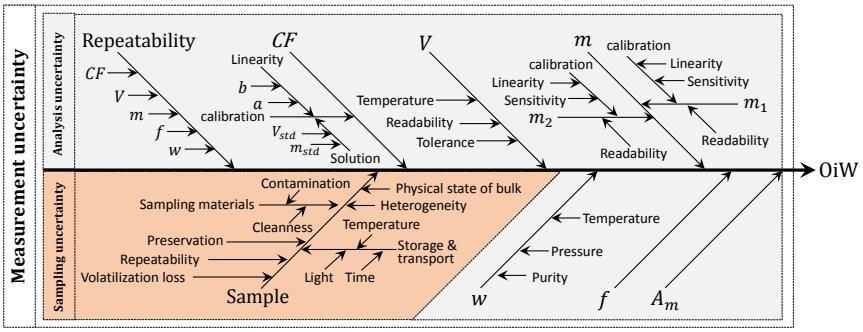

Figure 1. Cause-and-effect diagram of compounded uncertainties contribution to the measurement of OiW concentration by following the gas chromatography-flame ionization detector (GC-FID) reference method defined by OSPAR. The cause-and-effect diagram is divided into two sub-groups: Analysis uncertainty (gray) and sampling uncertainty (orange).

Calculating or estimating the individual uncertainty distribution for each parameter (known as Type B uncertainty), as in Figure 1, can be a complicated procedure as it is difficult to determine all possible uncertainties. Therefore, ISO 21748 suggests using the reproducibility standard deviation (S_R) between laboratories as a representation of the measurement uncertainty (known as Type A uncertainty): $S_R \simeq u_{meas}$, but it may be an overestimation depending on the quality of the laboratory [25,28]. Thus, a measurement uncertainty can only give a representative result as good as the sample that is provided from the sample target [14,31]. As inter-laboratory reproducibility values are measured on the same sample, it does not account for the uncertainty related to the target. Therefore, uncertainties associated with the sample target are as least as important to address as the uncertainties associated with the measurement. This sample should ideally have exactly the same OiW concentration as the target, but in reality, this is impossible for heterogeneous mixtures [31,32]. The combined or total uncertainty should then be described as:

$$u_c^2 = u_{target}^2 + u_{meas}^2. \quad (4)$$

The uncertainty's significance, related to the sample target, when measuring OiW concentrations is highly dependent on the location of the sampling point, sampling extraction process, the mixture of the heterogeneous solution, timing of sampling, etc. A study of environmental systems even shows that uncertainties between-operator and between-protocol are often much smaller than those caused by heterogeneity [32].

To measure the uncertainty related to the target for OiW concentration in an offshore oil and gas process, it must follow the sampling criteria from ISO 3171 to minimize the uncertainty related to heterogeneity. Then, to ideally measure the target uncertainty at more than one sampling point, at the exact same cross-sectional area of the pipe, could be utilized. The uncertainty between the extracted samples in a dynamic process could then be examined. However, for simplicity, the target uncertainty is always neglected, as most processes only have one sampling point at the same cross-section area of the pipe. Thus, if an online OiW monitor should be fairly tested against the reference method, the exact same sample must be used for both validation methods, online and manually, by sharing the target.

If assuming that the combined uncertainty can be expressed by the reproducibility, and the sample is a perfect representation of the body ($u_{target} = 0$), the uncertainty using the reference method can

intuitively be calculated from the data given in ISO 9377-2, as seen in Table 1. The reproducibility variance is assumed to be heteroskedastic, i.e., as OiW concentration increases, the variance increases with the same percentage for the entire range of OiW concentration of interest.

Table 1. Data of inter-laboratory trials published in ISO 9377-2 [30].

Sample No.	L [−]	n [−]	$\bar{\bar{x}}$ [mg/L]	x_{soll} [mg/L]	S_R [mg/L]	CV_R [%]	S_r [mg/L]	CV_r [%]
1	35	127	3.04	2.99	0.291	9.6	0.092	3.0
2	34	134	0.57	0.70	0.192	33.5	0.037	6.5
3	38	142	3.61	4.00	0.763	21.1	0.210	5.8
4	41	156	0.74	1.04	0.300	40.5	0.105	14.1

The variables in Table 1 are as follows. L is the number of laboratories after exclusion of outliers; n is the number of results after exclusion of outliers; $\bar{\bar{x}}$ is the grand mean of all results free from outliers; x_{soll} is the true value; S_R is the reproducibility standard deviation; CV_R is the reproducibility coefficient of the sum of repeatability within-laboratories and between-laboratory variance; S_r is the repeatability standard deviation; CV_r is the repeatability coefficient of variation within-laboratory consistency [30].

If considering that an extracted sample from an offshore oil-producing platform has a "true" OiW concentration of 20 mg/L under ideal homogenous conditions, then

$$u_{target} = 0, \tag{5}$$

where the only uncertainties related to the true value is the reproducibility as a representation of the measurement uncertainty,

$$u_{meas} = CV_R \bar{\bar{x}}. \tag{6}$$

As CV_R varies randomly for each $\bar{\bar{x}}$ concentration, u_{meas} is calculated as examples for best and worst case of an extracted sample of $x = 20$ mg/L:

$$u_{meas_{best}} = CV_{R_1} x = 1.92 \tag{7}$$

and

$$u_{meas_{worst}} = CV_{R_4} x = 8.1. \tag{8}$$

A combined standard uncertainty (u_c) that accounts for contributions from all important uncertainty components, in these particular examples $u_{meas_{best}}$ or $u_{meas_{worst}}$ as $u_{target} = 0$ is

$$u_c = \sqrt{u_{meas}^2 + u_{target}^2}. \tag{9}$$

As u_c's probability is only 68%, it is necessary to express it as expanded uncertainty (U) with a coverage factor (k). In these examples, a normal distribution with 95% confidence interval is considered ($k = 1.96$):

$$U_{best} = u_{c_{best}} k = 3.76 \tag{10}$$

and

$$U_{worst} = u_{c_{worst}} k = 15.88. \tag{11}$$

For these particular examples, the OiW concentration should be described as:

$$OiW_{best} = 20 \pm 3.76, k = 1.96, norm \tag{12}$$

and

$$OiW_{worst} = 20 \pm 15.88, k = 1.96, norm. \tag{13}$$

By considering those examples, it is within 95% confidence that the OiW in the best case does not exceed the discharge limit of 30 mg/L. For OiW_{worst}, the probability of measuring above 30 mg/L with a true solution of 20 mg/L is ≈5.5%, without even including the uncertainties related to the sampling target.

Due to the significant amount of uncertainties associated with the GC-FID method, the "error" of the measured values from an online monitor could potentially be a result of the GC-FID method rather than the performance of the online monitor. In worst case, an acceptable online monitor could be rejected despite being truly accurate and may have a negative influence on the reputation of all online OiW measurements. However, reaching a good understanding of the uncertainties associated with the reference method could facilitate the industrial acceptance of online OiW monitors [9].

3. Materials and Methods

This section describes the investigated four OiW monitors in this paper and the experimental setups used for validating the performance of the OiW monitors under different operating conditions.

3.1. Setup and Calibration of the OiW Monitors

The Turner TD-4100XDC online monitor detects the content of aromatic hydrocarbons in PW using fluorometry. The relative fluorescence units (RFU) are then converted to parts per million (ppm) through a calibration curve. As the OiW monitors are very sensitive to different compositions of atomic structures in its spectral excitation region, it must be calibrated to the mixture of the oil composition. Based on previous results using ARDECA SAE 30 motor oil, a non-detergent SAE 30 motor oil from Midland has been selected instead, as it is free from any surfactants dispersing and dissolving the OiW [34,35]. Even though the OiW monitors are able to detect dissolved oil, the separation process is unable to separate dissolved oil, and the separation efficiency will be inadequate. As the accuracy is nothing more than a comparison and adjustment of the relationship between the readings of the OiW monitors and the GC-FID method, the reproducibility between the four OiW monitors is investigated and not the OiW concentration according to the reference method. More detailed descriptions of the instrument and the calibration procedure are described in previous work [12,34,36]. The calibration of the OiW monitor follows the guideline (multipoint direct calibration) documented by the manufacturer, where at least two samples for a linear situation are recommended covering at least 50% of the desired monitoring range [37]. However, if the fluorescence of oil follows a nonlinear trend, multiple points are necessary. It should be evaluated whether a linear or nonlinear calibration equation produces the best calibration curve. The RFU sensitivity was adjusted by a physical sensitivity screw that sets the basic operating level. The aim of adjusting the operating sensitivity level was to secure the RFU response of all four OiW monitors are as similar as possible before calibration. 400 ppm was chosen as the highest value of interest, as the oil concentration is often less than 200 ppm, but noted to by another author to be below 400 ppm, before entering the deoiling hydrocylone as the second stage of the separation process [38,39].

The default identification from the manufacturer uses ordinary least square (OLS) regression to estimate the best-fit to a first- or second-order polynomial, and thereby implicitly assume homoskedastic random error (ϵ) by using unweighted regression calibrations. For OLS to be the best linear unbiased estimator (BLUE), five assumptions must be assumed according to the Gauss–Markov theorem: the true data trend is linear and that for all values of x the ϵ's are independent, normally distributed with a mean of zero and have the same standard deviation throughout the region of interest (homoscedasticity) [40,41]. Although the first assumptions simplify the reality, proper calibration of the instrument might still achieve a close approximation to the true value. However, if heteroskedasticity is present, OLS loses its efficiency and is not BLUE anymore [41]. By looking at the box plot of the calibration data for all four OiW monitors in Figure 2, the combined 280 samples, 70 samples for each OiW monitor, clearly indicates that ϵ exhibit heteroskedasticity.

The variance increases when the signal intensity increases, and that the RFU and ppm relation follows a linear trend.

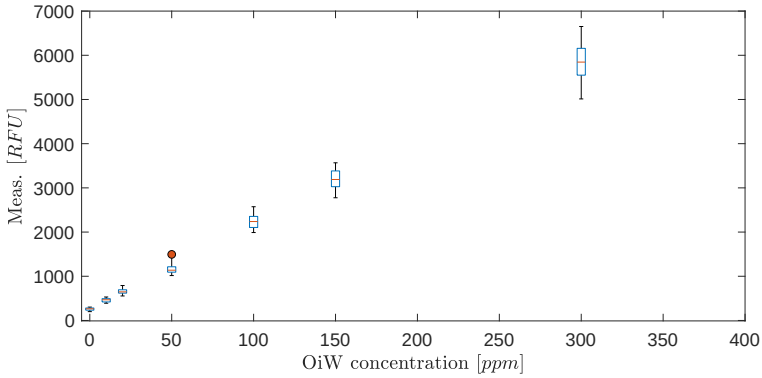

Figure 2. Combined box plot at each oil-in-water (OiW) concentration of all four OiW monitors' calibration data. The calibration data consist of 280; 70 samples for each OiW monitor at following OiW concentrations: 0, 10, 20, 50 100, 150, 300 ppm.

Ignoring the fact that nonconstant variance might result in suboptimal calibration and invalid uncertainty estimates [41,42], instead, weighted least square (WLS) could be used as it may not be reasonable to assume that every calibration concentration should be treated equally. One disadvantage of using WLS is the weighting is often unknown, but an appropriate weighting factor (w_i) for WLS may well be the reciprocal of the variance (σ^{-2}) for each calibration concentration. This weighting will strengthen the influence on the parameter estimates the lower the variance is. The calibration function of interest for both OLS and WLS follows the linear function

$$y = ax + b, \tag{14}$$

where x is the dependent concentration of OiW [RFU], y is the independent measurement unit of each the OiW monitors [ppm], a is the slope (sensitivity), and b is the intercept on the y-axis (offset). The two parameters a and b can be calculated by the regression formulas:

$$b = \frac{SS_{xy}}{SS_{xx}} \tag{15}$$

and

$$a = \overline{y} - b\overline{x}, \tag{16}$$

where $\overline{x}$ and $\overline{y}$ are the arithmetic weighted means of x_i and y_i, respectively, for every i observations from 1 to n. SS_{xx} and SS_{xy} are the weighted sum of squares around the mean and the weighted cross-product of sum of squares for x_i and y_i, respectively. For determining $\overline{x}$, $\overline{y}$, SS_{xx}, SS_{xy}, SSE, and $\hat{s}$, they are measured as in Equations (17)–(22), where the only difference between OLS and WLS is w_i. For WLS, $w_i = s_i^{-2}$, where $s_i = \sqrt{\frac{\sum_{i=1}^{n} e_i^2}{n-2}}$ and $e_i = y_i - \hat{y}_i$. "^" denotes that it is predicted based on observed data. By simply making the weighting factor $w_i = 1$, the OLS is equivalently achieved:

$$\overline{x} = \frac{\sum_{i=1}^{n} w_i x_i}{\sum_{i=1}^{n} w_i}, \tag{17}$$

$$\overline{y} = \frac{\sum_{i=1}^{n} w_i y_i}{\sum_{i=1}^{n} w_i}, \tag{18}$$

$$SS_{xx} = \sum_{i=1}^{n} w_i (x_i - \overline{x})^2, \tag{19}$$

$$SS_{xy} = \sum_{i=1}^{n} w_i (x_i - \overline{x})(y_i - \overline{y}), \tag{20}$$

$$SSE = \sum_{i=1}^{n} w_i (y_i - \hat{y})^2, \tag{21}$$

and

$$\hat{s} = \sqrt{\frac{SSE}{DOF}}. \tag{22}$$

As the estimation of the parameters for a linear regression a and b uses two degrees of freedom; $DOF = n - 2$. The confidence interval (CI) and prediction interval (PI) are calculated, respectively, where the subscript "$_0$" indicates the set of values which falls within the CI and PI [40,41]:

$$CI = ax_0 + b \pm t_{0.025}\hat{s}\sqrt{\frac{1}{n} + \frac{(x_0 - \overline{x})^2}{SS_{xx}}} \tag{23}$$

and

$$PI = ax_0 + b \pm t_{0.025}\hat{s}\sqrt{\frac{1}{w_0} + \frac{1}{n} + \frac{(x_0 - \overline{x})^2}{SS_{xx}}}. \tag{24}$$

The $t_{0.025}$ is the t-score with two-tailed 95% confidence of a t-distribution with $DOF = 68$. The true linear regression line should, with 95% probability, lie within the CI calculated from the sample data, and the PI should be an estimation of which future observations will fall within 95% probability. The attentiveness of this subject is due to when heterogeneity of variance is present, a substantial impact on prediction and calibration may occur, which will affect the precision and accuracy of the OiW monitor. Figure 3 illustrates the linear regression for each of the four OiW monitors with a 95% CI bounded by the inner dashed lines, and a 95% PI bounded by the outer dashed lines for both OLS and WLS.

As the true variance throughout the calibration region of interest is unknown, w_0 is estimated based on the predicted variance function:

$$s(\hat{y}) = c_1\hat{y} + c_0 \tag{25}$$

and

$$w_0 = s^{-2}(\hat{y}), \tag{26}$$

where c_0 and c_1 are obtained by OLS on known sample standard deviation (s_i) in $y_i = (0, 10, 20, 50, 100, 150, 300)$ ppm. Equation (25) may only be a suboptimal representation of the variance function for the OiW monitor. However, a large amount of calibration replicates would be needed to determine whether or not Equation (25) is the best variance function. Noblitt et al. [41] describe other candidates of variance functions, though they will not be part of this paper.

Whether OLS or WLS provides better predictions of the true OiW measurement will be evaluated in the experiment *"Performance evaluation of the four OiW monitors' calibration procedure and the related uncertainties"*.

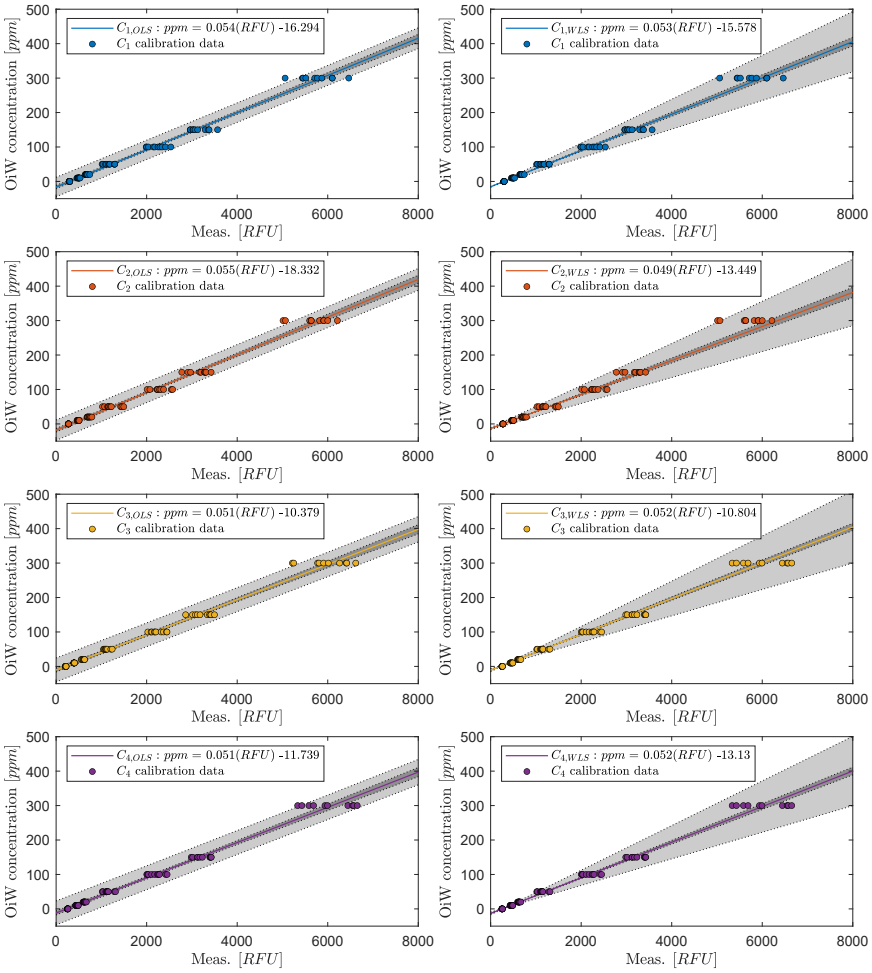

Figure 3. Parameter calibration for each of the four OiW monitors fitting to a linear regression: (**a**) illustrate the linear regression using OLS. (**b**) illustrate the linear regression using WLS.

3.2. Experiment Setups

The setup, located at Aalborg University in Esbjerg, is mainly used to emulate the main parts of an offshore deoiling process to validate potential performance improvements of different applied control strategies. An overview of the main process parts is shown in Figure 4. The system has, in the past, been used for several investigations to test/develop new control algorithms for process systems, modeling, slugging, fault detection/diagnosis, instrumentation performance, and HMI design [13,43–47].

As the pilot-plant is a laboratory setup, it is equipped with an excess of sensors and actuators, even at locations that might be nonexisting at industrial plants, to gain knowledge of indeterminate flow states and conditions. In this investigation on the OiW monitors' performance, only the support section and the hydrocyclone section are used, the rest are bypassed. A more detailed illustration of the components and instructions, used in this paper for executing the experiments on the pilot-plant, can be seen in Figure 5a and Table 2, respectively. Notice a T-junction was used for splitting the two-phase flow

between sidestream and mainstream. The T-junction's branch-arm has a $^{3}/_{8}$" diameter (1"= 25.4 mm) leading the flow into the sidestream of the process, and the mainstream of the two-phase OiW flow continuing through the run-arm of the T-junction.

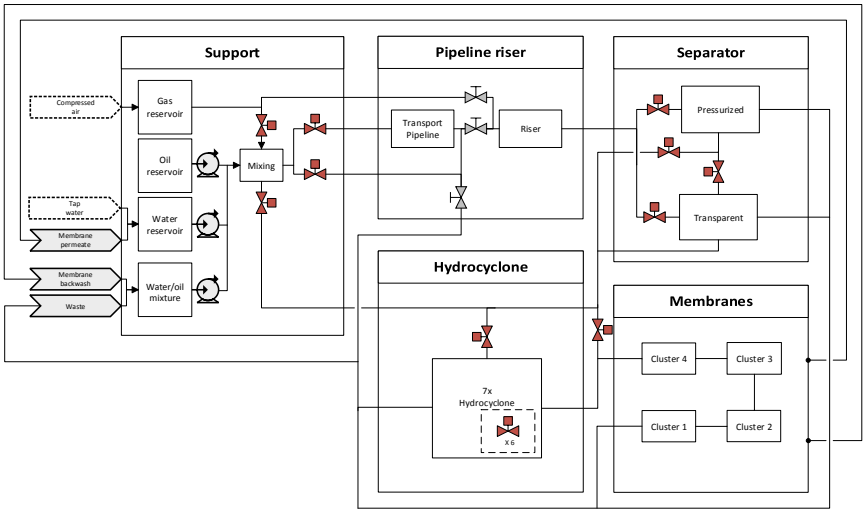

Figure 4. An overview of the bypass structure of the offshore pilot-plant at Aalborg University in Esbjerg.

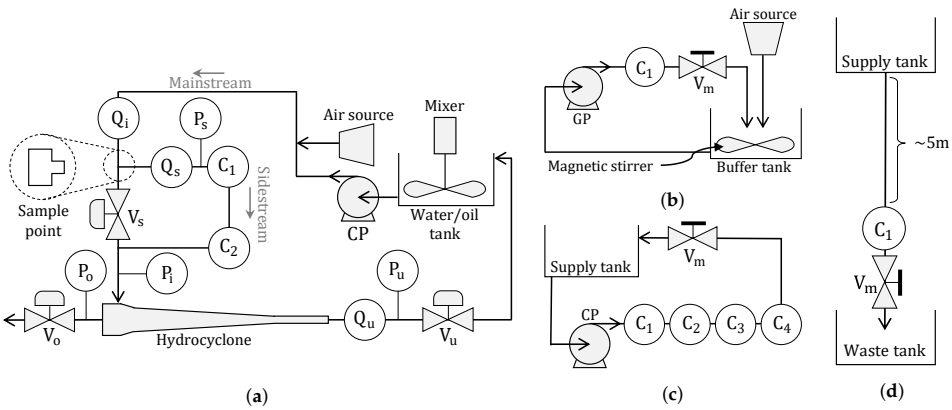

Figure 5. Piping and instrumentation diagram of the by-passed pilot-plant and three standalone setups: (**a**) illustrates the by-passed pilot-plant. (**b**) illustrates the setup for investigating gas bubbles' influence on a OiW monitor. (**c**) illustrates the setup for comparison of the four OiW monitors' calibration. (**d**) illustrates a gravitation feed setup to isolate internal influences.

Three standalone setups have been constructed, as seen in Figure 5b–d, with the corresponding Table 3, to isolate different parameters that can affect OiW measurements, and to evaluate the performance of calibrating the OiW monitors based on OLS and WLS.

Table 2. Specifications of instruments used in the pilot-plant process. An illustration of the instruments' position is seen in Figure 5a.

Component	Type	Description	Specifications
Water/oil tank	Custom made	Supply and waste tank for the oil and water mixture	2.48 m^3
Mixer	2 × Milton Roy Mixing VRP3051S90	Two mixers for mixing the immersible oil in water	N_{max} = 137 rpm, 3 × 550 mm blades
CP	Grundfos CRNE5-9 A-P-G-V-HQQV	Centrifugal pump feeding the OiW separation system	6.9 m^3/h at h = 68 m, h_{max} = 93.3 m
Air source	-	Addition of air into the system if necessary	(1–7) barA
Hydrocyclone	Vortoil 35 mm liner	Single industrial cased hydrocyclone liner	-
Q_i and Q_u	Bailey-Fischer-Porter 10DX4311C	Magnetic flowmeters measuring the inlet and underflow outlet of the hydrocyclone, respectively	0–1.64034 (0–1) L/s
Q_o	Emerson Micro Motion ELITE CMFS010M300N0ANACZZ	Coriolis flowmeter measuring the overflow outlet flowrate from the hydrocyclone	@0.002-97.0 kg/h
P_i, P_i, and P_o	Siemens Sitrans P200	Pressure transmitters measuring the pressure at their respective locations	(0–16) barA
C_1 and C_2	Turner-Design TD-4100XDC	Fluorescence-based OiW monitors measuring the OiW concentration before and after the hydrocyclone	(0–5000) ppm
V_s, V_o, V_u and V_{ub}	Bürkert type 8802	Pneumatic continuous control valves controlling the flow in the system	$\Delta t \lesssim 1$ s, Hysteresis 1%, P_{max} = 16 bar

Addition to Figure 5a, the flow path with nominal diameter and length of pipes between instruments is going through C_1, C_2, and Q_s on the sidestream, hydrocyclone, and end through V_u before returning to the water/oil tank, are illustrated in Figure 6. This is particularly important to consider when analyzing the fluid mechanics of the pilot-plant and to evaluate if the OiW monitors are properly connected according to the specification from the manufacturer.

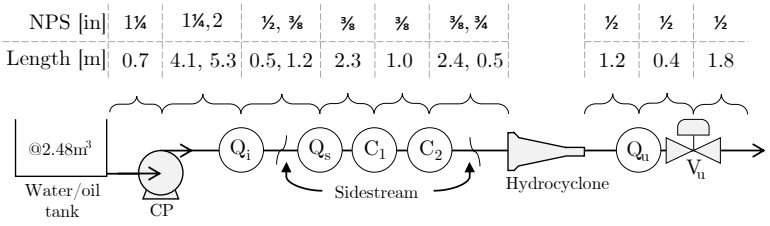

Figure 6. Illustration and table of the flow path with nominal diameter and length of pipes between instruments going through the sidestream.

Table 3. Specifications of instruments used for the standalone systems. An illustration of the instruments' position is seen in Figure 6.

Component	Type	Description	Specifications
Buffer tank	VWR 213-1128	Supply and waste beaker with/without a magnetic stirrer for mixing the solution	1000 mL
Supply tank	3H1/Y1.8/200	Supply plastic jerrycan gravity-feeding the OiW monitor	20 L
Waste tank	3H1/Y1.8/200	Plastic jerrycan for capturing the waste of the gravity-feeding system	20 L
GP	Greylor PQ-12	Gear pump supplied by a 0–24 V AC/DC power supply, feeding the standalone systems; Figure 5b	$Q_{max} =$ 0.132 m^3/h, P_{max} ≈2.4 bar
CP	Grundfos CRNE5-2 A-P-G-V-HQQV	Centrifugal pump feeding the standalone system; Figure 5c	6.9 m^3/h at h = 12.9 m, $h_{max} =$ 20.6 m
Air source	-	Addition of air into the system	(1–7) barA
V	Swagelok	Ball valve manipulating the flow in the standalone systems	-
C_1, C_2, C_3, and C_4	Turner-Design TD-4100XDC	Fluorescence-based OiW monitor measuring the OiW concentration	(0–5000) ppm

4. Experiment Design

This section will describe the design and objective of all executed experiments with the common aim to investigate various interferences that could affect the OiW monitor. Due to previous results, which showed how a varying Q_i influences the OiW concentration measured by one OiW monitor on sidestream, see Bram et al. [24], it is of interest to investigate whether this phenomenon on the pilot-plant is a consistent trend, by replicating the experiment. To observe the performance of the OiW monitors and the pilot-plant design, the following experiments were designed and executed.

- Experiment designs executed on the by-passed pilot-plant setup, see Figure 5a:
    - Q_i's influence on C_1 and C_2.
    - Direct flow through sidestream.
    - Constant Q_i with varying Q_s.
    - Constant pump speed with varying Q_s.
- Experiment designs executed on different standalone systems, see Figure 5b–d:
    - Gas bubbles' influence on C_1.
    - Repeatability investigation of flow-dependency of C_1.
    - Performance evaluation of the four OiW monitors' calibration procedure and the related uncertainties.

Following the manufacturer's recommendations, the flow rate should be within 1–2 L/min. Therefore, flow rates of 1.1 L/min and 1.9 L/min were chosen as the minimum and maximum flow rate, respectively, throughout all experiments executed through the OiW monitors.

4.1. Experiment Designs Executed on the By-Passed Pilot-Plant Setup

Two OiW monitors in series located on the sidestream were used to measure the OiW concentration. For all five experiments on the pilot-plant, there was no air injected into the setup, and the two mixers rotating with a constant speed of ≈137 rpm (maximum speed). The performance

of the hydrocyclone was not to be evaluated in this paper. However, if the performance and robustness of the OiW monitors are high, it will be of interest to investigate the optimal process conditions for the separation process of the hydrocyclone to lower the amount of discharge or increase production due to lower OiW concentration.

Q_i's influence on C_1 and C_2: Investigate the observation observed by Bram et al. [24], to validate the OiW monitors' flow-dependency in the pilot-plant.

- Q_i was stepped two times between 0.1 L/s and 0.4 L/s, and last time between 0.1 L/s and 0.5 L/s. This was accomplished using Q_i as feedback to a PI-controller for controlling the rotational speed of CP.
- Q_s is kept constant at 1.1 L/min by using Q_s as feedback to a PI-controller for controlling V_s opening degree.
- V_u and V_o were fully open throughout the experiment.

Constant Q_i with varying Q_s: Isolate the varying flow rate by only affecting the sidestream, like the experiment with direct flow through sidestream. This was executed by varying Q_s while compensating for having a constant Q_i. Note that this is only valid if the heterogeneous content is adequately mixed, and the pilot-plant physical design does not have any effect on the OiW mixture.

- Q_i was kept constant at 0.4 L/s by controlling the rotational speed of CP.
- Q_s was stepped from 1.1 L/min to 1.9 L/min and back again by manipulating the V_s opening degree.
- V_u and V_o was fully open throughout the experiment.

Constant pump speed with varying Q_s: Executed to investigate the pilot-plant's design effects on the measurement. This was done by keeping the pump speed constant, meanwhile keeping Q_i constant. Ideally, all parameters that would affect the OiW monitors will be at a constant level, except the uncertainty related to the heterogeneous mixture. However, as uncertainty related to the heterogeneous mixture is assumed normally distributed, the mean of the OiW concentration should be constant, even when Q_s is changing. If not, the OiW monitors' flow-dependency must be questioned and taken into consideration.

- CP was kept at a constant 90% pump speed.
- Q_s was stepped from 1.1 L/min to 1.9 L/min and back again by manipulating the opening degree of V_s.
- Q_i is kept constant at 0.4 L/s by controlling V_u's opening degree.
- V_o was fully closed throughout the experiment.

4.2. Experiment Designs Executed on Different Standalone Systems

To isolate the OiW monitors from the pilot-plant, different standalone systems were constructed to investigate different parameters that were suspected to influence the measurement of the OiW monitors.

Gas bubbles' influence on C_1: Like turbidity monitors, the OiW monitors were suspected difficulties with interference from gas bubbles. For turbidity monitors, air bubbles are known to cause a false high turbidity reading when measuring the amount of light scattered [48]. However, results from another report testing a fluorescence-based monitor indicate that gas bubbles significantly reduce the measurement, as the gas bubbles potentially reduce the strength of both excitation light and fluorescence [22]. The change in fluorescence intensity occurs as gas bubbles scatter the light that distorts the fluorescence spectrum [49]. The setup used for detecting gas bubbles' influence on C_1 can be seen in Figure 5b. The conditions of the experiment were as follows.

- Fixed *GP* speed to have a constant flow rate of ≈1.1 L/min.
- Constant stirring speed of the magnetic stirrer.
- Constant air flow rate introduced down into the buffer tank, creating different sizes of air bubbles, together with the mixing behavior from the magnetic stirrer.

Repeatability investigation of flow-dependency on C_1: As entrained-air was observed to have an influence on the OiW measurement in the previous experiment, the pump and mixer were suspected of introducing unwanted bubbles into the system. This could be due to the motion of the mixer, inlet suction of the pump, or leakage. Increasing the flow rate also increased the number of bubbles observed in the outlet, which intuitively could be the reason for an increasing OiW concentration and not the flow rate itself. To eliminate the influence of the pump, one OiW monitor was gravity-fed instead with only tap water or demineralized water. The gravity-fed setup is illustrated in Figure 5d.

- Flow rate was constant ≈1.1 L/min and ≈1.7 L/min, respectively, by manipulating V_m's opening degree.

Performance evaluation of the four OiW monitors' calibration procedure and the related uncertainties: Even though different parameters were observed to influence the measurement of the OiW concentration, the OiW monitors could still be feasible to use in the pilot-plant, if the monitors are consistent in their measurements and between each other. Four OiW monitors are used in this experiment for comparison of the instrument, see Figure 5c.

- Nine different concentrations are tested: 0, 5, 10, 20, 40, 80, 160, 320, and 400 ppm. Demineralized water is used with a solution of oil and isopropanol to reduce the uncertainty in the heterogeneous mixture of OiW significantly. Demineralized water was chosen as the laboratory tap water was observed to fluoresce and change on a day-to-day basis.
- 1.9 L/min was kept constant by controlling V_m's opening degree.
- Fixed CP speed of 74%.

5. Results

This section provides the results of which flow regimes influence the four fluorescence-based monitors' OiW measurements. The calibration presented in Figure 3 was not added to these experiments as only the trend of the OiW monitors' measurements were of interest under different flow regimes. The investigations were divided into experiments executed on the pilot-plant and experiments executed on the standalone systems, as described in Section 4.

5.1. Experiment Results Executed on the By-Passed Pilot-Plant Setup

Before each experiment on the pilot-plant, the mixers had a run time of >20 min to ensure the OiW volume in the supply tank was well mixed. Noise was observed in all experiments on the pilot-plant originating from the mixers in the supply tank. The first part of the execution time for each experiment are used to ensure that the system had reached nominal operation. The initialization time depends on the experiment and mainly ensures that the system is flushed sufficiently as contents of oil, algae, and particles tend to settle or stick to the pipeline inner wall when the system is not in operation. Each experiment's execution time was >100 min, to obtain steady-state measurements from the OiW monitors between each change of flow rate. The results of each experiment will be described and discussed in this section, and Section 6 will provide a holistic discussion of each topic.

Q_i's influence on C_1 and C_2: According to Figure 7, there is an indication that the OiW monitors are flow-dependent in the pilot-plant. Q_i was stepped two times between 0.1 L/s and 0.4 L/s, and one last time between 0.1 L/s and 0.5 L/s. Q_s was kept constant at 1.1 L/min. Figure 7 shows the same positive correlation as Bram et al. [24], when Q_i increases the RFU increases. As Q_i was controlled by the *CP*, the output signal of the *CP* has a similar shape as Q_i.

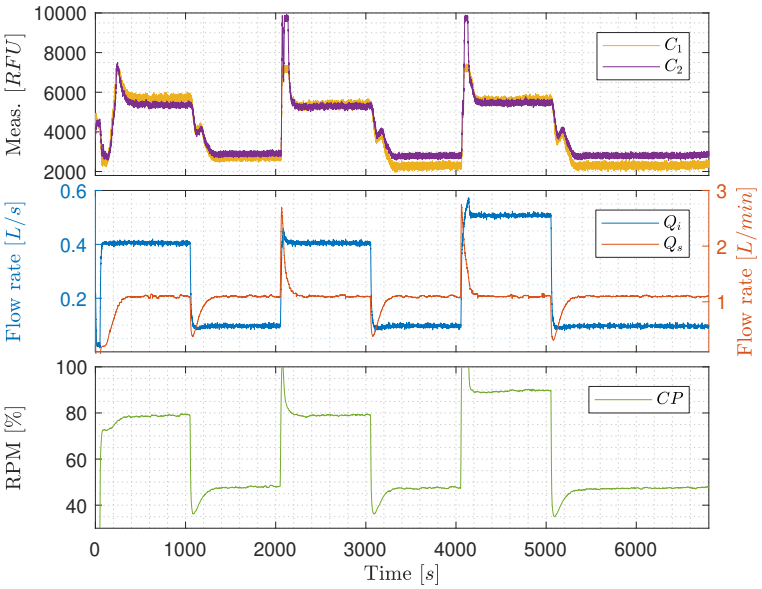

Figure 7. Q_i's influence on C_1 and C_2.

In this experiment the increment of the two OiW monitors was $C_1 \approx 3000$RFU and $C_2 \approx 2600$RFU, when Q_i was increased from 0.1L/s to 0.4 L/s. The last step from 0.1 L/s to 0.5 L/s does not appear to increase the RFU measurement compared to $Q_i = 0.4$ L/s. This could indicate that the oil and water are separating differently in the process, depending on the flow rate. Looking at Figure 6, the transportation delay of the OiW mixture before reaching the sample point is relatively long, which will be a problem if the flow rate is not highly turbulent through the entire system. The worst condition for achieving sufficient turbulence is when the superficial velocity is lowest. For that particular experiment on the pilot-plant, this occurred when Q_i is 0.1 L/s and the pipeline diameter (D) is 2":

$$A = \frac{\pi}{4} D^2, \tag{27}$$

$$v = \frac{Q}{A}, \tag{28}$$

and

$$Re = \frac{\rho v D}{\mu} \simeq 2545, \tag{29}$$

where $A = 0.002$ m^2, $v = 0.05$ m/s, $\rho = 998.2$ kg/m^3, and $\mu = 0.001$ Ns/m^2 @ 20 °C. As $Re < 10,000$ (even close to laminar $Re < 2300$) in some situations of the experiment, it could indicate that the oil experience significant gravitational separation throughout the pipelines. Thus, making the measurements from the OiW monitors unjustifiably flow-dependent. It will also explain why there is little to no difference in the RFU measurement when $Q_i = 0.4$ L/s or $Q_i = 0.5$ L/s as $Re \simeq 10,182$ and $Re \simeq 12,727$, respectively. This also concludes that it is not possible to determine whether the OiW monitors are flow-dependent based on this experiment. The high spikes of RFU observed when Q_i is increased, could be due to the presences of dead volume in the sidestream that is pushed through the OiW monitors after increasing the flow rate of Q_i, and a small systematic peak when Q_i is decreased.

Constant Q_i with varying Q_s: Figure 8 shows results of keeping Q_i constant at 0.4 L/s, ensuring that the flow through the entire part of the pilot-plant is highly turbulent, and stepping Q_s between

1.1 L/min and 1.9 L/min. Even though at high turbulence, where Q_i is kept constant, RFU and Q_s are still positively correlated. The increment of RFU after the increase of Q_s is, nevertheless, only 200 RFU compared to the results in Figure 7, that has a tenfold increment. This narrows the issue down to being either due to the OiW monitors are, in fact, flow-dependent, even within its operation range recommended by the manufacturer, the T-junction sample point which is not a standardized way of sampling by ISO 3171, or it could be due to gas bubbles' interference.

The result of *CP* increases slowly through the experiment as V_s is closing gradually in order to force more flow through the OiW monitors. The back-pressure is increased due to the decreasing opening degree of V_s, which is the consequence of the increasing *CP*'s rotational speed. The steady increase of *CP*'s rotational speed does not appear to influence the RFU.

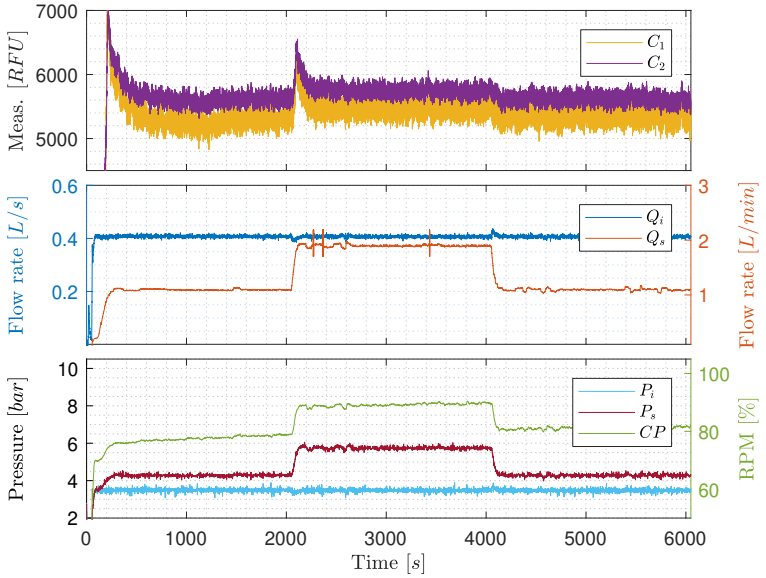

Figure 8. Constant Q_i with varying Q_s.

Constant pump speed with varying Q_i: Figure 9 is similar to Figure 8, but *CP* is kept constant at 90% rotational speed throughout the experiment, meanwhile controlling the varying Q_s by manipulating the opening degree of V_s. However, the results in Figure 9 are distinguished from Figure 8 as no clear changes occurs when Q_s is stepped from 1.1 L/min to 1.9 L/min and back again. This either indicates that increasing the rotational speed of *CP* decreases average droplet size by shear forces or increases entrained air and oil by having higher velocities of the carrier phase-flow near the water/oil tank's outlet. To further investigate the OiW monitors, three different standalone systems were constructed to determine gas bubbles' influence on the OiW monitors, the repeatability of each monitor under different flow conditions, and an extensive analysis of the calibration for the OiW monitors was carried out.

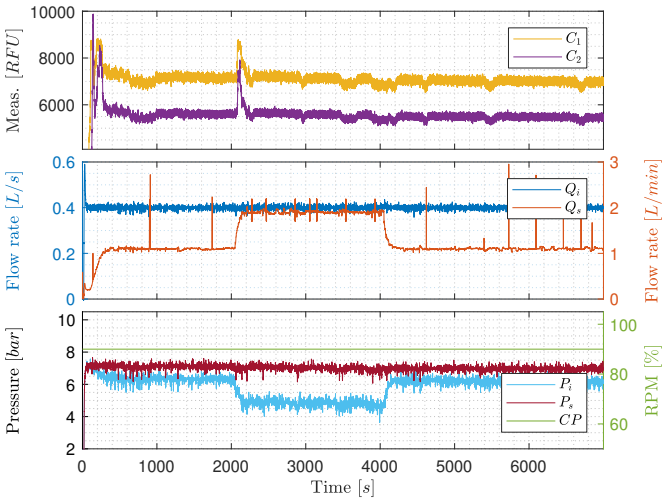

Figure 9. Constant pump speed with varying Q_s.

5.2. Experiment Results Executed on Standalone Systems

Gas bubbles' influence on C_1: Figure 10 shows the results of introducing air bubbles into the standalone system Figure 5b. The solution used for this experiment only consists of tap water from the laboratory to isolate the heterogeneity of OiW, as it could be challenging to determine whether the difference in RFU was due to air introduction or due to a shift in the volume of oil droplets entering the OiW monitor. As presumed, a relatively high RFU was measured in the tap water by the OiW monitor, and the RFU value of the tap outlet was observed to change on a day-to-day basis. In this experiment, a mean of 1665 RFU was measured from 0 to 600 s when no air is added into the system. After 10 min, air was added into the system, as indicated in Figure 10 with a blue vertical line. Air pressure was applied until visible air bubbles were apparent in the buffer tank. The RFU increased and fluctuated during the injection of air, with a mean of 1783 RFU during 650–1200 s. The fluctuation is assumed as an outcome of the random sizes of air bubbles introduced by the air source passing the view cell. After ending the air injection, the RFU measurement slowly converged to its initial RFU value. However, the difference in mean before and after the addition of air is 14 RFU. That is likely due to the execution time of the experiment was not long enough for the added air to dissipate to the surrounding environment. It is noteworthy that when only air was present in the view cell, with some uncertainty to small micro/macro water droplets, the measurement was 80–90 RFU consistently. Nevertheless, it makes sense as the content of only air should ideally not fluoresce.

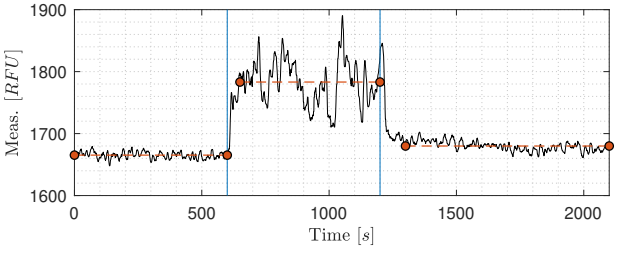

Figure 10. Gas bubbles' influence on the OiW monitor.

Repeatability investigation of flow-dependency on C_1: The results from gravity feeding one OiW monitor with both tap water and demineralized water with two different flow rates of 1.1 L/min and 1.7 L/min are seen in Figure 11. For experiments with tap water, the first three experiments with a flow rate of 1.7 L/min was rejected as the OiW concentration was consistently off compared to the other. The first three experiments inconsistencies were assumed happening due to start-up after a cleaning process. Demineralized water was selected as a reference, as ideally, it should not contain any matter capable of fluorescing. Tap water was known to fluoresce and was used for testing flow-dependency in another RFU range.

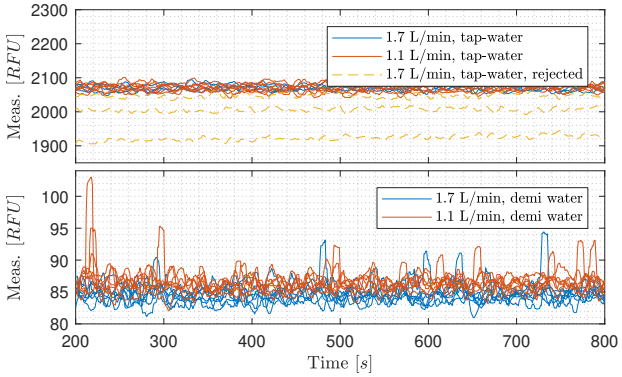

Figure 11. Repeatability investigation of flow-dependency on C_1 with demineralized water and tap water at two different flow rates.

One-way analysis of variance (ANOVA) was carried out to test the null hypothesis (H_0) that differences in flow rate through the OiW monitor have equal mean RFU measurements. As for the F-statistic of ANOVA to be meaningful, it requires that the dependent variable is normally distributed in each group.

According to the one-way ANOVA test on the tap water with different flow rates, there is a 95.7% chance that the mean of RFU is equal at a flow rate of 1.7 L/min and 1.1 L/min. Thus, H_0 cannot be rejected. The boxplot in Figure 12 shows that the medians of the to flow rates are within the same range for tap water. Based on the results with different flow rates of tap water, if the H_0 is instead rejected, the flow-dependency is still insignificant compared to other variables' influence on the measurements from the OiW monitors, as the difference in grand means and grand medians are 0.3 RFU and 4.0 RFU, respectively.

The one-way ANOVA test on the demineralized water with different flow rates shows that H_0 can be rejected and the boxplot shows similar result. Even though H_0 is rejected for demineralized water, the measurement grand mean and grand median is close to the result with tap water; 1.7 RFU and 2.1 RFU, respectively. The results from Figure 12 supports that the measurement from the OiW monitor on demineralized water is flow-dependent, though, it is insignificant. Interestingly, the experiments also show that the measurement of RFU is lower with a high flow rate of 1.7 L/min compared to a lower flow rate of 1.1 L/min. That is exactly the opposite as was observed in Figures 7 and 8. Notice, measurement within 95% confidence interval are larger for tap water than demineralized water:

$$\overline{\overline{x}} \pm 11.64 \text{ @ tap water, 1.7 L/min,} \tag{30}$$

$$\overline{\overline{x}} \pm 8.24 \text{ @ tap water, 1.1 L/min,} \tag{31}$$

$$\overline{\overline{x}} \pm 0.51 \text{ @ demi water, 1.7 L/min,} \tag{32}$$

and

$$\overline{\overline{x}} \pm 0.38 \text{ @ demi water, 1.1 L/min,} \tag{33}$$

where $\overline{\overline{x}}$ denotes the grand mean as reference. The big difference in 95% confidence interval between tap water and demineralized water is most likely due to fluorescence substances in the tap water compared to the demineralized water, that ideally should not contain any fluorescence substances.

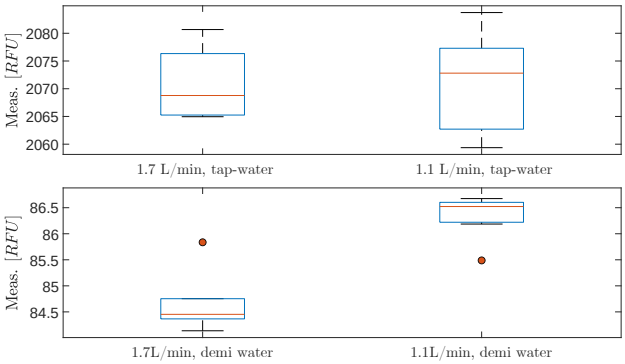

Figure 12. Boxplots for each type of water with different flow rates.

Performance evaluation of the four OiW monitors' calibration procedure and the related uncertainties: As mentioned in Sections 1 and 2, having a good understanding of the uncertainties associated with the online monitors would help their industrial acceptance. However, for them to be accepted, proper calibration is vitally important to ensure trustworthy data. A 100 min experiment with eight different OiW concentrations were added throughout the experiment: 5, 10, 20, 40, 80, 160, 320, and 400 ppm starting at 0 ppm, as seen in Figure 13. All equipment was thoroughly cleaned before running the experiment to reduce the presence of contamination. Even though the accepted true value of the OiW concentration cannot be guaranteed without the use of the GC-FID reference method, the concentration uncertainties related to preparing the samples can be estimated based on Type B uncertainties, which will be presented later in this subsection. By analyzing the settling time for each injection of a new OiW concentration in Figure 13, it takes less than three minutes for the OiW concentration to settle in the system. The exact injection times are highlighted in Figure 13.

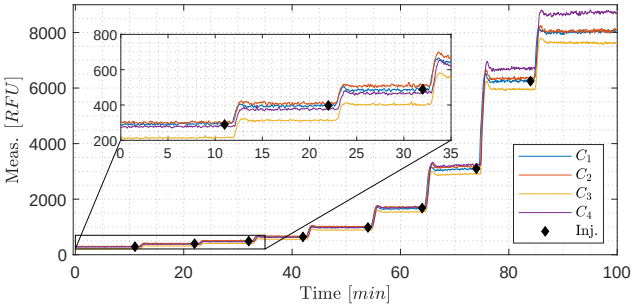

Figure 13. A 100 min experiment with eight different OiW concentrations were added throughout the experiment: 5, 10, 20, 40, 80, 160, 320, and 400 ppm starting at 0 ppm. The injection time is marked with black diamonds. The OiW measurements from the four OiW monitors are displayed in RFU, to evaluate the raw data of the OiW monitor before analyzing the calibration methods.

Based on the precision data presented in Table 1, the repeatability and reproducibility of the GC-FID method were calculated based on four different concentrations, in several different laboratories, with n number of samples for each OiW concentration. The repeatability and reproducibility followed the guidelines provided by ISO 21748 [25,50]. The same procedure was executed on the calibration

data in Figure 3, to estimate the reproducibility as representation of the measurement uncertainty for both OLS and WLS, see Tables 4 and 5, respectively. The Grubbs criterion was used for examining outliers, and the hypothesis of no outliers is rejected if

$$G > \frac{n-1}{\sqrt{n}} \sqrt{\frac{t^2_{a/(2n),n-2}}{n-2+t^2_{a/(2n),n-2}}}, \tag{34}$$

where G is the Grubbs criterion.

Table 4. Data of inter-laboratory trials from the four OiW monitors based on ordinary least square (OLS) calibration.

Sample No.	n [−]	$\bar{\bar{x}}$ [ppm]	x_{soll} [ppm]	S_R [ppm]	CV_R [%]	S_r [ppm]	CV_r [%]
1	39	−0.54	0	2.11	–	0.25	–
2	39	10.13	10	1.68	16.58	0.94	9.27
3	37	20.58	20	1.42	6.93	1.26	6.16
4	38	47.27	50	5.99	12.78	5.92	12.60
5	40	103.76	100	8.97	8.64	8.89	8.57
6	38	154.53	150	9.80	6.34	9.48	6.13
7	40	294.26	300	24.50	8.33	23.39	7.95

The CV_R's can be added to the calibration measurements with an expanded uncertainty of coverage factor $k = 1.96$ as in the previous Section 2. Based on the results in Tables 4 and 5, a rough estimate of CV_R = 10% was made for both OLS and WLS. Note that the reproducibility estimation is closely related to the repeatability for both OLS and WLS. This is highly due to not fulfilling all conditions for measuring the reproducibility stated in ISO 21748 [25]. The OiW measurement, on the same measurand, is done by different individuals but at the same time and in the same laboratory, which affects the results between-laboratory variance (S^2_L):

Table 5. Data of inter-laboratory trials from the four OiW monitors based on weighted least square (WLS) calibration.

Sample No.	n [−]	$\bar{\bar{x}}$ [ppm]	x_{soll} [ppm]	S_R [ppm]	CV_R [%]	S_r [ppm]	CV_r [%]
1	39	0.04	0	0.26	–	0.24	–
2	39	10.42	10	0.96	9.23	0.91	8.77
3	37	20.52	20	1.91	9.31	1.19	5.80
4	38	46.20	50	5.71	12.37	5.54	11.98
5	40	101.73	100	8.66	8.51	8.62	8.47
6	38	151.57	150	10.28	6.78	9.32	6.15
7	40	287.92	300	26.42	9.18	23.01	7.99

$$S^2_R = S^2_r + S^2_L. \tag{35}$$

The prediction interval is another way to define the combined uncertainty of the OiW monitor. However, there is a chance that both PI and reproducibility, as a representation of combined uncertainty, are overestimated [28]. Even though overestimation often has its advantages for not exceeding the safety limit, it becomes difficult to predict the expected result and thereby misrepresents the ability to estimate an actual outcome, e.g., if the OiW monitors should be used as control feedback. Another way of predicting uncertainties is by calculating the type B uncertainties of the sampling and the type A uncertainty of the OiW monitors' confidence interval. Like in Section 2, a cause-and-effect diagram is constructed to identify all relevant uncertainty sources. The parameters in the equation of measuring

the OiW concentration are represented by the main branches in Figure 14. Although, it can be difficult to determine all related uncertainties. The cause-and-effect diagram in Figure 14 is divided into type B uncertainties (gray area), related to the manufactures of the different equipment stated uncertainties, and type A uncertainties (green area), related to the OiW monitors measured confidence interval from the calibration. The orange area in Figure 14 is related to sources of uncertainties due to the nature of the solution and human errors, which will not be included in the measurement of the combined uncertainty. This can be problematic as human errors always will be present, and the combined uncertainty might be underestimated. However, it will give a good indication of what the lowest amount of uncertainty would be based on the different equipment used for mixing the eight different solutions.

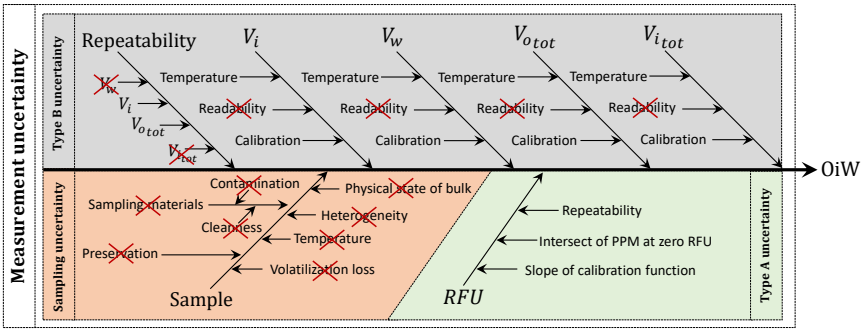

Figure 14. Cause-and-effect diagram of compounded uncertainties contribution to the measurement of OiW concentration by following the uncertainty related to each equipment used for mixing the eight different solutions. The cause-and-effect diagram is divided into three sub-groups: type B uncertainties (gray), type A uncertainties (green), and sampling uncertainties (orange).

The different equipment used for preparing the different OiW concentrations can be seen in Table 6, and their additional systematic error and random error stated by the different manufacturers.

Table 6. A list of the six different equipment used for preparing the samples of the experiment seen in Figure 13, and the corresponding systematic and random error.

Abbreviation	Volumetric Equipment	Volume	Systematic Error	Random Error
VR_1	Graduated cylinder, tall form, BLAUBRAND®, class A, 1000 mL	1000 mL	±5.00 mL	–
VR_2	VWR® Volumetric Flask, Class A, 500 mL	500 mL	±0.25 mL	–
VR_3	Graduated cylinder, tall form, BLAUBRAND®, class A, 250 mL	250 mL	±1.00 mL	–
VR_4	Graduated cylinder, tall form, BLAUBRAND®, class A, 100 mL	100 mL	±0.50 mL	–
VR_5	Finnpipette® F2: (0.5–5) mL	(0.5–5) mL	±40.0 µL	15.0 µL
VR_6	Gilson™ F148504: (10–100) µL	(10–100) µL	±1.5 µL	0.6 µL

The standard uncertainty due to random error, $u(V, rep)$, is often stated in a datasheet provided by the manufacturer of the pipette and implies the assumption of being normally distributed. For the different volumetric flasks, VR_1, VR_2, VR_3, and VR_4, the random error cannot, however, be determined by the manufacturer as it is not a mechanical error but rather based on the end-users ability to measure

with the naked eye (human error). For simplicity, $u(V, rep)$ of VR_1, VR_2, VR_3, and VR_4 are assumed zero. VR_5 and VR_6 follows a standard deviation of a normal distribution

$$u(V, rep) = \sigma. \tag{36}$$

The standard uncertainty due to calibration or systematic error of a volume, $u(V, cal)$, is commonly specified by the manufacturer on the equipment as $\pm u_i$. There is no information on the distribution or coverage factor of this uncertainty estimate, and the uncertainty is therefore conservatively assumed to be uniformly distributed. To convert the calibration uncertainty to standard uncertainty the calibration uncertainty is converted using

$$u(V, cal) = \frac{u_i}{\sqrt{3}}. \tag{37}$$

Uncertainty, due to the temperature, affects the thermal expansion of both equipment and liquids. Although, the volumetric thermal expansion coefficient of Borosilicate glass is insignificant (9.9×10^{-6} °C^{-1}) and is therefore neglected. All the equipment is calibrated at 20 °C according to the manufacturers, and the laboratory's temperature normally around 20 ± 3 °C, the uncertainty is conservatively assumed to be uniformly distributed as the deviation of temperature was not measured when the experiment was carried out:

$$u(V, temp) = \frac{V \Delta t \alpha_V}{\sqrt{3}}, \tag{38}$$

where α_V is the volumetric thermal expansion coefficient of each different material (isopropanol, water, and oil), temperature error $\Delta t = \pm 3$ °C, and V is the specific volumetric measurement. For the design of the experiment 495 mL isopropanol, 5 mL oil, and 10 L of water was used. Uncertainties due to the temperature effects can then be calculated for water, isopropanol, oil, and as mixtures by using Equation (38).

To calculate the combined uncertainty for each concentration it is important to note that for every time the equipment is used, an amount of $u(V, rep)$ and $u(V, cal)$ is added to the total volume:

$$u(V) = \sqrt{u(V, rep)^2 + u(V, cal)^2 + u(V, temp)^2} \tag{39}$$

Table 7 shows the amount of equipment used for mixing the eight different concentrations from 5–400 ppm.

Table 7. A list of used equipment used for mixing each concentration, $V_i - V_{i-1}$ represent the amount of stock solution that should be added to reach the target concentration.

V_w [mL]	Used Equipment		
10,000	$10 \times VR_1$		
Wanted [ppm]	**V_i [mL]**	**$V_i - V_{i-1}$ [mL]**	**Used Equipment**
10,000 *	500	–	$1 \times VR_2$, $1 \times VR_5$
0	0	0	–
5	5.00	5.00	$1 \times VR_5$
10	10.01	5.01	$1 \times VR_5$, $1 \times VR_6$
20	20.04	10.03	$2 \times VR_5$, $1 \times VR_6$
40	40.16	20.12	$4 \times VR_5$, $2 \times VR_6$
80	80.65	40.48	$8 \times VR_5$, $5 \times VR_6$
160	162.60	81.96	$1 \times VR_4$
320	330.58	167.96	$1 \times VR_3$
400	416.67	86.09	$1 \times VR_4$

* Stock solution of isopropanol and oil (C_{stock}).

As a new concentration is added to the previous mixture of OiW, the total amount of mixture increases every time. This implies that the uncertainty from the previous mixture is added current one, see Table 8. The equations for estimating the predicted OiW concentration are as follows:

$$C_{stock} = \frac{V_{o_{tot}}}{V_{o_{tot}} + V_{iso_{tot}}} \times 10^6 = \frac{V_{o_{tot}}}{V_{stock}} \times 10^6 \tag{40}$$

and

$$C_i(V_i) = \frac{V_i}{V_w + V_i} C_{stock}. \tag{41}$$

C_{stock} is the 10,000 ppm stock solution of isopropanol and oil, $V_{o_{tot}}$ and $V_{iso_{tot}}$ are the total amount of oil and isopropanol added to the stock solution respectively. C_i is the eight wanted OiW concentration that is aimed for, V_w is the total amount of water used in the experiment, and V_i is the different amounts of volumetric stock solution added to the experiment. Based on the standard uncertainties for each volumetric measurement of each equipment, the concentration uncertainty of the calibration can be determined by EURACHEM/CITAC [51]:

$$U_{cB}(C_{stock}) = C_{stock} \sqrt{\left[\frac{u(V_{o_{tot}})}{V_{o_{tot}}}\right]^2 + \left[\frac{u(V_{stock})}{V_{stock}}\right]^2} \tag{42}$$

and

$$U_{cB}(C_i) = C_i \sqrt{\left[\frac{u(V_w + V_i)}{V_w + V_i}\right]^2 + \left[\frac{u(V_i)}{V_i}\right]^2 + \left[\frac{u(V_{o_{tot}})}{V_{o_{tot}}}\right]^2 + \left[\frac{u(V_{stock})}{V_{stock}}\right]^2}, \tag{43}$$

where each OiW concentration's uncertainties can be seen in Table 8. u_{cB} is the type B uncertainties obtained from the uncertainty information given by the manufacturer of the used equipment, and u_{cA} is the mean of all type A standard uncertainties obtained within one standard deviation (68% confidence interval) from the calibration of all four OiW monitors at the specific concentration, see Figure 3. Each OiW concentration's uncertainties based on type A and type B can be seen in Table 8. Note that the previous u_{cB}, for each OiW concentration, is added to the continuous.

Table 8. Measured type B uncertainties of sampling and type A uncertainties of the OiW monitors' confidence interval estimated in the calibration.

Volume Unit	Equipment	No. of Times	Volume [mL]	u_{cB} [ppm]	$u_{cA,OLS}$ [ppm]	$u_{cA,WLS}$ [ppm]
V_{Stock}	VR_5 VR_2	1 1	5.00 500	59.38	–	–
V_{0ppm}	VR_1	10	10,000	-	1.92	0.03
V_{5ppm}	VR_5	1	5.00	0.04	1.87	0.04
V_{10ppm}	VR_5 VR_6	1 1	5.00 0.01	0.09	1.83	0.09
V_{20ppm}	VR_5 VR_6	2 1	10.00 0.03	0.18	1.74	0.21
V_{40ppm}	VR_5 VR_6	4 2	20.00 0.12	0.35	1.59	0.44
V_{80ppm}	VR_5 VR_6	8 5	40.00 0.48	0.70	1.42	0.91
V_{160ppm}	VR_4	1	81.96	1.31	1.74	1.86
V_{320ppm}	VR_3	1	167.98	2.54	3.60	3.74
V_{400ppm}	VR_4	1	86.09	3.15	4.68	4.68

By JCGM [27] it is denoted that if the contributions to u_c of the type A and type B standard uncertainties are denoted by u_{cA} and u_{cB}, the combined uncertainty u_c can be calculated as

$$u_c = \sqrt{u_{cA}^2 + u_{cB}^2}, \tag{44}$$

and the expanded uncertainty, with 95% confidence interval ($k = 1.96$) as

$$U = u_c k \tag{45}$$

This is done for both OLS and WLS, as seen in Table 9.

Table 9. Combined and expanded uncertainty for each OiW concentration for both calibration methods: OLS and WLS.

Volume Unit	$u_{c,OLS}$ [ppm]	$u_{c,WLS}$ [ppm]	U_{OLS} [ppm]	U_{WLS} [ppm]
V_{0ppm}	1.92	0.03	3.76	0.06
V_{5ppm}	1.87	0.06	3.67	0.11
V_{10ppm}	1.83	0.13	3.59	0.25
V_{20ppm}	1.75	0.28	3.43	0.54
V_{40ppm}	1.63	0.56	3.19	1.10
V_{80ppm}	1.58	1.15	3.10	2.25
V_{160ppm}	2.18	2.28	4.28	4.47
V_{320ppm}	4.41	4.52	8.64	8.86
V_{400ppm}	5.65	5.65	11.07	11.07

Summarizing the three different methods of estimating the uncertainty related to preparing a sample and measuring the OiW concentration by the four OiW monitors:

- Using the prediction interval directly from the calibration of the OiW monitors.
- Estimating the reproducibility based on the calibration data.
- The estimated combined uncertainty based on type A and type B uncertainties.

Instead of looking at the RFU measurement of each OiW monitor in Figure 13, the OiW concentrations are measured by each OiW monitor for both OLS and WLS, which are shown in Figures 15 and 16, respectively.

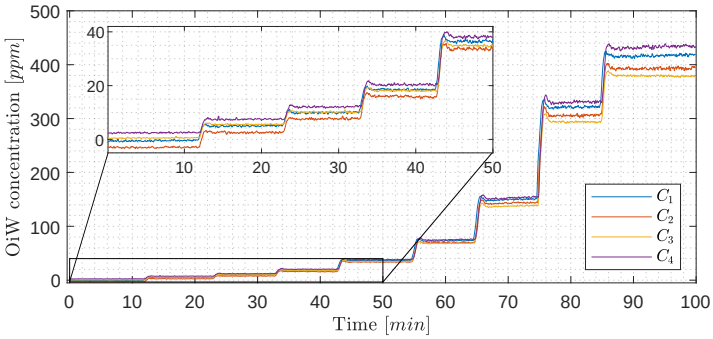

Figure 15. A 100 min experiment with eight different OiW concentrations as in Figure 13. The measurements from the four OiW monitors are displayed in ppm based on the OLS calibration method.

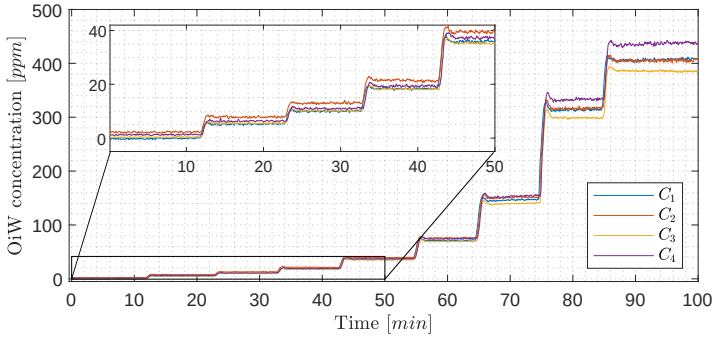

Figure 16. Similar as Figure 15; however, the measurements from the four OiW monitors are based on the WLS calibration method instead of OLS.

Only by looking at the two different ways of estimating the least square of the experiment in Figures 15 and 16, there is a clear tendency that the deviation of WLS, in the lower region, is smaller than with OLS. At high concentrations, it is more difficult to determine which of the two ways deviates from the predicted concentration. This tendency also agrees with the theory that OLS tends to fit points that are at the upper calibration levels better than those points at the lower calibration levels. To evaluate the performance of OLS and WLS, an average for each OiW concentration is calculated based on the duration time between injection time minus the first three minutes listed in Tables 10 and 11. As the accepted true OiW concentration cannot be given without the GC-FID reference method, the grand mean ($\overline{\overline{C}}$) of each OiW concentration based on all four monitors are calculated and their predicted OiW concentrations (X_{pred}) that were aimed for.

Table 10. Data of the experiment containing the predicted concentration, each steady-state value of the four OiW monitors based on OLS calibration, and the grand mean of all four monitors for each concentration.

X_{pred} [ppm]	$\overline{C}_1$ [ppm]	$\overline{C}_2$ [ppm]	$\overline{C}_3$ [ppm]	$\overline{C}_4$ [ppm]	$\overline{\overline{C}}$ [ppm]
0	−0.45	−1.83	0.57	2.49	0.19
5	5.02	4.05	5.60	7.48	5.54
10	9.93	9.53	10.19	12.08	10.43
20	18.54	18.43	18.10	20.36	18.85
40	36.48	37.39	34.88	38.19	36.74
80	73.04	75.81	68.26	74.98	73.02
160	149.62	154.81	137.39	152.60	148.61
320	321.31	328.94	293.83	330.24	318.58
400	417.58	422.98	378.92	434.06	413.39

By analyzing the performance of OLS and WLS with the three different ways of determining uncertainties, a good indication of the OiW monitors' reproducibility can be given. Figures 17 and 18 show the results of the mean OiW concentrations from each OiW monitor for both OLS and WLS listed in Tables 10 and 11, respectively. The $\overline{\overline{C}}$'s are used as a reference for each specific OiW concentration and both calibration methods, denoted as categories on the y-axes. The black squared marker in Figures 17 and 18 represent the predicted OiW concentration for each target, and the numbered marker (①, ②, ③) represent the three different ways of determining the uncertainty.

Table 11. Data of the experiment containing the predicted concentration, each steady-state value of the four OiW monitors based on WLS calibration, and the grand mean of all four monitors for each concentration.

X_{pred} [ppm]	$\overline{C_1}$ [ppm]	$\overline{C_2}$ [ppm]	$\overline{C_3}$ [ppm]	$\overline{C_4}$ [ppm]	$\overline{\overline{C}}$ [ppm]
0	−0.13	1.43	0.34	1.26	0.72
5	5.21	6.75	5.46	6.31	5.93
10	10.00	11.69	10.13	10.95	10.69
20	18.39	19.72	18.18	19.33	18.90
40	35.89	36.83	35.26	37.36	36.34
80	71.55	71.50	69.24	74.56	71.71
160	146.23	142.79	139.60	153.06	145.42
320	313.67	299.91	298.81	332.69	311.27
400	407.55	384.78	385.42	437.68	403.86

By looking at the results for both OLS and WLS, in most cases, X_{pred} lies within the measurements of the four OiW monitors. However, for the target at 40, 80, and 160 ppm solutions the OiW concentration of all four monitors were lower than the prediction aimed for with both calibration methods, which might be a result of insufficient amount of stock solution added to the setup.

Evaluating the performance of predicting the uncertainty related to the OiW monitors, each method's performance is described for both calibration methods:

OLS:

① As the weighting factor within PI of OLS is equal to one, the result of using PI as uncertainty boundary are equal in all OiW concentration. Resulting in overestimation of uncertainty at a lower concentration, and might end in an underestimation at high OiW concentrations.
② The 10% uncertainty estimation based on the reproducibility is applied, covering almost all OiW steady-state values the entire range except at 5 ppm. It is clearly the best way to represent the uncertainty related to OLS measurement compared to the other two methods.
③ The measurement of type B uncertainty was, as expected, difficult to include all uncertainties, resulted in an underestimation of the uncertainty above 40 ppm. The type A uncertainty from the CI of the OLS calibration is the main reason for the joined type A and type B uncertainty measurement fits within its boundary at the lower OiW concentration.

WLS:

① The weighting factor within PI of the WLS method is equal to the sample variance measured at each OiW concentration. The uncertainty estimation covers all OiW steady-state values in all ranges.
② The same as for OLS, a 10% uncertainty estimation based on the reproducibility calculation is applied. The uncertainty range is lower than the PI but still cover all OiW steady-state values in the entire range.
③ As for OLS, the measurement of type B uncertainty for WLS was, as expected, also underestimated.

Even though the reproducibility may be a good representation of the uncertainty related to the OiW monitors for both calibration methods, it usually requires a substantial amount of inter-laboratory trials for calculating the reproducibility. Therefore, it may not be the best approach to achieve an uncertainty boundary related to the OiW concentration obtained from the OiW monitor. However, using the PI as uncertainty estimation is only valid for the WLS method due to the weighting factor.

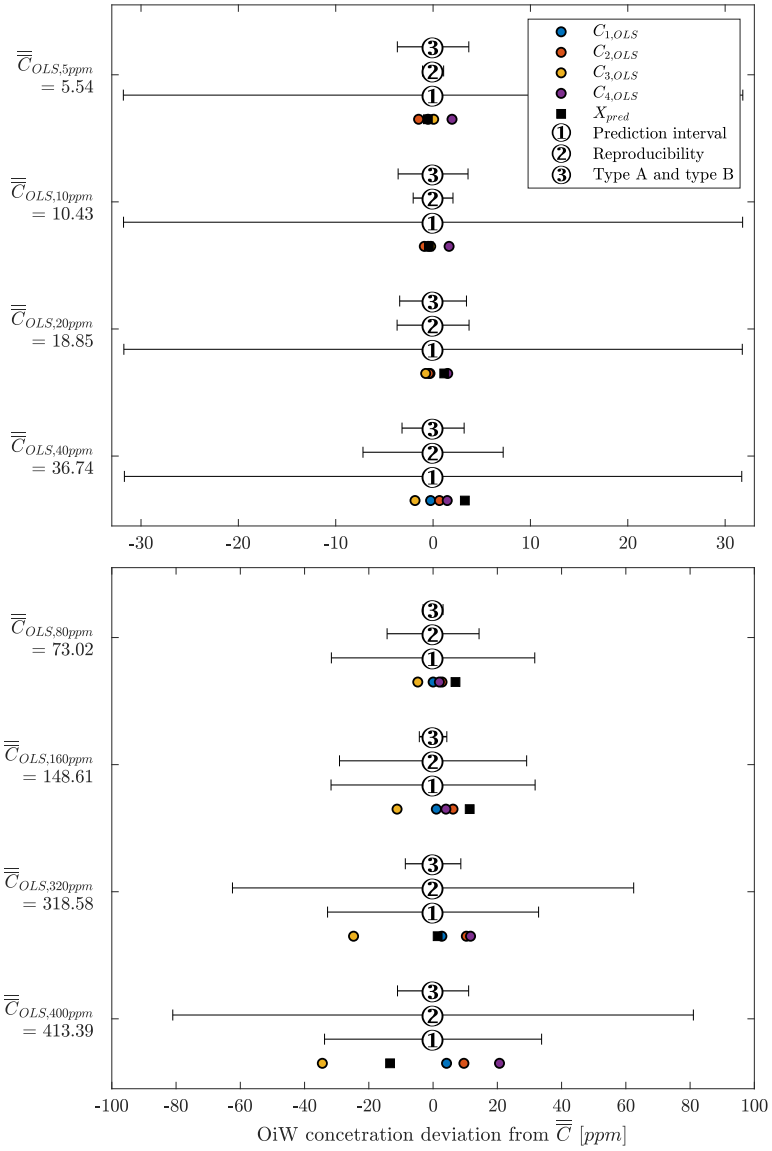

Figure 17. The analysis of three different methods for determining the best estimation of the OiW monitors' uncertainty based on OLS in the entire range of interest. The grand mean for each concentration is used as a reference point and categorized on the y-axes. The plot is divided into two subplots for better visualization of the OiW concentration range of interest.

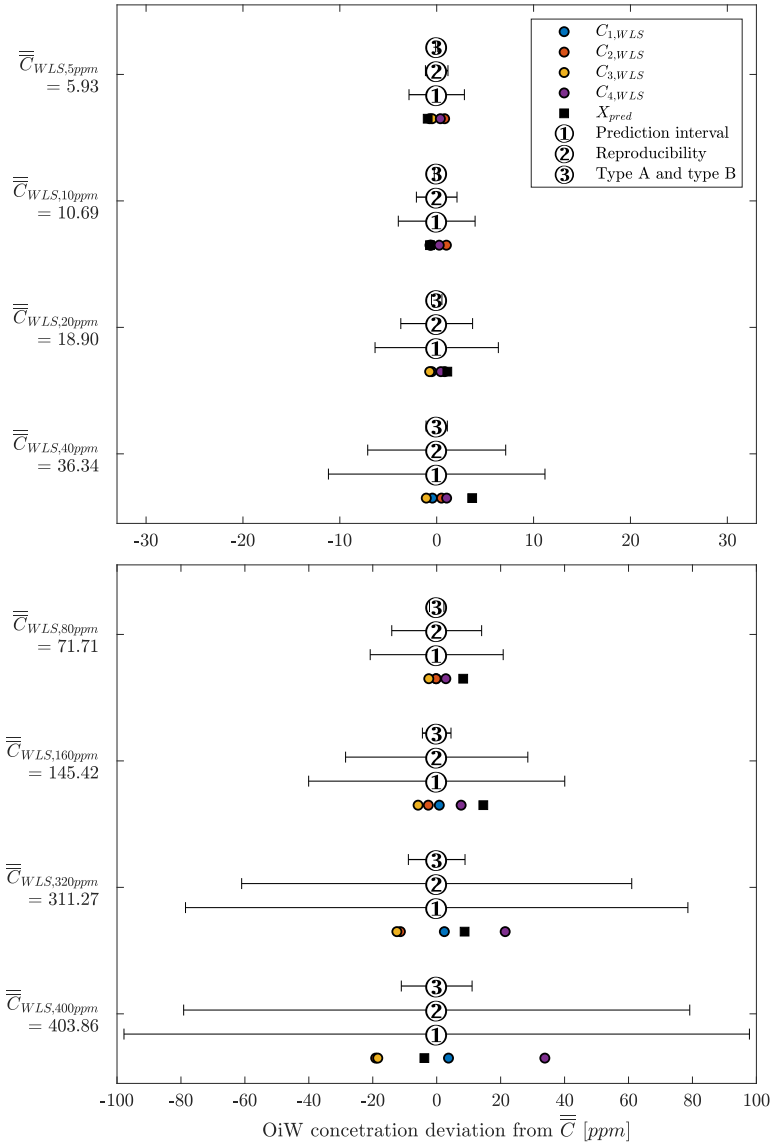

Figure 18. The analysis of three different methods for determining the best estimation of the OiW monitors' uncertainty based on WLS in the entire range of interest. The grand mean for each concentration is used as a reference point and categorized on the y-axes. The plot is divided into two subplots for better scaling of the OiW concentration range of interest.

6. Discussion

In general, RFU was used to represent the trend of OiW concentration, as the accepted true value of the fluid quantity was not able to be guaranteed on the pilot-plant. It will require a vast amount of cleaning to ensure that no previous dead volumes are present in the pilot-plant and all pipes are free of algae, bacteria, oil, grease, etc., all of which will influence the measurement. Even then, it can still not be guaranteed that contamination might inadvertently enter the system. Furthermore, samples

of the OiW solution used in the pilot-plant should be analyzed by the GC-FID method to validate if the OiW monitors measure the accepted true value. As mentioned in Sections 2 and 3.1, the most desirable outcome of the OiW monitors will be both high accuracy with high precision, but to achieve high accuracy with low uncertainty, it is necessary to have high precision. As directly investigating the OiW monitors' precision can be challenging to accomplish with relatively high uncertainty in sampling, reproducibility was investigated to determine whether the OiW monitors can be used as a non-reference method. Figures 15 and 16 show the result of calibrating the OiW monitors using OLS and WLS on the same data set. Based on the calibration data in Figure 3, there is a clear tendency of heteroskedasticity, where the variance increases when the signal intensity increases, and that the RFU and ppm relation follows a linear trend.

Looking at the results in Table 12 obtained from Figures 15 and 16 of the two calibration methods, at no given time did the WLS have a larger deviation between the OiW monitors' measurements than the OLS calibration method. Especially at the low OiW concentrations, the deviation of OLS was 2–3 times larger than with WLS. This indicates that WLS, as a calibration method, provides the higher reproducibility of the OiW monitors compared to OLS. Another analysis was to investigate if the uncertainty of the OiW monitors could be represented to an operator either for direct reporting of the OiW concentration with related uncertainty or as decision support. Including the uncertainty to the measurements will also fundamentally impact the control system design for expressing the discharge limit, if OiW monitors in the future should be used as control feedback for advanced control with the aim to achieve better operation in both the separation and treatment process. The results in Figure 18 show that PI and reproducibility are two good candidates for representing the uncertainty of OiW monitors' measurements. However, reproducibility typically requires a substantial amount of inter-laboratory trials. Therefore, it is suggested that PI, which can mathematically be expressed based on calibration data, should represent the uncertainty of the OiW measurement, and reproducibility may be given as a reference to update the uncertainty parameter in the calibration curve. Note that the results from this experiment are taken under ideal conditions for the fluorescence-based monitors to investigate the calibration comparison, as isopropanol was added to the mixture for dissolving oil into the water phase.

Table 12. Data of the results in Figures 15 and 16, containing the predicted concentration, biggest deviation between all four OiW monitors for each concentration and each calibration method, and biggest deviation from $\overline{\overline{C}}$ for each concentration and each calibration method.

X_{pred} [ppm]	Biggest div. between $\overline{C}_1, \overline{C}_2, \overline{C}_3, \overline{C}_4$ with OLS [ppm]	Biggest div. between $\overline{C}_1, \overline{C}_2, \overline{C}_3, \overline{C}_4$ with WLS [ppm]	Biggest div. from $\overline{\overline{C}}_{OLS}$ [ppm]	Biggest div. from $\overline{\overline{C}}_{OLS}$ [%]	Biggest div. from $\overline{\overline{C}}_{WLS}$ [ppm]	Biggest div. from $\overline{\overline{C}}_{WLS}$ [%]
0	4.34	1.56	2.30	–	0.86	–
5	3.43	1.54	1.95	35.1	0.82	13.8
10	2.55	1.70	1.64	15.8	1.00	9.4
20	2.26	1.54	1.50	8.0	0.82	4.4
40	3.31	2.10	1.86	5.0	1.08	3.0
80	7.55	5.33	4.76	6.5	2.85	4.0
160	17.42	13.46	11.21	7.5	7.64	5.3
320	36.41	33.88	24.75	7.8	21.42	6.9
400	55.14	52.91	34.46	8.3	33.83	8.4

During the experiments, variations of flow conditions caused the sidestream not to be a representation of the mainstream in the process. The results of Figure 7 raised the suspicion that the OiW monitors were flow-dependent, though further investigation confirmed that it was not the case. The results in Figures 11 and 12, from the experiment on flow-dependency, showed an insignificant relationship between OiW concentration and flow rate based on the boxplot and the ANOVA tests, both with demineralized water and tap water. Demineralized water was selected as the basis of the reference as, ideally, it should not contain any fluorescence-sensitive matter. The tap water was known to fluoresce and was therefore used as a second RFU concentration for flow-dependency. Oil with

emulsifiers could also have been used for this experiment to ensure that the results were not limited to water, but uncertainties related to homogeneity could increase due to oil, and isopropanol must be fully dissolved in the water phase. It was, therefore, debatable whether the extracted sidestream was representable due to operating conditions. By comparing Figures 7 and 8, Reynolds number did have a huge impact on the measurement, and it is safe to conclude that the system cannot be operated below a mainstream of 0.4 L/s if turbulence is required throughout the system. It was furthermore questioned if the two-phases of the flow were uneven split in the T-junction due to hydrodynamics, and a phase maldistribution might have taken place between the run and the branch [52]. The T-junction sample point was also questioned to influence OiW concentration measurement, even when the flow is assumed highly turbulent; gravity, inertia, and pressure might still influence how the two-phase flow is divided between the run and branch of the T-junction [53]. Another drawback of using the T-junction as the sampling point is the propagation or amplification of other upstream processes effects that cause an uneven concentration split. An example of this could be the increasing shear forces of the *CP* that change the droplet size distribution, which should not ideally affect the OiW concentration. However, a shift in droplet sizes might affect the split between the run and the branch, which could potentially be the source of the observed increment in RFU as the flow rate is increased in Figure 8. This hypothesis is supported when comparing the results in Figures 8 and 9, as the step input signal to Q_i and Q_s in both experiments are identical. By changing the controller and actuator in Figure 8 from controlling Q_i by *CP* to controlling Q_i by V_s, meanwhile keeping *CP* constant in Figure 9, the OiW measurement was kept constant. The dispersed liquid is likely more stable throughout the process when *CP* is kept constant, as increasing shear forces from the *CP* would probably decrease the average droplet size and thereby a better representation in the entire mainstream. Even though this is a positive effect for investigating the OiW monitors, it is undesirable as the average droplet size decrease, which heavily reduces the separation efficiency of the process [54]. The measurement of the OiW somewhat seems to be constant in Figure 9, but the system still has issues that can be addressed in the future to lower the uncertainty as much as possible related to sampling:

- Change the sample point from horizontal to be vertical.
- Use a sample probe for directing the rising flow through the sidestream.
- Use isokinetic sampling.
- Minimize the transport delay between the sample point and the OiW monitor as the manufacturer recommends a $^1/_2$" connection with a maximum flow rate of 2.0 L/min, which relates to transitional flow ($Re = 3358$) and stratification can happen in the transport pipeline.

Air's influence on the OiW monitors was also investigated on a standalone system. Figure 10 shows that the injection of air both introduces systematic and random error in the measurement of OiW. As the random error of air introduction only increases the uncertainty, seen as noise on the RFU signal, it might be acceptable if using a moving average of the OiW concentration, assuming zero-mean random noise, preferably including the measurements of the past minutes or more. Variations in the systematic error based on the volume and size distribution of gas bubbles will be a problem, as it will not be feasible accounting for air's influence by simply recalibrating. However, seen from a normal oil separation process, systematic error due to gas bubbles might not be an issue as a three-phase separator will reduce the volume and size distribution of gas bubbles before the sample point. Further investigation should examine how the volume and size relationship of gas bubbles influences the OiW concentration.

Most of the discussion has focused on implementation and process criteria to reduce parameters that influence the OiW concentration, but it is not necessarily only a process design issue. The inner filter effect is a common internal issue of fluorescence-based monitors that describes the nonlinear relationship between the fluorescence intensity and the concentration of a fluorophore [55]. A decrease in fluorescence emission due to inner filter effect is caused by the absorption of the exciting light closer to the incident beam, which significantly diminishes the light intensity further away from it.

Secondary inner filter effects are caused by reabsorption of fluorescence [55]. Inner filter effects could also have affected the results observed in Figures 8 and 10. When the concentration is high, or the light absorption is high, the excitation beam is attenuated by the sample so that the surface perpendicular to the excitation beam fluoresces most powerful [56]. This effect might explain why the OiW monitors output a higher RFU even though the concentration is still the same, as smaller droplets that are generated by the high shear pump (*CP*) increases the oil droplets' total surface area, which is at the current time under investigation.

Other effects that can influence the analysis are chemical quenchers, such as oxygen and chloride, where a quenching mechanism refers to decreases in the fluorescence intensity of a sample [57–59]. The most significant mechanism of oxygen quenchers is the collision of oxygen and phosphor molecules in the excited triplet state [56,57,60]. Even though chlorine has not been used in these experiments, it is necessary to address if the quenching mechanism happens when chlorine is present, as chlorine is often added to the process for killing microorganisms. In [58], the results showed that all polynuclear aromatic hydrocarbon (PAH) molecules decreased in fluorescence due to the presence of chlorine. Some of the PAH types did even show a 41% decrease in fluorescence due to chlorine [58]. Other more physical differences between the measurement of the OiW monitors could be due to differences in the photomultiplier or degradation of the fluorescent lamp over time. However, it should be possible to account for those by recalibration.

Based on the authors' knowledge, one of the most significant issues with the use of fluorescence-based monitors is the big uncertainty related to what is fluorescing in the excitation region. Due to the high sensitivity to the presence of other atomic structures, in the same excitation region as aromatic hydrocarbons, the OiW monitors might not be feasible for measuring the exact OiW concentration in a highly dynamic separation facility with consistent changes of substances. As high reproducibility of the OiW monitors can be achieved with proper calibration, they can still be useful to determine the separation efficiency of separation equipment, such as deoiling hydrocylcones. As the separation efficiency is not dependent on OiW accuracy, but rather the ratio of OiW concentration across the hydrocyclone, the OiW monitors will still be feasible for enhancing the hydrocyclones deoiling performance. Another use of the OiW monitors could be in cooperation with other sensors, as a single monitor is unable to reduce uncertainty in its perception [61]. As uncertainty arises from various conditions for measuring the OiW concentration, it could be of interest to combine several sensors to gain more rich information. This can be done in several ways by using sensor fusion to increase the quality of data, increase reliability, or estimate unmeasured states. Redundancy of identical monitors would reduce the amount of uncertainty by averaging the value, seen in Figures 15 and 16, and to compensate for sensor deprivation by fault-tolerant design [61]. However, it might not be the best solution as interference will affect all identical monitors, as discussed throughout the paper. Instead, a combination of different sensor types can be fused, i.e., Kalman filter, which provides a likelihood estimation of the measured OiW concentrations based on the different sensors [61]. As traditional Kalman filter requires the sensor measurement uncertainties, knowing the uncertainty of the OiW monitors will benefit the Kalman filter prediction [62]. This is usually executed by predicting the true value by producing estimates of the current state variables, along with their uncertainties [63]. The most weight is given to the value with the least uncertainty. As a result, the estimates produced by the Kalman filter tend to be closer to the true values than sensors used separately.

7. Conclusions

The paper presented an evaluation of four fluorescence-based monitors (Turner TD4100-XDC) that are sensitive to the content of aromatic oil in a mixture. The fluorescence-based monitor was thoroughly calibrated to a specific oil type used in all experiments. The "true" values of the fluorescence-based monitors, compared to the OSPAR GC-FID reference method, were at no given time measured, as the measurement of oil-in-water (OiW) is known to be highly methodology-dependent. Additionally, a relatively high amount of uncertainties are potentially associated with the reference method.

From this assessment, the precision, repeatability, and reproducibility of the fluorescence-based monitors were investigated.

Testing the OiW monitors' calibration method revealed that the weighted least square (WLS) is preferred to achieve higher reproducibility, compared to ordinary least square (OLS), due to the heteroskedastic behavior. Having a good understanding of the uncertainties associated with the OiW monitors will also help the industrial acceptance of including online monitors.

Previous studies of the fluorescence-based monitors raised concerns about the measurement of OiW concentration being flow-dependent. However, based on the results of the fluorescence-based monitors, they are not or at least insignificantly flow-dependent within its recommended flow rate range. The flow-dependency phenomenon of two fluorescence-based monitors, discussed by Bram et al. [24], was caused by insufficient representation of the process flow. To circumvent the transport stratification in the pipelines, the mainstream of the process must be operated at $Re > 10,000$. Furthermore, the horizontal used T-junction as a sampling point was questioned to split the two phases unevenly, and as a result, the testing facility is scheduled for replacement of the sampling point to further lower uncertainties.

The measurements of the OiW monitors were also observed and discussed to be affected by other interferences such as gas bubbles, droplet sizes, quenchers introduced by the solution's composition, and presences of other atomic structures in the same excitation region. Due to the high sensitivity to different compositions of atomic structures other than aromatic hydrocarbons, the fluorescence-based monitors might not be feasible for measuring OiW concentrations in highly dynamic separation facilities with continuous changes of the fluid composition. Thus, different interference parameters influenced the measurements of the fluorescence-based monitors, they still have a high precision between each other, and it could still be of interest for measuring the separation efficiency of OiW separation processes downstream the gravity separator, such as deoiling hydrocyclones and membrane filtration systems, to enhance their deoiling performance. One advantage of measuring inlet and outlet OiW concentration of a separation process is that separation efficiency is a ratio of the two measurements, and therefore robust to interference that affects both of the monitors.

Author Contributions: D.S.H. and S.J. designed and executed the experiments; D.S.H. and M.V.B. analyzed the data; Z.Y. contributed with materials and analysis tools; S.J., M.V.B., and Z.Y. assisted with technical discussion, feedback, and paper refinement; D.S.H. wrote the paper. All authors have read and agreed to the published version of the manuscript.

Funding: This research was funded by the DHRTC projects "Injection Water Quality and Control" (Proj-No.: 878040) and "Laboratory Testing at AAU-Esbjerg and Development" (Proj-No.: 878039).

Acknowledgments: The authors would like to thank the support from DHRTC and the colleagues; S. Pedersen, L. Hansen, and P. Durdevic at AAU Esbjerg, for many valuable discussions and supports.

Conflicts of Interest: The authors declare no conflicts of interest.

Abbreviations

The following abbreviations are used in this manuscript.

OiW	Oil-in-Water
PWRI	produced water re-injection
PW	produced water
IW	injection water
MIC	microbiologically influenced corrosion
OSPAR	Oslo and Paris convention (for the Protection of the Marine Environment of the Northeast Atlantic)
GC-FID	gas chromatography-flame ionization detector
TEX	toluene, ethylbenzene, and xylene
ISO	International Organization for Standardization
RFU	relative fluorescence units
ppm	parts per million
OLS	ordinary least square

BLUE	best unbiased estimator
WLS	weighted least square
CI	confidence interval
PI	prediction interval
ANOVA	analysis of variance
PAH	polynuclear aromatic hydrocarbon

References

1. Ahmed, U. Making the Most of Maturing Fields. *Oilfield Rev.* **2004**, *16*, 1.
2. Blanchard, E. Oil in Water Monitoring is a Key to Production Separation. *Offshore* **2013**, *73*, 104–105.
3. Maxwell, S. *Implications of Re-Injection of Produced Water on Microbially Influenced Corrosion (MIC) in Offshore Water Injection Systems*; CORROSION 2005; NACE International: Houston, TX, USA, 2005; p. 9.
4. OSPAR Commission. *List of Decisions, Recommendations and Other Agreements Applicable within the Framework of the OSPAR Convention—Update 2018*; Technical Report; OSPAR: London, UK, 2018.
5. Marle, C.M. Oil entrapment and mobilization. In *Basic Concepts in Enhanced Oil Recovery Processes*, 1st ed.; Bavière, M., Ed.; Critical Reports on Applied Chemistry Volume 33; Elsevier: Paris, France, 1991; Volume 33, Chapter 1, pp. 3–39.
6. Hartmann, D.J.; Beaumont, E.A. Predicting Reservoir System Quality and Performance. In *Handbook of Petroleum Geology: Exploring for Oil and Gas Traps*, 1st ed.; Beaumont, E.A., Foster, N.H., Eds.; Handbook of Petroleum Geology; The American Association of Petroleum Geologists: Tulsa, OK, USA, 1999; Volume 3, Chapter 9, p. 154. [CrossRef]
7. OSPAR Commission. *Produced Water Discharges from Offshore Oil and Gas Installations 2007–2012*; OSPAR: London, UK, 2014; p. 2.
8. Larsen, I. *Denmark's Oil and Gas Production—And Subsoil Use 09*; Technical Report; Energistyrelsen: Copenhagen, Denmark, 2010.
9. Yang, M. Analysing Oil Pollution. *Awe Int.* **2018**, *56*, 31–37 .
10. Kokal, S.; Al-Dawood, N.; Fontanilla, J.; Al-Ghamdi, A.; Nasr-El-Din, H.; Al-Rufaie, Y. Productivity Decline in Oil Wells Related to Asphaltene Precipitation and Emulsion Blocks. *SPE Prod. Facil.* **2003**, *18*, 247–256. [CrossRef]
11. Bennion, D.; Thomas, F.; Imer, D.; Ma, T.; Schulmeister, B. Water Quality Considerations Resulting in the Impaired Injectivity of Water Injection and Disposal Wells. *J. Can. Pet. Technol.* **2001**, *40*, 54–61. [CrossRef]
12. Hansen, D.S.; Bram, M.V.; Yang, Z. Efficiency investigation of an offshore deoiling hydrocyclone using real-time fluorescence- and microscopy-based monitors. In Proceedings of the 2017 IEEE Conference on Control Technology and Applications (CCTA), Mauna Lani, HI, USA, 27–30 August 2017; pp. 1104–1109. [CrossRef]
13. Bram, M.V.; Hansen, L.; Hansen, D.S.; Yang, Z. Grey-Box Modeling of an Offshore Deoiling Hydrocyclone System. In Proceedings of the 2017 IEEE Conference on Control Technology and Applications (CCTA), Mauna Lani, HI, USA, 27–30 August 2017; pp. 94–98. [CrossRef]
14. Yang, M. Measurement of Oil in Produced Water. In *Produced Water*, 1st ed.; Lee, K., Neff, J., Eds.; Springer: New York, NY, USA, 2011; Chapter 2, pp. 57–88. [CrossRef]
15. Department for Business Energy & Industrial Strategy. *Methodology for the Sampling and Analysis of Produced Water and Other Hydrocarbon Discharges*; Technical Report; United Kingdom Government Digital Service: London, UK, 2018.
16. Miløstyrelsen. *Generel Tilladelse for Maersk Olie og Gas A/S (Maersk Olie) til Anvendelse, Udledning og Anden Bortskaffelse af Stoffer og Materialer, Herunder Olie og Kemikalier i Produktions- og Injektionsvand fra Produktionsenhederne Halfdan, Dan, Tyra og Gorm for Per*; Technical Report; Mærsk Olie og Gas A/S: Copenhagen, Denmark, 2016.
17. Danish Energy Agency. Yearly Production, Injection, Flare, Fuel and Export in SI Units 1972–2019. Available online: https://ens.dk/ (accessed on 7 August 2020).
18. Gao, C. Factors affecting particle retention in porous media. *Emir. J. Eng. Res.* **2007**, *12*, 7.
19. Danish Energy Agency. *Production*; Technical Report; Danish Energy Agency: Esbjerg, Denmark, 2016.

20. Durdevic, P.; Raju, C.; Bram, M.; Hansen, D.; Yang, Z. Dynamic Oil-in-Water Concentration Acquisition on a Pilot-Scaled Offshore Water-Oil Separation Facility. *Sensors* **2017**, *17*, 124. [CrossRef]
21. Henriksen, A. Online Oil-in-Water Monitoring Experience. Available online: http://www.advancedsensors.co.uk/ (accessed on 7 June 2019).
22. Zhang, J. *RPSEA Subsea Produced Water Discharge Sensor Lab Test Results and Recommendations Final Report*; Technical Report 3; Clearlew Subsea LLC: Houston, TX, USA, 2016.
23. Jepsen, K.L.; Bram, M.V.; Hansen, L.; Yang, Z.; Lauridsen, S.M.Ø. Online Backwash Optimization of Membrane Filtration for Produced Water Treatment. *Membranes* **2019**, *9*, 68. [CrossRef]
24. Bram, M.V.; Hansen, L.; Hansen, D.S.; Yang, Z. Extended Grey-Box Modeling of Real-Time Hydrocyclone Separation Efficiency. In Proceedings of the 2019 18th European Control Conference (ECC), Naples, Italy, 25–28 June 2019; pp. 3625–3631. [CrossRef]
25. Dansk Standard. *Vejledning i Brug af Estimater for Repeterbarhed, Reproducerbarhed og Korrekthed ved Estimering af Måleusikkerhe*d; Technical Report; DS/ISO: Copehagen, Denmark, 2017.
26. Howell, M. *A Closer Look at Accuracy of Measuring and Test Equipment*; Currents; EASA: St. Louis, MO, USA, 2014; pp. 3–5.
27. JCGM. *Evaluation of Measurement Data—Guide to the Expression of Uncertainty in Measurement*; Technical Report; BIPM: Saint-Cloud, France, 2008.
28. Magnusson, B.; Näykki, T.; Hovind, H.; Krysell, M. *Handbook for Calculation of Measurement Uncertainty in Environmental Laboratories*; Technical Report; Nordtest: Espoo, Finland, 2004.
29. Dansk Standard. *Olieproducter. Automatisk Prøveudtagning fra Rørledninger*; Technical Report; DS/ISO: Charlottenlund, Denmark, 1999.
30. Dansk Standard. *Water Quality—Determination of Hydrocarbon Oil Index—Part 2: Method Using Solvent Extraction and Gas Chromatography*; Technical Report; DS/ISO: Copenhagen, Denmark, 2001.
31. Ramsey, M.H.; Thompson, M. Uncertainty from sampling, in the context of fitness for purpose. *Accredit. Qual. Assur.* **2007**, *12*, 503–513. [CrossRef]
32. Eurachem/EUROLAB/CITAC/Nordtest/AMC Guide. *Measurement Uncertainty Arising from Sampling: A Guide to Methods and Approaches*; Technical Report; Eurachem: Torino, Italy, 2019.
33. Lava, R.; Zanon, F.; Menegus, L. *Issues with Monitoring and Analysis of Hydrocarbons in Italy*; NEL Produced Water Workshop; In Proceedings of the Produced Water Workshop 2017, Aberdeen, UK, 13–14 June 2017; p. 41.
34. Hassan, A.A.; Bram, M.V.; Hansen, D.S. Monitoring and Control of a Deoiling Hydrocyclone Utilizing Oil-in-Water Measurement. Master's Thesis, Aalborg University, Esbjerg, Denmark, 2016.
35. Midland. *Midland Non Detergent 30*; Technical Report; Midland: Hunzenschwil, Switzerland, 2011.
36. Durdevic, P.; Pedersen, S.; Yang, Z. Evaluation of OiW measurement technologies for deoiling hydrocyclone efficiency estimation and control. In Proceedings of the OCEANS 2016, Shanghai, China, 10–13 April 2016; pp. 1–7. [CrossRef]
37. Turner Designs Hydrocarbon Instruments. *E09 TD-4100XDC Oil in Water Monitor User Manual*; Technical Report; Turner Designs: Fresno, CA, USA, 2014.
38. Coca-Prados, J.; Gutiérrez-Cervelló, G.; Benito, J.M. Treatment of Oily Wastewater. In *Water Purification and Management*, 1st ed.; Coca-Prados, J., Gutiérrez-Cervelló, G., Eds.; NATO Science for Peace and Security Series C: Environmental Security; Springer: Dordrecht, The Netherlands, 2011; Chapter 1, pp. 1–55. [CrossRef]
39. Schubert, M.F.; Skilbeck, F.; Walker, H.J. Liquid Hydrocyclone Separation Systems. In *Hydrocyclones*, 1st ed.; Svarovsky, L., Thew, M.T., Eds.; Fluid Mechanics and its Applications; Springer: Dordrecht, The Netherlands, 1992; Volume 12, pp. 275–293. [CrossRef]
40. Gonick, L.; Smith, W. *The Cartoon Guide to Statistics*, 4th ed.; HarperCollins Publishers Inc.: New York, NY, USA, 2005; p. 230.
41. Noblitt, S.D.; Berg, K.E.; Cate, D.M.; Henry, C.S. Characterizing nonconstant instrumental variance in emerging miniaturized analytical techniques. *Anal. Chim. Acta* **2016**, *915*, 64–73. [CrossRef]
42. Martin, J.; de Adana, D.D.R.; Asuero, A.G. Fitting Models to Data: Residual Analysis, a Primer. In *Uncertainty Quantification and Model Calibration*; Hessling, J.P., Ed.; InTech: London, UK, 2017; Chapter 7, pp. 133–173. [CrossRef]
43. Hansen, L.; Durdevic, P.; Jepsen, K.L.; Yang, Z. Plant-wide Optimal Control of an Offshore De-oiling Process Using MPC Technique. *IFAC-PapersOnLine* **2018**, *51*, 144–150. [CrossRef]

44. Jepsen, K.L.; Pedersen, S.; Yang, Z. Control pairings of a deoiling membrane crossflow filtration process based on theoretical and experimental results. *J. Process Control* **2019**, *81*, 98–111. [CrossRef]
45. Pedersen, S.; Durdevic Løhndorf, P.; Yang, Z. Influence of riser-induced slugs on the downstream separation processes. *J. Pet. Sci. Eng.* **2017**, *154*, 337–343. [CrossRef]
46. Durdevic, P.; Yang, Z. Application of H_∞ Robust Control on a Scaled Offshore Oil and Gas De-Oiling Facility. *Energies* **2018**, *11*, 287. [CrossRef]
47. Nielsen, E.K.; Bram, M.V.; Frutiger, J.; Sin, G.; Lind, M. A water treatment case study for quantifying model performance with multilevel flow modeling. *Nucl. Eng. Technol.* **2018**, *50*, 532–541. [CrossRef]
48. Scardina, P.; Letterman, R.D.; Edwards, M. Particle count and on-line turbidity interference from bubble formation. *J. Am. Water Work. Assoc.* **2006**, *98*, 97–109. [CrossRef]
49. Edinburgh Instruments. Scattering. Available online: https://www.edinst.com/blog/raman-scattering-blog/ (accessed on 27 July 2020).
50. Fridman, A.E. Assurance of Measurement Accuracy in Compliance with ISO 5725 Standards. In *The Quality of Measurements: A Metrological Reference*, 1st ed.; Springer: New York, NY, USA, 2012; Chapter 8, pp. 179–195. [CrossRef]
51. EURACHEM/CITAC. *Quantifying Uncertainty in Analytical Measurement*; Technical Report; EURACHEM: Torino, Italy, 2012.
52. Wang, L.Y.; Wu, Y.X.; Zheng, Z.C.; Guo, J.; Zhang, J.; Tang, C. Oil-Water two-Phase Flow Inside T-Junction. *J. Hydrodyn.* **2008**, *20*, 147–153. [CrossRef]
53. Sam, B.; Pao, W.; Nasif, M.S.; Norpiah, R.B. Simulation of two phase oil-gas flow in T-junction. *ARPN J. Eng. Appl. Sci.* **2016**, *11*, 12011–12016.
54. Young, G.; Wakley, W.; Taggart, D.; Andrews, S.; Worrell, J. Oil-water separation using hydrocyclones: An experimental search for optimum dimensions. *J. Pet. Sci. Eng.* **1994**, *11*, 37–50. [CrossRef]
55. Wang, T.; Zeng, L.H.; Li, D.L. A review on the methods for correcting the fluorescence inner-filter effect of fluorescence spectrum. *Appl. Spectrosc. Rev.* **2017**, *52*, 883–908. [CrossRef]
56. Edinburgh Instruments. What Is the Inner Filter Effect? Available online: https://www.edinst.com/blog/inner-filter-effect/ (accessed on 26 August 2019).
57. Ware, W.R. Oxygen Quenching of Fluorescence in Solution: An Experimental Study of the Diffusion Process. *J. Phys. Chem.* **1962**, *66*, 455–458. [CrossRef]
58. Momin, S.A.; Narayanaswamy, R. Quenching of fluorescence of polynuclear aromatic hydrocarbons by chlorine. *Analyst* **1992**, *117*, 83. [CrossRef]
59. Lakowicz, J.R. (Ed.) Quenching of Fluorescence. In *Principles of Fluorescence Spectroscopy*, 3rd ed.; Springer: Boston, MA, USA, 2006; Chapter 8, pp. 277–330. [CrossRef]
60. Wilson, D.F. Oxygen Dependent Quenching of Phosphorescence: A Perspective. In *Oxygen Transport to Tissue XIV*, 1st ed.; Erdmann, W., Bruley, D.E., Eds.; Advances in Experimental Medicine and Biology; Springer: New York, NY, USA, 1992; Volume 317, pp. 195–201. [CrossRef]
61. Elmenreich, W. An introduction to sensor fusion. *Vienna Univ. Technol. Austria* **2002**, *502*, 28.
62. Shi, L.; Johansson, K.H.; Murray, R.M. Kalman Filtering with Uncertain Process and Measurement Noise Covariances with Application to State Estimation in Sensor Networks. In Proceedings of the 2007 IEEE International Conference on Control Applications, Singapore, 1–3 October 2007; pp. 1031–1036. [CrossRef]
63. Ma, H.; Yan, L.; Xia, Y.; Fu, M. *Kalman Filtering and Information Fusion*, 1st ed.; Springer: Singapore, 2020; p. 291. [CrossRef]

Paper D

Offshore Online Measurements of Total Suspended Solids using Microscopy Analyzers

Dennis S. Hansen, Stefan Jespersen, Mads V. Bram, and Zhenyu Yang

The paper has been submitted to
IEEE Sensors Journal, IEEE, 2020.

Offshore Online Measurements of Total Suspended Solids using Microscopy Analyzers

Dennis Severin Hansen, Stefan Jespersen, Mads Valentin Bram, and Zhenyu Yang*

***Abstract*— Accurate online water quality measurements have gained attention during the last decades in the oil and gas industry for improving operational performance and protecting the surrounding environment. One potential solution to extend the reservoirs' economic life and put less strain on the environment is by re-injecting the produced water, but the quality of the injected water must be high and consistent to prevent injectivity reduction. This paper evaluates two different online microscopy analyzers that utilize a high-resolution video camera for capturing images of the particles passing their view cell. The calibration procedure for both online microscopy analyzers has been thoroughly validated for steady-state and real-time measurements. The real-time measurements were achieved by post-processing the data captured by the microscopes and applying a trailing moving average window. The performance of measuring the oil-in-water concentration was compared with an online fluorescence-based monitor. The paper addresses the statistical considerations when defining the level of accuracy of the predicted particle size distribution within a defined confidence interval. Both microscopes showed promising results for measuring known particle sizes and oil-in-water concentration, both in steady-state and real-time.**

***Index Terms*— oil and gas industry, produced water, microscopy analyzer, oil-in-water concentration, real-time measurements, calibration procedure**

I. Introduction

EVEN as a general global goal is to consume energy from renewable energy sources, oil and gas are needed in the transition [1]. Oil production is expected to increase during the next three decades globally, which entails the oil and gas industry to significantly impact the world's energy consumption in the coming decades [2]. The general trend towards more sustainable energy production also affects the offshore oil and gas industry as discharge legislation become stricter [3], [4]. With stricter policies produced water re-injection (PWRI) has gained growing attention to extend the reservoirs' economic life and decrease produced water (PW) discharge to minimize environmental impacts [5]. However, the re-injected PW and the injected seawater must contain a continually high quality to prevent formation damage and unpredicted injectivity reduction [6]–[10]. Currently, only $\sim 14.5\%$ of the PW in the Danish sector of the North Sea is re-injected, which is a reduction over 50% since 2009 due to reservoir challenges according to the Danish Environmental Protection Agency [3], [11]. To increase the percentage of PWRI, efficient management of PW and seawater involves proper treatment to maintain continually high quality and accurate monitoring. The water quality in offshore injection water treatment (IWT) processes is usually assessed in terms of particles' plugging tendency, also addressed as suspended solids or total suspended solids (TSS) [8], [12]. In this paper, TSS is defined as any particles that can be retained by a filter, including oil droplets. However, the quality of the injection water (IW) should be economically viable to achieve and counterbalanced against well-stimulation [12]. Currently, offshore IWT processes rely on off-line measurements of TSS concentration following the ISO 872; thus in case of a decrease in IW quality, the reaction time is long, due to the use of onshore laboratory measurements [13].

Even if at-line execution significantly reduces the reaction time of the off-line TSS concentration measurements, it is difficult for operators to investigate where and what is the root cause of the decreased quality, when there is no available information related to TSS. Especially as significant water quality decline often occur downstream [8]. Online TSS and oil-in-water (OiW) concentration measurements have not become standardized in the oil and gas industry, despite the long history of measuring particle sizes online [13]. Although PWRI is a solution for extending the economic life of oil production, it is beneficial to measure particle sizes to increase the performance of IWT processes. Several different methods for measuring particle sizes exist, each based on several design options from different manufacturers. Besides microscopy, which is based on direct observation, all other techniques are challenged by their property assumptions that only the equivalent diameter of a sphere is measured, and the existing morphologies is not taken into the equation, which complicates the ability to classify particles. Another advantage of microscopy is the manual discrimination of particles captured to evaluate the results. This paper aims to examine two different online microscopy analyzers: Jorin ViPA and Canty InFlow. Both microscopes are based on the

Manuscript submitted December 12, 2020. This work was supported by the DHRTC projects "Injection Water Quality and Control" (Proj-No.: 878040) and "Laboratory Testing at AAU-Esbjerg and Development" (Proj-No.: 878039).

D. S. Hansen, S. Jespersen, M. V. Bram, and Z. Yang* are with the Aalborg University, Department of Energy Technology, 6700 Esbjerg, Denmark (e-mail: dsh@et.aau.dk; sje@et.aau.dk; mvb@et.aau.dk; yang@et.aau.dk). *Corresponding author.

same technique of utilizing a high-resolution video camera to capture images of the particles' projected area passing the view cell. Both monitors are based on bright field illumination techniques, presenting a dark image of particles passing the depth of field with a bright background. The resolution of Jorin ViPA is fixed by the manufacturer, and the Canty InFlow is adjusted to a specific resolution. A fluorescence-based monitor (Turner TD-4100XDC) is used as a benchmark to evaluate the two online microscopes' performance to measure OiW concentrations. The fluorescence-based monitor is selected based on a previous work by Hansen *et al.* [6]. This paper addresses the problems that petroleum engineers must subjectively decide what particles are considered in focus. Furthermore, the calibration procedure will be validated on known solid particle sizes and their ability to measure different OiW concentrations accurately and in real-time.

II. Materials and Methods

Two setups have been constructed to execute the experiments presented in this paper. The two systems are shown in Fig. 1 and 2. The setup shown in Fig. 1 is used to calibrate both online microscopes using different known polystyrene particle sizes produced by BS-Partikel [14].

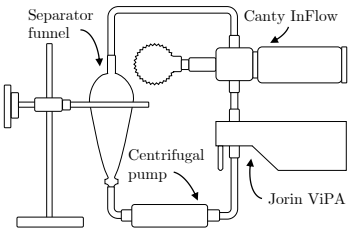

Fig. 1. A recirculating test setup for measuring known particle sizes to calibrate both online microscopes.

The three different polystyrene particle sizes follow a statistically Gaussian distribution, and the measured means and standard deviations presented in parentheses, are given by the manufacturer:

- Nominal diameter of 10µm: $x_3 = 9.8(0.3)\mu m$
- Nominal diameter of 20µm: $x_1 = 20.1(0.4)\mu m$
- Nominal diameter of 40µm: $x_2 = 40.3(0.9)\mu m$

Fig. 2 illustrates a skid mounted testing platform for validating the two online microscopes' performance. The platform is equipped with a centrifugal pump (CP), pressure transmitters (P_x), flowmeters (Q_x), and pneumatic control valves (V_x). The system is configurable to direct the liquid through the sidestream and the mainstream by manipulating the control valves.

By taking advantage of on-line sampling, both microscopes: Jorin ViPA (C_2) and Canty InFlow (C_3) are installed on a sidestream, making them applicable in most installations regardless of the flow velocity and the pipeline's dimensions. Although on-line measurement complicates the sampling procedure, as a maldistribution between the run and the branch

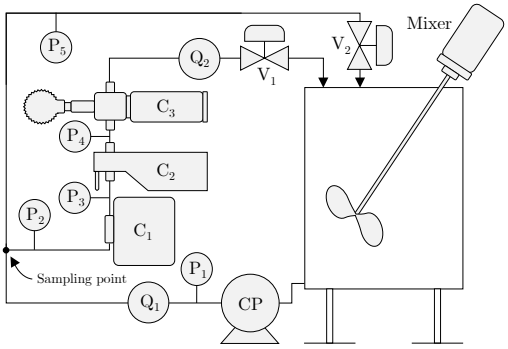

Fig. 2. Skid mounted testing platform for validating quality monitors' performance on a sidestream installation during different flow regimes.

can occur. Execution specifications of both microscopes are listed in Table I.

TABLE I
Execution specifications of both microscopes.

	Jorin ViPA	Canty InFlow
Pixel length	0.375µm/pixel	0.513µm/pixel
Resolution	1292×964 pixels	1920×1200 pixels
Frame rate	∼30fps	∼30fps

A fluorescence-based monitor (C_1), that are sensitive to the aromatic content, is installed to measure the OiW concentration. C_1 is installed as benchmark to facilitate the investigation of measuring OiW concentrations by C_2 and C_3. The accuracy of C_1 has been extensively studied by Hansen *et al.* [6], and will not be evaluated in this paper.

The difficulty of online microscopy analysis is related to the narrow focus area, where only a fraction of the entire flow is directed into the sidestream and through the view cell. Further complication occurs as only a narrow depth of field of the passing flow are captured by the microscope; thus not all TSS that passes the view cell will be observed, and are therefore excluded from being measured as shown in Fig. 3.

To achieve statistical results, it is necessary to sample a sufficient amount of particles which is constricted by the small depth of field. The quantity of captured particles strongly relate to the accuracy of the predicted particle size distribution (PSD). The accuracy of the PSD can be determined within a region of relative error, δ, from a defined confidence level with its represented z-score value, u. The number of sufficient particles, n^*, that are required is based on δ and sample standard deviation, s, has been proposed by Masuda and Iinoya [15]. The approach is based upon the assumption that the PSD is follows a log-normal distribution.

$$\log(n_*) = -2\log(\delta) + \log(\omega), \tag{1}$$

where

$$\omega = u^2\alpha^2 s^2(2c^2 s^2 + 1). \tag{2}$$

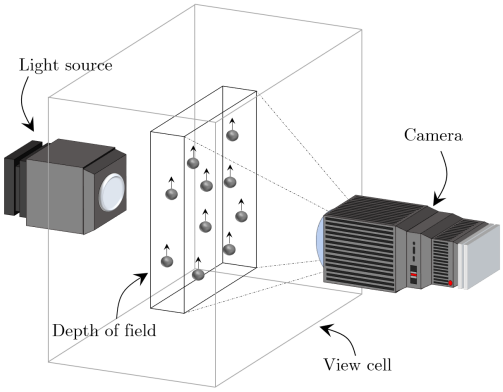

Fig. 3. The depth of field of the measured volume within the view cell.

α is the non-zero exponential constant that defines the particle distribution, for log-normal distribution $\alpha = 2$ [16]. c can be calculated as

$$c = \beta + \frac{\alpha}{2} \tag{3}$$

where β is a basis number, for the count basis $\beta = 0$. The number of particles required within a certain range of error changes depending on how the data is scattered. Thus, the number of particles increases as the deviation of the data increases. Simultaneously, the number of particles increases proportionately to the error of magnitude required. On the contrary, the relative error can be estimated based on the number of particles observed.

Experimental Design

This subsection describes the design and objective of all executed experiments on both setups from Fig. 1 and 2. The two microscopes were calibrated according to a known particle size from BS-Partikel, followed by a performance validation on known sizes, larger and smaller than the known particle size used for calibration. The two microscopes were installed in series together with the fluorescence-based monitor to observe their performance of measuring OiW concentrations.

Experiments executed on the setup presented in Fig. 1:

Experiment I: calibration of both microscopes, by addition of known particle sizes with a mean and standard deviation: $x_1 = 20.1(0.4)\mu\text{m}$.

Experiment II: validation test of the calibration procedure executed in Experiment I, by addition of a known particle size larger and smaller than x_1: $x_2 = 40.3(0.9)\mu\text{m}$ and $x_3 = 9.8(0.3)\mu\text{m}$.

The pump speed was fixed at the same value in both Experiment I and II. Most of the presented data in Experiment I are based on data from C_2, although the exact same procedure was executed on C_3. Both microscopes have three calibration parameters:

- Threshold value (THV): an 8-bit integer, resulting in a greyscale image with pixel values in the range of $0-255$, from black to white for both microscopes.
- Edge strength/focus rejection value (ESV/FRV): an edge detection method running a convolution kernel for estimating the gradient at each pixel on the image. The most common method is Sobel, which have been used on C_3. Other methods are also available when using C_3. C_2's edge detection method is classified. The ESVs of C_2 are in a range of $0-10$, where ESV $= 10$ only includes particles with a large gradient. C_3's FRV ranges from $0-1000$, although FRV > 45 did not include any particles in the calibration analysis.
- Depth of field: only necessary to adjust if the user is interested in the sample's concentration. Depth of field normally defines the distance between the closest and farthest particle in the image that appears acceptably sharp. The virtual depth of field used for these microscopes determines the depth of the captured images to equal the known concentration.

Only the first two calibration parameters were analyzed in Experiment I and validated in Experiment II by addition of the particle sizes: x_2 and x_3. The depth of field value was tuned in Experiment III.

Experiment executed on the setup presented in Fig. 2:

Experiment III: a performance evaluation of the microscopes, to measure OiW concentrations in steady-state and real-time measurements, benchmarked according to the predicted OiW concentration and the measurements obtained from C_1. Six nominal OiW concentrations were investigated $(55, 100, 150, 200, 250, 400)\text{ppm}$.

CP was kept at 100% pump speed to ensure that the droplet size distribution does not change over time due to the high shear occurring in CP. V_2 was kept at a fixed opening degree, and the flow rate through the sidestream was kept constant by manipulating V_1.

III. Results

The results are divided into three sections based on Experiment I, II, and III.

Experiment I:

A 2h recirculation experiment with particle size x_1 dispersed in $1\mu\text{m}$-filtered tap water, was executed with both microscopes and used as calibration data.

Firstly, the THVs were adjusted so that the known particle size x_1 can statistically be represented by the microscopes. A high ESV was selected only to determine the THVs on captured particles in focus. Determining the THV before the ESV is essential as the edge detection method depends on the THV. Furthermore, for comparison of both microscopes' performance, particle sizes were based on equivalent area diameter during post-processing of the data. Note that choosing another method of determining the particle diameter will most likely shift the distribution of measured sizes. The measurement in Fig. 4 presents mean results of the first 100

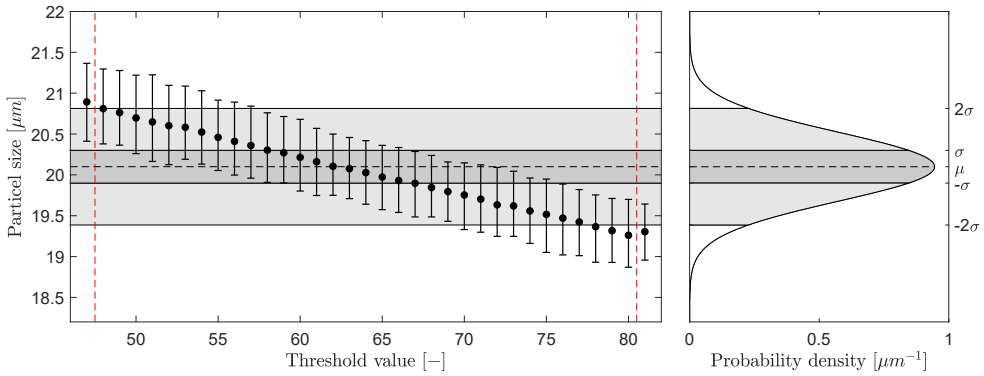

Fig. 4. Selected particles, all with maximum ESV on C_2. The error bars represent the mean, minimum, and maximum particle sizes at different THVs. The Gaussian distribution is calculated based on information from BS-Partikel: $\mu = 20.1\mu$m and $\sigma = 0.4\mu$m.

images with particles captured at maximum ESV. The THV was then toggled in a range of $47 - 81$, where at THV$\leq$47 and THV$\geq$81, particles no longer fulfill the ESV's criteria and are no longer counted. The Gaussian distribution in Fig. 4 represent the information analyzed by BS-Partikel: $\mu = 20.1\mu$m and $\sigma = 0.4\mu$m.

Based on the results in Fig. 4, a THV $= 62$ for C_2 was selected. For C_3, a THV $= 182$ was selected. The analysis results with a THV $= 62$ and maximum ESV $= 10$ are shown in Fig. 5. A probability density function (PDF) is included on the graphs in Fig. 5, to visualize the performance of estimating the particle sizes.

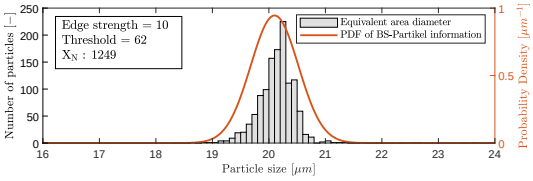

Fig. 5. Included particles with a THV $= 62$ and ESV $= 10$, measured by C_2.

Selecting the ESV is more subjective as it is a perception of what appears to be acceptably sharp. Fig. 6 presents eleven different particles captured by C_2 with a THV $= 62$, each with different acceptable ESV between $0 - 10$. Associated information of each particle, presented in Fig. 6, is shown in Table II.

Furthermore, Fig. 7 and Table III show an artifact of selecting a weak ESV. Even though an ESV of one outputs a measured size within 1σ from the μ of x_1, selecting an ESV $= 2$, the gradient of the particle is no longer accepted and is considered out-of-focus. Although a smaller, but stronger gradient within the particle, fulfills the requirement and is included as a particle.

Selecting a too high ESV will reduce the counted number of accepted particles in the analysis, or even worse not represent

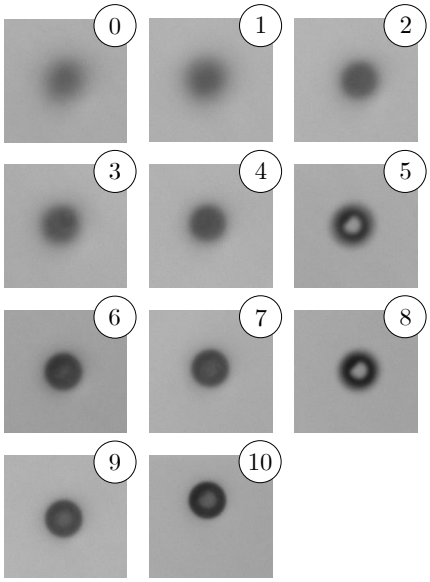

Fig. 6. Eleven different particles in captured by C_2 with a THV $= 62$, each with different acceptable ESV between $0 - 10$. Associated results based on ESV are shown in Table II.

other types of particles in the process that has a weaker gradient by nature. A further validation of selecting a proper ESV or FRV was executed by analyzing the corresponding results of the first three particles in Table II that are within 2σ from μ of x_1 (ESVs: 5, 6, and 7). The results are shown in Fig. 8. The same evaluation procedure was executed on C_3.

Increasing the ESV from 5 to 7 counted 24% fewer particles in Experiment I. Another phenomenon occurs at a ESV $= 5$, as the size histogram is skewed left due to the acceptable edge is found closer to the center of the particles as the peripheries are less in focus. Selecting between an

TABLE II
ASSOCIATED RESULTS TO FIG. 6, BASED ON DIFFERENT ESV.

Edge strength	Size	Aspect ratio	Shape factor
0	6.53	0.69	0.36
1	16.86	0.92	0.86
2	15.59	0.92	0.87
3	17.18	0.87	0.89
4	17.27	0.96	0.97
5	19.82	0.99	0.94
6	19.56	0.97	0.96
7	19.43	0.99	0.97
8	20.50	0.96	0.93
9	19.56	0.97	0.96
10	19.97	0.97	0.98

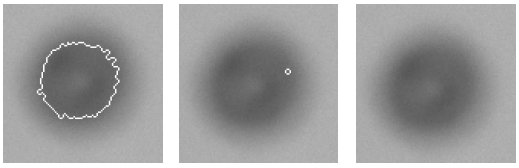

(a) (b) (c)

Fig. 7. Three images of the same particle with a THV = 62, but with different ESVs: (a) ESV $\leq$1; (b) ESV =2; (c) ESV $\geq$3. Associated results are shown in Table III.

TABLE III
ASSOCIATED RESULTS TO FIG. 7.

Edge strength	Size	Aspect ratio	Shape factor
$\leq$1	19.70	0.94	0.80
2	1.81	0.71	0.96
$\geq$3	–	–	–

ESV = 6 or ESV = 7 is a tradeoff between obtaining less countable particles and reducing the phenomena of underestimating the size of particles that are less in focus. An ESV = 6 was chosen for C_2, and a FRV = 25 was chosen for C_3. The calibration results of C_3 are shown in Fig. 9. The number of particles captured by C_3 was $\sim$5 times larger than the amount captured by C_2. This is primarily a result of higher image resolution and larger pixel size than C_2 as shown in Table I.

Experiment II:
A 2h validation test was executed by adding two additional particle sizes: x_2 and x_3, along with x_1. The raw data from C_2 and C_3, without any classification, are shown in Fig. 10.

For each known particle size, 1ml aqueous surfactant solution containing the polystyrene particles was added. Both microscopes observed a high number of x_3 in the validation test, a result of containing more particles per volume than the others. By truncating the sample for each known particle size with a fixed range of $\pm$4µm from the known μ of x_1, x_2, and x_3, the statistical information can be obtained as shown in Table IV.

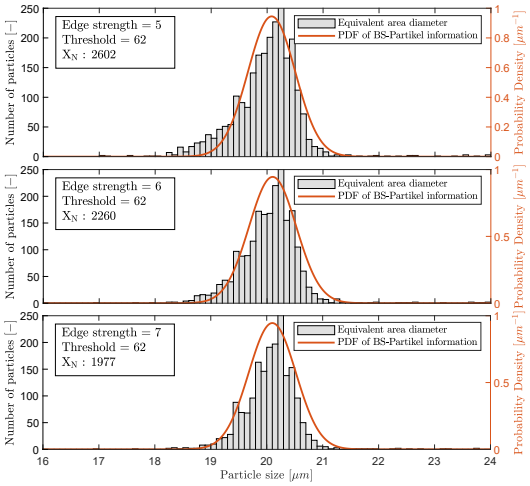

Fig. 8. Included particles with a THV = 62 and three different ESVs: 5, 6, and 7, respectively, measured by C_2.

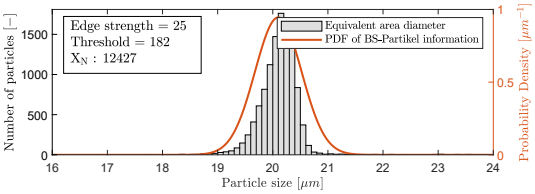

Fig. 9. Included particles with a THV = 182 and a FRV = 25, measured by C_3.

TABLE IV
ASSOCIATED RESULTS TO FIG. 10.

	Known $\mu(\sigma)$ [µm]	$\mu_{estimat.}$ [µm]	$\sigma_{estimat.}$ [µm]
C_3	9.8(0.3)	9.5	0.6
	20.1(0.4)	20.0	0.6
	40.3(0.9)	40.9	0.5
C_2	9.8(0.3)	9.6	0.6
	20.1(0.4)	20.3	1.0
	40.3(0.9)	41.4	0.6

Experiment III:
A 6h experiment was carried out with the addition of oil after at least 30min between each OiW concentration of observation. Fig. 11 shows the time series of measured OiW concentration from C_1. The vertical line marks a truncated time series of $\sim$3.5h that was left out. The depth of field value in C_2 and C_3 was at that period adjusted to match a OiW concentration of 55ppm during the first 30min after the injection of oil into the process and to classify oil droplets.

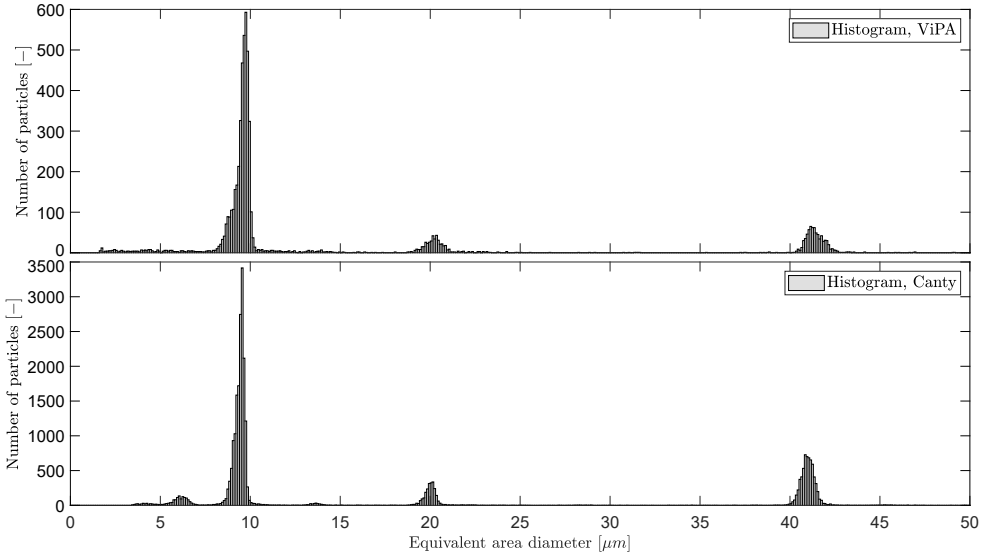

Fig. 10. Three known particle sizes were measured simultaneously by C_2 and C_3. The mean and sample standard deviation are listed in Table IV.

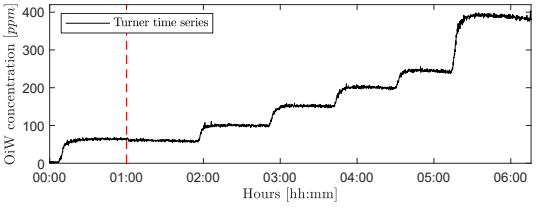

Fig. 11. Time series of measured OiW concentration measured by C_1 executed on the setup shown in Fig. 2. The vertical line marks the truncated time series of ∼3.5h.

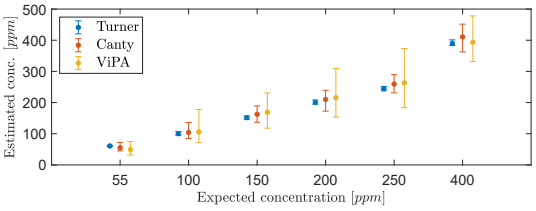

Fig. 12. Error bars representing the mean, minimum, and maximum OiW concentrations based on the average concentration obtained each minute from C_2 and C_3, together with error bars based on measurement every 10s from C_1.

During the last expected OiW concentration of 400ppm, the mixed concentration can no longer be maintained in the setup according to the measurement of C_1. Fig. 12 presents an error bar of each OiW concentration measured in a duration of 30min for each online monitor. Each error bar represent the mean, minimum, and maximum OiW concentration measured, where C_1 was selected to have a sample frequency of 0.1Hz, and C_2 and C_3 outputting an averaged concentration measurement every minute.

Fig. 13 and 14 present the PSD histogram of the measured OiW concentrations at 55ppm and 400ppm for each microscope. Furthermore, the Fig. 13 and 14 presents the mean of the log-normal distribution, μ_0, the standard deviation of the log-normal distribution, σ_0, and the number of counted particles, X_N.

Both OiW concentrations follow a log-normal size distribution measured by both microscopes with only small changes in the distribution with respect to the concentration. Following the proposed calculation by Masuda and Iinoya [15]

TABLE V
ASSOCIATED RESULTS TO FIG. 12.

Expected conc.		55ppm	100ppm	150ppm	200ppm	250ppm	400ppm
C_1	minimum:	56.2	94.7	146.1	193.9	237.6	379.0
	μ:	60.9	100.1	151.8	200.7	244.6	390.0
	maximum:	67.7	105.4	159.5	207.7	255.8	398.4
C_2	minimum:	31.6	71.4	118.0	153.5	183.7	331.9
	μ:	49.2	106.1	168.9	215.7	263.1	393.6
	maximum:	75.1	177.8	230.7	309.3	373.4	478.0
C_3	minimum:	44.9	84.6	136.9	172.4	231.2	362.6
	μ:	55.1	104.0	162.4	210.0	259.3	410.6
	maximum:	72.3	136.1	189.2	239.6	289.4	451.7

in (1)−(3), for obtaining a sufficient statistical representation within 95% confidence level, δ of the PSD can be calculated as shown in Table VI.

A trailing moving average window of 1min was selected, for measuring the OiW concentration real-time by C_2 and C_3. Fig. 15 and 16 show the results of real-time measurements at

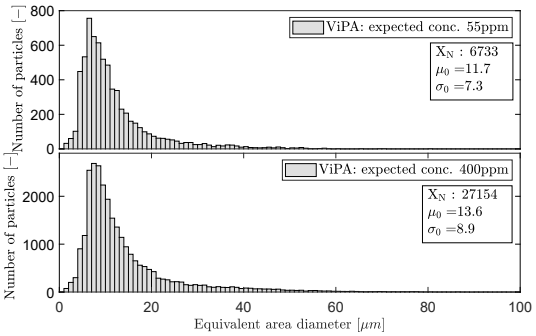

Fig. 13. Droplet size distribution obtained with C_2 based on the measured OiW concentrations at the expected concentration of 55ppm and 400ppm, respectively.

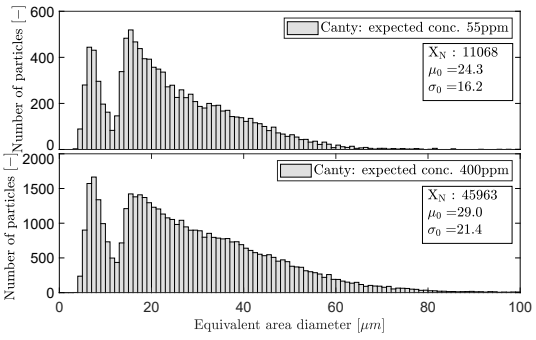

Fig. 14. Droplet size distribution obtained with C_3 based on the measured OiW concentrations at the expected concentration of 55ppm and 400ppm, respectively.

TABLE VI
ASSOCIATED RESULTS TO FIG. 13 AND 14, CALCULATING THE δ, RELATED TO EACH PSD OF EACH OIW CONCENTRATION MEASURED WITH C_2 AND C_3.

Expected OiW conc.		55ppm	400ppm
C_2	μ_0:	11.7	13.6
	σ_0:	7.3	8.9
	X_N:	6733	27154
	δ	3.5%	1.9%
C_3	μ_0:	24.3	29.0
	σ_0:	16.2	21.4
	X_N:	11068	45963
	δ:	3.0%	1.6%

the expected OiW concentration of 55ppm from C_2 and C_3, respectively, together with real-time measurements from C_1. The calculated OiW concentration, based on post-processed equivalent volume measurements and the depth of field volume, are presented for each captured image.

The results presented in Fig. 15 and 16 have also been executed at the expected OiW concentration of 400ppm and

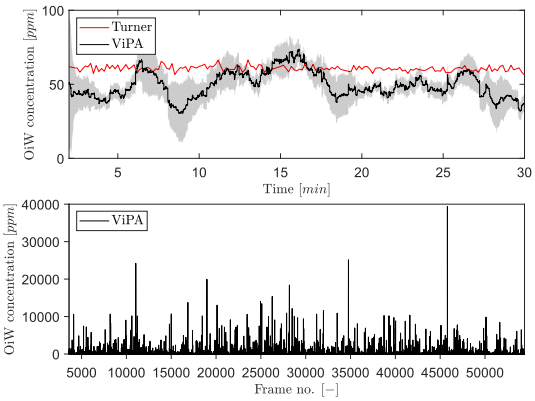

Fig. 15. Real-time OiW concentration measurements calculated using a trailing moving average window of 1min of the post-processed oil volume ratio in each image captured by C_2. Top graph shows the real-time measurement measured by C_1 and C_2. A 95% confidence interval of the averaging window is shadowed behind the signal. Bottom graph shows the volume concentration of each frame captured.

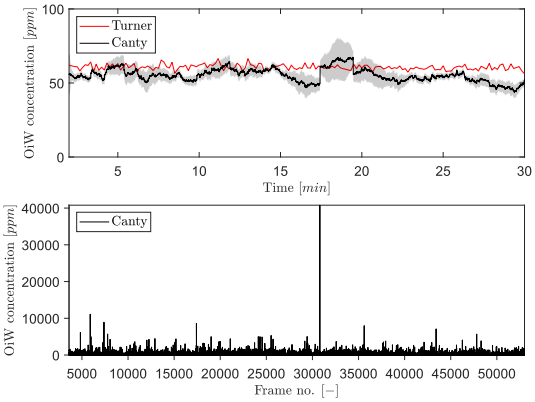

Fig. 16. Real-time OiW concentration measurements calculated using a trailing moving average window of 1min of the post-processed oil volume ratio in each image captured by C_3. Top graph shows the real-time measurement measured by C_1 and C_3. A 95% confidence interval of the averaging window is shadowed behind the signal. Bottom graph shows the volume concentration of each frame captured.

presented in Fig. 17 and 18.

IV. DISCUSSION

The process of calibrating the two online microscopes is highly based on the perception of what is considered in focus. To ensure consistent results when calibrating the three main calibration parameters: THV, ESV/FRV, and depth of field, the calibrating procedure must be well documented to reduce the difference between each calibration execution. Fig. 4 and 8 presented one solution for selecting the THV and ESV/FRV that outputs an estimation that matches the

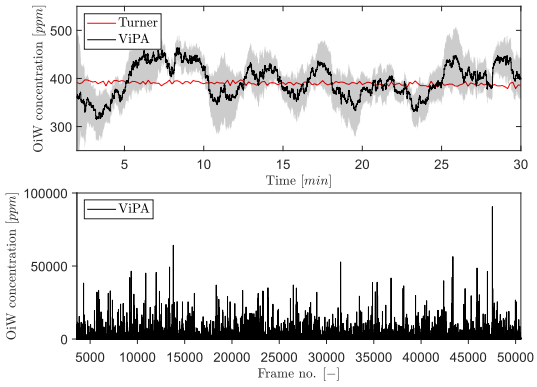

Fig. 17. Same procedure as in Fig. 15 for real-time OiW concentration measurement based on captured images from C_2 at another measurement range of ∼400ppm

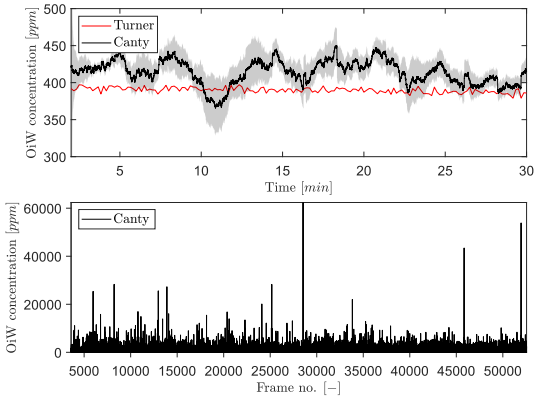

Fig. 18. Same procedure as in Fig. 16 for real-time OiW concentration measurement based on captured images from C_3 at another measurement range of ∼400ppm.

Gaussian distribution of the known particle sizes based on the information from the manufacturer of the produced particles. The skewness observed in Fig. 8 when calibrating the ESV could be a result of selecting a slightly too low THV; thus a lower ESV may have yielded better results. Although, based on the results shown in Fig. 10 the calibration procedure presented in Experiment I revealed only a small deviation from the known PSDs. For further improvement of online microscopy analyzers, auto-calibration or human-computer interaction (HCI) of the calibration procedure can lower the subjective perception of what is acceptably sharp.

The steady-state values of measuring OiW concentration in Fig. 12 showed promising results in relation to the expected OiW concentrations. The measurement of C_1 confirmed that C_2 and C_3 are able to measure the mean OiW concentrations.

Moreover, C_1 also confirmed what the setup was able to keep a well mixed OiW concentration, apart from high OiW concentrations where a declining tendency of measured concentration was observed. The observed declining tendency may occur due to accumulation within the setup (dead volumes), natural separation in the supply tank, or pipelines and equipment becoming oil-wet.

Regardless of these sources of error, both microscopes were able to measure the mean OiW concentration of 30min in close relation to the expected concentration. A high deviation was observed when outputting OiW concentration every minute in steady-state, especially considering the steady concentration measured by C_1 as shown in Fig. 11. Fig. 19 shows the results of extending the averaging time duration of both microscopes in steady-state. The results in Fig. 19, shows that increasing the averaging time to 3min reduces the fluctuation of measured OiW concentration greatly. Meanwhile, the negative impact is that the time resolution of dynamics will be reduced accordingly.

Another solution is to measure the OiW concentration in real-time by incorporating a trailing moving average window. The size of the moving average window is highly based on the plant's dynamics. Based on the results in Fig. 15, 16, 17, and 18, both microscopes are able to measure the the OiW concentration and thus they have the potential to track the transient behavior when it occurs in an IWT process. The fluctuating real-time results obtained with both microscopes, using a trailing moving average window of 1min, can be questioned to be sufficient to provide qualitative feedback to an operator. However, by extending the moving average window to 3min, the real-time measurements of OiW concentration from both microscopes are naturally more consistent, as shown in Fig. 20. Extending the moving average window is only valuable if the dynamic of the plant is not faster than the moving average window. The higher resolution of C_3 caused the microscope to capture twice as many particles compared to C_2, thus when using the moving average window, C_3 yields a more stable measurement.

One important procedure that has not been addressed in this paper is the classification within both microscopy analyzers. Oil droplets in Experiment III have been classified and withdrawn from the rest of the observed particles. The classification process has not been addressed as the procedure are very different in each microscope. C_2 entrust the operator in selecting the classification range of each measured variable. C_3 uses machine learning by letting an operator train the classification process by manually defining the captured particles. The different results of PSDs shown in Fig. 13 and 14, could be a result of classifying differently. The results obtained by C_3 are not representable around $13\mu\text{m}$ if the PSD truly follows a log-normal distribution. Another consequence to the bimodal PSD obtained by C_3 could be the installment right after the narrow view cell of C_2, which may change the PSD of oil droplets by breakups or coalescence. Another statical consideration was addressed when outputting a PSD, as the PSD should be trustworthy if an operator should draw any conclusion based on the presented PSD. Masuda and Iinoya [15] presented an estimation for predicting the required number of particles to be counted for a certain accuracy. In this paper, δ of the PSDs shown in Fig. 13 and 14 were calculated

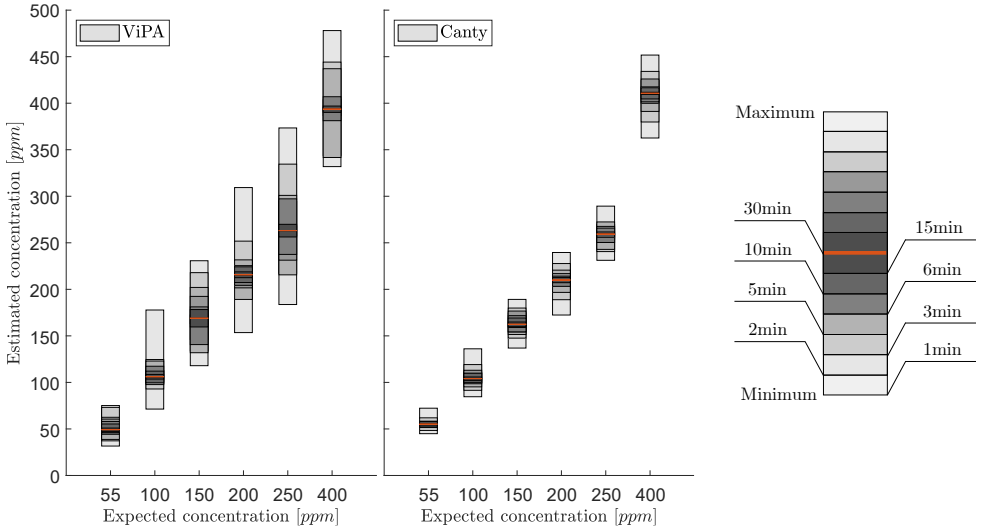

Fig. 19. Error bars representing the minimum and maximum OiW concentrations based on different time durations of averaging the OiW concentrations obtained by C_2 and C_3, respectively. The right error bar illustration shows different time durations according to the greyscale value. The red indicator shows the grand mean of the OiW concentrations obtained within the execution time of 30min.

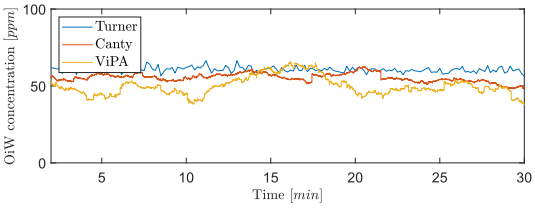

Fig. 20. Real-time OiW concentration measurements calculated extending the trailing moving average window to 3min for both C_2 and C_3.

based on the number of particles obtained within 30min at two different OiW concentrations (55ppm and 400ppm) for both microscopes. Based on the results in Table VI, a $\delta < 5\%$ was observed within a 95% confidence interval of all the presentable PSDs. If the $\delta < 5\%$ is not enough more particles must be counted, i.e., at $\delta = 1\%$ roughly $100,000 - 130,000$ for C_3 and $90,000 - 100,000$ for C_2 must be counted based on the measured OiW concentrations, respectively. Seen from another point of view, if a PSD update every 30min is too slow, the allowed δ in the presented PSD must be defined to determine the minimum number of particles required in order to achieve a defined level of accuracy.

V. Conclusion

The paper presented an evaluation of two different online microscopy analyzers that utilize a high-resolution video camera for capturing images of the particles passing their view cell. The three main calibration parameters: threshold, edge strength/focus rejection, and depth of field, were validated and discussed in order to address the difficulty in determining which particles are considered to be in focus. The procedure for selecting the three different calibration parameters must be well documented to increase the reproducibility when installed in an offshore oil and gas process. It was discussed whether the manufacturer could accommodate to reduce the use of perception when calibrating the instrument by integrating auto-calibration or human-computer interaction to minimize the uncertainties related to calibrating the microscope. Both microscopes were able to discriminate the particle size distribution of three known particle sizes with high precision, indicating a successful calibration procedure for accurately measuring the particle sizes.

A fluorescence-based monitor was installed as a benchmark to evaluate both online microscopes' performance to measure oil-in-water (OiW) concentrations, both for steady-state measurements, and for real-time purposes. The fluorescence-based monitor was selected due to previous work by Hansen *et al.* [6] showing promising results for measuring OiW concentrations. Both measurements from the microscopy analyzers were reasonable compared to the expected OiW concentration and the measured concentration from the fluorescence-based monitor. Real-time measurements from both microscopy analyzers were achievable by post-processing the data captured by the microscopes and applying a trailing moving average window of 1min. Although selecting the size of the moving average window should be based on the plant's dynamics.

Lastly, a statical consideration was addressed to determine the minimum number of particles required in order to achieve a defined level of accuracy within a defined confidence interval when outputting the particle size distribution to an operator.

ACKNOWLEDGMENT

The authors would like to thank the support from the DHRTC and thank the colleague, L. Hansen from AAU, for many valuable discussions and supports. A special thanks go to colleagues at Total Denmark A/S in Esbjerg for valuable supports.

REFERENCES

[1] IPIECA, UNDP, and IFC, "Mapping the Oil and Gas Industry To the Sustainable Development Goals: An Atlas," The global oil and gas industry association for environmental and social issues, London, Tech. Rep., jul 2017.
[2] EIA, "International Energy Outlook 2019: World Energy Projection System Plus," Washington, DC, 2019. [Online]. Available: www.eia.gov/aeo
[3] Miløstyrelsen, "Generel tilladelse for Total E&P Danmark A/S (TOTAL) til anvendelse, udledning og anden bortskaffelse af stoffer og materialer, herunder olie og kemikalier i produktions- og injektionsvand fra produktionsenhederne Halfdan, Dan, Tyra og Gorm for perioden 1," Total E&P Danmark A/S, Copenhagen, Tech. Rep., dec 2018.
[4] OSPAR Commission, "Overview assessment of the implementation of OSPAR Recommendation 2001 / 1 for the management of produced water from offshore installations Offshore Industry Series," OSPAR Commission, London, Tech. Rep., 2010.
[5] E. Blanchard, "Oil in Water Monitoring is a Key to Production Separation," *Offshore*, vol. 73, no. 11, pp. 104–105, nov 2013.
[6] D. Severin Hansen, S. Jespersen, M. V. Bram, and Z. Yang, "Uncertainty Analysis of Fluorescence-Based Oil-In-Water Monitors for Oil and Gas Produced Water," *Sensors*, vol. 20, no. 16, p. 36, aug 2020.
[7] A. Ostroff, "Injection Water Problems Identified By Laboratory Analysis," in *Middle East Technical Conference and Exhibition*. Manama: Society of Petroleum Engineers, mar 1981, pp. 523 – 526.
[8] C. C. Patton, "Water Quality Control and Its Importance in Waterflooding Operations," *Journal of Petroleum Technology*, vol. 40, no. 9, pp. 1123–1126, sep 1988.
[9] D. Bennion, D. Bennion, F. Thomas, and R. Bietz, "Injection Water Quality - A Key Factor to Successful Waterflooding," in *Annual Technical Meeting*, vol. 37, no. 6. Calgary: Petroleum Society of Canada, apr 1994, pp. 53–62.
[10] B. L. Ogden, "Water Technology: Understanding, Interpreting and Utilizing Water Analysis Data," in *Southwestern Petroleum Short Course Conference 2008*. Lubbock, TX: Southwestern Petroleum Short Course, apr 2008, p. 12.
[11] I. Larsen, "Denmark's Oil and Gas Production – and Subsoil Use 09," Energistyrelsen, Copenhagen, Tech. Rep., jun 2010.
[12] K. Bansal and D. Caudle, "A New Approach for Injection Water Quality," in *SPE Annual Technical Conference and Exhibition*. Washington, DC: Society of Petroleum Engineers, apr 1992, pp. 383 – 396.
[13] M. Yang, "Measurement of Oil in Produced Water," in *Produced Water*, 1st ed., K. Lee and J. Neff, Eds. New York, NY: Springer-Verlag, jul 2011, ch. 2, pp. 57–88.
[14] K. Eslahian, "Certificate of Traceability," 2020, certificates.
[15] H. Masuda and K. Iinoya, "Theoretical Study on the Scatter of Experimental Data due to the Particle-Size-Distribution," *Journal of Chemical Engineering of Japan*, vol. 4, no. 1, pp. 60–66, feb 1971.
[16] A. Jillavenkatesa, S. J. Dapkunas, and L.-S. H. Lum, *Particle Size Characterization: Recommended Practice Guide*, 1st ed., ser. NIST Recommended Practice Guide. Gaithersburg, MD: National Institute of Standards and Technology, 2001.

Dennis Severin Hansen was born in Odense, Denmark in 1990. He received the BSc and MSc degrees in Offshore Energy Systems at Aalborg University, Esbjerg, Denmark, in 2016 and currently a Ph.D. student at Aalborg University at the Department of Energy Technology, Esbjerg. From 2016 to 2017, he was a Research Assistant at the department where he is currently a P.hD. student. His research interests include online water quality measurements in fluid processes, microscopy analysis, process optimization, and control, with oil and gas industry as the domain. He was a recipient of the DHRTC Technology Conference best poster presentation in 2017.

Stefan Jespersen was born in Rødding, Denmark in 1993. He received his BSc and MSc degrees in Offshore Energy Systems at Aalborg University, Esbjerg, Denmark in 2017. From 2017 to 2020 he was employed as a Research Assistant at the Department of Energy Technology, Esbjerg where he is currenly enrolled as a Ph.D. student. His research interests include modeling and control of process systems.

Mads Valentin Bram was born in Sønderborg, Denmark in 1992. He received his BSc and MSc degrees in Offshore Energy Systems at Aalborg University, Esbjerg, Denmark, in 2016 and finished his Ph.D. in 2020 at Aalborg University at the Department of Energy Technology, Esbjerg. His research interests include modeling, control, and performance of offshore deoiling hydrocyclones.

Zhenyu Yang received his BSc and MSc degrees in control theory from Shandong University (China), in 1991 and 1994 respectively, and received his Ph.D. degree in control engineering from Beihang University (China) in 1998. He had been post-doctor at TUDelft during 1998−1999, post-doctor and Assistant Professor at Aalborg University (AAU) during 1999−2003. Since 2003 he has been an Associate Professor at AAU, Denmark. His research areas include control theory, modeling and identification, fault detection and diagnosis, fault tolerant control, hybrid dynamical systems, AI & machine learning, as well as their industrial applications. Recent years he has been extensively committing research on advanced automation and monitoring on the produced/injection water treatment for offshore oil & gas production. He has authored/co-authored over 155 peer-reviewed journal/conference publications. He has been leader/PI for a number of international/national research projects and raised up about 40 million DKK project funding in the past 10 years. Currently he is the leader of Offshore Energy Systems Research Program at AAU and has been secretary of IEEE joint Danish Chapter of CS023 and RA024 since 2012.

Paper E

Human Machine Interface Prototyping and Application for Advanced Control of Offshore Topside Separation Processes

Dennis S. Hansen, Stefan Jespersen, Mads V. Bram, and Zhenyu Yang

The paper has been published in the proceeding
IECON 2018 - 44th Annual Conference of the IEEE Industrial Electronics Society. Washington, DC: IEEE, 21-23 Oct. 2018, pp. 2341–2347.

Human Machine Interface Prototyping and Application for Advanced Control of Offshore Topside Separation Processes

1st Dennis Severin Hansen
Dept. of Energy Technology
Aalborg University Esbjerg
6700 Esbjerg, Denmark
dsh@et.aau.dk

2nd Stefan Jespersen
Dept. of Energy Technology
Aalborg University Esbjerg
6700 Esbjerg, Denmark
sje@et.aau.dk

3rd Mads Valentin Bram
Dept. of Energy Technology
Aalborg University Esbjerg
6700 Esbjerg, Denmark
mvb@et.aau.dk

4th Zhenyu Yang
Dept. of Energy Technology
Aalborg University Esbjerg
6700 Esbjerg, Denmark
yang@et.aau.dk

***Abstract*—This paper establishes an implementation framework, as a proof of concept, of how to reduce the uncertainty of deploying advanced control offshore. The majority of process research tends to consider improvements in performance, but with less emphasis on how to realize implementation. For control methods to be successfully applied offshore, the methods must be sufficiently simple, trustworthy, and transparent. This is mainly due to the severe consequence of incidences offshore. As it is ultimately the operators that decide which control methods are toggled on/off, the operators need to be aware of the control's behavior. The focus of this paper is not process performance, nor control theory, but rather how to convey the status, state, and action of the controllers to the offshore operators. A design approach is given for displaying and explaining the control for the operators. The is based on uniting the fast prototyping capability of Simulink Real-Time with the graphical capabilities of a Human Machine Interface system. As a case study, experiments are carried out to compare Model Predictive Control to conventional Proportional Integral Derivative control on a scaled offshore pilot-plant, which can emulate different separation processes at the topside of offshore oil & gas installations. The results show that the established connection makes it possible to investigate and compare control systems real-time, which data should be available to an operator and how to represent it.**

***Index Terms*—Human-Machine Interface, Model Predictive Control, Open Platform Communication, Simulink Real-Time, Offshore topside separation process**

I. Introduction

Unlike many other industries, the upstream offshore oil & gas industry has been relatively slow to adopt new technological approaches [1]. The oil & gas industry has benefited from the steady profits and optimistic forecasts prior to the oil crisis in 2014. As Trond Ellefsen, Head of IT and Special Adviser Strategy from former Statoil in U.S. comments; *Why question something that apparently works?* [2]. Today, the scenery has changed to analyze the effectiveness of the end-to-end value chain by adopting new approaches [2]. However, convincing the industry to implement new technology remains difficult. According to Dave Savelle hardware costs and change of management challenges are often the barrier to faster adoption [3]. Therefore, adoption of new technology and changes have to show significant value, compared to cost, before achieving general acceptance. One way of increasing the adoption speed could be reducing the gap between academic research and industrial implementation. The academic oil & gas society aims to create new solutions with a high innovation rate, while the industry prefers thoroughly proven solutions with low risk and significant profit [4].

One example of a gap between the oil & gas industry and academia exists in the application of advanced controllers. A specific example is the use of Model Predictive Control (MPC), which is often disabled due to operators lacking understanding and trust of it [5], [6]. Operators switch to manual mode if they lose understanding or confidence in the action of the advanced controller, even though it operates as intended [7]. Hence, the benefits of an advanced control system will never be achieved if the operators cannot evaluate the outcome of the controller's actions.

The Importance of Human-Machine Interface

According to Abnormal Situation Management (ASM) Consortium, abnormal events are due to 3-8% production loss of the plant's capacity, where 42% is due to human incidents (operators) [8]. An abnormal situation is considered as an event which deviates from the normal operating state. Based on the percentage from ASM Consortium and statistical review of Denmark's oil production, from BP in 2016, at least $100 million is lost annually due to abnormal situations caused by human incidents in the Danish sector alone [8], [9]. Furthermore, 90% of these abnormal events caused by human incidents are estimated to be preventable [8].

Incidents can occur when operators are exposed to an excessive amount of information and are therefore prone to miss critical information due do the large amount data/alarms flooding the operators' displays [10]. Therefore, suggestions are given to emphasize the "human factors" when designing Human Machine Interface (HMI) for the operators [10].

HMI is the platform on which the operator monitors the process and where counteractions can be executed. For a simple system, with a well-defined operating point, the task of identifying abnormal situations might be easy. However, for a

978-1-5090-6684-1/18/$31.00 ©2018 IEEE

complex interdependent system, where the optimal operating point is varying due to uncontrollable inputs, the situation could be much harder to interpret. In addition, an MPC system could be implemented to increase production, improve product quality, and/or lower OPEX, but at the cost of increased complexity that renders the system harder to comprehend for the operators [7].

Reducing the Gap Between Academic Research to Industrial Implementation

Developing solutions on a scaled experimental test setup, running commercially used offshore HMI software, could potentially reduce the gap between academic research and industrial implementation. This enables researchers to adapt their solutions to an industry-like environment. Experiments are particularly useful when developers have an incomplete knowledge of the physics governing the system, when designing new control structures. The experiment improves confidence in the theoretical model that has been developed, especially if the theory is questionable for its purpose.

A scaled experimental test setup at Aalborg University in Esbjerg has been constructed and modified over a period of six years, and new updates and additions to the experimental test setup is still ongoing. In this paper, connection has been established between Simulink Real-Time and ABB 800xA HMI software. Although it is possible to display systems using Simulink; displaying results from Simulink in the HMI software gives a more realistic presentation of what the real implementation could output and still keep the fast prototyping capability of Simulink Real-Time.

As an example of using this connection between Simulink Real-Time and HMI, this paper also investigates how to improve the operators' awareness of the MPC procedure and compare the results with a Proportional Integral Derivative (PID) controller. To the authors knowledge, connection between Matlab/Simulink and industrial SCADA/HMI software have not been established in same method, operation, and context as described in this paper. However, there exists some related work that uses the connection to study wind-PV-battery power systems, where instead of using the real power plants, a Simulink model is generated of a hybrid power system, which is connected to the SCADA software via serial connection [11]. Another method of the connection between Matlab/Simulink and SCADA software, focuses on auto-generating Programmable Logic Controller (PLC) code from Simulink models and implementing it into B&R Automation software in which an HMI display was generated [12]. Both design methods and operation approaches of the connection are based on using Simulink to model a simulation of the process. The method presented in this paper is running the entire scaled test setup through Simulink Real-Time and establishing connection to an ABB HMI software via an Open Platform Communications (OPC) server, which can send and receive information between Simulink Real-Time and ABB HMI software. Data exchange with OPC was also tested with a software program, developed by a third-party company, making root-cause analysis of alarm events.

The rest of this paper is organized as: Section II describes how the OPC connection is established between Simulink Real-Time and ABB 800xA HMI; section III presents the experiment setup and design used for MPC; section IV illustrates the results; section V gives a discussion of the results of the MPC experiment and the benefits of HMI; lastly the paper is concluded in section VI.

II. OPC Connection Between Matlab/Simulink Real-Time and Industrial HMI

The setup, located at Aalborg University in Esbjerg, is mainly used to emulate the main parts of an offshore separation process to validate potential performance improvements of different applied control strategies. A picture of the main process parts is shown in Fig. 1. The system is used to develop and test new control algorithms, modeling, and fault detection/diagnosis for process systems. The focus in this paper is to include the HMI software, where the OPC server is the central node in the system to which an external software/hardware can be connected.

Fig. 1. The offshore pilot-plant at Aalborg University in Esbjerg.

As a laboratory setup the plant is equipped with an excess of sensors and actuators, even at locations that are unfeasible for real plants, to gain understanding of the mechanisms and characteristics of any experiment. The centralized control system of this offshore pilot-plant is implemented in an assigned computer (TARGET Computer) running Simulink Real-Time, as shown in Fig. 2. The control algorithms running in the

Matlab/Simulink software give inputs to the actuation systems, such as valves and pumps, while the outputs from all sensors and actuators are sent to the Matlab/Simulink. The system is configurable with isolation valves, such that specific parts of the entire plant can be bypassed if needed. The system consists of supply tanks from which a defined mixture of water, oil, and gas can be pumped into the system. It has a long horizontal pipeline to emulate pipelines on the seabed and a vertical pipeline which emulates the riser. The offshore pilot-plant consist of three separation stages; first stage is a gravimetric separator, the second stage consists of enhanced gravity separation using hydrocyclones, and the third stage is filtration using ceramic membranes.

In total the system has 250+ sensors which enable the emulation of a scenario in which an operator is exposed to an excessive amount of information on the screens or a situation where the system is flooded with alarms. Developed controllers for different processes/facilities can be implemented in Matlab/Simulink and tested in both simulation mode or directly on the pilot-plant. The fast prototyping of Simulink Real-Time is favorable compared to conventional industrial control solutions implemented in SCADA & PLC systems. However, the standard representation of real-time data in Simulink is a screen with only data and graphs, making it a poor representation of an operator's display. Instead, a connection to an industrial HMI software is used to generate more realistic situations.

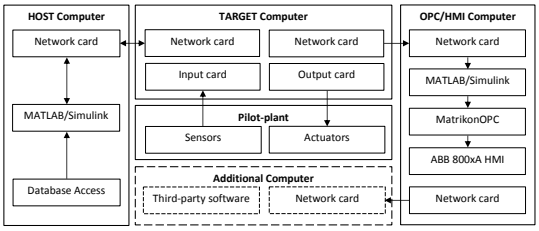

Fig. 2. Connection configuration of different computing systems. Each main block represents a computer with its respective software and hardware.

Fig. 2 illustrates the connection configuration of different computing systems, each implemented in one dedicated digital computer. When starting a test, the system's controllers are configured in Simulink on the HOST Computer. The computer compiles the program onto a dedicated real-time TARGET Computer over ethernet connection between two network cards. The TARGET Computer is connected to nine I/O cards which drive actuators as well as read sensor data. The second network card on the TARGET Computer transmits data from the TARGET Computer to the OPC/HMI Computer. This is done by User Datagram Protocol (UDP) packages from Simulink Real-Time on the TARGET Computer to Simulink Desktop Real-Time on the OPC/HMI Computer. The reason for selecting UDP instead of TCP is due to the concerns to overly delay segment transmission from the TARGET Computer when running in real-time [13].

The OPC/HMI Computer reads all sensor and actuator data from the Target Computer with a sampling rate of 1Hz, which is a common sampling rate for offshore installations. The data is then transmitted from Simulink Desktop Real-Time to the MatrikonOPC internally in the computer. Finally, the MatrikonOPC sends data to ABB 800xA HMI software from which data can be visualized in the configured workplace. The OPC server works as a central point from which data can be requested and is widely used in industry. This enable additional interfaces that can be connected to the pilot-plant system and was tested with an Additional Computer, running a developed software program from a company. The data is then used for fault diagnosis and root-cause analysis, see Fig. 2 [14].

III. MPC Experiment Illustration

Connection between Simulink Real-Time and an ABB HMI software was established, and an investigation was carried out;

- How can MPC be illustrated and explained in an intuitive way for an operator?

The investigation will serve as an example of the value of including the HMI to the pilot-plant. To visualize the behavior of the MPC solution in the ABB HMI software a simplified interface version was designed, as shown in Fig. 3. In the ABB HMI, an attempt was made to visualize the behavior of the MPC and the process without going into details about the underlying control theory. More information about the MPC solution used in this experiment can be found in [15].

The MPC was responsible for controlling the level in the separator and the pressure drop ratio (PDR) of the hydrocyclone. As separation efficiency measurements of hydrocyclones are often unreliable or inaccurate, PDR is the most commonly used hydrocyclone control objective, as PDR serves as an intermediate variable and is defined as [16];

$$PDR = \frac{P_i - P_o}{P_i - P_u}. \tag{1}$$

In a conventional solution, the level control in the separator tank is realized by manipulating the opening degree of the underflow valve (CV04) and the PDR is controlled by manipulating the overflow valve (CV09) as shown in Fig. 3. A set of PI controllers has been developed and used as a baseline to emulate the current industrial case, in order to make a comparison with the newly developed MPC solution, which is developed as a Multiple Input Multiple Output (MIMO) control solution to coordinate the level and PDR control loops [15]. For comparison study, two experiments were carried out. One experiment running a standard PID control solution, which is often used offshore (Baseline control experiment) and one experiment running an MPC solution (MPC model experiment).

Baseline control experiment:

- PI controller controlling the pressure at inside the separator tank. The setpoint is 7barA.

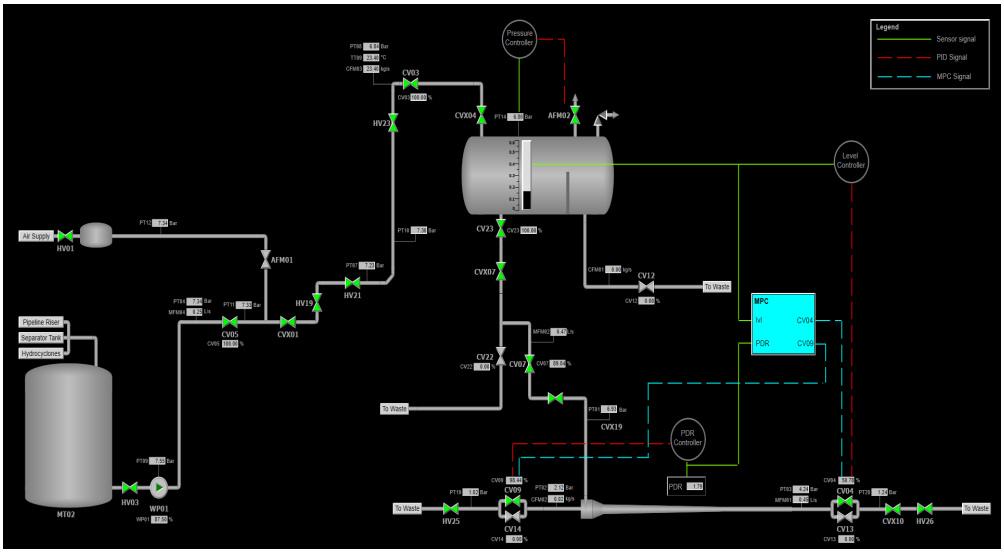

Fig. 3. Screen-shot of the HMI, showing the sub-systems designed for implementing an MPC model to the pilot-plant. The HMI illustrates the state and value of each actuator, tag name, and location of the pilot-plant for all actuators and sensors.

- PI controller controlling the level inside the separator tank. The setpoint is 15cm.
- PI controller controlling the PDR over the hydrocyclone. The setpoint is 2.

MPC model experiment:

- PI controller controlling the pressure at inside the separator tank. The setpoint is 7barA.
- MPC controlling the level inside the separator tank and PDR over the hydrocyclone. The setpoints are 15cm and 2 respectively.
- The constraints of the MPC are as follow:
  - Separator level constraints 10cm $\leq h_s \leq$ 20cm
  - Underflow valve opening degree 10% $\leq V_u \leq$ 100%
  - Overflow valve opening degree 3% $\leq V_o \leq$ 100%

IV. Results

A visual presentation of the pilot-plant is designed in ABB HMI software as seen in Fig. 3. Compared to the standard representation on the Simulink Real-Time target screen as seen in Fig. 6, the HMI gives better illustrations of the gravity separator, hydrocyclone, supply tank, etc. This is important for an operator in order to swiftly comprehend the process status of the plant.

Simulink Real-Time only shows sensor tag names and values, whereas the HMI also shows the respective sensor's physical location in the setup. As seen in Fig. 6, it is possible to generate a trend curve on the Simulink Real-Time target screen, but it does not have tick marks on the axes.

Fig. 6. The Simulink Real-Time display of the TARGET Computer.

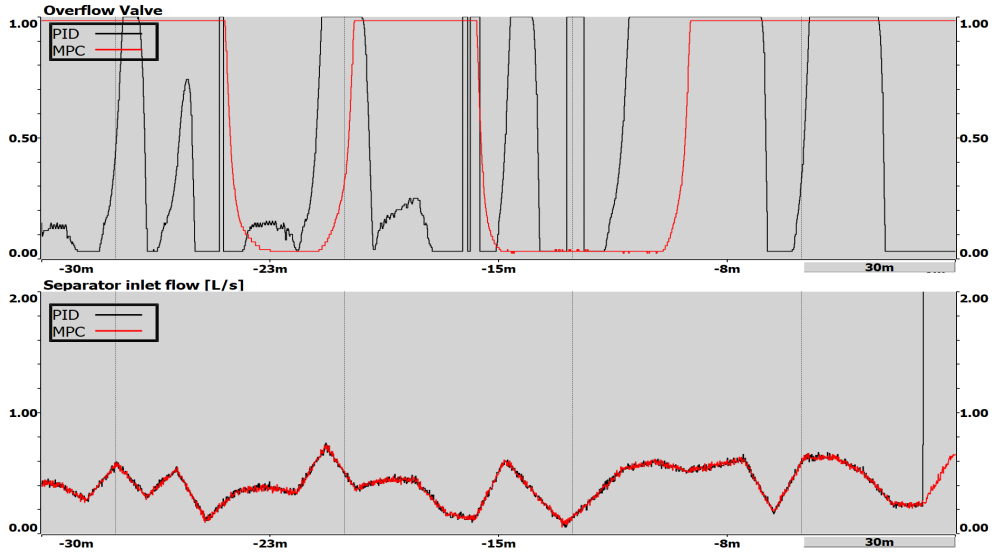

Fig. 4. Trend curves in HMI displaying the overflow valve opening degree on the upper graph and the inlet flow in the bottom graph. It is seen that the inflow conditions are the same for both the PI controllers and the MPC controller in the two experiments.

In the HMI software tick marks were added along with lines that represents the level constraints that were specified in the MPC, as seen in Fig. 5. In this paper, only a fairly simple illustration of the pilot-plant is designed as a proof of concept. The separator tank and hydrocyclone have sensor values shown with numerical displays, tag names, and units. The level in the separator tank is displayed with a graphical bar indicator instead of a numeric value to give a more intuitive representation of the level, where the weir is illustrated for reference. Valves light up green when active and are gray when closed. The control systems are displayed with a legend to indicate which signals the controllers use for feedback and which control signals they transmit. Even though it is either the MPC or the two PI controllers, which are active at a time during the experiment, both are shown for comparison. Pumps are displayed as round icons with a direction arrow and the text boxes are used to indicate connections between distant points such as the overflow and underflow outlets that return to the waste tank.

This work established a framework in which multiple solutions can be tested and benchmarked. The inclusion of the HMI increases the similarity between offshore industrial systems and the experimental setup. This increases the chance of research to be understood and acknowledged by the industry.

The inclusion of OPC and HMI also means that researchers can pitch their research to industry. Results can be illustrated in a live demonstration to get the feedback needed to improve or redirect the research.

The results of the experiment are shown in Fig. 4 and Fig. 5. Fig. 4 shows two trend curves, one shows the current valve position right after the hydrocyclone overflow outlet, the other shows the current measurement of the separator inlet flow. Fig. 5 shows two trend curves, one displays the current PDR value and the other shows the current level value in the separator tank. Along with the trend curves, two indication lines of the level constraints (black horizontal lines). For all four trend curves, in Fig. 4 and Fig. 5, there are two trend lines, representing the online MPC solution (red) and the PI control solution (blue). The PI control data is ghosted from a previous experiment while the MPC is running in real-time for this particular demonstration. In Fig. 4 it is evident that the flow is identical in the two experiments. The plots show the data for the last 30min. Note that the PI control experiment ends a few minutes before the MPC experiment, thus the last few minutes should not be compared.

A typical industrial plant with interconnected systems, like a PID controller controlling the level in the separator tank, and another controlling the PDR, can counteract each other [17]. Fig. 5 shows how the PDR fluctuates when controlled by a PI controller, whereas the level is strictly kept around the operating point of 15cm. Because the level controller is very strict, it actuates the underflow valve aggressively when the measured level is deviating from the reference. The underflow valve acts as a disturbance to the PDR control-loop, and the PDR controller compensates for this by actuating the overflow valve. However, with the situation that the overflow valve is less dominant, compared to the underflow valve, it often

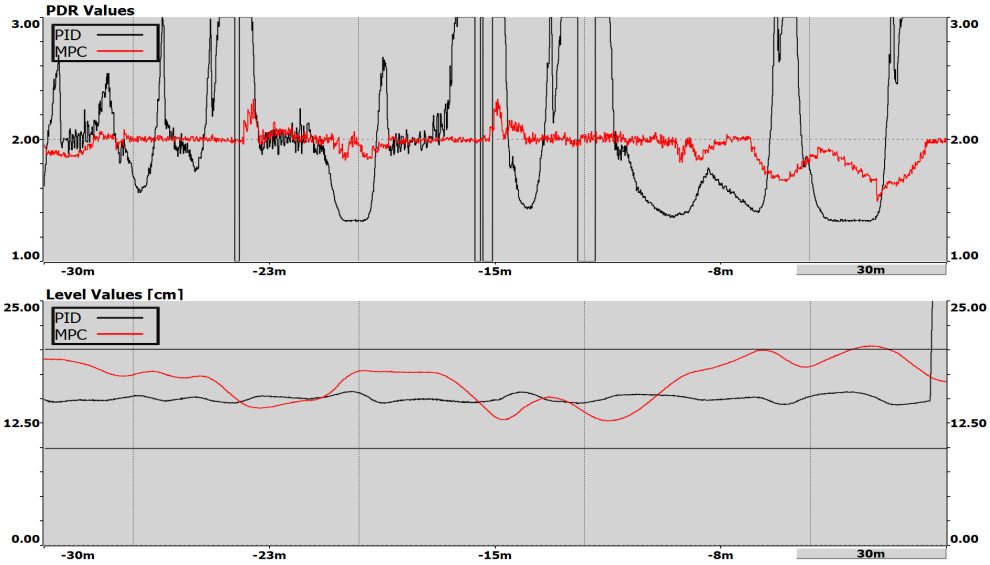

Fig. 5. Trend curves of hydrocyclone PDR in the upper graph and separator level in the bottom graph. It is seen that the MPC keeps the PDR relatively steady while keeping the level within bounds. The MPC only sacrifices the PDR when the level approaches the level constraints, indicated with black lines.

saturates or acts aggressively causing the oscillatory behavior as seen in Fig. 4. In reality, the level does not have to be this strict but only has to stay within certain limits. The PI controller was tunes to resemble data form an offshore platform [18].

One benefit of MPC, is that constraints can be implemented in the mathematical design of the controller. In Fig. 5 it is seen that the MPC attempts to keep the level bounded between the level constraints illustrated with black lines. The MPC controls both the level and the PDR simultaneously. It relies on a mathematical model which is used to do a prediction of the future outputs. From the predictions, a cost function is set up which can consist of the output reference tracking, the manipulated variable tracking, the change in manipulated variables, and constraint violations. All of those can be assigned weights which are tuning parameters along with the prediction horizon and the control horizon. A solution which minimizes the cost is found on-line and the first-step of the control inputs is applied in the next time step. The use of a cost function enables the MPC to make a trade-off between different control objectives and suppress too large deviations and fast changes in manipulated variables. This means that a trade-off can also be made between the control objective and the actuation energy or control effort. It is seen that when the level reaches the upper boundary, the MPC reacts by putting less effort in keeping the PDR and more effort into keeping the level within the limits. Even though the MPC is more complex it still has the intuitive behavior of trying to find a trade-off between control objectives. In this example, the MPC keeps the PDR relatively constant by relaxing the level tracking when possible.

V. Discussion

As a proof of concept, a comparison between the offshore data-based PI control solution and MPC solution was presented using the established connection between Simulink Real-Time and ABB 800xA HMI software. As expected the MPC clearly outperforms the PI control solution in terms of keeping the PDR constant. However, the controller is not limited to being MPC to yield process improvements, but merely a controller which relaxes the level controller in order for the PDR to remain steady around the reference. A more relaxed PI-based level controller could also have been implemented and would also have shown improved results over the baseline PI control presented. The purpose of this experiment was, however, merely to show that the established connection with the HMI can be used to compare control solutions in real-time. Robust controllers like MPC does however have the advantage of easy implementation of boundary conditions and its capability of handling more control objectives at once while handling trade-offs.

It was observed that the actions of the controller can be explained by looking at the trend curves. However, during the 30min of demonstration, the level reaches the constraint line once and actually crosses it shortly afterwards. The question is thus whether the operator would trust the MPC once it approaches the constraints. In that case more information should probably be shown to convince the operator that the

MPC can handle the situation. If the inlet flow, as seen in Fig. 4, is not measured or estimated the operator should decide whether the system is about to become uncontrollable by looking at the underflow valve opening degree and the trend of the level curve. If the valve is saturated and the level is still rising unaffected, the system is no longer controllable. Some of the information from the MPC could be implemented in the HMI, thus making the controller's characteristics more transparent. The level constraints displayed on the trends are an example of MPC characteristics being given for the operator to see. Other information from the cost function or predictions could be displayed as well, to understand how the controller makes its decisions. Whereas Simulink Real-Time is fast for prototyping controllers, the HMI software was used to prototype a way of displaying data from the MPC. With the HMI it can be investigated how control information is best presented to an operator.

To fully meet the industry's implementation requirement, one could argue that the developed control systems should be implemented on a PLC, instead of running the control system through Matlab/Simulink. One solution could be implementing the MPC or similar advanced control solution in digital computer environment. The computed control signals can then be transmitted to PLC systems, via an OPC server, assuming that the PLC is OPC compatible.

VI. Conclusion

The scaled pilot-plant is a testing facility capable of running different sections of the plant in series or bypass different sections. The plant provides a good testing environment for developing new features to the upstream offshore oil & gas industry. However, concerns arising from developing new features in an academic used software as Matlab/Simulink are often met as a barrier for implementation of found solutions into an industrial application. Therefore, to mimic the industrial practice, a connection has been established between Simulink Real-Time and ABB 800xA HMI software. To demonstrate the use of this connection a case study was carried out by investigating how to potentially improve the operators' comprehension of the MPC procedure and how different controllers can be demonstrated in real-time. The results show how a PI control solution can be ghosted from a previous experiment, with the same operating condition as for the MPC solution, while the MPC is running real-time. By doing so, a demonstration of the benefits or/and limitations can be given for interested industrial partners in a known industrial HMI software. This can inspire the oil & gas industry to adopt new solutions and provide crucial feedback for research, thus reducing the gap between the academia and industry.

Acknowledgment

The authors would like to thank support from the DTU-DHRTC Projects: *"Laboratory Testing at AAU-Esbjerg and Development"* and *"Injection Water Quality and Control"*. The authors will also like to thank the colleagues S. Pedersen, K. Jepsen, L. Hansen, and P. Durdevic from AAU-Esbjerg, for many valuable discussions and supports.

References

[1] M. Andrew. (2017) How technology is saving the oil and gas industry. Inc., Agent Beta. [Online]. Available: https://www.inc.com/andrew-medal/how-technology-is-saving-oil-gas-industry.html

[2] E. Trond. (2015) Oil and gas industry slowly and surely adapting to demands of modern times. Energy CIO Insights. [Online]. Available: https://smart-grid.energycioinsights.com/cxo-insights/oil-and-gas-industry-slowly-and-/surely-adapting-to-demands-of-modern-times-nwid-46.html

[3] D. Savelle, "The oil industry, technology and the field ticket of the future," *PennEnergy*, March 2018.

[4] A. Khlaifat, H. Qutob *et al.*, "Bridging the gap between oil and gas industry and academia," in *North Africa Technical Conference and Exhibition*. Society of Petroleum Engineers, 2013.

[5] C. Lindscheid, A. Bremer, D. Haßkerl, A. Tatulea-Codrean, and S. Engell, "A test environment to evaluate the integration of operators in nonlinear model-predictive control of chemical processes1," *IFAC-PapersOnLine*, vol. 49, no. 32, pp. 129–134, 2016.

[6] M. Campos, H. Teixeira, F. Liporace, and M. Gomes, "Challenges and problems with advanced control and optimization technologies," *IFAC Proceedings Volumes*, vol. 42, no. 11, pp. 1–8, 2009.

[7] M. G. Forbes, R. S. Patwardhan, H. Hamadah, and R. B. Gopaluni, "Model predictive control in industry: Challenges and opportunities," *IFAC-PapersOnLine*, vol. 48, no. 8, pp. 531–538, 2015.

[8] A. Consortium, "Abnormal situation management -effective automation to improve operator performance." ASM Consortium, 2007.

[9] B. Dudley, "Bp statistical review of world energy june 2017," *Global, British Petroleum*, 2017.

[10] S. Guerlain, G. A. Jamieson, P. Bullemer, and R. Blair, "The mpc elucidator: A case study in the design for human-automation interaction," *IEEE Transactions on Systems, Man, and Cybernetics-Part A: Systems and Humans*, vol. 32, no. 1, pp. 25–40, 2002.

[11] A. Soetedjo, A. Lomi, Y. I. Nakhoda, and Y. P. Tosadu, "Combining web scada software and matlab-simulink for studying wind-pv-battery power systems," *ARv*, vol. 2, no. 2, p. 1, 2013.

[12] R. Salunke, P. Vikhe, and T. Sarode, "Implementation of automatic plc code from matlab simulation model using b&r automation target for simulink," in *2nd International Conference on Control, Communication and Power Engineering*, 2011.

[13] J. F. Kurose and K. W. Ross, *Computer networking: a top-down approach*. Addison-Wesley Reading, 2010.

[14] E. K. Nielsen, M. V. Bram, J. Frutiger, G. Sin, and M. Lind, "Modelling and validating a deoiling hydrocyclone for fault diagnosis using multilevel flow modeling," in *International Symposium on Future Instrumentation & Control for Nuclear Power Plants*, 2017.

[15] L. Hansen, P. Durdevic, K. Jepsen, and Z. Yang, "Plant-wide optimal control of an offshore de-oiling process using mpc technique," *IFAC Workshop on Automatic Control in Offshore Oil and Gas Production*, vol. 3, no. 49, pp. 144–150, 2018.

[16] D. S. Hansen, M. V. Bram, and Z. Yang, "Measuring efficiency of offshore deoiling hydrocyclones utilizing real-time oil-in-water monitors," in *2017 IEEE Conference on Control Technology and Applications (CCTA)*. IEEE Press, 2017, pp. 1104–1109.

[17] Z. Yang, S. Pedersen, and P. Durdevic, "Cleaning the produced water in offshore oil production by using plant-wide optimal control strategy," in *Oceans-St. John's, 2014*. IEEE, 2014, pp. 1–10.

[18] P. Durdevic and Z. Yang, "Application of h_∞ robust control on a scaled offshore oil and gas de-oiling facility," *Energies*, vol. 11, no. 2, p. 287, 2018.

ISSN (online): 2446-1636
ISBN (online): 978-87-7210-866-7 AALBORG UNIVERSITY PRESS